THE UNIVERSITY OF HULL

POLYACRYLAMIDE NANOPARTICLE DELIVERY SYSTEMS IN PHOTODYNAMIC THERAPY

Being a Thesis submitted for the Degree of Doctor of Philosophy

in the University of Hull

By

Kuruppuarachchi Appuhamilage Dona Surani

Maheshika Kuruppuarachchi,

BSc (Hons) Keele University, UK

September 2011

Acknowledgements

I would firstly like to thank my supervisor, Dr. Ross W. Boyle for providing me with the opportunity to study for this PhD, all his help, guidance and continuous encouragement throughout the time in the lab and also whilst writing up – thank you for all your endeavours. I also want to thank Dr. Steve Archibald, my second supervisor, for his help during this time.

Special thanks go to Prof. John Greenman for letting me use the facilities in his lab to carry out my biology studies. I would like to thank Huguette Savoie for her help in photobiology work and Dr. Cristina Alonso for assisting in the organic chemistry lab. Many thanks go to Dr. Leigh Madden for sharing his expertise in the biology techniques and Dr. Vicky Green for her help in flow cytometry. I would also like to thank Dr. Tim Paget for teaching me how to work with bacteria. Further, many thanks go to Dr. Mark Lorch, Dr. Robert Lewis for their help with NMR, Dr. Kevin Welham for his help with MS, Ann Lowry for helping in obtaining TEM images and Carol Kennedy for help with CHNS Analysis. My thanks also go to all I worked with, especially, Dr. Abigail Webster, Emily Lumley, Rachel Smith, Dr. Mike Benstead, Dr. Abid Khan, Dr. Chris Welch, Dr. Francesca Giuntini and Dr. Aaron Bullous for all the interesting discussions along the way.

I will always be grateful to Dr. Leanne B. Josefsen for sharing her expertise in nanoparticle synthesis and kindly volunteering to read through my entire thesis. Your beautiful encouraging emails and texts have inspired me many a time.

I am eternally indebted to my parents, Anton and Sriya and my parents-in-law, Markus and Bernedette, for always encouraging me to go the extra mile. The reminder, “How is your thesis going?” every time we spoke did keep me going. A bunch of thanks also goes to my little sister Dinesha, brother Dananjeya, and my friends, Melanie, Sakinah, Delphine, Claudia, Dawid, Agnieszka, Susan for making this a pleasant experience. Thank you!

Lastly, a big thank you goes to my husband. Pascal, you have been tremendously supportive throughout my whole PhD career. You always believed in me, cheered me up whenever I needed it, helped me to stay awake late at night writing up and made sure I would not forget to switch off every once in a while.

Without you all, this journey would not have been possible! Thank you once again!

****

Abstract

In treating many diseases, including cancer and bacterial infections, drug resistance has emerged as a major obstacle limiting the therapeutic efficacy of chemotherapeutic agents. One area which may prove to be particularly attractive is Photodynamic Therapy (PDT). Reactive oxygen species (ROS) which cause damage to tumour tissue are not generated until the drug is activated by light, minimising generalised toxicity and giving a high degree of spatial control over the clinical effect.

The application of nanoparticles (NPs) in the field of drug delivery is extensively studied as a potential for delivering high payloads of drugs site selectively. They can be targeted towards, and accumulate in, tumour tissue by the enhanced permeability and retention effect, if sequestration by the reticuloendothelial system (RES) is avoided.

This project aimed to develop an efficient drug delivery system based on nano-sized particles. Polyacrylamide nanoparticles were chosen to deliver photosensitisers due to the chemical and biological inertness of polyacrylamide, in addition to its optical transparency. The porous three-dimensional particles produced from microemulsion polymerisation reactions are typically prepared in the nanometre range.

In the study, two types of NPs loaded with photodynamic sensitisers are synthesised: photosensitiser (i.e. phthalocyanine) entrapped NPs (PCNP) and photosensitiser (i.e. phthalocyanine) entrapped NPs coated with a second photosensitiser (i.e. porphyrin) (PCNP-P) to enhance the capacity for ROS generation, and hence therapeutic potential. The mean sizes of these particles were 45±10nm and 95±10nm respectively.

NP uptake by human Caucasian colon adenocarcinoma cells (HT29) was determined by flow cytometry and confocal microscopy. Cell viability assays using two chosen NPs (PC-NP and PCNP-P) corresponding to the minimum uptake time (<5 minutes) and maximum uptake time (25 hours), quantified by flow cytometry, demonstrated that these cancer cells can be damaged by activation of the photodynamic NPs both when in the external media and post internalisation.

Results suggest that in order to induce photodynamic damage, the NPs need only be associated with the tumour cell closely enough to deliver singlet oxygen - their internalisation within target cells may not be necessary. Clinically, this could be of great importance as it may help to combat the ability of many cancer cells to actively expel conventional anti-cancer drugs.

Some of this work has already been published, under the title **Polyacrylamide Nanoparticles as a Delivery System in Photodynamic Therapy**, in *Mol. Pharmaceutics*, **2011**, *8* (3), pp 920–931.

Abbreviations

$^1O_2$ / $^1\Delta_g$	singlet oxygen
$^3O_2$	molecular oxygen
$\lambda_{max.}$	maximum absorption
Φ	quantum yield
5 ALA	5-aminolevulinic acid
5FPorphyrin	5,10,15,20-tetra(pentafluorophenyl)porphyrin
AlPc	aluminium phthalocyanine
APS	ammonium persulphate
BSA	bovine serum albumin
CDDP	cisplatin; *cis*-dichlorodiammineplatinum(II)
CME	clathrin-mediated endocytosis
DCM	dichloromethane
DMF	dimethylformamide
DMSO	dimethyl sulfoxide
DSRuCl	disulphonated 4,7-diphenyl-1,10-phenanthroline ruthenium (II) chloride; disulphonated ruthenium chloride dye
EMS	electromagnetic spectrum
EPR	enhanced permeability and retention
FACS	fluorescence activated cell sorting
FCS	fetal calf serum
FL	fluorescence
FSC	forward scatter
FRET	fluorescence resonance energy transfer

GPC	gel permeation chromatography
GTP	group transfer polymerisation
HPLC	high performance liquid chromatography
HRP	horseradish peroxidise
HT29	human caucasian colon adenocarcinoma cells
ICG	indocyanine green
LSCM	laser scanning confocal fluorescence microscopy
LPS	lipopolysaccharides
MB	methylene blue
MS	mass spectrometry
MR	magnetic resonance
MRI	magnetic resonance imaging
MRSA	methicillin resistant *Stapholococus aureus*
MSNs	mesoporous silica nanoparticles
MTS	3-(4,5-dimethyl thiazol-2-yl)-5-(3-carboxymethoxyphenyl)-2-(4-sulfophenyl)-2H-tetrazolium inner salt
MW	molecular weight
NHS	National Health Service
NHS Porphyrin	5-[4-(succinimide-N-oxycarbonyl)phenyl]-10,15,20-tris-(4-*N*-methylpyridimiumyl)porphyrin trichloride
NMR	nuclear magnetic resonance
NP	nanoparticles
OPE	one-photon excitation
ORMOSIL	organically modified silica
PACT	photodynamic antibacterial chemotherapy

PBS	phosphate buffered saline
PC	aluminium phthalocyanine tetrasulfonyl chloride
PCNP	polymer bound tetrasulfonato-aluminium phthalocyanine entrapped nanoparticles
PCNP-A	polymer bound amino functionalised tetrasulfonato-aluminium phthalocyanine entrapped nanoparticles
PCNP-P	polymer bound tetrasulfonato-aluminium phthalocyanine entrapped porphyrin conjugated nanoparticles
PCS	photon correlation spectroscopy
PDT	photodynamic therapy
PEBBLE	probes encapsulated by biologically localized embedding
PEG	polyethylene glycol
PEG(750)Porphyrin	5,10,15,20-tetrakis(2,3,5,6-tetrafluoro-4-{PEG(750)-sulfanyl}patt-phenyl)-porphyrin
PGPs	P-glycoproteins
POLPC	polylysine conjugated aluminium - phthalocyanine
PI	propidium iodide
PS	photosensitiser
PyPorphyrin	5,10,15,20-tetrakis-(4-*N*-methylpyridiniumyl)porphyrin tetraiodide
QDs	quantum dots
RES	reticuloendothelial system
ROS	reactive oxygen species
SSC	side scatter
Surfactant	surface active substances

TEGTs	4-toluenesulfonic acid 1-(2-(2-(2-methoxy)ethoxy) ethoxy)ethyl ester
TEM	transmission electron microscopy
TEMED	*N*,*N*,*N'*,*N'*-tetramethylethylenediamine
TET	triplet energy transfer
THF	tetrahydrofuran
TLC	thin layer chromatography
TOAB	tetraoctylammonium bromide
TPE	two-photon excitation
UV-vis.	ultra violet visible
W/O	water-in-oil
$z_{ave.}$	average size

Contents

List of figures

List of schemes

List of tables

Chapter 1: Introduction

This chapter briefly discusses how drug delivery is carried out with polymers and nanoparticles (NPs) mainly for photodynamic therapy (PDT) and photodynamic antimicrobial chemotherapy (PACT).

1.1 Polymers

Polymers are large molecules (macromolecules), composed of repeating small elementary units joined by chemical bonds; these elementary units are called monomers [*i.e.* a vinyl polymer (polyvinyl) is composed of the vinyl monomer unit (–CH_2-CH(X)-)]. A constitutional replicating unit incorporates more than one monomer in the formation of a polymer[1].

Polymers can be divided into two major categories, living polymers and non-living polymers. Living polymers are well-defined polymers with closely defined structures and sizes combined with low polydispersity (range of polymer lengths), whereas non-living polymers are significantly less well characterised and usually have much greater polydispersity.

1.1.1 Living polymers

Living polymers are molecules with known molecular weights and architecture. These polymeric chains are dynamic objects that maintain a narrow molecular weight distribution[2, 3]. They adapt according to the environment (*i.e.* the addition of a monomer or a sudden change in temperature) by polymerisation and depolymerisation reactions allowing a new thermodynamic equilibrium to be attained.

Living polymers are synthesised *via* ionic polymerisation. Living polymerisation is usually further categorised into cationic polymerisation and anionic polymerisation. Cationic polymerisation involves addition of a positively charged monomer, whereas anionic polymerisation initiates with a negatively charged monomer[1]. Living polymers possess unique features: (i) the easy addition or subtraction of monomers from the chain ends[4] and a fixed total number of chains[2]. These polymers can be synthesised by controlling the initiator and the active end-group monomers and can either be end-functionalised or block-copolymerised with other monomers, enabling the synthesis of a variety of well characterised polymers (Figure 1.1).

In a living polymer system, the polymerisation ceases only if all the monomers present are consumed as long as oxygen and water (*i.e.* free radical sources) are absent from the media. Addition of a monomer would resume the polymer chain growth, even if the "new" monomer added is different to the initial monomer used.

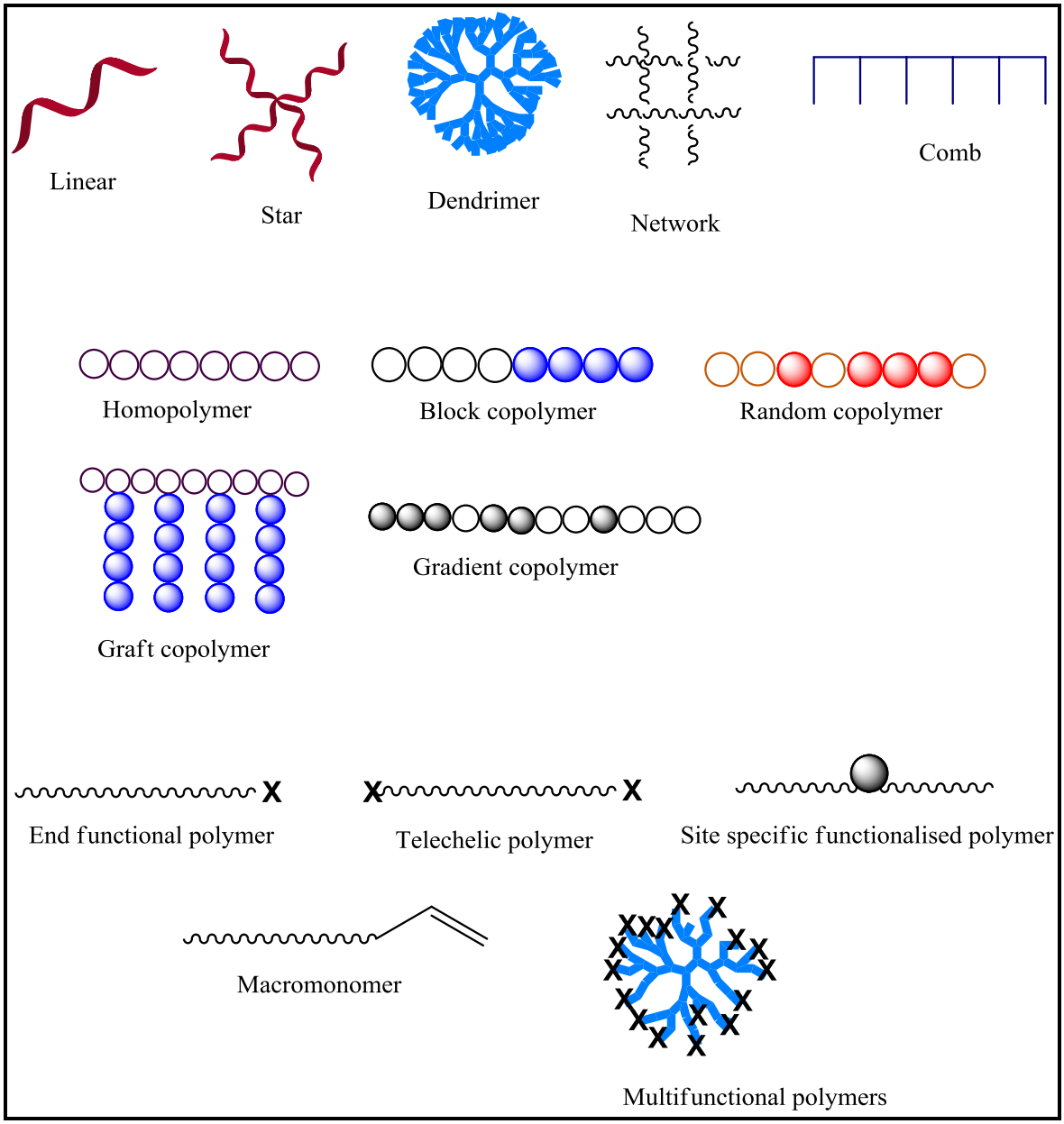

Figure 1.1: A schematic diagram of polymers synthesised using living polymerisation

(modified from reference[3])

Non-living polymers are synthesised by radical polymerisation. Some key differences between ionic and radical polymerisation are listed in the below table (Table 1.1)[1,2].

Ionic polymerisation	Free radical polymerisation
The distribution of chain lengths is very small. Poisson fluctuations around the mean with a low polydispersity index (~1) (Polydispersity index is a measure of the molecular mass range of a polymer sample.)	The distribution of chain lengths of the polymers is broad with a relatively high polydispersity index (~2).
Polymer architecture can be controlled.	Architecture of the polymer cannot be controlled.
Possibility of controlling the molecular weight of the polymer.	Molecular weight of the polymer cannot be controlled.
The solvent that is used in the reaction has a considerable influence on the nature of the polymers synthesised: polymerisation reactions are carried out in solvents with relatively low polarity.	The solvent serves as a vehicle for the soluble species but shows no influence on the rate or the stereochemistry of the products.
Polymer termination cannot involve two growing chain ends – due to charge repulsion.	Polymer termination can involve two growing chain ends.
Limitation in the range of monomers that can be used for polymerisation.	A very broad variety of monomers can be used for the polymerisation reaction.

Table 1.1: Comparison between ionic polymerisation and free radical polymerisation

1.1.2 Group Transfer Polymerisation (GTP)

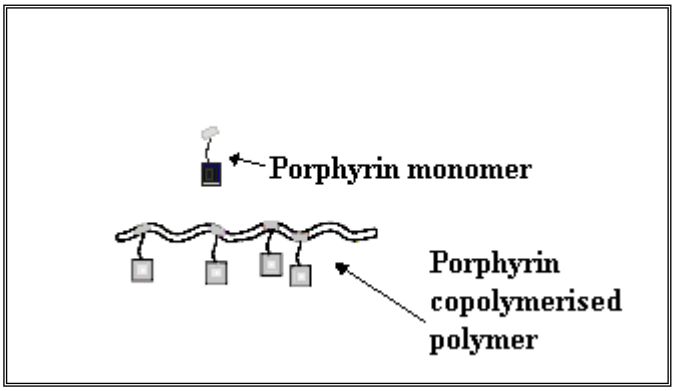

Figure 1.1: Copolymerisation of a porphyrin in a polymer chain

GTP is a reasonably new technique for polymerisation of acrylic and methacrylic monomers. This is an easy, fast, living polymerisation method and can be carried out at room temperature or above. This method is appropriate for synthesising porphyrin copolymerised polymers (Figure 1.1), due to its cost efficiency and ability to control the architecture and molecular weight of the polymer[5]. GTP relies on functionalised groups such as methacrylate and acrylate as the monomers.

Following on from microtechnology, nanotechnology has been referred to as the technology of the 21st century. Nanotechnology has already impacted significantly on the material world, in the fields of medicine, electronics and energy production. The section below briefly discusses the origin of nanotechnology by introducing different types of NPs used in biomedicine, mainly in drug delivery. The subsequent discussion focuses more specifically on NPs formed from a polyacrylamide matrix. The section ends with a discussion on how NPs can be taken up by cells.

1.2 Nanotechnology

Nanotechnology is not new: Nobel Laureate Richard Feynman, inspired the concepts of nanotechnology back in 1959 in his visionary lecture,

‘’There is plenty of room at the bottom”[6]. He noted “What I want to talk about is the problem of manipulating and controlling things on a small scale...What I have demonstrated is that there *is* room---that you can decrease the size of things in a practical way. I now want to show that there is *plenty* of room”.

He further continued his vision,

“The principles of physics, as far as I can see, do not speak against the possibility of manoeuvring things atom by atom. It is not an attempt to violate any laws; it is something, in principle, that can be done; but in practice, it has not been done because we are too big. The problems of chemistry and biology can be greatly helped if our ability to see what we are doing, and to do things on an atomic level, is ultimately developed, a development which I think cannot be avoided”.

Although the concept of nanotechnology was laid down with this lecture in 1959, it did not emerge as a separate scientific discipline until some 20 years ago.

Nanotechnology can be defined as the engineering of functional systems at a molecular level. It modifies matter at the lower nanometric (1-100 nm) level. Particles of this size behave as an intermediate between macroscopic sized solids and atomic or molecular systems[7]. The properties and functions of NPs primarily depend upon their size[8]. The

increased surface area (surface area per mass) of the nanosized particle having a huge influence on its overall properties.

The application of nanotechnology in medicine and biology is advancing rapidly in areas such as cancer therapy[9, 10], manipulation of genetic materials[11-13], rapid colorimetric detection[14], disease diagnosis[11, 15], intracellular glucose imaging[16], detection of zinc[17] bioimaging[18] *i.e.* brain tumour diagnosis and imaging[19]. Research is now expanding into rational delivery and targeting of pharmaceutical, therapeutic and diagnostic agents through intravenous and interstitial routes of administration with nanosized particles. A very interesting study was reported by Russell *et al.*, on intelligent fingerprinting, where they showed how it's possible to obtain direct chemical information from drugs or drug metabolites present in miniature amounts of sweat deposits[20]. Further, NPs can be embedded with proteins[21], to provide ratiometric methods for pH measurement using fluorescent dyes[22, 23] and horseradish peroxidise (HRP)[24].

Optical PEBBLE (probes encapsulated by biologically localized embedding) nanosensors, using ORMOSIL (organically modified silica) NPs as a matrix, have demonstrated some excellent results confirming the validity and high sensitivity of the delivery method for intracellular studies of PEBBLE sensors, which is required to achieve real-time measurements of intracellular dissolved oxygen concentration[25]. Another study by the same group developed a ratiometric singlet oxygen nano-optode where they observed relatively high singlet oxygen solubility due to the highly permeable structure, hydrophobic nature of the outer shell and longer lifetime of oxygen in the ORMOSIL matrix compared to the aqueous solution[26]. Josefsen *et al*. reported some excellent results on a nanosystem that can generate ROS and monitor the cell reaction as a function of

calcium ion concentration using a porphyrin conjugated calcium green entrapped NP system[27, 28].

Quarta *et al.* reviewed the most significant *in vitro* studies using magnetic-fluorescent nanocomposites based on colloidal iron oxide nanocrystals combined with different classes of fluorophores (*i.e.* cyanines and porphyrins) on living cells, applications in biology and medicine[29]. Further it also gives an insight into how fluorescent-magnetic NPs, previously mainly focused on diagnosis *via* MRI and fluorescence imaging, have now developed a step further towards a number of multifunctional magnetic targeting drug delivery systems for diagnosis and therapy in the past couple of years.

Nanomedicine can be defined as the diagnosis, identification, monitoring, repair, construction and control of human biological systems at the molecular level using engineered nanodevices and nanostructures[30]. In short, particles in nanomedicine bridge the gap between the 'structure' and the biological 'function'[31]. Multidisciplinary functions of these particles can be divided into pharmacogenomics, gene therapy[32], DNA manipulation[33], drug delivery[34], nanodevices, nanotools and/or nanodiagnostics[31].

Selective subcellular delivery is more likely to have therapeutic benefits because the cytosolic delivery of drugs is generally affected by efflux mechanisms. However, entrapping the compound in a nanoparticle creates a barrier protecting the drug by acting as a drug/photosensitiser (PS) depot within the cell. Thus, nanotechnology can be used in certain therapies, establish sustained release drug profiles and protect therapeutic compounds within cells from efflux transporters such as multi-drug resistance proteins and P-glycoproteins which continuously reduce therapeutic drug concentrations[35].

NPs are being extensively investigated as targeted and localised drug delivery systems[34, 36-43]. Drug delivery using NPs is particularly promising due to the possibility of engineering NPs to control their fundamental properties such as drug release characteristics[44, 45], solubility or diffusibility. Further, in tumour targeting, NPs can be used in antigen-dependent (specific) or antigen independent (non-specific) mechanisms[19].

1.2.1 Nanoparticles

Nanoparticles (NPs) represent a relatively new trend in drug delivery. Large particles (>200 nm) are usually captured by macrophages. However, NPs below 200 nm are more likely to be eventually removed from the body by renal clearance. Having small particles can help to maintain higher circulating levels of the therapeutic agents once administered[11]. Drugs or sensors can be entrapped in the nanoparticle matrix, conjugated to the nanoparticle surface or covalently linked to the matrix. There are advantages to entrapping drugs/sensors in the core of porous NPs[24]. Primarily, the particle matrix acts as a barrier between the intracellular environment and potentially toxic dyes, while inhibiting interactions of the dye with circulating serum components which might alter its photophysical properties[46]. Surface conjugated NPs however retain many of the drawbacks of using free dyes.

1.2.2 Nanoparticles in Drug Delivery

NPs used in drug delivery should be 3-200 nm in size, ideally ~100 nm[36]. Most of the properties, *i.e.* the surface curvature of the NP, especially relevant to surface interactions[47] that make NPs attractive for novel applications are found when the NPs are around 100 nm. In targeting NPs to tumour tissue, provided they avoid sequestration by the reticuloendothelial system (RES), accumulation can occur in the tumour stroma as a result of the enhanced permeability and retention effect[48].

Particles synthesised to avoid the RES can lead to longer circulation times, resulting in greater potential to target the site of interest. Ideally, these NPs are ~100 nm in size, with a hydrophilic surface (to avoid clearance by fixed macrophages), this can be achieved by coating the particles with hydrophilic polymers that create a cloud of chains on the particle surface repelling plasma proteins[48]. This method creates a hydrophilic protective layer around the NPs that is able to repel the absorption of opsonin proteins *via* steric repulsion forces, thereby blocking and delaying the first step in the opsonisation process[4].

Depending on the method of preparation, drugs can either be physically entrapped in (encapsulated) or covalently bound to the NPs[31]. Some of the different structures of NPs used in drug delivery such as polymeric NPs, polymeric micelles, dendrimers and liposomes can be seen in Figure 1.2.

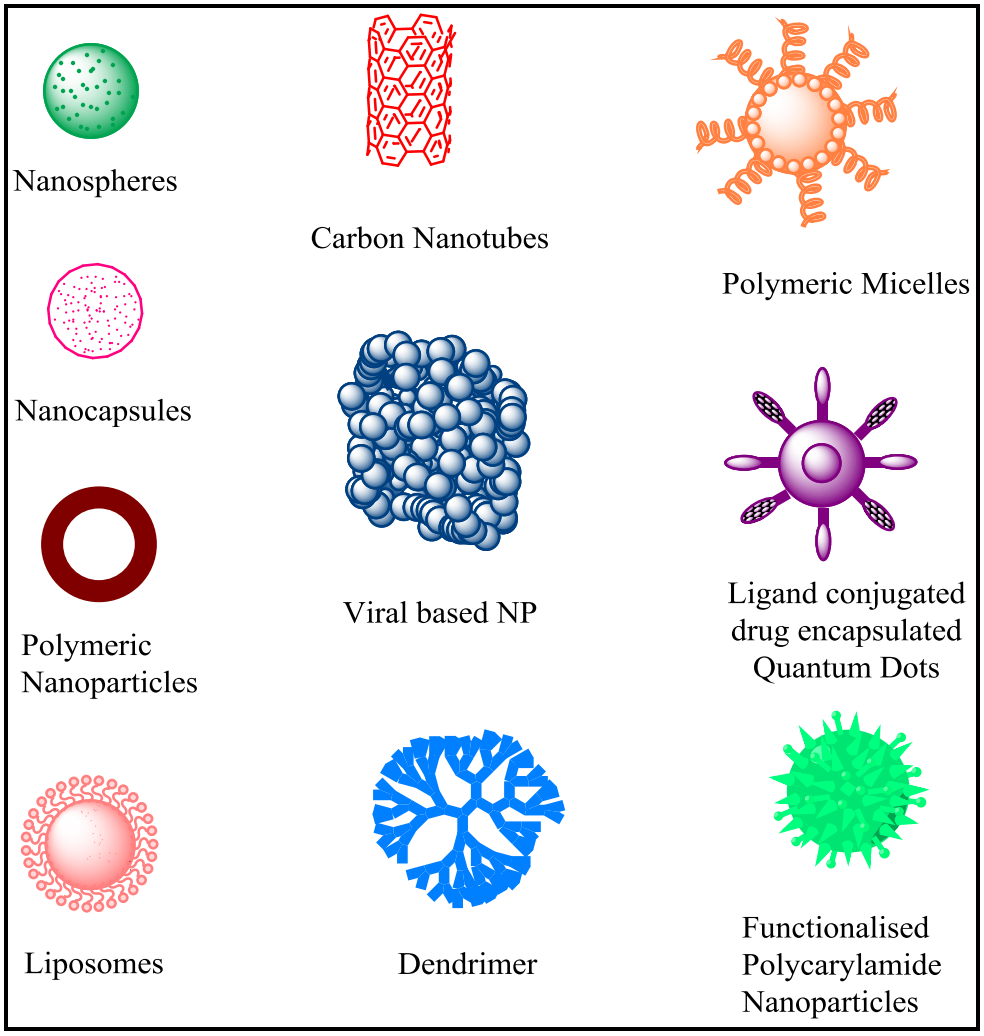

Figure 1.2: Schematic representation of polymer based drug carriers

(modified from reference[49])

Nanospheres have matrix type structures, where drugs may be absorbed at the sphere surface or encapsulated within the structure[50]. Nanocapsules consist of an inner liquid core surrounded by a polymeric membrane, with the drug confined to its cavity. Generally, the active compounds are dissolved in the inner core of the nanoparticle but may also be adsorbed onto the surface[49]. Drugs can be conjugated to or encapsulated within polymeric NPs[36]. Liposomes are layered lipid structures, generally of much greater size, compared

with micelles and present both polar and non-polar regions within their structures. Polymeric micelles are self-assembled block co-polymers, with an inner hydrophobic core (that can be assembled to include hydrophobic drugs), and in an aqueous solution can arrange to form an outer hydrophilic layer. Quantum dots are fluorescent nanocrystals that can be conjugated to a ligand[49]. Dendrimers are monodispersed symmetric macromolecules. These are synthesised with a large number of reactive end-groups surrounding a small internal molecule. Viral-based NPs in general are multivalent self-assembly protein cage structures. Carbon nanotubes are carbon cylinders composed of allotropes of carbon[36].

Drug encapsulating NPs are solid, nanosized (generally 3-200 nm), drug carriers that may or may not be biodegradable. They can be engineered to selectively deliver biologically active compounds to targeted tissues resulting in improved drug efficacy and low drug toxicity[51-53].

NPs can also be attached to other molecules that act as markers to detect the early stages of diseases[54]. As seen in Table 1.2, the unique properties of different nanoparticle materials make them appropriate for drug delivery[54].

Nanoparticle Material/Technique	Property
NPs (50-100 nm).	Penetrate easily through blood vessel pores.
Nano-capsules and nano-porous materials.	Avoid the host immune system and deliver the therapeutic vehicle to the target site.
Polymers.	High degree of engineering precision.
Enhanced particle adhesion.	Increase localised drug retention, slowing down drug release.
Ligand attached NPs.	High degree of engineering precision.

Table 1.2: Nanoparticle Properties

Further, there are cost benefits in using nanotechnology for drug delivery, including advanced performance characteristics of the product due to the enhanced delivery and effective patent protection[49].

1.2.3 Nanoparticle Synthesis

There are many methods and techniques described in the literature for nanoparticle synthesis[55-57]. The most common synthetic materials could be classified as pre-formed polymers, macromolecules and bio-based or inorganic materials[58-62]. Most commonly, NPs are synthesised by polymerisation reactions[63, 64]. This can be achieved either by emulsion or interfacial polymerisation. Emulsion polymerisation[65-69] involves a radical polymerisation reaction that is initiated within an emulsion, including a monomer, **Surf**ace **act**ive subst**ances** (surfactant) and two immiscible liquids (*i.e.* water and oil).

Emulsions are mixtures of two immiscible liquids such as oil and water, stabilised by an emulsifier. Emulsions do not form spontaneously. To form an emulsion, an energy input is required through a homogenizing process. Over time, the unstable phases convert to a stable state comprising the emulsion. The term microemulsion refers here to a system composed of non-polar phase (oil), water (containing monomers) and an amphiphilic compound. However, in the strictest sense, the phase rich in amphiphilic compound is a microemulsion. Depending on the size of the droplets emulsions can be classified as macroemulsions (droplet size 50–500 nm) or microemulsions (droplet size 5–50 mm). In relation to thermodynamics, this phase executes the condition of maximum mutual solubilisation of water and oil where the interfacial tension between aqueous phase and oil is at a minimum[70]. Surfactants can increase the kinetic stability of emulsions greatly so that, once formed, most often the emulsion does not change significantly over years of storage. Interfacial polymerisation[71-75] is a polymerisation reaction that occurs at or near to the interfacial boundary of the two immiscible solvents. Here, the monomers present in one of the solvents react with different monomers present in the other solvent. These

reactions are generally spontaneous. To stay within the scope of this review, the discussion will mainly focus on the emulsion polymerisation technique[65-69].

1.2.4 Emulsion Polymerisation

Emulsion polymerisation can be divided into two categories based on the phases used in the polymerisation method (*i*) organic phase and the (*ii*) aqueous phase[50].

The organic phase method is the more widely used method for nanoparticle preparation and is a radical polymerisation involving a monomer, surfactant and water (See Table 1.1, for the characteristics of the radical polymerisation method). These are combined in suitable ratios[76] to form emulsions, in which micelles of discrete dimensions are formed (Figure 1.3).

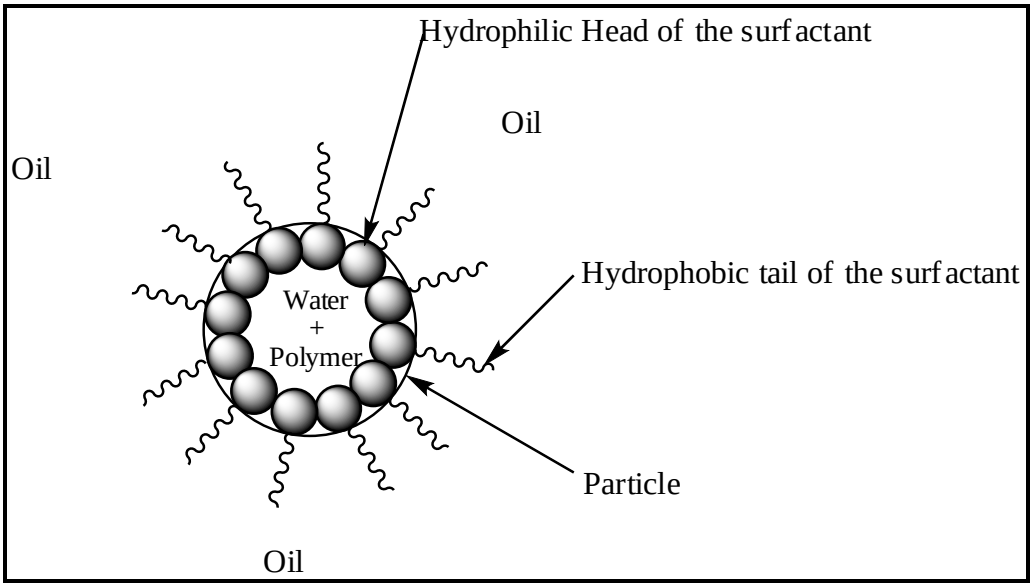

Figure 1.3: Schematic representation of a synthesised nanoparticle *via* microemulsion technique

Micelles are particles that form due to the spontaneous arrangement/migration of surfactant molecules in the microemulsion reactions. The addition of an initiator (*e.g.* ammonium persulphate) initiates the polymerisation process/reaction and forms porous solid particles of nanometre dimensions. Assemblies of surfactant molecules trap the particles formed in one phase, preventing any aggregation in the early stages of the polymerisation. Size and porosity can be controlled by varying the composition of the mixture used to form the micelles. The ability to control the pore size, charge of the nanoparticle, and the ability to entrap PSs within the nanoparticle core, makes this an attractive method for the preparation of NPs for delivery of photodynamic agents[50].

In the aqueous phase method, the monomer is dissolved in an aqueous solution without having to use emulsifiers and surfactants in the solution. The polymerisation may be initiated when the monomer collides with an introduced initiator molecule, which could either be an ion or a free radical. Alternatively, a monomer molecule may be transformed into an initiating radical by a high energy radiation, such as strong visible light, gamma radiation, or UV radiation, leading to radical polymerisation[50].

1.2.5 Potential of NPs to overcome drug resistance

In treating diseases, such as cancer or bacterial infection, drug resistance has emerged as a major obstacle limiting the efficacy of chemotherapeutic and anti-bacterial agents.

Among several mechanisms of drug resistance[77-81], P-glycoprotein mediates one of the best known and most extensively investigated[82]. P-glycoproteins (PGPs) are part of the efflux transporter family found in the gut, kidneys, brain and other organs. They act as a localised drug transport mechanism actively exporting drugs out of the cell. Recent studies[83] have suggested that NPs may be able to circumvent P-glycoprotein–mediated resistance.

One possible mechanism by which NPs may avoid recognition by the P-glycoprotein efflux pump is as a result of being enveloped in an endosome when entering the cell[84]. Ligand-targeting strategies involving NPs, especially those using receptor-targeting ligands, may have particular potential for overcoming drug resistance, as these ligands are generally internalised *via* receptor-mediated endocytosis. It has been suggested that transferrin-conjugated paclitaxel-loaded NPs[85], folate receptor–targeted NPs, and pH-sensitive polymeric micelles containing doxorubicin[86], all exhibit greater inhibitory activity against the drug-resistant breast cancer cell line (MCF-7 cells) compared with their non-targeted free drug counterparts.

1.2.6 Cellular uptake of NPs

The eukaryote cell membrane is an active semi-permeable lipid bilayer that segregates the intracellular environment (cytoplasm) of a cell from the extracellular environment (Figure 1.4). It regulates and coordinates the entry and exit of small and large molecules to and from the cell. Small molecules, such as sugars, ions and amino acids can pass through the plasma membrane *via* protein pumps or channels present in the membrane.

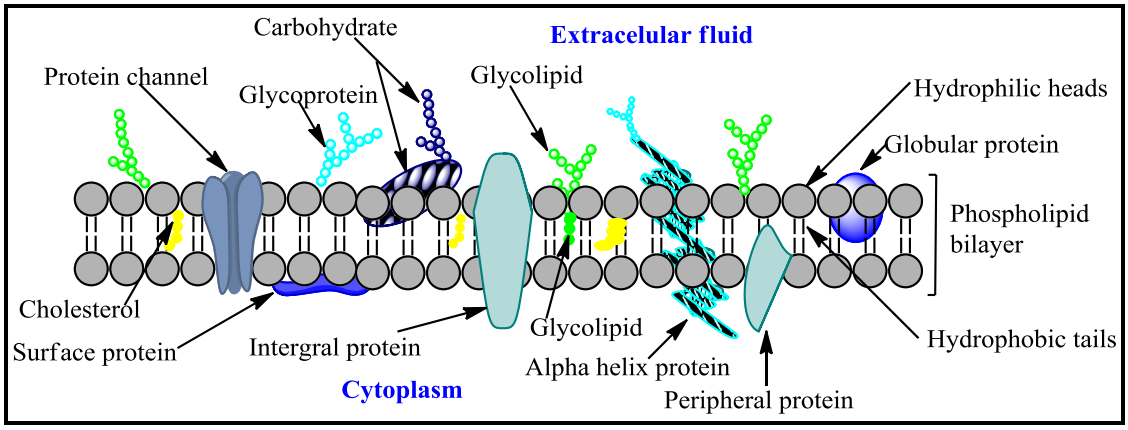

Figure 1.4: Schematic cell membrane model

Cells have evolved a variety of strategies to absorb material from the external environment. Predominantly for particles of nanometre size endocytosis is one such strategy[87-90]. Endocytosis is the process by which cells internalise material by engulfing it with their cell membrane. It regulates many processes that are essential to cells including nutrient uptake, receptor signalling, neurotransmission, mitosis and growth.

Endocytosis is one of the major pathways of nanoparticle cellular uptake[91-93] and this process is both concentration and time dependent.

Endocytosis can be categorised into three broad categories, depending on the size of the vesicle formed and the cellular machinery involved:

- Phagocytosis[94,95]: uptake of large particles
- Pinocytosis[95,96]: uptake of fluid and solutes
- Receptor-mediated endocytosis[97,98]: more specific active event where the cytoplasm membrane folds inward to form coated pits.

Uptake of NPs *via* endocytosis can occur through phagocytosis, fluid phase pinocytosis or receptor mediated endocytosis. NPs less than 200 nm are known to be imported to cells by pinocytosis while larger particles (>500 nm) are internalised through phagocytosis[99]. Panyam and Labhasetwar reported no phagocytotic activity with NPs approximately 100 nm in size[90].

Pinocytosis occurs in almost all cells[87], whereas, phagocytosis (Figure 1.5) is typically restricted to specialised mammalian cells[87] like macrophages[94], neutrophils[100] and monocytes[101]. Innes and Ogden in 1999[102] described the possibility of pinocytotic endocytosis taking place in oral epithelial cells with microspheres of 0.01 µm and 0.1 µm. They found no endocytosis taking place with 1.0 µm microspheres[99]. In 2009 Hu *et al*. confirmed these findings by reporting that colloidal particles of less than 0.2 µm can be imported into cells by pinocytosis whereas larger particles (0.2-0.5 µm) would be internalised *via* phagocytosis[99].

Pinocytosis (Figure 1.5) can be sub-classified into at least four fundamental mechanisms: macropinocytosis, clathrin-mediated endocytosis (CME), caveolae-mediated endocytosis

and clathrin and caveolae independent endocytosis. Macropinocytosis[103] represents an efficient route for non-selective endocytosis of solute macromolecules and is preferred for the uptake of smaller particles. The remaining three uptake mechanisms are differentiated depending on the sizes of vesicles formed in particle uptake. Approximately, the sizes are clathrin ~120 nm, caveolin ~60 nm and clathrin-caveolin ~90 nm.

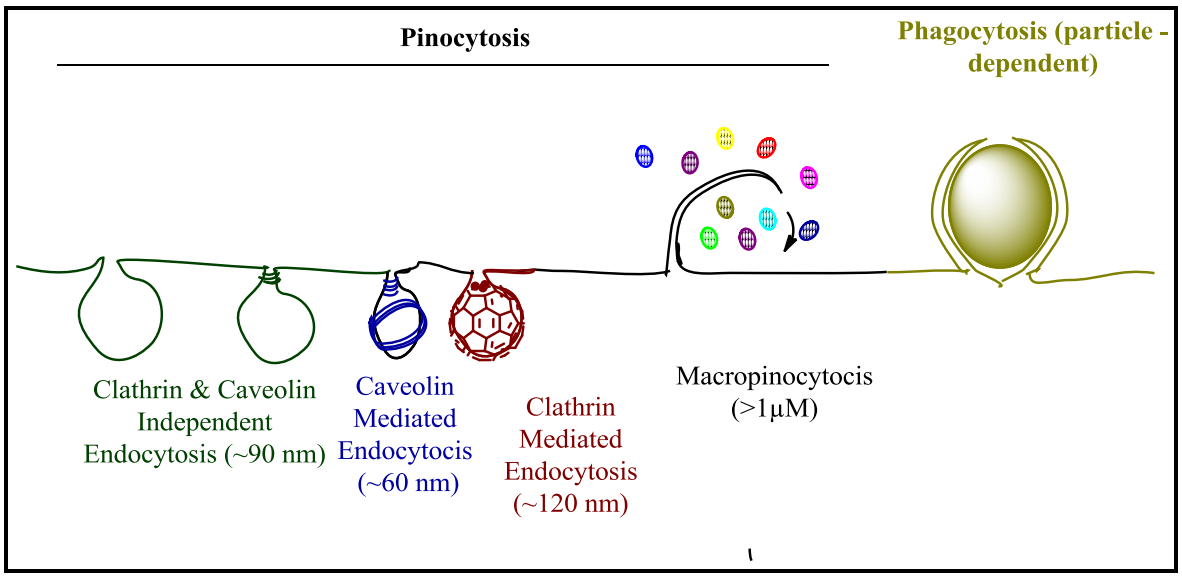

Figure 1.5: Multiple means of particle entry to mammalian cells (modified from reference[87])

Clathrin mediated endocytosis[104] occurs in all mammalian cells and is the most important mechanism for receptor mediated uptake. Caveolae can be found in endothelial cells, smooth muscle cells and adipocytes. In contrast to other mechanisms, caveolae endocytosis is interesting for nanoparticle delivery as the particles are neither trapped in endosomes nor degraded in lysosomes[105]. Technically, this makes the delivery of NPs to intracellular targets possible, with physical characteristics of the NPs resulting in delivery to the Golgi complex, endoplasmic reticulum or other sites by transcytosis. Transcytosis is a process by which various macromolecules are transported across the interior of a cell.

Clathrin and caveolae independent endocytosis is described only in few instances, *i.e.* recovery of neuron membrane proteins.

Receptor-mediated endocytosis is an active event where the cytoplasm membrane folds inward to form coated pits in protein or particle uptake. In the event of uptake, the particles are first locked into ligands or receptors in the cells plasma membrane prior to the engulfing event. Any particles entering the cells in this mechanism are frequently enveloped by endosomes. This bypasses the initiation of one of the main drug resistance mechanisms involving P-glycoprotein[106].

It has been established that NPs can be taken up by cells and they are an effective drug delivery method[107]. Depending on the size of the NPs, theoretically, all the mechanisms described above could feature in the cellular uptake of the particles. However, it is still unclear as to how endocytosis can be selectively targeted by NPs[18,87]. The mechanism of internalisation and intracellular localisation of NPs could be determined by the surface properties of NPs.

Exocytosis is the reverse process to endocytosis in eukaryotic cells[108]. Endocytosis and exocytosis are both dynamic and energy dependent processes[90]. At any point in time, the nanoparticle concentration within a cell results from the net difference between these two processes. The intracellular population consists of NPs that are recycling inside the cell, in the lysosomes or in the cytoplasm[90]. Jin *et al.* reported a comparison of internalisation (endocytotic uptake), exocytosis rates and net accumulation of carbon nanotubes over time (8000 s) compiled from single particle tracking and found that the net accumulation fluctuates with time[109].

1.3 Photodynamic Therapy (PDT)

Life on earth, directly or ultimately, depends on light. The energy of the sun promotes processes that maintain human existence through photosynthesis. In medicine, PDT represents a unique combination of light, a photosensitising drug and oxygen to treat cancer and bacterial infections. The following discussion highlights the properties of light, describes the photophysics, photochemistry and photobiology of PDT, and the various PSs used in PDT.

Conventional therapies such as surgery, chemotherapy and radiation therapy involve a subtle balance between removing and/or destroying diseased tissue and sparing the surrounded healthy tissue from destruction. Due to the indiscriminate cytotoxic properties of the latter two of these treatments towards healthy and diseased tissue, serious side effects may result. Hence, it is essential to focus the development of new treatments on selectively targeting the diseased tissue.

The phenomenon of photodynamic reactions was first discovered by Raab in 1900 while studying the effects of light and dyes on paramecia[110]. Paramecia are a group of unicellular ciliate protozoa. In his study, the paramecia that were exposed to sunlight and an acridine dye were killed, while the ones which were in the dark survived. This was an oxygen rich biological system, containing a sensitiser which absorbed light causing a photochemical reaction. This effect was given the name *'photodynamisagerscheinung'* or *'photodynamic reaction'* by Tappeiner and Jodlebauer in 1904 differentiating it from the photochemical reactions that occur without involving oxygen *e.g.* the use of ultra violet light to treat psoriasis[111]. Since the origin of PDT, many researchers have been involved in its development. Excellent reviews from McCaughan in 1999[111], MacDonald and

Dougherty in 2001[112] and Josefsen and Boyle in 2008[113] highlight the development of PDT.

PDT requires the combination of light and photosensitising agents in an oxygen-rich environment. The technique relies upon selective accumulation of the PS in target tissue followed by activation with light[114-116].

1.3.1 The Nature of Light

Light is a form of radiant energy. All radiant energy exists as electromagnetic waves. Light exhibits wave-like and particle-like properties. Light can thus be described by wave-like properties: light undergoes reflection, refraction, interference, diffraction and polarisation. However, light can also be described by its particle-like behaviour, due to its photoelectric effect (the phenomenon in which electrons are emitted from matter after the absorption of energy from electromagnetic radiation). Light is composed of small packets of energy called quanta or photons travelling in periodic waves.

Wavelength is inversely proportional to the frequency (the number of waves that pass a certain point in a second). Once the electromagnetic radiation is arranged in the order of increasing wavelength, it is called the electromagnetic spectrum (EMS). Visible light is the radiant energy to which the human (mammalian) eye responds and covers the region, approximately from 360-780 nm in the EMS. In fact, since the sensitivity of the human/mammalian eye to radiation is very low at the two extremes, the range visible to mammals is considered to be 380-720 nm[117]. Colour is ascribed to and associated with different/specific wavelengths.

Colour is said to require the presence of three factors: a source of illumination, an object for the light to interact with and the human/mammalian eye to observe[117]. Dean B. Judd, one of the founders of colour science, defined colour as,

"that aspect of the appearance of objects and lights which depends upon the spectral composition of the radiant energy reaching the retina of the eye and upon its temporal and spatial distribution thereon"[118].

When light strikes any object, including cells, it can undergo one or more of the following processes: 1. reflection, 2. transmission, 3. scattering and 4. absorption. Light needs to first be absorbed for any photochemical/photobiological reaction to occur (as the source of energy)[111].

In the context of PDT, PSs are compounds which absorb light of a specific wavelength and utilise this energy to generate (*via* the interaction with molecular oxygen) highly cytotoxic singlet oxygen. Further, in PDT, the measurement of the absorption of light by the PS is called its 'absorption coefficient' for that wavelength. This phenomenon changes with their environment, *i.e.* tissue and wavelength[111].

The therapeutic outcome of PDT is related to the activation wavelength of the PS, which in turn is related to the depth of light penetration in human tissue. The optimal spectral window for biological tissue penetration of light lies in the red to near infrared part of electromagnetic spectrum (Figure 1.6), approximately 600 to 800 nm[119], implying that photodynamic sensitisers must have a strong absorption band in this region to be effective[120].

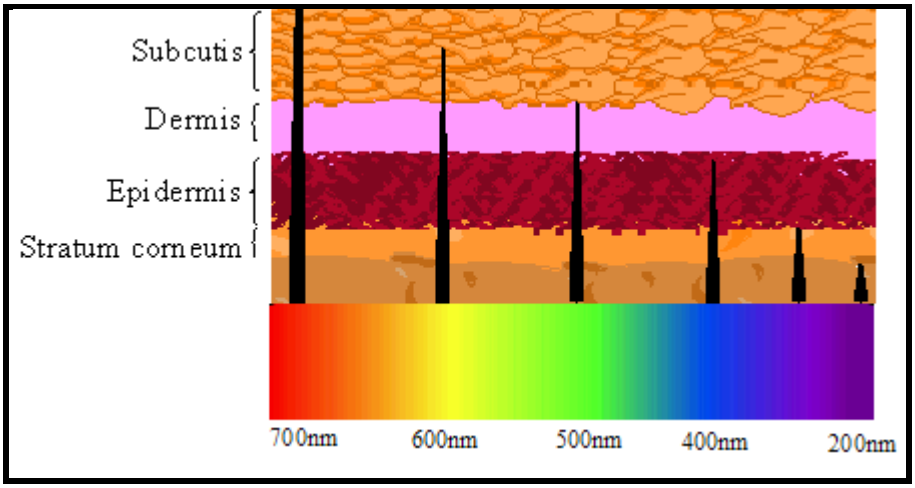

Figure 1.6: Schematic diagram of the wavelength versus skin penetration (modified from[121])

1.3.2 Photophysical Mechanisms in PDT

Absorption of energy by chromophores occurs between the electronic energy levels of molecular orbitals. The various energy levels involved in the absorption and emission of light are classically represented by a Jablonski energy diagram.

PSs absorb light energy and therefore increase the energy of the PS's electrons from the ground state to the excited state. PSs in the ground state ($^1S_0$) possess electrons in a singlet state (no net spin, S=1). But once the light is absorbed by the sensitiser, the electron becomes 'excited' ($^1S^*$), and will remain in a singlet state unless one of the spin-paired electrons can undergo spin inversion, and *via* intersystem crossing (ISC), resulting in a spin aligned pair of electrons (Figure 1.7).

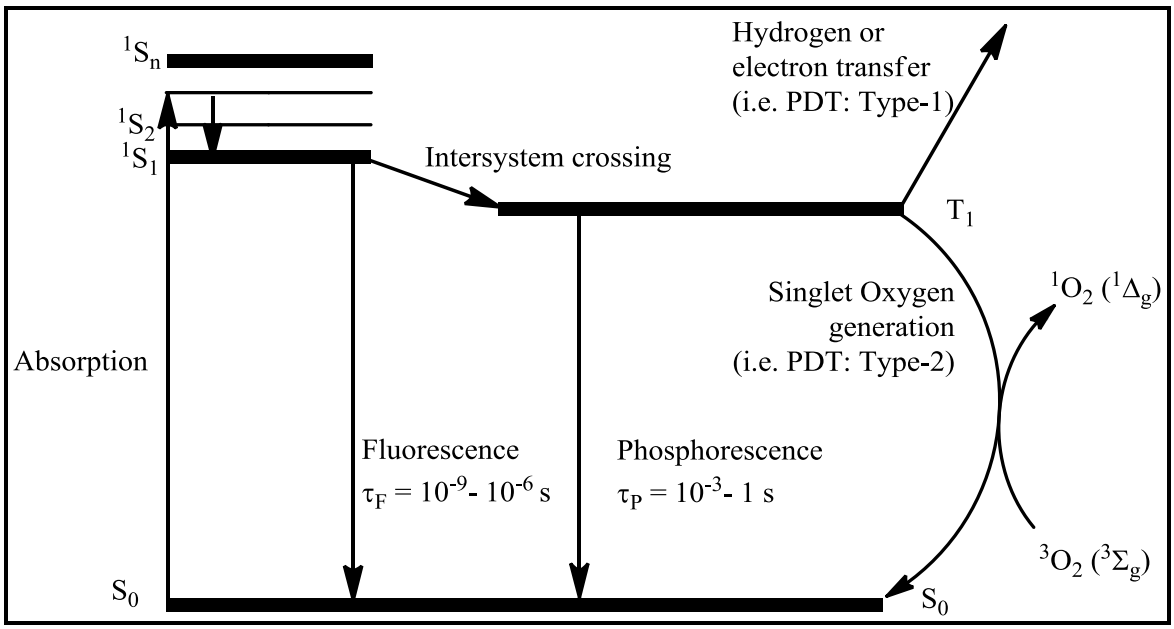

Figure 1.7: A Modified Jablonski Diagram

The PS is now in its triplet state (T) (net spin, S=3)[88] and can react chemically in two ways: by Type I and Type II (Figure 1.7) pathways.

Type-I reaction: the PS reacts directly with a substrate molecule resulting in hydrogen atom abstraction or electron transfer, both generating a reactive, cytotoxic free radical leading to oxidative damage[114,122].

Type-II reaction: in a biological system where oxygen is present, a PS transfers its energy to the stable triplet state of molecular oxygen. Gaining the energy provided from the PS, one of the oxygen's unpaired electrons undergoes spin inversion, rendering the net electronic spin zero[111, 114, 123]. Thus, oxygen is now in its extremely reactive singlet excited state, referred to as singlet molecular oxygen. The type-II mechanism and the cytotoxicity of singlet oxygen is considered predominant in PDT[124], although changes to oxygen levels in the microenvironment of diseased tissue may affect a greater dependence on type-I.

Photons can be absorbed repeatedly by PSs after it has returned to the ground state and the above processes can continue until the PS degrades (photobleaching)[111]. Once the PS is excited, excess energy can be lost *via* a number of pathways, including radiative and non-radiative decay. Fluorescence results directly from radiative decay of a singlet excited state, while phosphorescence is the result of radiative decay of the triplet excited state. Since a change of spin is required, intersystem crossing and phosphorescence are quantum mechanically forbidden processes (Spin Selection Rule). The lifetime of fluorescence (τ_F) is in the range 10^{-9}- 10^{-6} s, whereas the life time of phosphorescence (τ_P) is in the range 10^{-3}- 1 s. Since phosphorescence allows more time for collision of the singlet oxygen with substrates in its environment, this longer triplet state life time (τ_P) is an important parameter in PDT.

1.3.3 Two-photon Excitation (TPE)

TPE is simultaneous absorption of two photons by a PS usually in the near-infrared region of the electromagnetic spectrum. TPE achieves the same effect as one-photon excitation (OPE) at half the wavelength, promoting a molecule into its singlet excited state, provided that the combined energy of the two photons matches the energy of a single photon that is required to excite the molecule using light of double the wavelength (Figure 1.8). Practically, this means that optimal excitation of PSs can be achieved by deeply penetrating light, thus maximising the clinical PDT effect.

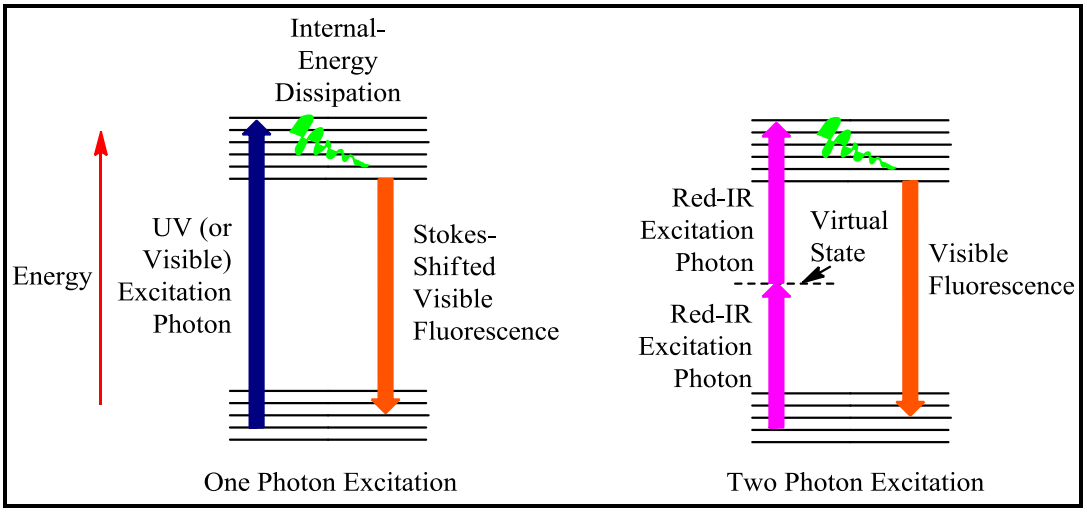

Figure 1.8: Schematic diagram of photon excitation of a molecule

1.3.4 Beer-Lambert Law (Beer's law)

The law states that absorbance (**A**) is directly proportional to the path length (**l**), of the sample and its molar concentration (**c**):

$$A = \varepsilon cl$$

ε - the molar extinction coefficient (with dimensions of $dm^3.mol^{-1}cm^{-1}$) of the solute

c - the molar concentration (in $moledm^{-3}$)

l - the path length, is measured in centimeters

The Beer-Lambert law is particularly important for determining the concentration of solutions from absorbance measurements.

1.3.5 Singlet Oxygen

The first excited state of oxygen, which is commonly known as singlet oxygen, O_2 ($^1\Delta_g$) is an extremely reactive and highly cytotoxic species. It is responsible for many photochemical processes such as photodegradation of dyes and photocarcinogenesis. Reactions of singlet oxygen are associated with applications in several fields, including organic synthesis and bleaching processes. It is also the main damaging element in PDT[125, 126]. Both type-I and type-II photochemical reactions occur in parallel[127]. The concentration of oxygen present and the PS used has a predominant effect on the ratio[128]. However, for most photosensitisers employed in PDT, the type-II photochemical reaction represents the dominant process[124].

A second excited singlet state, O_2 ($^1\Sigma_g^+$), can be formed in competition with the first excited state, O_2 ($^1\Delta_g$). In solution, this O_2 ($^1\Sigma_g^+$) deactivates very rapidly to the longer lived O_2 ($^1\Delta_g$) species[129]. Singlet oxygen reacts with a variety of electron rich bio-molecules, resulting in oxidised products, such as hydroperoxides and endoperoxides[122]. Singlet oxygen can also generate other reactive oxygen species (ROS), such as superoxide radicals causing damage to the cell's DNA, lysosomes, mitochondria or membranes, which could result in cell apoptosis (programmed cell death) or necrosis (accidental cell death)[130].

Singlet oxygen can be detected directly through its extremely weak emission at 1270 nm. However, this is not visible to the naked eye. Nonetheless, at high singlet oxygen concentrations, dimolecular light emission (simultaneous emission from two singlet oxygen molecules upon collision) can be observed as a red glow at 634 nm[131].

Oxygen exhibits a few rather unusual properties with respect to magnetic behaviour, spectroscopy, energy-transfer processes and chemical reactivity. These peculiarities are a result of the open-shell electronic structure of the molecule Figure 1.10[126]. In the isolated (molecular) oxygen molecule, the transition to form singlet oxygen is strictly forbidden by the Spin Selection Rules. In other words, direct excitation of ground state oxygen by light to form singlet oxygen is very unlikely.

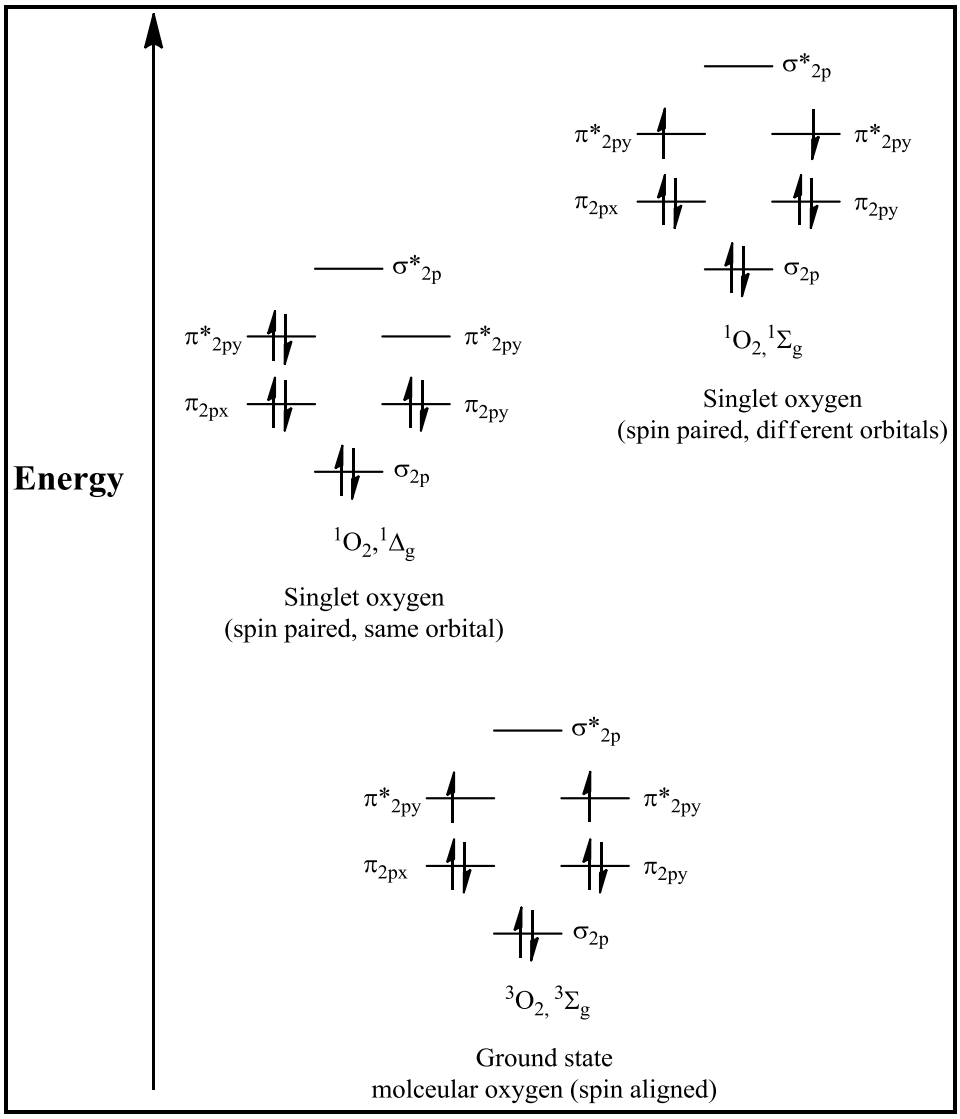

Figure 1.9: Molecular orbital diagram of oxygen (reproduced with permission from[28]).

1.3.6 Photosensitisers

Photosensitisers (PSs), in the context of PDT, are compounds which absorb light of a specific wavelength and utilise this energy, in combination with molecular oxygen ($^3O_2$), to generate highly cytotoxic singlet oxygen. PSs are generally, aromatic structures that are efficient at undergoing intersystem crossing and forming long-lived triplet excited states[132]. The selective accumulation of a drug in diseased tissue is the key requirement for photodynamic sensitisers[114]. An ideal PS[114, 119] would have the properties listed in Table 1.3.

Chemical Property	**Biological Reason for Property**
Chemically pure and of known constant composition.	To effectively test, understand and formulate the PS.
Minimal or no dark toxicity.	To minimise damage to healthy tissue.
Appropriate balance between lipophilic/hydrophilic characters.	Rapid excretion from the body. Target localisation to minimise the damage to neighbouring healthy tissue.
High singlet oxygen quantum yield (Φ).	To enable the efficient generation of singlet oxygen.
A high molar absorbance at longer wavelengths.	Longer wavelengths of light penetrate deeper into tissue (see Figure 1.6).
Easy to dissolve and stable in aqueous media at physiological pH.	To avoid aggregation of the PS and aid in drug administration.
The pharmacokinetic elimination from the patient should be rapid *i.e.* less than one day.	To avoid the necessity for post-treatment protection from light exposure and prolonged skin photosensitivity.

Table 1.3: Properties of an ideal PS

Some common basic structures of PSs are represented in Figure 1.11. The majority of the PSs used in PDT are based on cyclic tetrapyrroles. However, the existence of efficient PSs such as methylene blue (MB) and indocyanine green suggest that it is not a prerequisite that efficient PDT agents possess similarities to naturally occurring porphyrins.

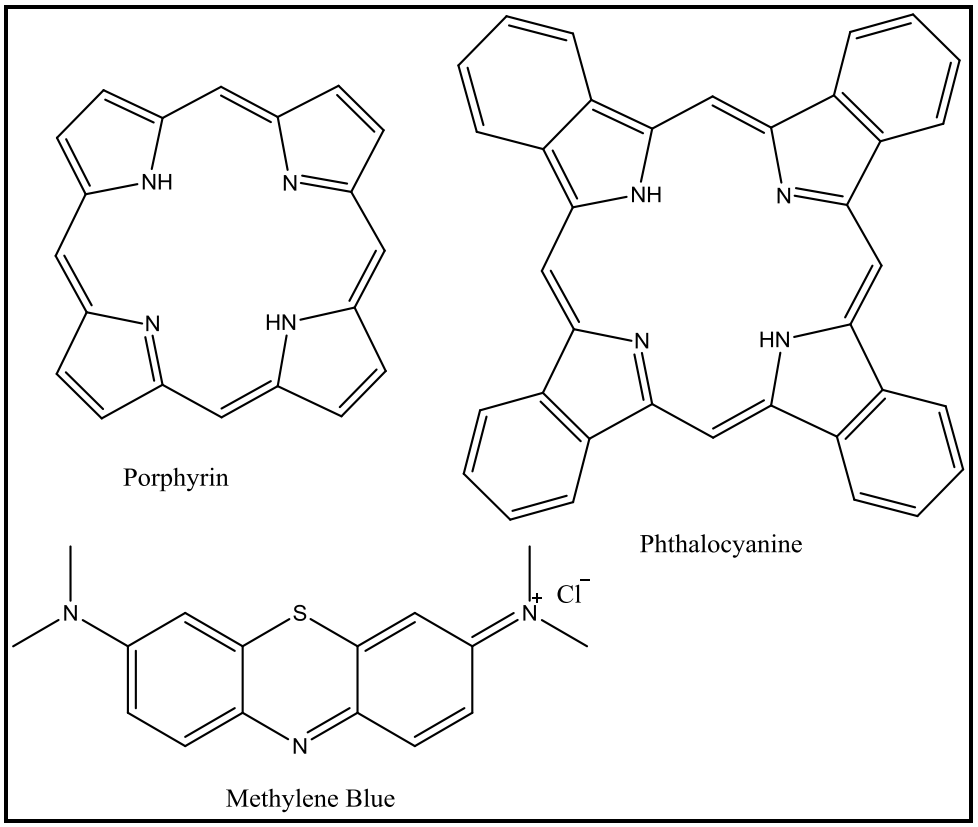

Figure 1.10: Some basic structures of PSs

Some photodynamic sensitisers cause cell death directly, while others cause cell death *via* vascular shutdown, thus depriving the cell of nutrients and oxygen. The exact means of tumour destruction depends on the specific PS, light dose used and localised oxygen concentration, which can vary depending on existing physiological conditions [114, 123].

Although there are numerous naturally occurring and synthetic agents which can act as PSs, very few have progressed to the commercial market, and hence, into clinical practice. Each PS has its own specific characteristics that can benefit patients but none of the PSs are totally acceptable. Below is a summary of few common drawbacks of clinically available PSs:

- Hydrophobicity
- Difficulty of synthesis
- Suboptimal pharamacokinetic half life
- Lack of specificity
- Normal tissue uptake
- Dark toxicity
- Suboptimal wavelength for activation

An excellent review by Konan *et al.* summarises the current state and the potential of PS delivery in PDT[133].

1.3.7 Cancer

It is estimated that about one in three people now living will develop some type of cancer. Cancer is an abnormal growth of cells caused by multiple changes in gene expression leading to deregulated balance of cell proliferation and cell death and ultimately evolving into a population of cells that can invade tissues and metastasize to distant sites causing significant morbidity and if untreated death of the host. One of the main problems in treating cancer is the inability to selectively target tumour cells and tissues[134] without resulting in severe side effects to healthy tissues and organs. However, in treating this complex multiple abnormal cell growth, tumour vasculature has been identified as a potential target since the 1970's[52].

In healthy tissue, the smooth muscle layer plays a significant role in responding properly to vascular mediators such as adrenalin and acetylcholine calcium. Autonomic nervous system and vascular mediators *via* receptors on smooth muscle cells generally control the muscle tone. Muscular tension surrounding the vessel walls achieving a constant blood flow, volume and blood pressure maintains the vascular tone. However, this refined system does not function in tumour vasculature. There is a highly abnormal transport dynamic across tumour capillaries. Further, significantly enhanced or almost unrestricted leakages of plasma proteins from the luminal side of the wide endothelial gap openings with large pore sizes are apparent in these tissues. Frequent signs of tumour tissue are blood vessels that are irregular in shape, leaky, defective, dilated, abnormal or missing perivascular cells, basement membrane, deficiency of smooth muscle layer in the vascular wall, vessels with fairly wide lumen, lack of functional lymphatics and lymphatic drainage. Angiogenesis supports the abnormal tumour growth and due to over expression of the vascular permeability factor/vascular endothelial growth factor gene, enhanced permeability and

retention (EPR) effect is apparent in all solid tumours. Hence, passive targeting should be appropriate to treat most solid tumours. Active targeting has the potential to selectively eradicate the tumour cells through specific binding of targeting moieties linked to a drug vehicle with tumour-derived specific markers. However, the drug needs to be first extravasated, as the tumour cells are generally located outside of microvasculatures[135]. Due to the deteriorated lymphatic system, the concentration of any introduced macromolecules/lipids would remain high for longer periods; the rate of accumulation of substances in tumour tissue is inversely proportional to their clearance rate. Thus, to conclude the EPR effect entails not only the passive delivery but also prolonged retention of macromolecular drugs over weeks or even months[134].

1.3.8 PDT for Cancer

PDT tumour destruction can be caused mainly by combination of the following three mechanisms. However for long term tumour control, a combination of all three would be suitable[136]:

1. Direct tumour destruction

- ROS that are generated by PDT can kill tumour cells directly[137]. However, obtaining complete tumour eradication is not always possible due to (*a*) non-homogeneous distribution of the PS in the tumour and (*b*) shortage of available oxygen in tumour.

2. Tumor vasculature shutdown

- The viability of the tumour tissue depends on the nutrients received *via* the blood vessels and abnormally enhanced neovascularisation is the characteristic of tumor progression. In recent years, the focus on the tumor vascular shutdown has led to two novel therapeutic advancements, vascular targeting and anti-angiogenesis.

3. Anti-tumor immune response

- The formation and maintenance of blood vessels depend on growth factors produced by tumour or host cells. By activating an immune response against tumour cells, the intensity and nature in different tumour and normal cell immune response could contribute to PDT selectivity[136].

1.4 NPs as delivery agents for PDT

The main objective in the development of nanotechnology in PDT is to obtain targeted and efficient delivery of the appropriate levels of therapeutic or diagnostic agents for improved therapeutic efficacy, with reduced side effects to the patient. Different types of NPs, their recent developments, fundamental limitations and potential for improvement are reported in recent reviews[138-145].

1.4.1 Silica NPs

Control of mesoscopic order, pore dimensions in the (macro) molecular size range, pore volume and surface area, morphology and selective surface functionality including attachment of any moiety against tumour cells are all possible with mesoporous silica NPs (MSNs). This robust, biodegradable ceramic matrix also has the potential to incorporate drugs, proteins, imaging agents and PSs. Brevet *et al.* designed a functionalised MSN by covalently anchoring a PS (porphyrin) to the surface of the NP and targeting cancer cells with mannose attached to the surface[146]. Through mannose dependent endocytosis and control experiments with non-functionalised NPs, they proved that these MSNs presented a much higher photodynamic effect in human breast adenocarcinoma (MDA-MB-231) cells. Advances of MSNs in biomedical applications, with a special focus on cancer therapy and diagnostics were reviewed in detail recently[147].

Hydrophobicity, charge and the size of PSs play a significant role in nanoparticle encapsulation. Gupta *et al.* studied this relationship recently using organically modified silica NPs (ORMOSIL)[148]. They did some comparative studies on the above factors,

photophysical characteristics and release kinetics to determine the possibility of using ORMOSIL NPs in PDT.

PS encapsulated silica NPs have also been reported to excel in *in vitro* cell kill[149]. Liu *et al.* recently published a good review outlining few specific functionalised silica NPs as drug/gene delivery systems that have been applied in human disease therapy or detection (molecular and cellular imaging)[150].

1.4.2 Magnetic NPs

Magnetic NPs in PDT have an exclusive advantage due to the dual functionality of the system *i.e.* simultaneous magnetic resonance (MR) detection and fluorescence imaging. Photosensitisers (i.e. Chlorin e6) can be covalently anchored on to the surface of a magnetic NP to enable near infrared fluorescence imaging, MRI and PDT in a single species[151]. Also, a recent study by Wang *et al.* reported the development of a multifunctional magnetic NP system with dual-imaging (MR and optical) capabilities (superparamagnetic magnetite NPs and fluorescent dyes were co-encapsulated inside non-porous silica NPs), the PS (tetra-substituted carboxyl aluminium phthalocyanine) was then covalently linked to the mesoporous silica shell. The surface was further modified with folic acid to enhance the delivery of PSs to cancer cells that over-express the folate receptor, also decreasing toxicity to the surrounding normal tissues[152].

Magnetic chitosan NPs tailored as a drug delivery system for PS are reported to provide excellent biocompatibility, biodegradability, low toxicity and water solubility without

compromising their magnetic targeting properties/abilities[153, 154]. They can be used in MRI monitored PDT, producing excellent photodynamic efficacy both *in vitro* and *in vivo*.

1.4.3 Gold NPs

Gold NPs possess unique size-dependent physicochemical and optical properties that make them ideal for transporting small molecules as well as biomacromolecules to diseased cells/tissues[155].

Russell *et al.* investigated a gold nanoparticle PS delivery system, where a thiol moiety was used to link the gold nanoparticle to a phthalocyanine, which enhanced the singlet oxygen quantum yield (Φ) by 50% as compared with the free PS[156]. This increase is assumed to be the result of the presence of the phase transfer agent (tetraoctylammonium bromide; TOAB), used to coat the particles, which increases the triplet energy transfer to molecular oxygen. Recently some excellent results were reported by the same group, with a similar nanoparticle system, but modified with PEG units and an anti-HER2 antibody[157]. This study confirmed the ability to generate high levels of singlet oxygen while specifically targeting breast cancer cells.

Gold NPs can also be used as a biocompatible delivery vehicle to transport 5-aminolevulinic (5-ALA) acid for selective and efficient PDT[158]. In this study, a 50% increase in cytotoxicity towards tumour cells, relative to 5-ALA alone, was reported along with selective destruction of tumour cells using 5-ALA-conjugated NPs in co-culture with dermal fibroblasts.

Another gold NP – hydrophobic phthalocyanine delivery study reported the passive accumulation of NPs using EPR effect, delivery, pharmacokinetics and excretion dynamics *in vivo*[159]. They carried out a series a quantitative chemical analysis to show that gold NPs themselves did not enter the cells; however the adsorbed phthalocyanine was released and diffused into hydrophobic areas within tissues (cellular membrane). According to this study, the EPR effect was the driving force to accumulate the NP conjugates. While the drug (phthalocyanine) localised essentially in the tumour, NPs kept circulating in the body and had their own bio-distribution profile until excretion.

Recently, a gold nanosystem study was reported[160] with two porphyrin-brucine quaternary ammonium salts, and it was observed that the gold nanoparticle-bound conjugates were less effective than unbound conjugates in killing cells in *in vitro* studies. However, with the basaloid squamous cell carcinoma PE/CA-PJ34 cell line, the same system was reported to be more effective in reducing tumour size *in vivo*.

While there have been many developments in the area of gold NPs in recent years as cancer therapy and diagnostic agents, there are few challenges (biodistribution, pharmacokinetics and possible toxicity) that need overcoming to improve gold NPs as a drug delivery system[155].

1.4.1 Polyacrylamide NPs

Polyacrylamide NPs are synthesised through microemulsion polymerisation techniques and have been engineered for the intracellular delivery of sensors[16, 17, 23, 27, 161] drugs and PSs[28, 162, 163]. Some optimistic *in vivo* and *in vitro* studies have been reported recently with regard to NP distribution in cells[163] and tissue, pharmacokinetics and elimination of the NPs[164].

The PS encapsulated NP matrix has the potential to prevent the PSs from interacting or degrading in the physiological conditions *i.e.* methylene blue (MB) can be reduced to an inactive form by plasma enzymes and thus is not approved for systemic delivery. However, MB encapsulated in a polyacrylamide matrix can be used in intravenous applications due to the barrier between the PS and the enzymes[46]. By conjugating the dye with a monomer during the microemulsion polymerisation process it was also reported that there was a large increase in the loading of MB per nanoparticle and minimisation of dye leaching, which resulted in some excellent PDT effects[165]. Another interesting study was reported from the same group where MB was covalently loaded to polyacrylamide NPs while protecting the MB from the effects from the enzymes in the biological environment and leaching[166].

Multifunctional polyacrylamide NPs with targeting moieties *i.e.* Human breast cancer (MDA-435) cells using Photofrin® and iron oxide encapsulated NPs for detection using MRI and treatment of cancer using PDT[167] have shown some excellent prospects.

1.4.2 Quantum Dots

Quantum dots offer great promise as an emerging material in a variety of applications in PDT. The key benefit of quantum dots over molecular PSs is their tunable optical properties and surface chemistries. Targeting and imaging using semi-conductor quantum dots[168], generation of a photodynamic effect and of folic acid-conjugated QDs for targeted PDT[169] have been reported. Bakalova *et al.* demonstrated that quantum dot anti-CD antibody conjugates sensitised leukaemia cells to UV irradiation and promoted the effect of the classical PS, sulfonated aluminum phthalocyanine[170]. QDs could be used to sensitise the PS through a fluorescence resonance energy transfer (FRET) mechanism, or interact directly with $^3O_2$ *via* a triplet energy-transfer process (TET) in PDT[171].

An excellent review by Samia *et al.* assess the potential of using quantum dots and quantum dot conjugates as PSs for PDT while giving the recent developments in the preparation and photophysical characterisation of quantum dot energy transfer processes up until 2006[171]. Further, an interesting review by Yaghini *et al.* summarised the potential of QDs for photosensitisation in PDT compared with, and in combination with, conventional photosensitising organic dyes[172].

Ionisation radiation (X-rays and gamma rays) may be another novel approach to treat tumours in internal organs that needs a deeper penetration of light. Although less safe than visible light, this may be used in quantum dots and NPs to yield electrons and radicals in PDT[142].

1.5 Photodynamic Antimicrobial Chemotherapy (PACT)

1.5.1 Bacteria

Bacterial cells are extremely small (1-2 μm^3) and possess different shapes including coccus (spherical), bacillus (rod-like), spirillum (spiral) and filamentous. Bacteria fall into two categories, Gram-positive (*e.g. Staphylococcus, Streptococcus, Enterococcus*) and Gram-negative (*e.g. Escherichia coli* and *Pseudomonas auroginosa*).

Surrounding the cytoplasmic membrane, a rigid structure of peptidoglycan gives the bacteria its shape. Peptidoglycan is a polymer of interlocking chains of identical monomers connected by interpeptide bridges. All bacteria cells are similar from the peptidoglycan inwards. But, depending on how the peptidoglycan cell wall is structured, bacteria can be divided into two major classes: Gram-positive (Gram +) and Gram-negative (Gram -) (Figure 1.11).

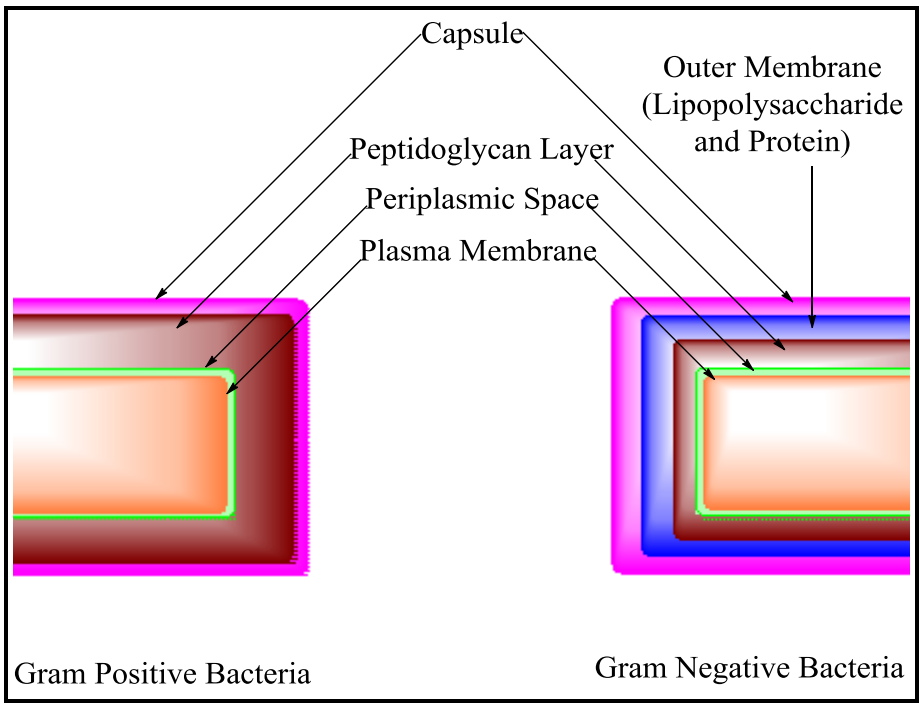

Figure 1.11: Schematic comparison of the thickness of peptidoglycan cell walls of Gram-positive and negative bacteria

In Gram-positive bacteria, the outermost membrane is made with peptidoglycan which makes up as much as 90% of the thick, compact cell wall, whereas in Gram-negative bacteria, the cell wall is more chemically complex, thinner and less compact. In Gram-negative bacteria, peptidoglycan makes up only 5–20% of the cell wall, and lies between the plasma membrane and an outer membrane. This outer membrane is similar in composition to the plasma membrane, but is less permeable and composed of lipopolysaccharides (LPS)[173]. In a Gram-staining test, Gram-positive bacteria retain the blue-violet colour in the test (crystal violet dye) contrasting to Gram-negative bacteria, which does not retain the colour.

1.5.2 Existing Treatments of Bacterial Infections

Chronic bacterial infection of wounds and ulcers is a major problem which costs the National Health Service (NHS) millions of pounds annually to treat. Orenstein *et al*. (1998)[174] have identified the following complications associated with surface infections (burn wounds). Direct heat on skin makes the resulting wound susceptible to infection *i.e.* the denatured protein present in the infected site becomes rich media for bacterial growth and proliferation. Additionally, thermal thrombosis (an obstruction formed inside a blood vessel disturbing the blood flow) prevents the delivery of cellular components of the host defence system and systemic antibiotics to the microorganisms in the infected site. The proliferating organisms in the infected site may penetrate the dead tissue by moving along hair follicles to reach the interface between non-viable and viable tissue, which will result in infection of the viable tissue underneath.

Generally, bacterial diseases are treated with antibiotics and antiseptics. These drugs, when incorporated into delivery vehicles (for example, creams and ointments), can be applied to the skin for local effect.

But there are problems associated with these treatments including the development of resistance towards drugs in the targeted organisms and disruption of the endogenous microflora[175]. Non-targeted drug delivery could also result in collateral damage to the nearby healthy cells, metabolism and excretion of drugs before reaching their target, difficulties in maintaining an appropriate drug concentration at the target site and cell permeability issues[51, 176].

1.5.3 Bacterial Antibiotic Resistance

A combination of rapid replication and mutation allows the microbial population to develop into different strains and it is this process that has led to the rise in antibiotic resistant strains of bacteria such as methicillin resistant *Stapholococus aureus* (MRSA).

Gram-positive bacteria lack the outer membrane, which plays a vital role in the resistance to antibiotics that is displayed by Gram-negative bacteria. Thus, Gram-positive bacteria are more susceptible to photodynamic inactivation, while Gram-negative bacteria are resistant to many PSs[177, 178].

Cationic PSs have been shown to be active against both Gram-positive and Gram-negative bacteria, while in general, neutral or anionic PS molecules only inactivate Gram-positive bacteria. Cationic PSs interact at sites on the outer membrane surface at which divalent cations cross bridge adjacent lipopolysaccharide molecules causing a destabilisation of the outer membrane and allowing ingress of the PS (self-promoted uptake). Neutral or anionic PS molecules bind only to the outer membrane of Gram-negative bacteria and thus, do not inactivate them after illumination[179].

1.5.4 Photodynamic Antimicrobial Chemotherapy (PACT)

PACT has the potential for treating bacterial infections by exploiting the combination of the PS and the appropriate wavelength of light and molecular oxygen, to result in excited, toxic oxygen which damages the bacteria[179, 180]. In the last decade, different approaches to combine nanotechnology with PACT have been investigated: NPs can either be used to improve the inactivation kinetics or to improve the delivery of PSs to the bacteria[181]. Photodynamic inactivation of bacteria is carried out in three stages. In the first stage, the PS accumulates in the targeted microbial cells. Next, the infected area is illuminated at the appropriate activation wavelength for the PS. Finally, the singlet oxygen that is produced results in oxidative damage to the targeted bacteria[182].

1.6 Concluding remarks

Polymer and nano-technology have shown great potential towards revolutionising cancer treatment in the last couple of decades. PDT is a rapidly evolving cancer treatment with significant advantages. One of the key challenges faced by PDT, inefficient delivery of drugs, has been addressed by NP based delivery systems and has demonstrated many advantages with fewer side effects. Although *in vitro* and *in vivo* studies have shown promising results, so far no NP based PDT agents are used in the clinic. However with the development of suitable NPs, we might finally bring PDT to the forefront of cancer treatment and other potential clinical applications.

1.7 Aim

The aim of the project was to synthesise a multiple PS delivery system based on a polyacrylamide nanosystem.

- To develop an efficient drug delivery system based on nano-sized particles for PDT and PACT.

- In the search for an efficient drug delivery system, a wide range of different NPs were investigated[34, 36-43]. This project primarily focuses on encapsulating a range of PSs (with different functionalities) within NPs and studying the systems behaviour in cell uptake, PDT and PACT.

1.8 Methodology

- To accomplish the requirements, first, a nanosystem with appropriate PSs was synthesised.
- Once successfully synthesised, a delivery method was developed for cellular internalisation of polyacrylamide NPs, which were then be qualitatively and quantitatively studied.
- Following, PDT *in vitro* studies were carried out (*i*) targeting cells when NPs are internalised and targeting the cellular environment when NPs have definitely not entered the cells. This would reflect *in vivo* targeting internalised NPs in tumour cells and the tumour vasculature.

Initially the project focused on two novel drug delivery approaches involving polymer based particles.

- In one route, the project investigates a nanotechnology based delivery system for PDT and PACT agents. NPs are produced from a bio-compatible matrix, polyacrylamide. These polymers were chosen as they are chemically inert, have shown efficient drug delivery and controlled and sustained release properties. The microemulsion environment used in synthesising these NPs gave rise to the techniques reliability and reproducibility in producing NPs of controlled size. PDT is a promising modality for removal of harmful or unnecessary cells that has been recently accepted in the clinic for cancerous and non-cancerous conditions [114, 127]. A range of PSs have been synthesised with varied physical properties: size and net charge. These PSs have been entrapped in the polyacrylamide matrix for investigation. NPs combined with PSs could mitigate many of the current problems

associated with drug delivery in PDT including drug resistance. In the project, nanoparticle uptake by cells (Human Caucasian colon adenocarcinoma cell line-HT29), has been quantified using fluorescence activated *cell* sorting (FACS). PDT cytotoxicity will be quantitatively investigated using PDT and PACT assays: cancer cell lines and bacteria assays and correlated with size, charge and porosity of the NPs carriers.

- Further in this project, it is considered important to recognise the approximate concentration of PS present per specified weight of NPs. This would be beneficial in biological studies allowing direct comparisons to be made.

- In the second approach, cationic hydrophilic polymers copolymerised with known amounts of porphyrin molecules were to be synthesised and compared with published results that have been obtained by attaching PSs to cationic polylysines[183, 184].

Chapter 2: Investigations and synthesis of photosensitiser entrapped nanoparticle systems

The aim of the project is to synthesise a multiple PS delivery system using polyacrylamide NPs to study their application in anticancer applications, *i.e.* PDT, and PACT. This chapter describes the attempts taken to synthesise/modify a number of PSs; their entrapment in polyacrylamide NPs, the cellular uptake and PDT cytotoxicity of the subsequent NPs.

2.1 Nanoparticle synthesis and characterisation

In this project, NPs are synthesised by adopting a well-documented microemulsion polymerisation method used in previous work from this laboratory[28] and others[185]. This procedure facilitates synthesising porous polyacrylamide NPs that have been shown to be compatible with biological environments[185-191].

The synthesis is carried out in a water-in-oil (W/O) microemulsion system where the monomers (acrylamide and N,N'-methylenebisacrylamide) and initiators (ammonium persulphate (APS) and NNN'N'-tetramethylethylenediamine (TEMED)) are brought together in an oily phase (hexane) containing surfactants (Brij® 30 and dioctyl sulfosuccinate sodium salt). The reaction mixture is a transparent media with a continuous oily domain and an aqueous domain compartmentalised by surfactants[16]. Surfactants host the reaction and act as steric barriers, inhibiting polymerisation between droplets during the reaction. Hydrophilic monomers and cross linking agents are effectively incorporated

in the reverse micelles and their hydrophilicity dictates their presence in the aqueous core of the micelle droplet. APS initiates the radical reaction in the presence of the co-monomers: acrylamide and N,N'-methylenebisacrylamide. APS is used for the generation of free radicals necessary for the polymerisation and is used with an accelerator, TEMED. TEMED enhances the formation of radicals from persulphate and they increase the rate of polymerisation[192].

These free radicals convert acrylamide monomers into free radicals which react with unactivated monomers to begin the polymerisation chain reaction[193]. It is assumed that the acrylamide polymerisation begins in water droplets containing monomers due to the initiator hydrophilicity. The polymerisation of the monomer leads to an increase in the viscosity of the water droplets. Initially it forms a gel and then inverts the phase of the W/O dispersion. When a sufficient amount of polymer is formed in the aqueous phase, a polymer dispersion containing water is formed due to the constant stirring of the microemulsion. A possible mechanism for the polyacrylamide polymerisation is shown in Scheme 2.1.

Once initiated, the chain grows by repeated additions of the co-monomer molecules until the free radical site is terminated. This can occur due to several reasons[1]:

1. A collision mechanism

- by collision of a growing particle containing a radical centre with a ‘dead’ particle containing a monomer combining their unpaired electrons to form a bond
- two chain ends simply coupling together to form one long chain

2. Disproportionation

- transfer of hydrogen atom to give a ‘dead’ polymer molecule
- a radical from one chain end can be abstracted to another, producing a polymer with a terminal unsaturated group and a polymer with a terminal saturated group

3. Combination of an active chain end with an initiator radical

4. Interaction with impurities or inhibitors *i.e.* oxygen

5. If all the monomers are consumed.

The number of propagation steps could vary due to several factors such as radical and chain reactivity, the solvent, and the temperature.

The elongating polymer chains are randomly crosslinked by N,N’-methylenebisacrylamide which results in the characteristic porosity of the NP. The porosity also depends on the polymerisation conditions and the monomer concentrations. A thorough literature review on porosity of polyacrylamide NPs was documented by Josefsen[28].

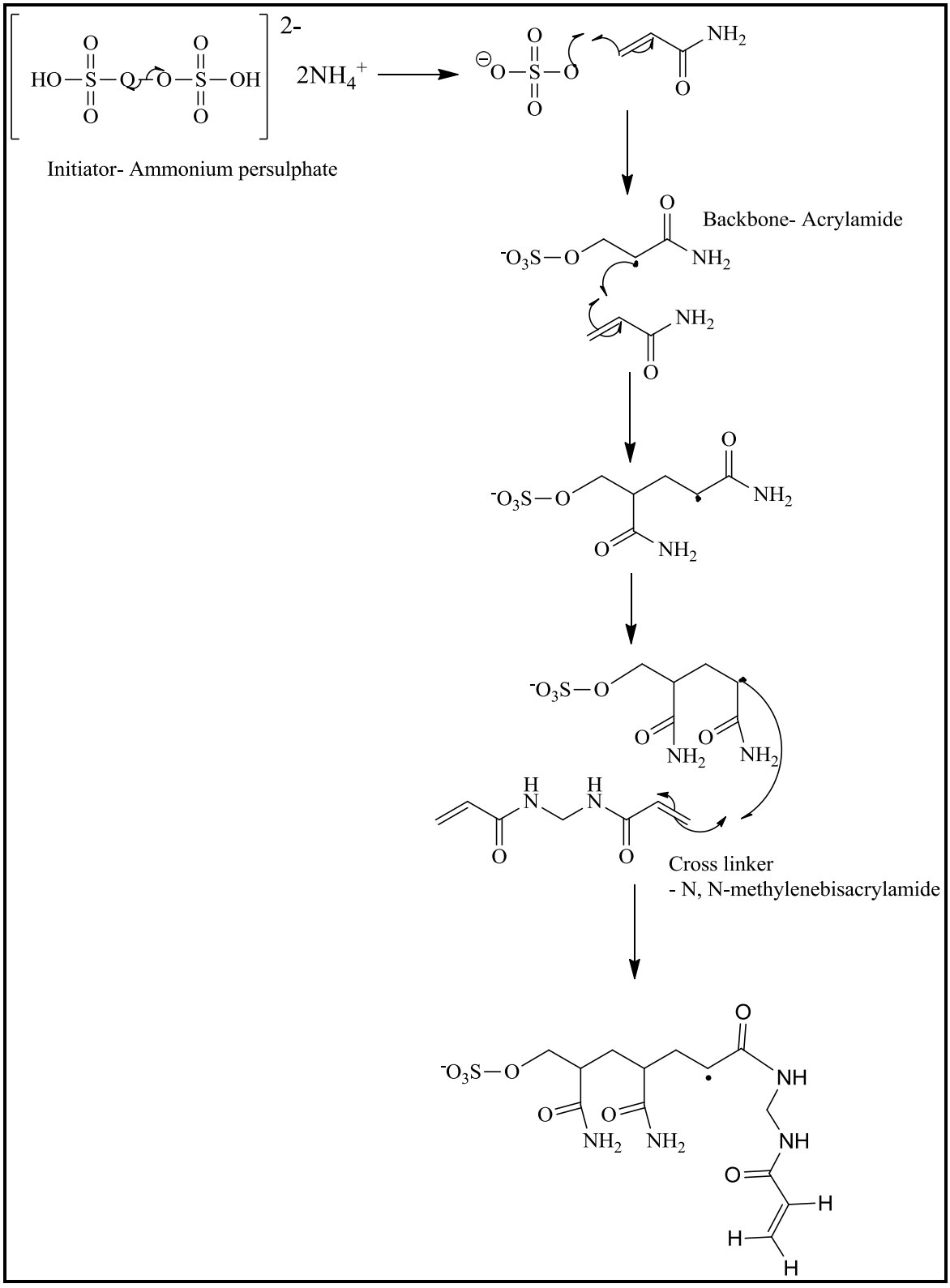

Scheme 2.1: Possible mechanism for polyacrylamide NP synthesis

The polymerisation can occur for up to 2 hours and thus the reaction typically is left undisturbed for two hours at room temperature, with constant stirring under a strictly controlled environment with argon gas. Purification of the polymeric NPs follows an ethanolic centrifugation after *in vacuo* removal of the hexane phase. The success of the polymerisation reaction was demonstrated by the recovery of porous three dimensional NPs by microfiltration. A reaction pathway with chemical structures and reagents of the NP synthesis procedure is shown in Scheme 2.2.

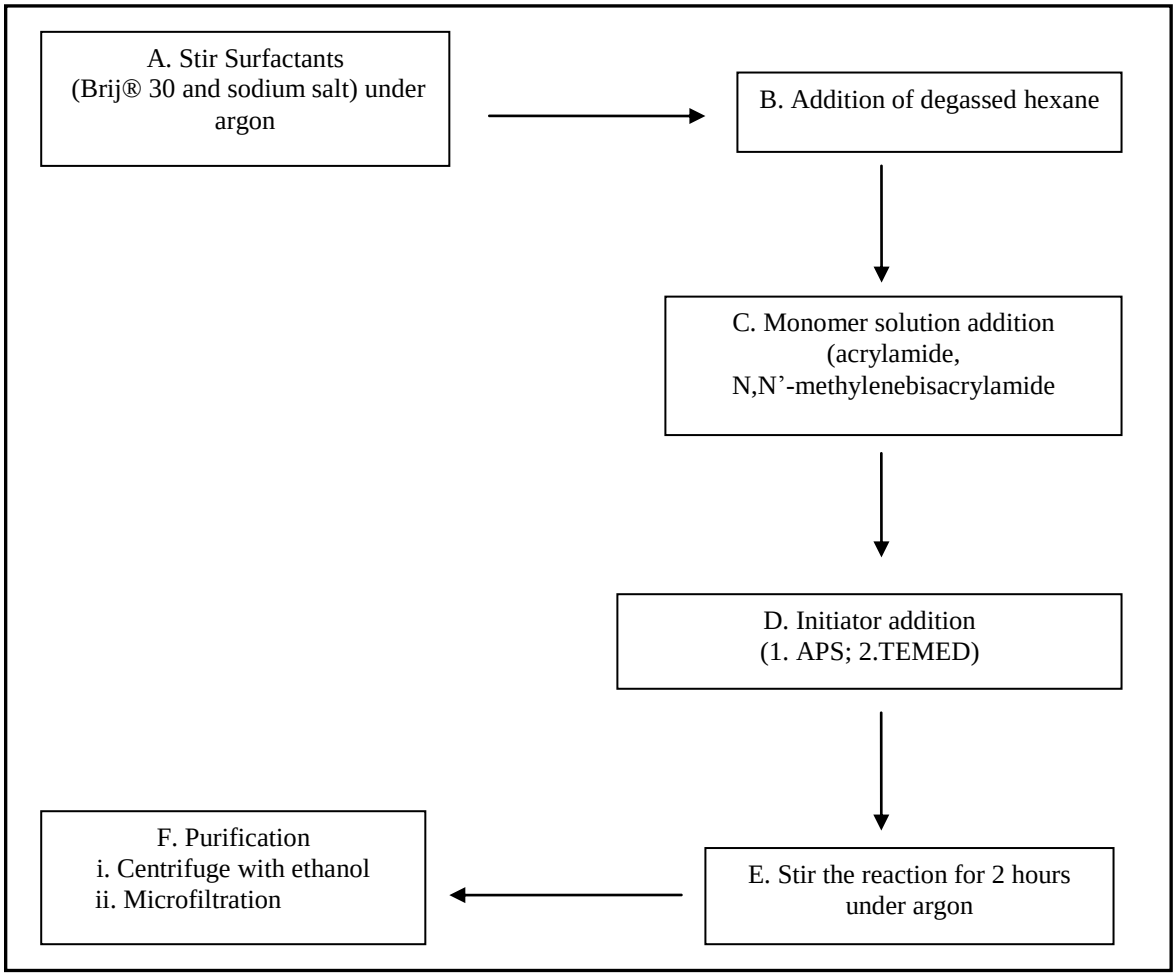

Scheme 2.2: Reaction pathway of the polyacrylamide NP preparation procedure

To understand the suitability of the polyacrylamide NPs for use in drug delivery, first it was important to characterise the NPs and understand their behaviour under different conditions. General characterisation techniques for NPs include size and polydispersity. In the project the size of the NPs was determined by both TEM and PCS techniques. PCS technique further enabled the size distribution of the NP populations to be quantified.

The NP size and size distribution were measured by the PCS using the Zetaplus^{TM} particle size analyser (Malvern 3000) at 25°C and at a scattering angle of 90°. To support the results obtained in NP characterisations, NPs were dispersed in MilliQ water. 3 mL of (1 mg/mL dispersion) was used to obtain a dilute sample for the size measurement. NPs synthesised in this technique are polydisperse. To obtain an approximately homogeneous suspension, the NPs used in all the applications in the project were filtered through a 0.22 µm filter unit, assuring that the size of the NPs that were used were less than 0.22 µm. Rapid sonication (30 seconds) was used to break up any loosely-held agglomerates. For NPs the intensity of the scattered light is uniform in all directions. So it was only necessary to measure scattering at a single angle. Thus 90° scattering angle was used in the measurements. The value was recorded as the average of 30 measurements. A typical size (Z_{ave}) distribution of a NP population is shown in Figure 2.1.

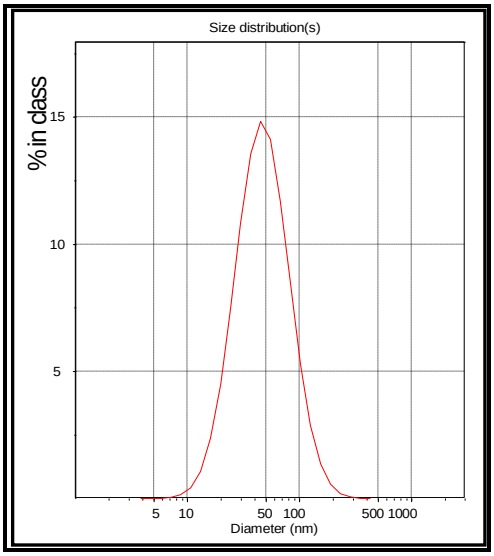

Figure 2.1: PCS spectrum of a typical NP: size distribution (z_{ave} 48 nm)

Transmission electron microscopy (TEM) was used to obtain images of the polyacrylamide NPs [18]. The first approach to obtain images was to stain the NPs with a negative stain *i.e.* uranyl acetate. In brief, a drop of uranyl acetate (1% solution) was deposited onto a drop of NP suspension that was deposited on a copper grid. After few seconds and once the grid was dry, the heavy metal salt, uranyl acetate, was deposited around the relatively transparent particles causing the NPs to appear light against the dark background acting as a negative stain (Figure 2.2).

In Figure 2.2, the visible spots are much smaller than 20 nm (scale bar). Z_{ave} of the NPs was 30 nm. These spots should be aggregates of uranyl acetate which either penetrated through porous NPs or attached to the surface during the staining procedure. The dark shadows seen in the image have subsequently been identified as NPs (Figure 2.3). Figure 2.3 is an image of one of those NPs with high resolution.

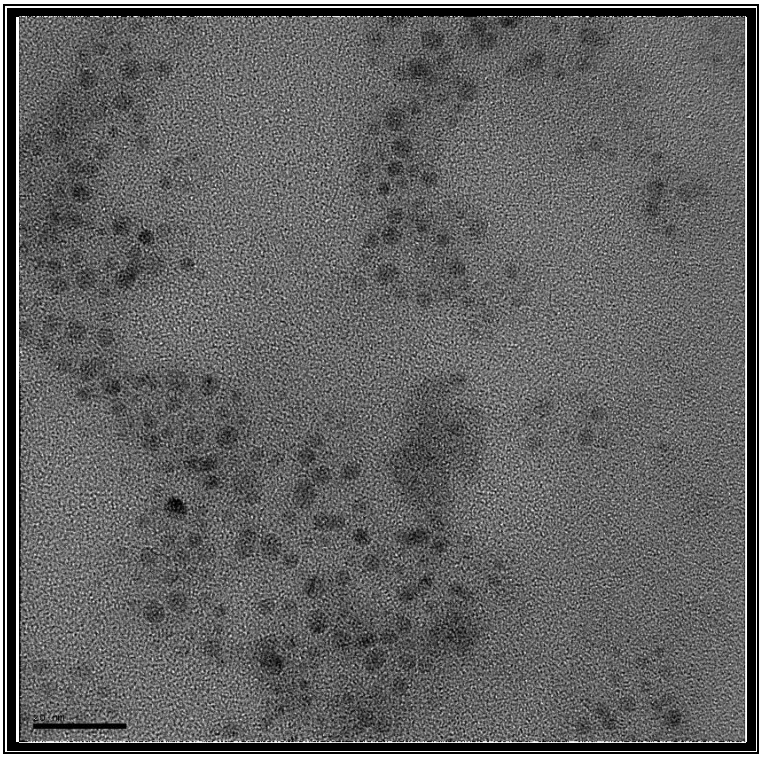

Figure 2.2: TEM image of a blank NP distribution (scale bar 20 nm)

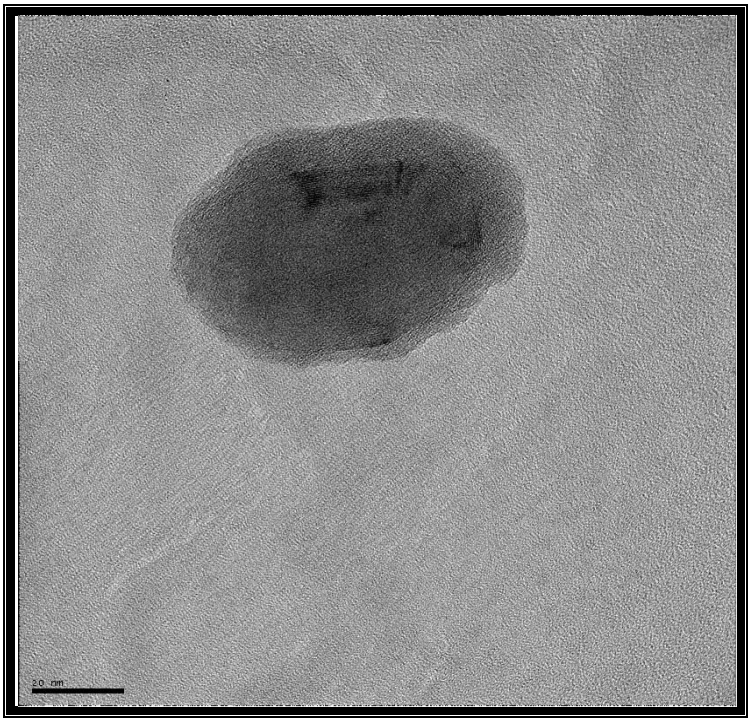

Figure 2.3: TEM image of a single blank NP (scale bar 20 nm)

The quality of obtained images was further improved by imaging NPs with uranyl acetate entrapped within the NP itself. To synthesise uranyl acetate encapsulated NPs [23], uranyl acetate (1 mg, 2.4 μmol) in water (50 μL) was added to the NP reaction mixture (Scheme 2.2) along with the monomer/at the monomer stage. In this way, the encapsulated uranyl acetate can be captured in the TEM images and circumvent the need to stain NPs prior to imaging. Figure 2.4 shows an image of an uranyl acetate encapsulated NP. Suspensions prepared for TEM imaging were used in imaging almost instantly, omitting any opportunity for leaching.

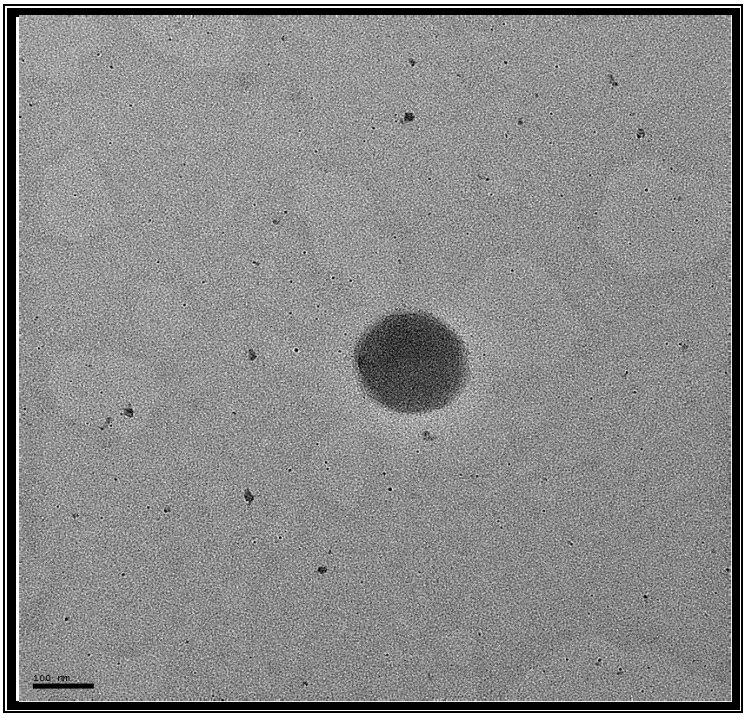

Figure 2.4: TEM image of an uranyl acetate encapsulated NP (scale bar 100 nm)

Uranyl acetate entrapped polyacrylamide NP population in Figure 2.5 confirms that the NPs synthesised in this procedure are polydisperse.

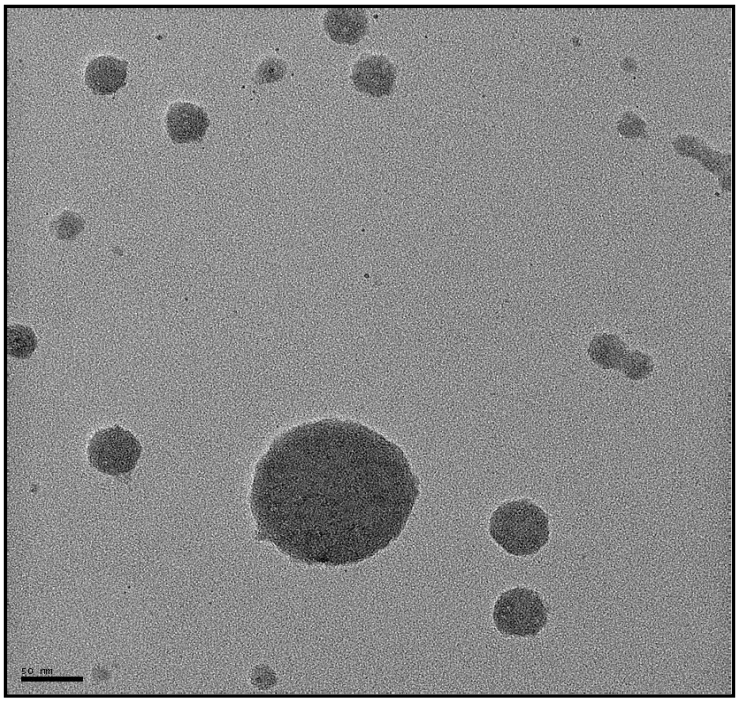

Figure 2.5: TEM Image of a polydisperse distribution of the uranyl acetate encapsulated NPs (scale bar 50 nm)

The method of imaging was optimised further to get a better quality image. One drop (5 μL) of a dilute suspension of uranyl acetate encapsulated NPs was added to the glow discharged carbon/copper grid. In imaging, glow discharge is used to make the power unit (carbon coated copper grid) hydrophilic. Once this was dried, a drop of ethanol was added and TEM images were taken (Figure 2.6).

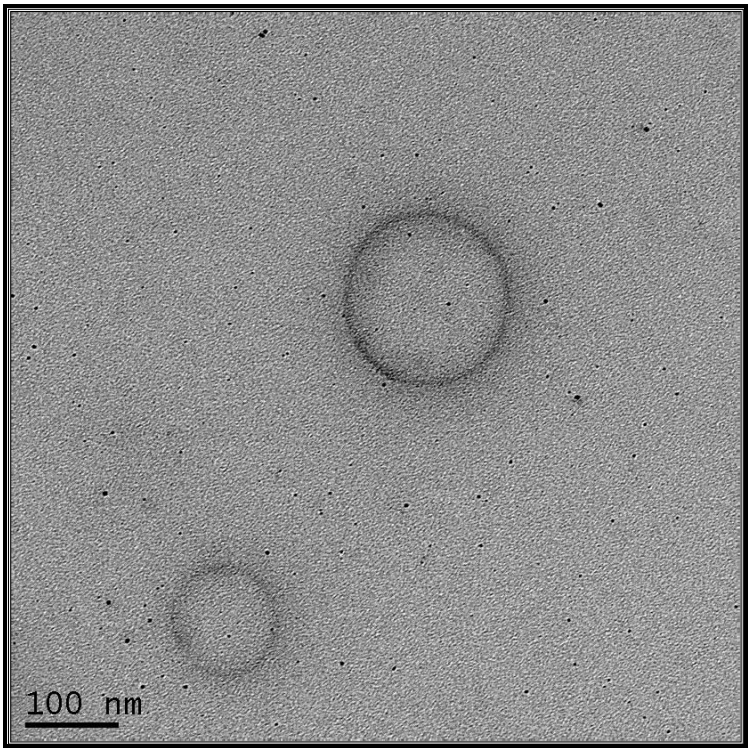

Figure 2.6: TEM image showing polydisperse distribution of the uranyl acetate encapsulated NPs in ethanol (scale bar 100 nm)

When using NPs in drug delivery, NP stability in suspension and the surface charge plays a vital role. The colloidal suspension stability and NP stability with time were also studied using size as a major factor.

Since in a colloidal system particles in a suspension can adhere to each other and form aggregates, it was interesting to observe whether or not NPs in suspension are susceptible to a high degree of aggregation over time. To this end, two suspensions of MB entrapped NPs [21] and dextran fluorescein entrapped NPs [29] were prepared with equal concentrations (10 mg NPs in 3 mL water). Due to the nature of the experiment, the suspensions were not filtered nor sonicated prior to measurement readings.

Size (Z_{ave}) measurements were taken at 0, 24, 48 and 72 hours by the PCS technique, Zetaplus^{TM} particle size analyser (Malvern 3000) at 25°C and at a scattering angle of 90°. The average NP size and the polydispersity increased from 37.1 nm to 76.6 nm over 72 hours. The reason for this increase in size could be flocculation. However, the NP population remained a normal distribution (Gaussian distribution); size distribution of the polydispersed NPs still clustered around the mean (Figure 2.7).

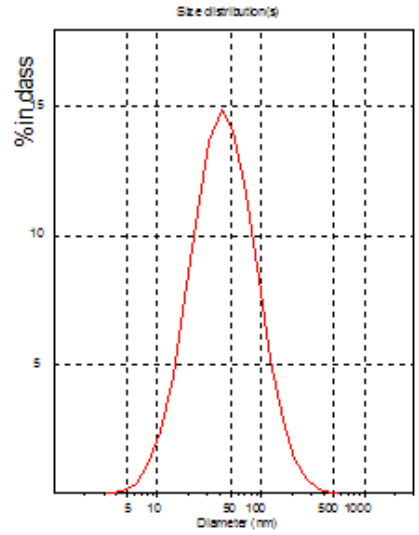

After 24 hours		
Run	ZAve	Poly
1	45.5	0.546
2	37.1	0.556
3	42.7	0.53
Average	41.7	0.544
+/-	4.3	0.013

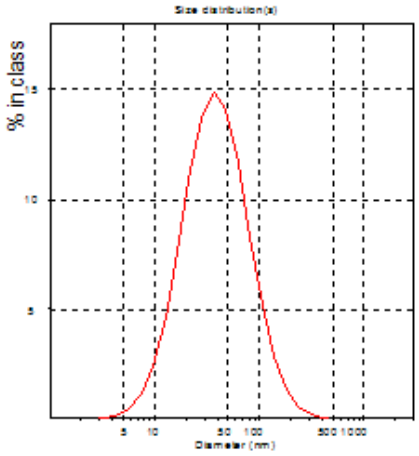

After 48 hours		
Run	ZAve	Poly
1	60.9	0.511
2	45.4	0.46
3	37.9	0.512
Average	48.1	0.494
+/-	11.7	0.029

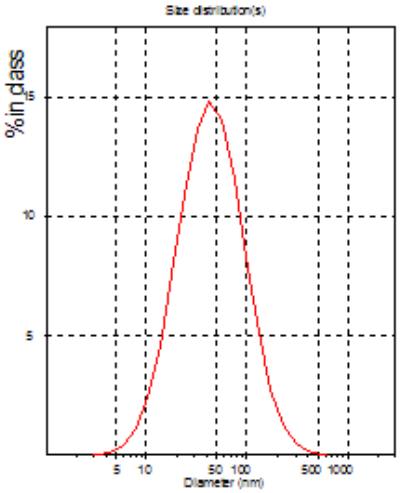

After 72 hours		
Run	ZAve	Poly
1	76.7	0.685
2	45.7	0.45
3	43.5	0.573
Average	55.3	0.569
+/-	18.6	0.118

Figure 2.7: Size distribution (Z_{ave}) over 72 hours

These aggregates are named ‘flocs’ and the process is called ‘flocculation’. Weak flocs can be stable and cannot be broken up by Brownian motion but may disperse under an external force such as vigorous agitation. The denser form of flocculation is named coagulation and the result could be sedimentation or creaming. Once sonicated for 10-20 seconds, average NP size decreased back to the 37 nm. The increased stability in solution confirmed the suitability of NPs to be used in longer experiments.

Further, since the NPs synthesised in the project are expected to be used in cellular assays, it was important to study the stability of the colloidal system.

There are two fundamental mechanisms that could affect dispersion stability.

• Steric repulsion – this is obtained by adding polymers to the system to adsorb onto the particle surface therefore preventing the particle surfaces coming into close contact.

• Electrostatic or charge stabilisation – this is the effect on particle interaction due to the distribution of charged species in the system. Due to the higher affinity of either cations or anions to one of the phases, there is usually electric charge separation occurring in interfacial layers. A layer of ions bound to one of the phases is called “surface charge” in a NP suspension; this is referred to as the charge of the NPs.

Since the NPs used in the project are synthesised by polymerisation a steric repulsion was clearly expected[194]. In order to further understand whether there is any surface charge zeta potentials of the suspensions were measured. Zeta potential is a parameter characterising electric properties of interfacial layers in dispersions, emulsions and porous bodies.

NP suspensions were prepared as for size determination and were measured using the Zetaplus^{TM} zeta potential analyser. The pH of the samples was recorded prior to each analysis. The value of a single sample was recorded as the average of 10 measurements. Most of the suspensions synthesised in the project were of zeta potential zero or slightly negative {(-1)-(- 3)}. Although large voltage measurements (>25 mV) were not obtained for zeta potentials, Josefsen carried out a series of polyacrylamide NP stability studies and confirmed that the NPs synthesised using the mentioned method were stable up to 6 months[28]. Therefore, the stability of the polyacrylamide NPs should be primarily controlled by steric repulsion.

Due to the nature of the NP synthesis technique only hydrophilic compounds could be entrapped in the aqueous core of the micelle droplet of the polyacrylamide NPs. Further, the identified compound needs to be compatible with radical polymerisation (NP synthesis), *i.e.* the compound needs to remain active when entrapped within the polymer matrix and the polymerisation process should not have any noticeable effect on the activity of the compound.

2.2 Synthesis/modification of photosensitisers and probes to entrap in nanoparticles

First, to verify the possibility of entrapping a PS in the NP matrix, commercially available PSs were investigated, initially the cyanine type PS indocyanine green (ICG, Figure 2.8) was chosen. The strong absorption band of ICG at 780 nm[195] (red /IR region) was one of the major reasons for this selection. An aliquot (30 µL, 1.3 mmoldm^{-3}) of a solution of ICG (1 mg, 1.3 µmol) in water (1 mL) was added to the reaction mixture at the same time as the monomer mixture.

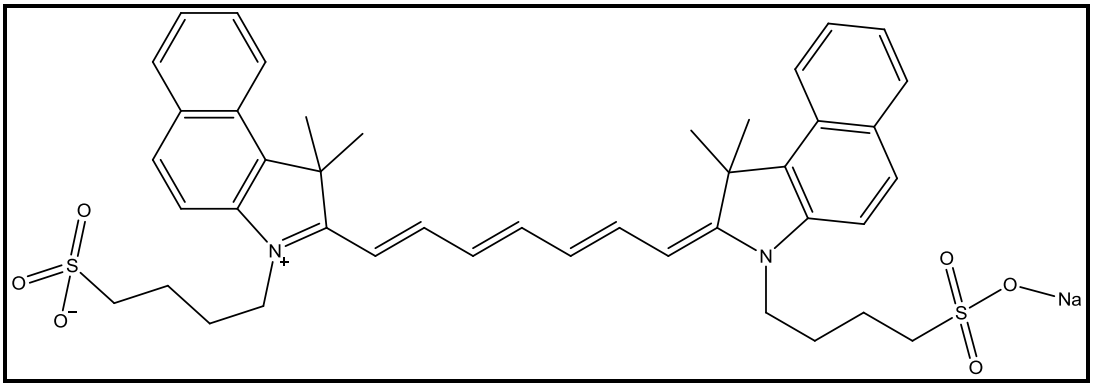

Figure 2.8: Indocyanine Green (ICG)

Within a few minutes of reaction initiation, the ICG colour transformed from green to yellow. Purification of the polymeric NPs followed an ethanolic centrifugation after *in vacuo* removal of the hexane phase. The spectroscopic analysis of the product using absorbance and emission spectroscopy revealed that ICG was no longer present in the NPs.

The ICG molecule contains a sequence of non-aromatic double bonds. The synthesis of the NPs follows a radical polymerisation mechanism. This raised the question whether or not the non-aromatic double bonds were attacked during the polymerisation reaction. Following this consideration, two parallel reactions were set up to find out whether or not the ICG was affected by the radical initiators.

Experiment-1: Monomers present and initiators absent - solution contained ICG, surfactants, water, hexane and monomers (acrylamide and N,N'-methylenebisacrylamide)

Experiment-2: Initiators present and monomers absent - solution included ICG, surfactants (Brij 30, sodium salt), water, hexane and initiators (APS and TEMED)

Results of the experiments were as follows.

Experiment-1: The solution was green in colour for the whole duration (2 hours) of the experiment. Spectroscopic analysis of the final aqueous media indicated the presence of ICG confirming that the monomers didn't have any influence on the reaction.

Experiment-2: The solution turned yellow as soon as the APS (radical initiator) was added, even before the addition of TEMED (initiator catalyst). The solution was stirred for 2 hours followed by spectroscopic analysis. The characteristic ICG absorbance and fluorescence peaks were not observed, suggesting that in fact, ICG was attacked by initiators in the radical reaction. It was concluded therefore that ICG was not a suitable PS to be encapsulated into the NPs, which use ammonium persulphate as the initiator in the radical polymerisation reaction which forms them.

Kopelman *et al.* has recently reported the possibility of post loading ICG into blank polyacrylamide NPs at room temperature by adding dyes in dimethyl sulfoxide into the NP mixture in PBS[162]. As most of the initiators are targeted to attack double bonds and ICG contains multiple non-aromatic double bonds, the above method might be the only method to use ICG with polyacrylamide NPs. However, the aim of the project at this stage was to verify the possibility of entrapping a PS in the NP matrix.

Following the disappointing results of ICG encapsulated NP synthesis, it was decided to attempt encapsulating MB (Figure 2.9), another PS with good absorbance at wavelengths suitable for PDT (668 and 609 nm) and with known activity in both PACT[196]/ PDT[197], but which contains no non-aromatic multiple bonds.

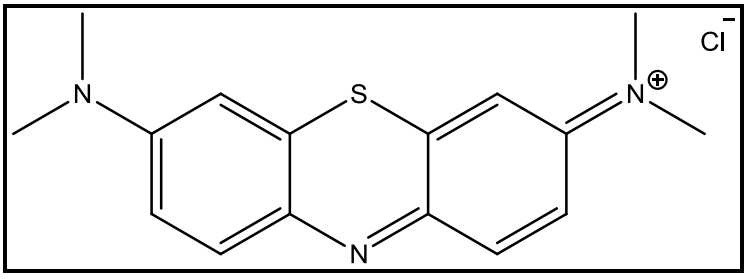

Figure 2.9: Methylene Blue (MB)

In synthesising MB encapsulated NPs [21] the NP synthesis procedure was followed as before but in this instance an aliquot (100 μL, 15.6 mmoldm^{-3}) of a solution of MB (5 mg, 15.6 μmol) in water (1 mL) was added to the monomer mixture to successfully obtain polyacrylamide particles (Z_{ave} 36 nm) (Figure 2.10).

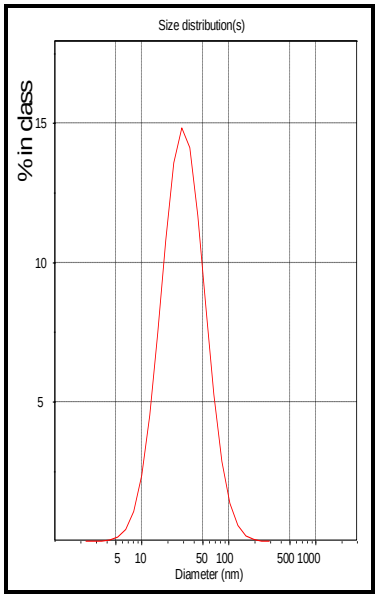

Figure 2.10: PCS spectrum of MB encapsulated NPs

Absorbance and emission spectra of MB showed no degradation and the MB entrapped concentration in NPs was determined using UV-vis. absorbance and the Beer-Lambert law. The calibration "straight" line (Figure 2.11) was plotted using the absorbance at 665 nm against known concentrations of MB. This calibration "straight" line was used in quantifying the approximate concentrations of MB present in a pre-determined weight of NPs (*i.e.* 1 mg) in 1 mL of H_2O by measuring its absorbance. Due to the heterogeneous nature of the nanoparticles and its contents, 1 mg of nanoparticles in 1 mL of H_2O was chosen as the standard to quantify the concentration of photosensitiser entrapped. The concentration of MB per 1 mg of NPs in 1 mL of H_2O is 5.6 $\mu moldm^{-3}$.

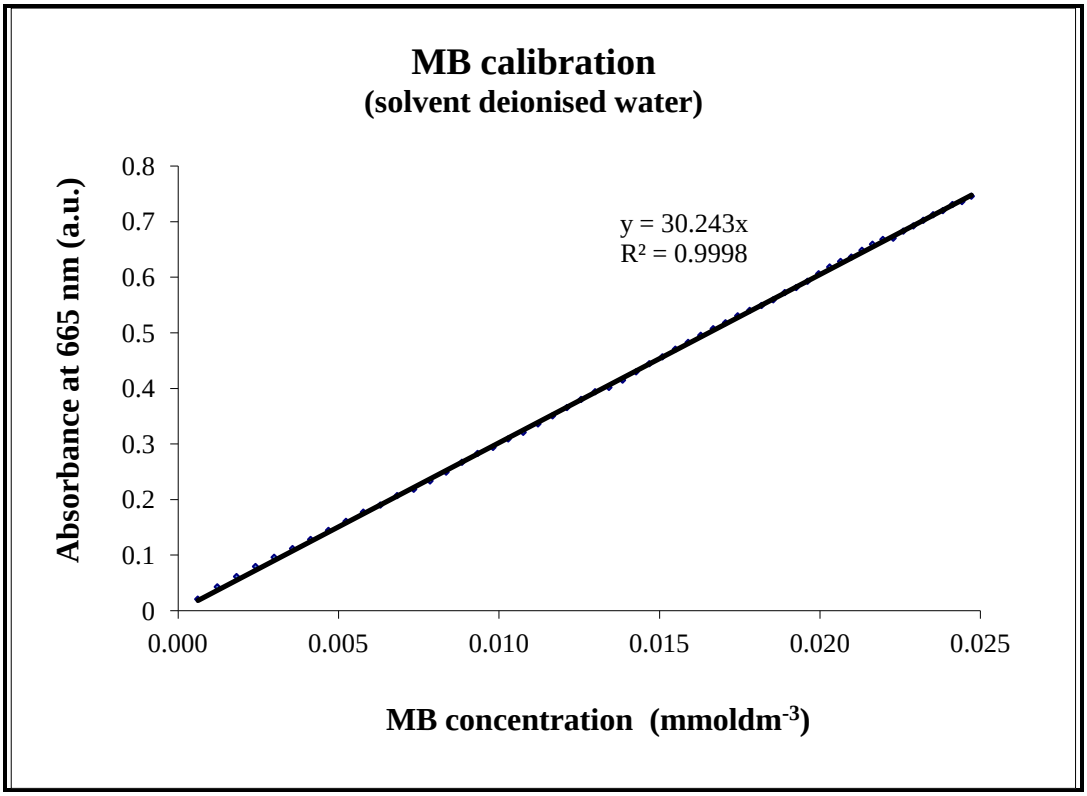

Figure 2.11: MB calibration "straight" line

Physically entrapped dyes in polyacrylamide NPs have previously been reported to leach 45-50% in a 48 hour[24, 189] period and up to 100% over seven days[189] when in an aqueous suspension. Factors such as the molecular size and hydrophilicity of the dye play a significant role in leaching properties of the dye from a polyacrylamide matrix[187]. Smaller hydrophilic dyes have an inclination to diffuse out through the pores of the matrix and into the hydrophilic environment. However, to comply with the aim of the project, it was important to entrap the dyes/PSs within the NPs, minimising dye leaching into the cellular environment. Thus, leaching experiments were performed to quantify the leached MB from the polyacrylamide NPs synthesised in the project.

Absorbance of the leached MB was measured to assess the porosity of the NPs. 200 mg of NPs were dispersed in 80 mL of MilliQ water and the dispersion was kept stirring at room

temperature. At given time intervals (hourly), three 2 mL samples were drawn from the suspension and the absorbance was measured using UV-vis. NP suspensions were microfiltered (Whatman® Anodisc 25, 0.02 µm, 25 mm filter) and the absorbance readings of the leachates were analysed. Average readings at each time point before and after filtration were taken for 24 hours. The results indicated that MB does leach from the polyacrylamide matrix over a 24 hour time period and is capable of slow release (Figure 2.12).

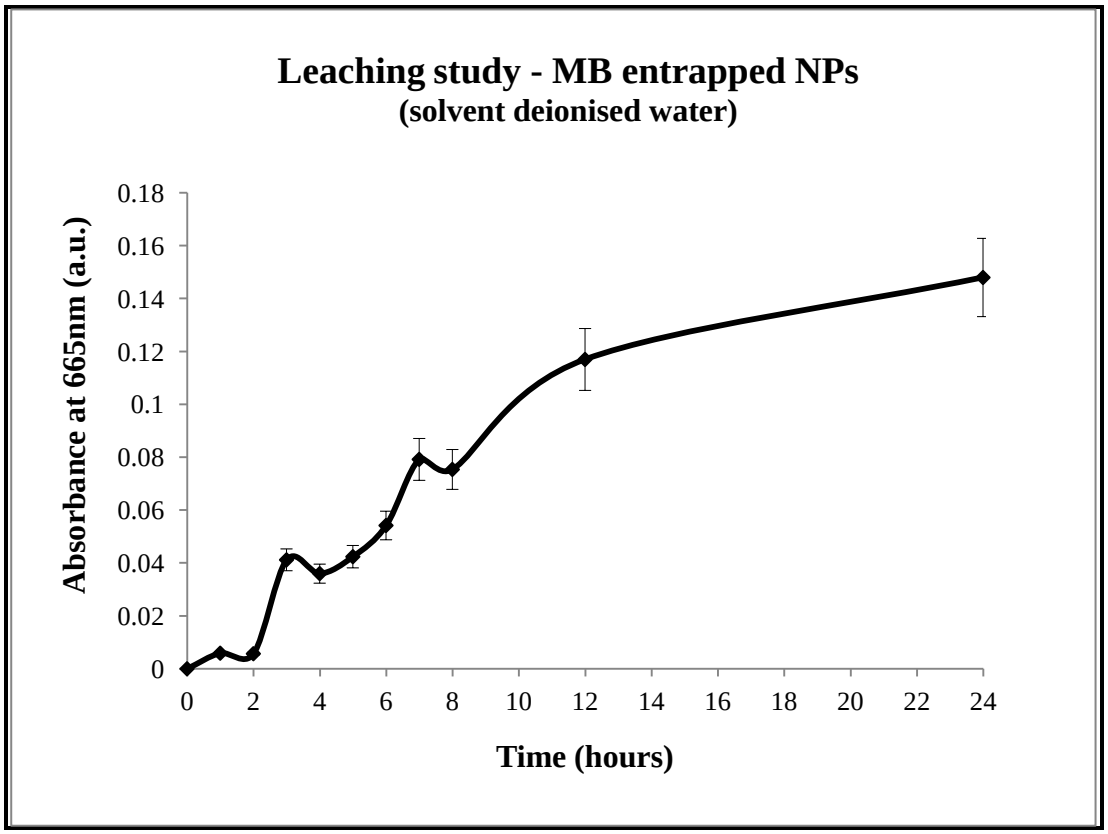

Figure 2.12: Leaching study of MB NPs

Percentage of leached MB was calculated using the formulae below.

% Leached = (Filtrate absorbance/NP suspension aliquot absorbance) * 100

No. of hours	% Leaching
0	0.00
1	3.47
2	9.24
3	24.24
4	21.18
5	24.94
6	31.88
7	46.59
8	44.35
12	68.82
24	87.06

The calculated results indicated that nearly 90% of MB does leach from the polyacrylamide matrix over a 24 hour time period (Figure 2.13).

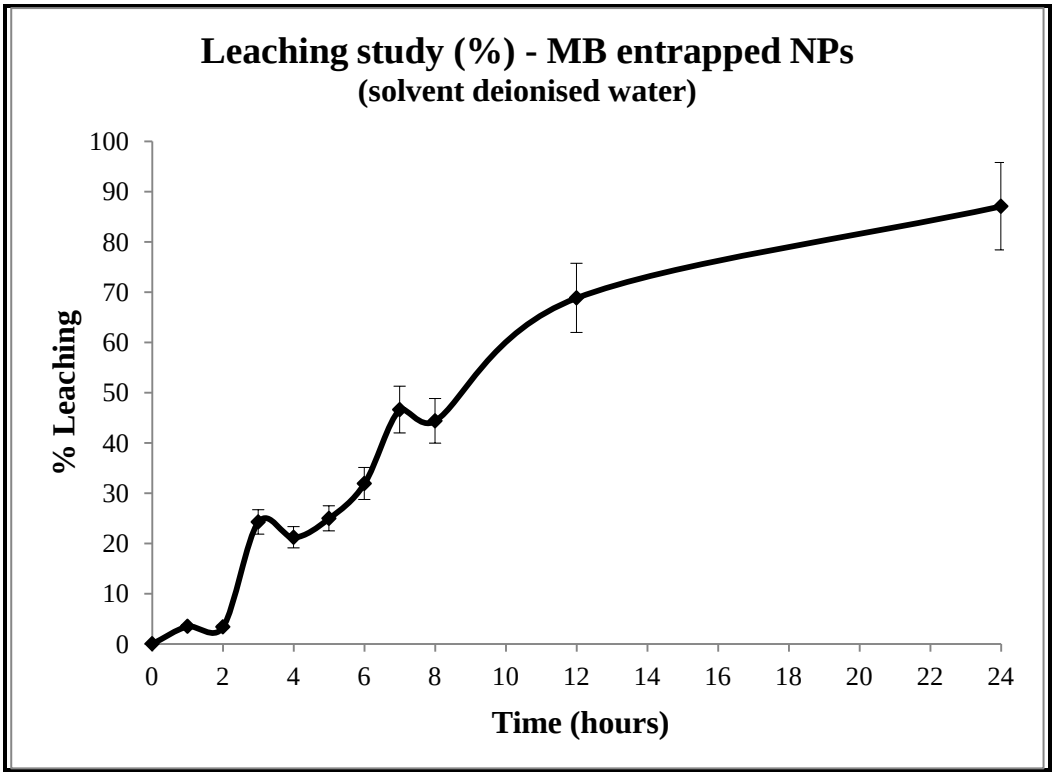

Figure 2.13: Percentage leaching study of MB NPs

Having successfully characterised the MB NPs the project progressed to synthesise NPs with further PDT agents entrapped.

As discussed previously, only hydrophilic compounds can be used in the w/o radical polymerisation reaction (NP synthesis). Thus, the synthesis of a non-macrocyclic hydrophilic PS, disulphonated 4,7-diphenyl-1,10-phenanthroline ruthenium (II) chloride; DSRuCl (Figure 2.14) was attempted using commercially available $RuCl_3$. The singlet oxygen Φ for $Ru(dpp(SO_3)_2)_3$ free in solution is 0.80 ± 0.05[191]. Although the production of singlet oxygen by DSRuCl is relatively modest it is still sufficient for PDT activity.

$RuCl_3$ was reacted with 3.5 molar equivalents of 4,7-diphenyl-1,10-phenanthrolinedisulfonic acid disodium salt in deionised water and refluxed with stirring

for 48 hours. The colour of the reaction mixture changed from dark green to red over a 48 hour period. The solution was cooled to room temperature, filtered and excess solvent removed *in vacuo*. The resulting red-brown solid was purified by size exclusion chromatography using Sephadex G25 (solvent distilled water). The bright red fraction was collected and concentrated *in vacuo* to obtain the hydrophilic DSRuCl [1]. It should be noted that this compound is a mixture of several isomers as SO_3Na substituents on the phenyl rings are randomly positioned.

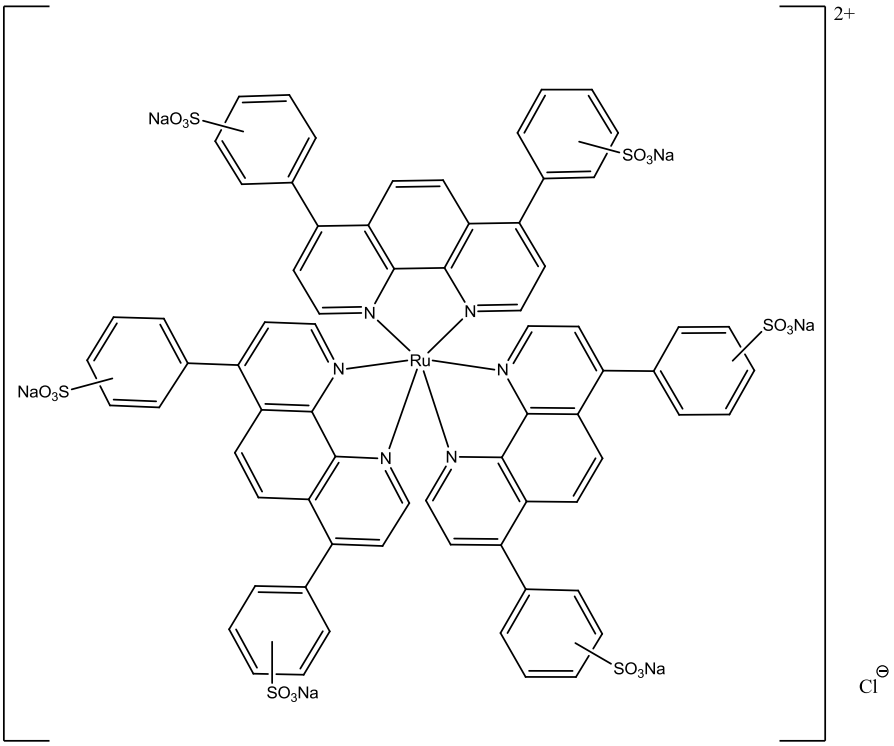

Figure 2.14: Disulphonated ruthenium chloride dye (disulphonated 4,7-diphenyl-1,10-phenanthroline ruthenium (II) chloride; DSRuCl)

The characterisation of the product was determined using elemental analysis. Elemental analysis of the compound demonstrated some discrepancies between the expected and

actual results[198]. This could be accounted for by extra water molecules in the sample. A comparison of the expected[199] and actual results for elemental analysis can be seen in Table 2.1: .

Element	Expected results %	Actual results %
Carbon	47.18	42.61
Hydrogen	3.96	2.81
Nitrogen	4.23	4.08
Sulphur	9.69	7.88

Table 2.1: Expected and actual results for elemental analysis for DSRuCl

Despite the discrepancies observed between the actual and expected elemental analysis, the characteristic absorbance peak associated with complex formation was observed in the UV-visible spectrum (Figure 2.15)[198, 199]. The absorbance and fluorescence peaks (Figure 2.16) were consistent with the literature[198] and no changes to the spectral shape or peak wavelengths were observed. The elemental analysis variation could have occurred due to a problem with the sample, instrumental contamination or instrumental inaccuracy[199]. Elemental analysis measures all material in the sample but absorbance and fluorescence only measure chromophoric material, so the error in the elemental analysis was most likely due to contamination of the sample with non-chromophoric impurities (for example salts).

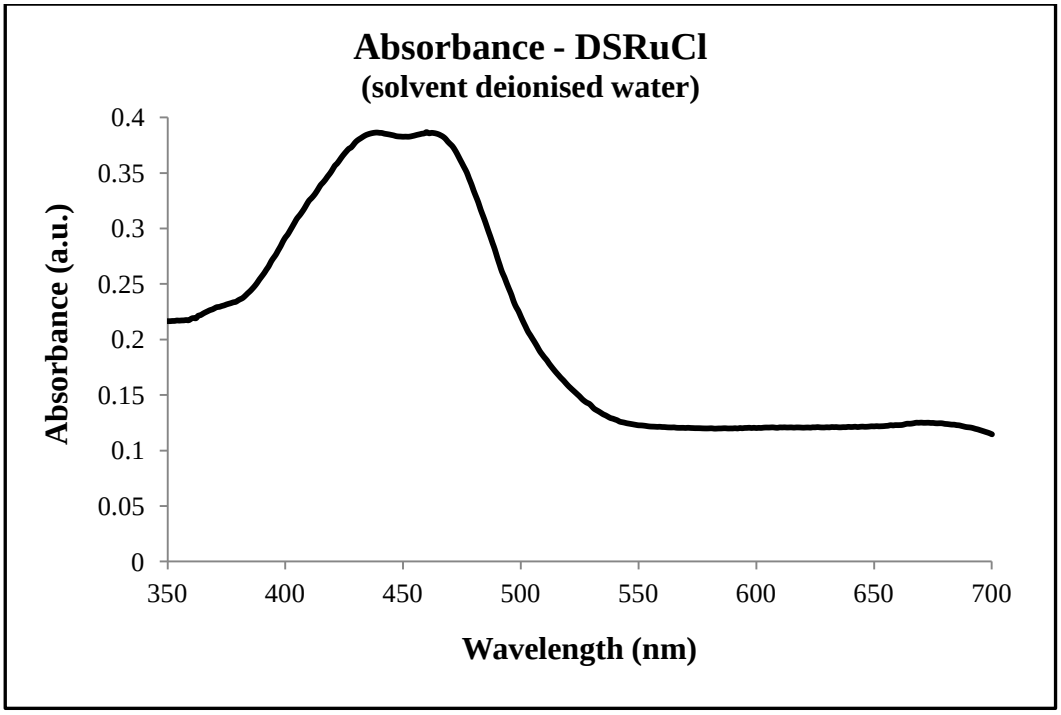

Figure 2.15: Absorbance spectrum of DSRuCl

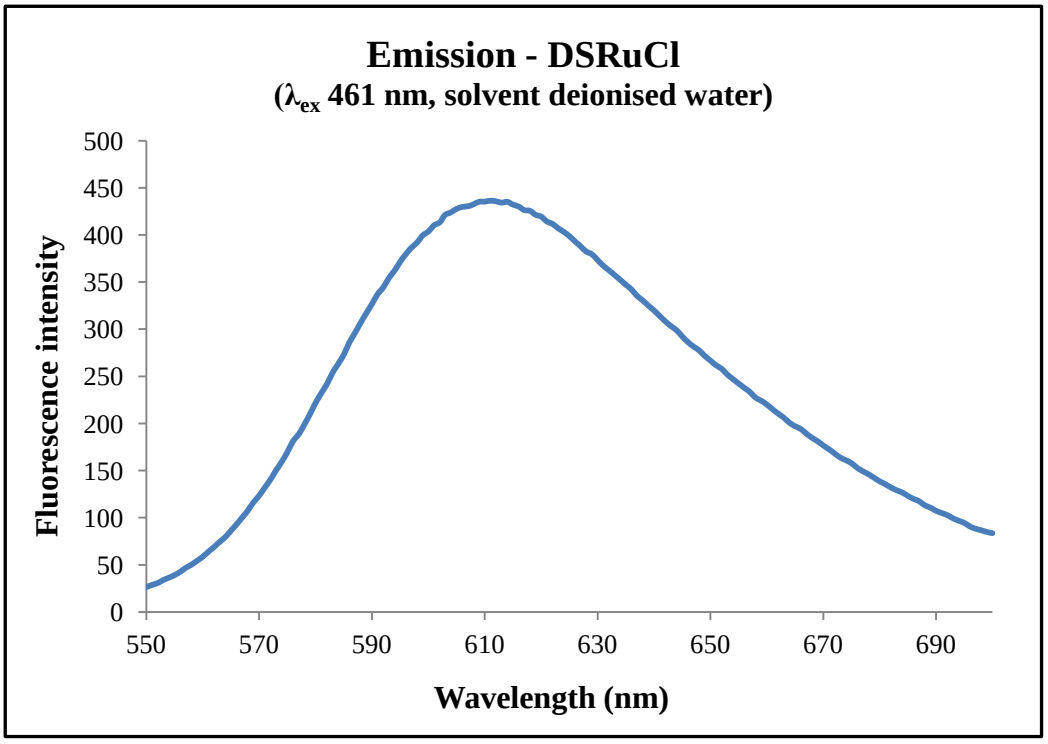

Figure 2.16: Emission spectrum of DSRuCl

NPs were synthesised encapsulating the obtained hydrophilic DSRuCl [24]. In the synthesis, the previously developed (see above) procedure was followed with the exception of adding an aliquot (100 μL, 2.8 mmoldm^{-3}) of a solution of DSRuCl (5 mg, 2.8 μmol) in water (1 mL), along with the monomer mixture. Size (z_{ave}) 58 nm (Figure 2.17).

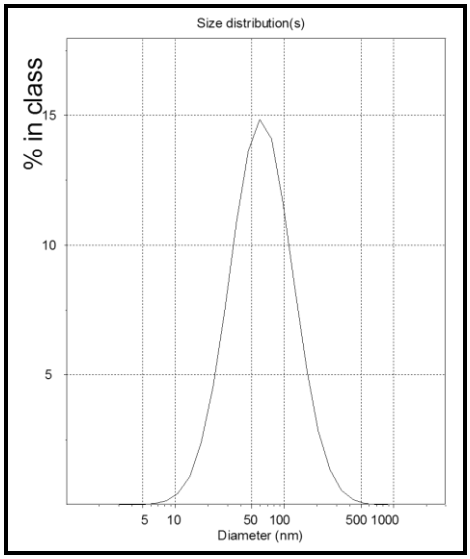

Figure 2.17: Size distribution of DSRuCl encapsulated NPs

After isolation of the NP the absorbance (Figure 2.18) and emission spectra (Figure 2.19) of a suspension of the particles confirmed the presence of the DSRuCl.

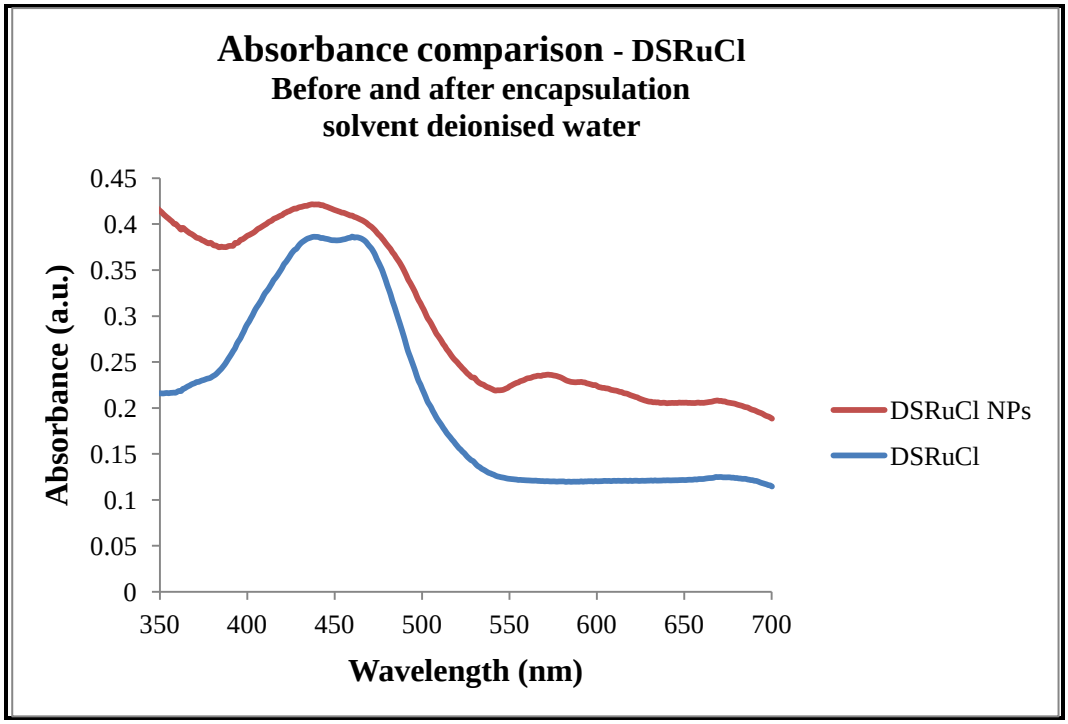

Figure 2.18: DSRuCl before and after encapsulation - absorbance spectra comparison

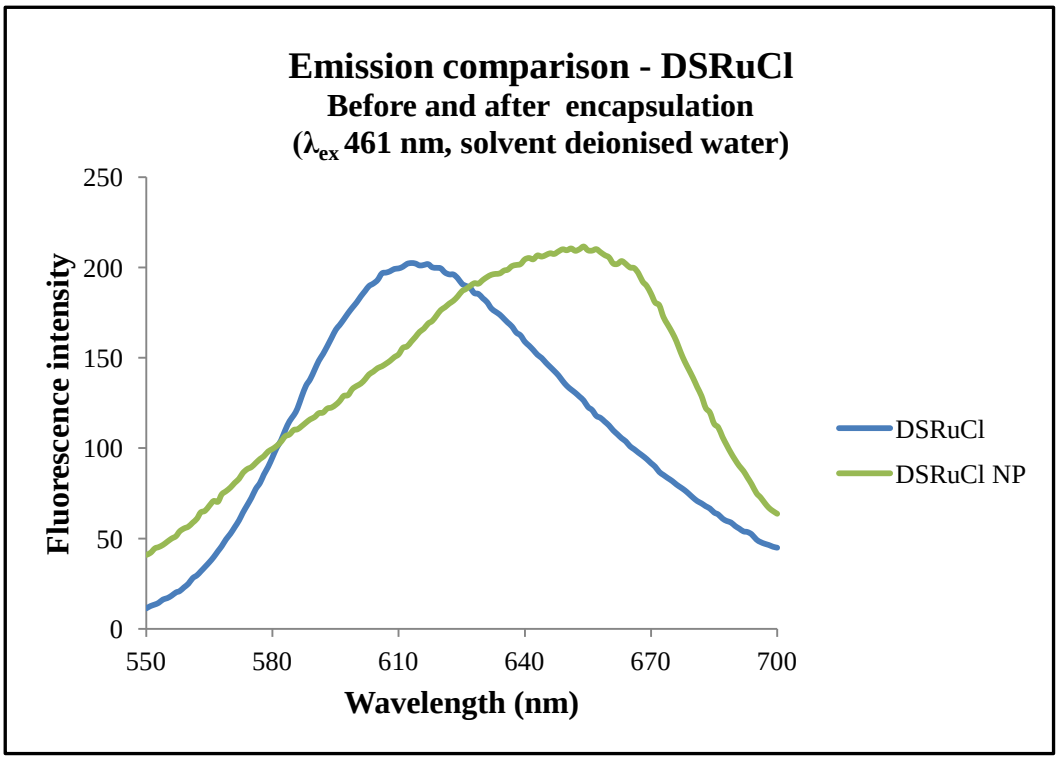

Figure 2.19: DSRuCl before and after encapsulation - emission spectra comparison

The calibration "straight" line (Figure 2.20) for DSRuCl was plotted against the absorbance at 461 nm for a known concentration range of the DSRuCl (solvent water). This calibration "straight" line was then used in quantifying the approximate concentrations of DSRuCl present in a pre-determined weight of NPs (*i.e.* 1 mg) in 1 mL of H_2O by measuring its absorbance. The concentration of DSRuCl per 1 mg of NPs in 1 mL of H_2O was 4.0 μmoldm^{-3}.

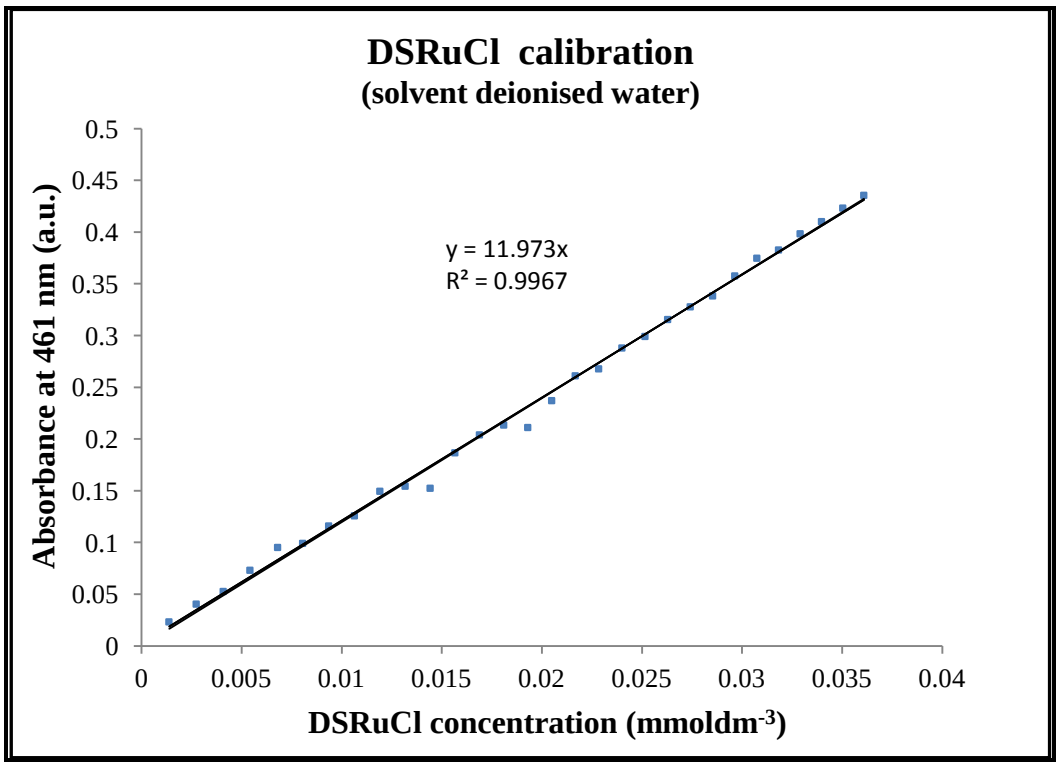

Figure 2.20: DSRuCl calibration "straight" line

Although the synthesised DSRuCl (hydrophilic) was successfully entrapped in the polyacrylamide NPs, since the DSRuCl was not 100% pure, the NPs were not used in any biological applications. However the compatibility of the DSRuCl in the polyacrylamide synthesis procedure encouraged the attempts to entrap other hydrophilic PSs. To this end, a small cationic porphyrin, 5,10,15,20-tetrakis-(4-*N*-methylpyridiniumyl)porphyrin

tetraiodide (PyPorphyrin), was chosen to be entrapped in the NP matrix. The porphyrin has previously shown good PDT/PACT activity against cultured cancer cells and bacteria[200].

The Adler[201] method was adopted to synthesise 5,10,15,20-tetrapyridyl porphyrin (Scheme 2.3). Briefly, pyrrole and pyridine-4-carboxyaldehyde were refluxed in propionic acid for 30 minutes and the reaction mixture was left to cool down to room temperature and filtered. The resulting solid was washed with methanol to yield 5,10,15,20-tetrapyridyl porphyrin as a purple solid. Subsequent functionalisation to achieve hydrophilicity was obtained by methylation of the pyridinium nitrogen atoms by adding excess iodomethane to a solution of the porphyrin in dimethylformamide (DMF). The reaction mixture was stirred for 17 hours at 40°C. After cooling, the product was precipitated and washed with diethyl ether to remove any remaining iodomethane. The product recovered was re-precipitated from acetone:water (1:1) to obtain PyPorphyrin [2] as a purple crystalline solid in a 98% yield (Scheme 2.3).

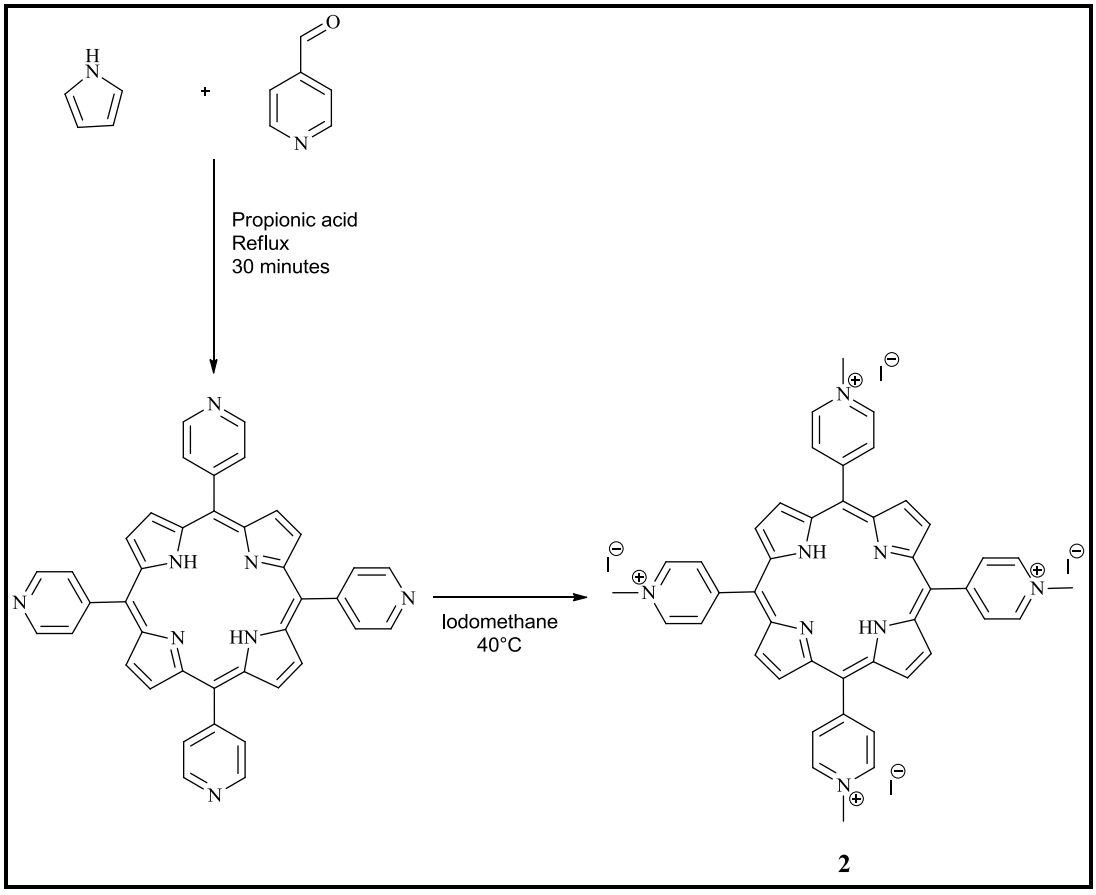

Scheme 2.3: PyPorphyrin synthesis

The porphyrin was then entrapped in polyacrylamide NPs [26] using the polyacrylamide NP synthesis procedure described (see Scheme 2.2) with the exception of the addition of an aliquot (100 μL, 4.2 mmoldm^{-3}) of a solution of PyPorphyrin (5 mg, 4.2 μmol) in water (1 mL), along with the monomer mixture to the hexane solution (z_{ave} = 48 nm). The absorbance (Figure 2.21) and emission spectra (Figure 2.22) confirmed that the PyPorphyrin was compatible with the radical polymerisation procedure.

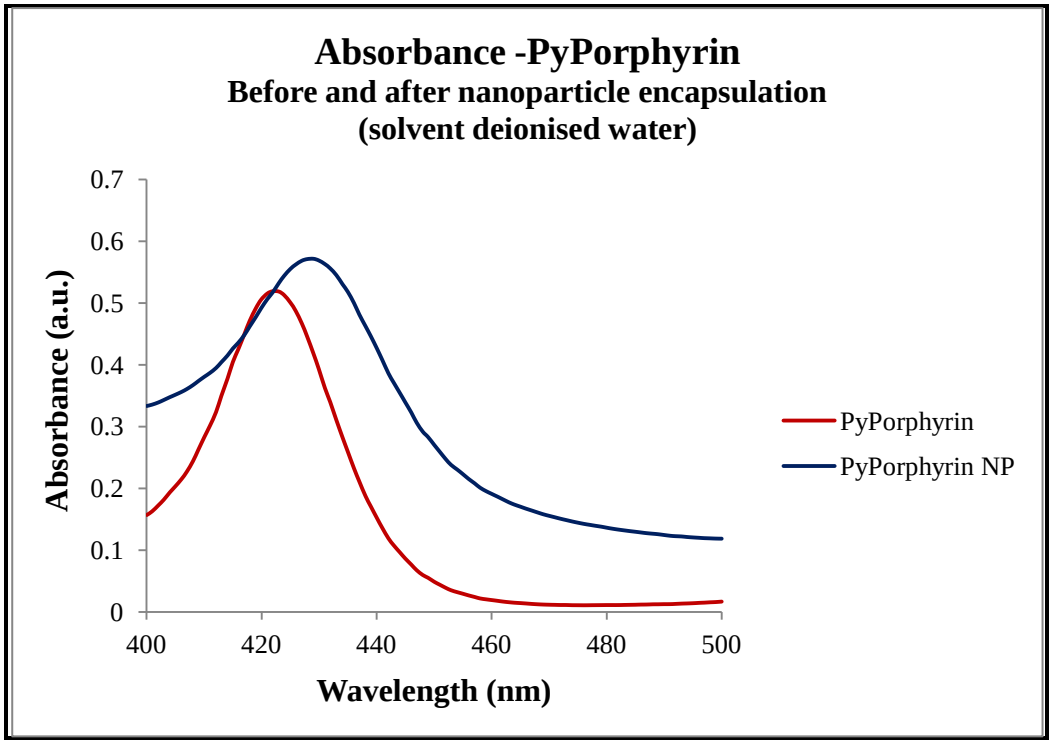

Figure 2.21: PyPorphyrin before and after NP encapsulation - absorbance spectra comparison

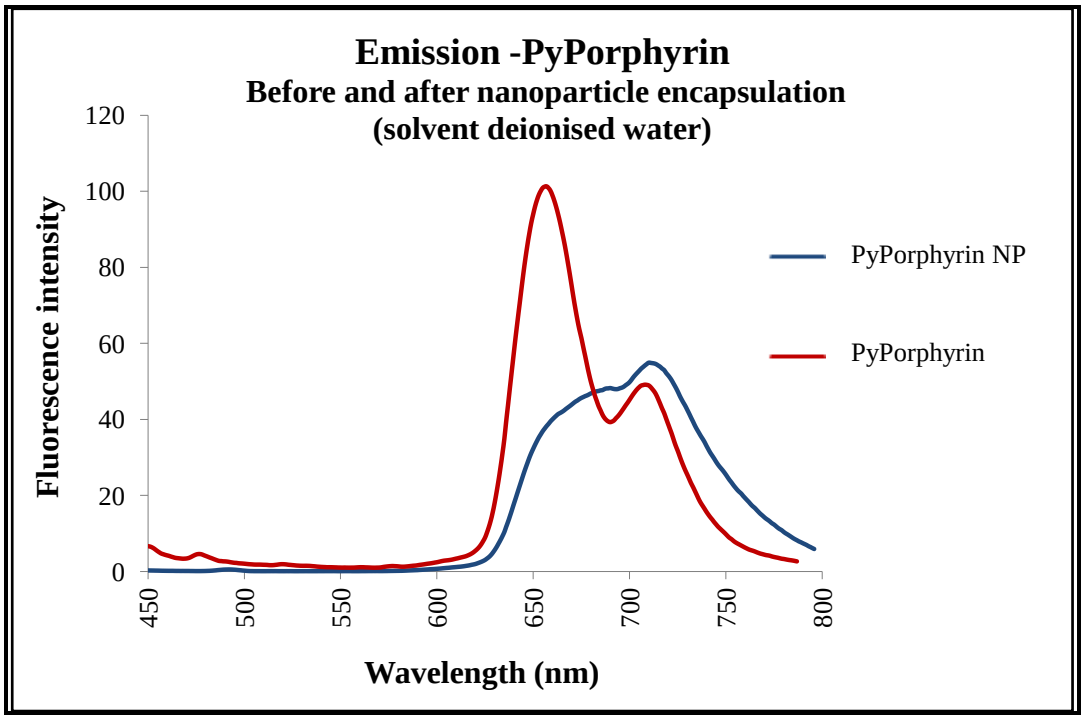

Figure 2.22: PyPorphyrin before and after NP encapsulation - emission spectra comparison

A calibration "straight" line (Figure 2.23) was used to measure the approximate concentrations of PyPorphyrin present per set weight of NPs by measuring its absorbance (solvent deionised water). This calibration "straight" line was then used in quantifying the approximate concentrations of PyPorphyrin present in a pre-determined weight of NPs (*i.e.* 1 mg) in 1 mL of H_2O by measuring its absorbance. The concentration of PyPorphyrin per 1 mg of NPs in 1 mL of H_2O was 0.34 μmoldm^{-3}.

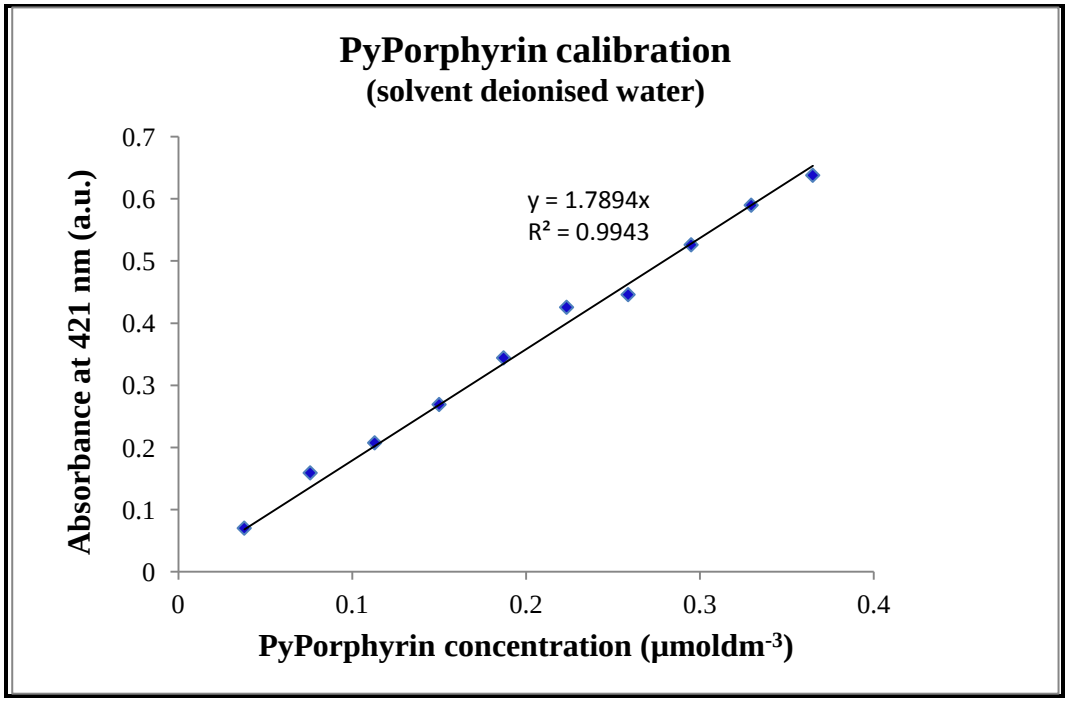

Figure 2.23: PyPorphyrin calibration "straight" line

Due to the smaller size of the entrapped porphyrins they were expected to leach from the NP matrix when in suspension. Thus, experiments were carried out to investigate potential leaching of PyPorphyrin. Fluorescence readings were taken at given intervals over 24 hours (Figure 2.24). After modest fluctuations for 6 hours the intensity started to increase.

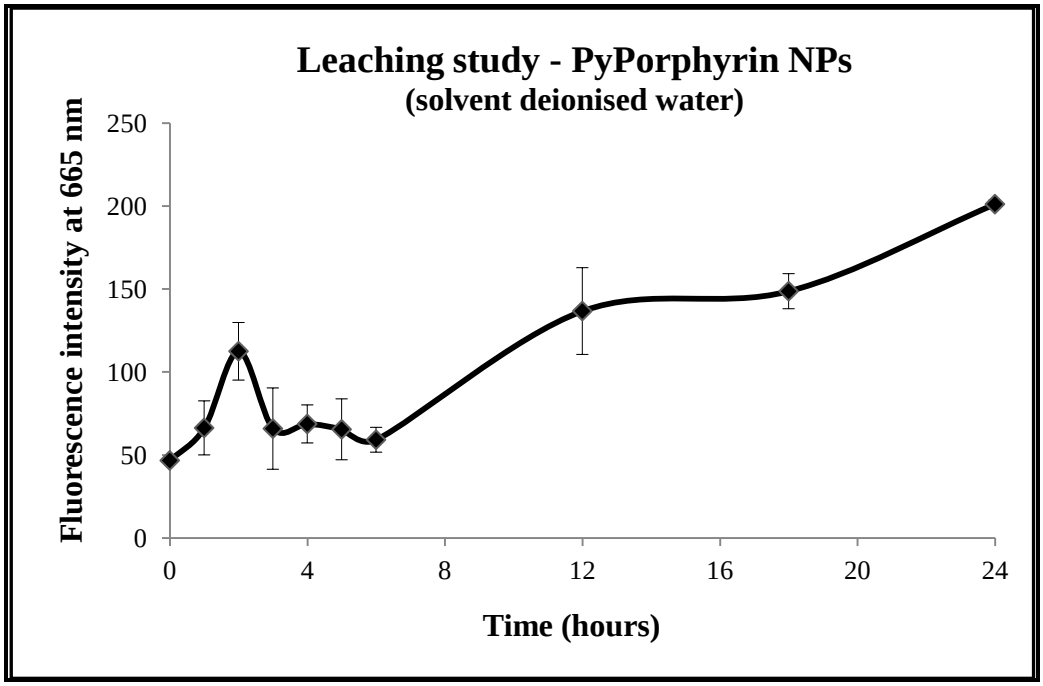

Figure 2.24: Leaching study of PyPorphyrin NPs

One of the main purposes of encapsulating/entrapping PSs in a particle matrix is to prevent loss of drug en route to the target tissue. Thus, now the most crucial problem that needed addressing was to reduce leaching. Most of the encapsulated molecules are prone to leach out of the particle over time unless they are anchored within the NP core[202, 203].

In principle, leaching can be minimised/stopped in two ways:-

- NP modification: variation in the particle pore size

To overcome leaching from the NP matrix, NP pore size can be decreased by varying the type and the concentration of the cross linker used in the NP synthesis[189] covalently attaching the dye to the NP matrix[23] or by adding cages or lipophilic tails[186] to the dye.

- PS modification: trapping the PS in the NPs by making the porphyrin more sterically bulky

As the dyes have the potential to leach out during the final washing stages of NP synthesis, we proposed that by attaching the PS to a soluble anchor, such that the size of the dye conjugate could be increased to prevent or minimise the leaching from the NP structure. Following this initiative, synthesis of cationic, water-soluble and reasonably sterically bulky PSs were attempted.

2.3 Sterically bulky PS synthesis

Sterically bulky PSs can be synthesised either by attaching a bulky group (*i.e.* dextran, polylysine or PEG) or covalently incorporating the PS into co-block polymers. Copolymerised porphyrins, which have shown some promising results in antibacterial PDT, have been obtained by attaching PSs to cationic polylysines[183,184]. Following a similar notion, cationic hydrophilic polymers copolymerised with known amounts of porphyrin molecules were investigated. The group transfer polymerisation (GTP) method was used in the copolymerisation synthesis.

2.4 Copolymerisation of porphyrins using group transfer polymerisation (GTP)

GTP relies on the functionalised groups methacrylate and acrylate. Thus, it was decided to synthesis a porphyrin with an acrylate reaction handle. First, it was decided to synthesise a copolymerised porphyrin using GTP. The procedure to synthesise 5-(4-propenoxyphenyl)-10,15,20-triphenylporphyrinatozinc [5] was completed in three steps.

- Adler method[201] was used in the synthesis of 5-(4-hydroxyphenyl)-10,15,20-triphenylporphyrin [3].
- Zinc was inserted into the porphyrin cavity to minimise interference with the polymerisation process by the exchangeable inner hydrogen atoms [4].
- Finally, the targeted acrylate group was incorporated onto the porphyrin[204] [5] as shown in Scheme 2.4

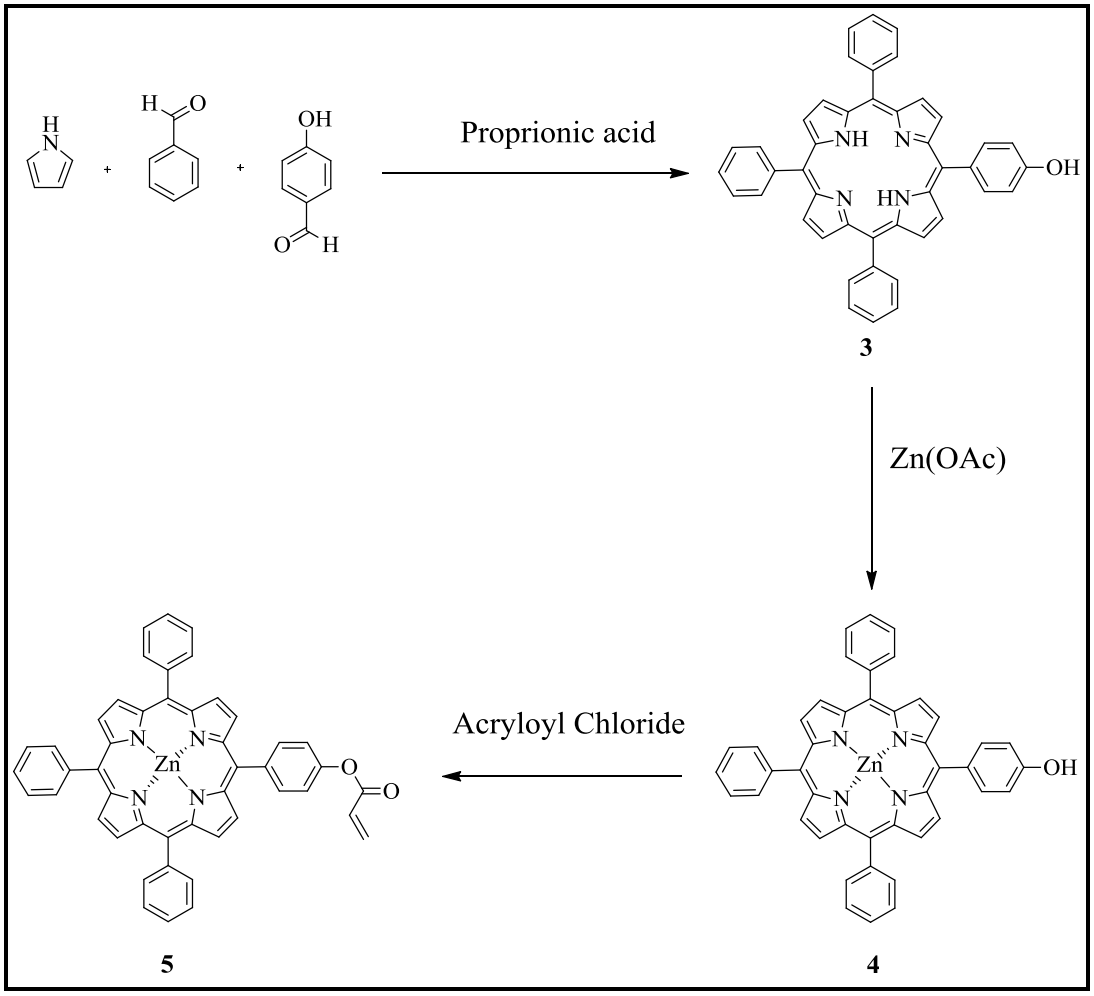

Scheme 2.4: 5-(4-Phenylpropionate)-10,15,20-triphenylporphyrinatozinc synthesis

The monomer [5] was used in the GTP polymerisation technique investigated by Dr. *T.* Georgiou's research group at the University of Hull. Unfortunately, gel permeation chromatography (GPC) data indicated that the monomer did not copolymerise. The GPC supported the hypothesis that only the 2-(dimethylamino)ethyl methacrylate monomer polymerised to form a homopolymer, while the porphyrin compound did not react. This can be attributed to the steric hindrance of the porphyrin molecule. The porphyrin is relatively large and/or may be too close to the acrylamide group, thus interfering with the polymerisation process. Bulky monomer reagents could be expected to take longer to

polymerise. GPC suggested that the reference monomer polymerised but without being copolymerised with the porphyrin monomer.

To facilitate the above unsuccessful copolymerisation reaction, the steps to consider were to increase the length of the link between the functional handle of the porphyrin to enable spacing the steric bulk of the porphyrin further from the polymerisation centre and to perform the reaction over a longer period. However, since the scope of this project was not specifically concerned with optimising this polymer reaction, the reaction was not further persuit. However optimising the above copolymerisation reaction would be an interesting area of future research.

With the aim of synthesising a sterically bulky PS to entrap in the NP matrix, the project was directed towards synthesising a reasonably sterically bulky porphyrin by conjugating a relatively large group onto the porphyrin molecule.

2.4.1 Bulky group incorporation

The attributes of the compound to synthesise were - that it should be water-soluble and have relative steric bulk in order to minimise leaching from the porous polyacrylamide NPs. Thus, as a starting point it was decided to synthesise a PEG substituted porphyrin. PEG can act as if it were 5-10 times as large as a soluble protein of comparable molecular weight[205] (Figure 2.25). PEG is soluble in both organic solvents and aqueous media, is often used to solubilise hydrophobic drug molecules, it typically binds 2-3 water molecules per ethylene oxide molecule and has a high degree of backbone chain flexibility.

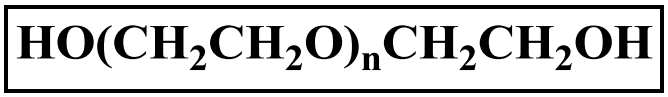

Figure 2.25: Structure of a PEG molecule

In order to couple PEG units to a porphyrin, it was first necessary to identify suitable functionalities on each of the two components. The method of Batinic-Haberle *et al.* (2006)[206] was adopted for this purpose: monomethoxy tri(ethylene glycol) is pre-activated by 4-toluene sulfonyl chloride, converting it to the corresponding tosyl derivative. This activated 4-toluenesulfonic acid 1-(2-(2(-2-methoxy)ethoxy)ethoxy)ethyl ester (TEGTs) [6] can then be coupled with tetrapyridyl porphyrin to obtain 5,10,15,20-tetrakis-(4-*N*-(1-(2-(2-(2-methoxyethoxy)ethoxy)ethyl)pyridiniumyl)porphyrin. To pre-activate the monomethoxy tri(ethyleneglycol) a dry chloroform solution was reacted with 4-

toluenesulfonyl chloride. The solution was stirred at room temperature for 17 hours under nitrogen before toluene was added and the solvents removed *in vacuo*. The residue was dissolved in ethyl acetate and the triethylammonium chloride removed by vacuum filtration, followed by further washing with ethyl acetate, base (sodium hydrogen carbonate solution) and water. The crude oil was separated by flash chromatography and was confirmed as 4-toluenesulfonic acid 1-(2-(2-(2-methoxy)ethoxy) ethoxy)ethyl ester (TEGTs) by ^{1}HNMR, ^{13}CNMR and mass spectrometry (MALDI).

The tosyl activated PEG was then treated with 5,10,15,20-tetrapyridyl porphyrin in dry dimethylformamide to facilitate the conjugation of the PEG to the pyridyl groups of the porphyrin. The reaction (Scheme 2.5) was followed by TLC and after 48 hours was terminated upon consumption of the starting material. Diethylether was added to the reaction mixture and the precipitated solid was washed with methanol.

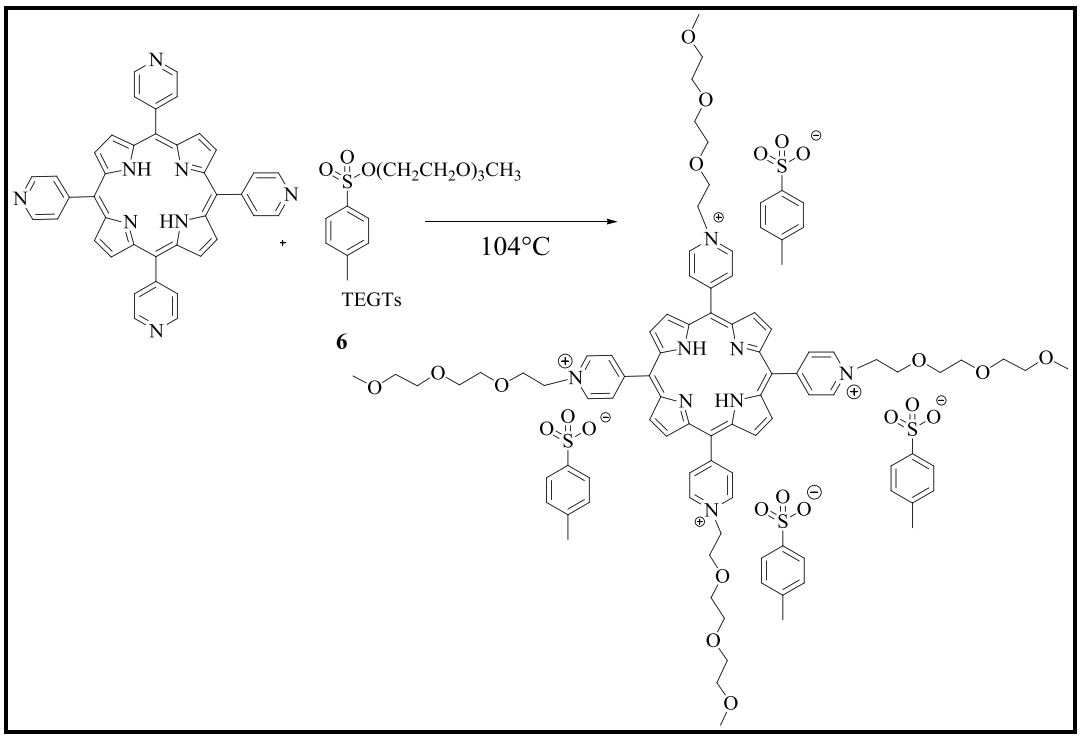

Scheme 2.5: PEGylated porphyrin synthesis

Several attempts were made to purify the product by gel permeation chromatography (LH20) and using a number of different solvents. However, the PEGylated porphyrin remained contaminated with residual tosyl PEG as indicated by ^{1}H NMR.

To this end, 5, 10, 15, 20-tetra-(4-tributylaminomethylphenyl)porphyrin tetrabromide was chosen as the next target molecule and a synthesis was designed based on previously reported work by Hall[207]. This involved using the Adler[201] method to obtain 5,10,15,20-tetra-(4-carbomethoxyphenyl)porphyrin followed by hydride reduction, bromination and finally the Menshutkin reaction with tributylamine (Scheme 2.6).

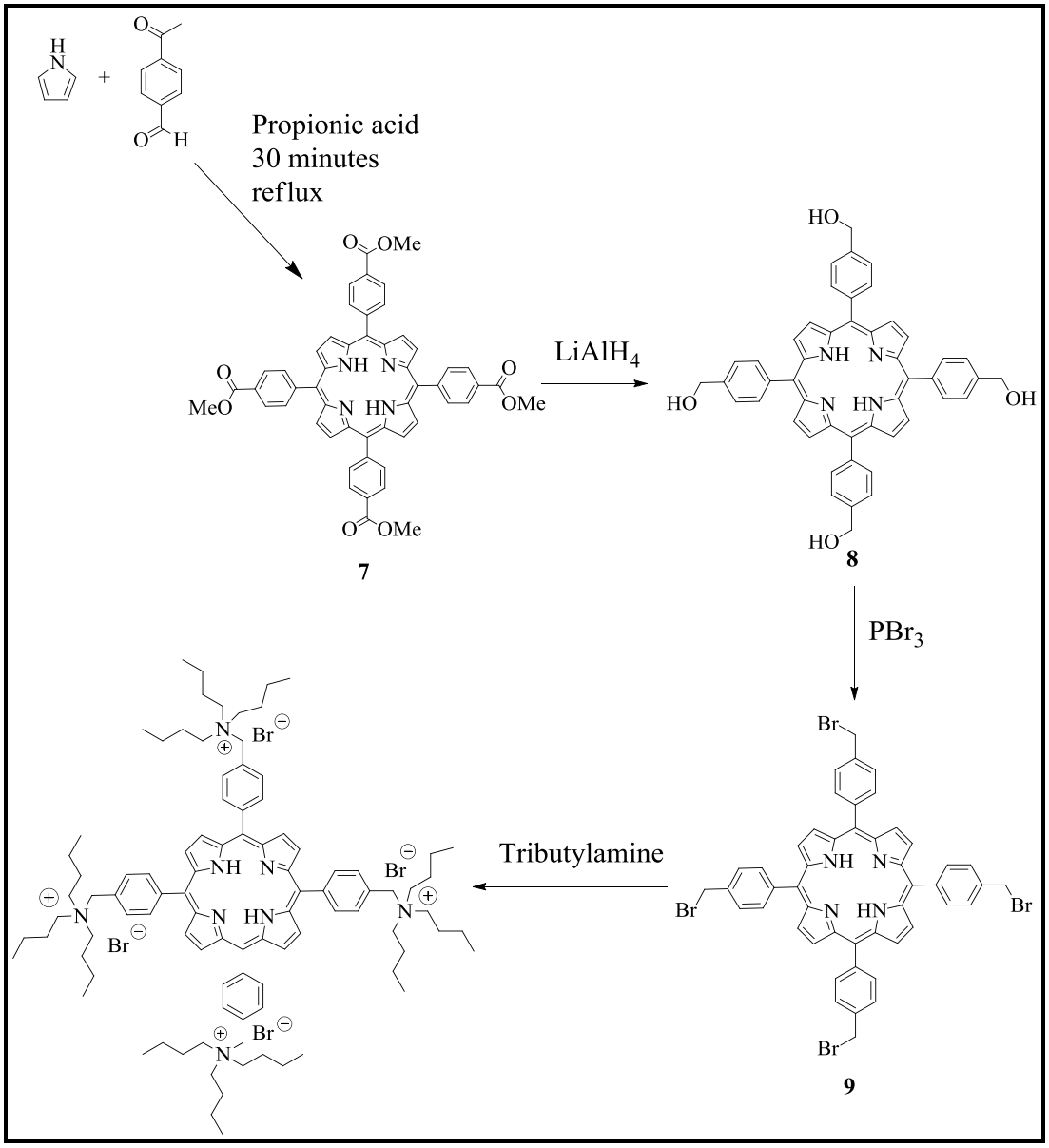

Scheme 2.6: 5, 10, 15, 20-Tetra-(4-tributylaminomethylphenyl)porphyrin tetrabromide synthesis

In the synthesis of 5,10,15,20-tetra-(4-carbomethoxyphenyl)porphyrin**[7]**, pyrrole and methyl-4-formylbenzoate were refluxed in propionic acid for 30 minutes, cooled and filtered. The crude reaction mixture was precipitated with methanol from dichloromethane (DCM) to obtain 5,10,15,20-tetra-(4-carbomethoxyphenyl)porphyrin as a fine purple solid in 22.2% yield. The next step in the synthetic sequence, reduction of the four

carbomethoxy groups to hydroxymethyl groups, proved problematic. The procedure of Datta-Gupta (1966)[208] was attempted.

The reaction was monitored by thin layer chromatography (TLC), however only incomplete reduction resulted. In an attempt to optimise the reaction a variety of conditions were employed which are summarised below:

- As lithium aluminium hydride ($LiAlH_4$) can decompose rapidly due to a number of factors (*i.e.* humidity) the ratio of excess $LiAlH_4$ to porphyrin was altered ranging from 18–200 (18, 31, 112, 115, 118, 200) molar equivalents. However, $LiAlH_4$ used in the experiments was always stored in a desiccator under vacuum.

- To understand whether changing the temperature would optimise the reaction, it was carried out at room temperature, 30°C, 40°C and 60°C (reflux).

- The reaction was also carried out for different lengths of time from 2 hours - 4 days analysing the progress by TLC.

  - 2 hours refluxing; 18 hours at room temperature; 18 hours refluxing; 41 hours at room temperature; 41 hours refluxing

  - 48 hours at room temperature with different $LiAlH_4$: porphyrin equivalents (molar equivalents of 18, 115, and 200)

  - 50 hours at room temperature followed by one hour refluxing;

  - 70 hours at room temperature (both $LiAlH_4$ and porphyrin in tetrahydrofuran (THF) solution and very slow addition of porphyrin in THF to the lithium aluminium hydride solution – so that the $LiAlH_4$ was in excess for porphyrin to react during the addition);

- 96 hours at room temperature

- Solvent alteration: DCM was attempted as a substitute for THF. THF was used in the reaction as $LiAlH_4$ is considered to be stable in THF. However, this solvent was changed due to increased porphyrin solubility in DCM. However, this substitution was also unsuccessful.

- Purification methods:

    - A celite bed was used to absorb the porphyrin followed by methanol: DCM (30:70), water wash and drying with magnesium sulphate.
    - Acid, base, water washes followed by drying with magnesium sulphate.

After several attempts to optimise and purify this porphyrin, the desired product [8] was obtained only once, in extremely low yield (1.2 mg, 1.4%). The conditions used to yield the desired porphyrin were: porphyrin: $LiAlH_4$ ratio - 115; reaction condition - room temperature for 48 hours; purification method - celite bed to absorb the porphyrin followed by methanol: DCM (30:70), washed with water and drying over magnesium sulphate.

5,10,15,20–Tetra-(4-hydroxymethylphenyl)porphyrin was a key intermediate and appeared to be accessible *via* a simple hydride reduction. A possible mechanism for the $LiAlH_4$ reduction relating to the ester reduction is shown in Scheme 2.7. Although, the mechanism appears to be relatively straightforward, stage (d) of the mechanism requires addition of H^+ to complete the reaction. The fact that this intermediate involves complexation of the porphyrin with the aluminium centre, combined with the presence of four reducible groups per porphyrin, suggested that large supramolecular structures may form, which could hinder access to residual carbomethoxy groups. Indeed, reduction of some proportion of the carbomethoxy groups always occurred but driving the reaction to completion, so that

there was no contamination of the tetra-hydroxymethyl product with tri-, di- and mono-reduction products proved impossible. This hypothesis could be a possible explanation for the disappointing reaction results.

It is noteworthy that this particular reaction, which would seem to be useful for gaining access to a variety of tetra-substituted porphyrins, is referred to in only two papers in the literature[208, 209]: Datta-Gupta 1966 and Robic *et al*. 1990.

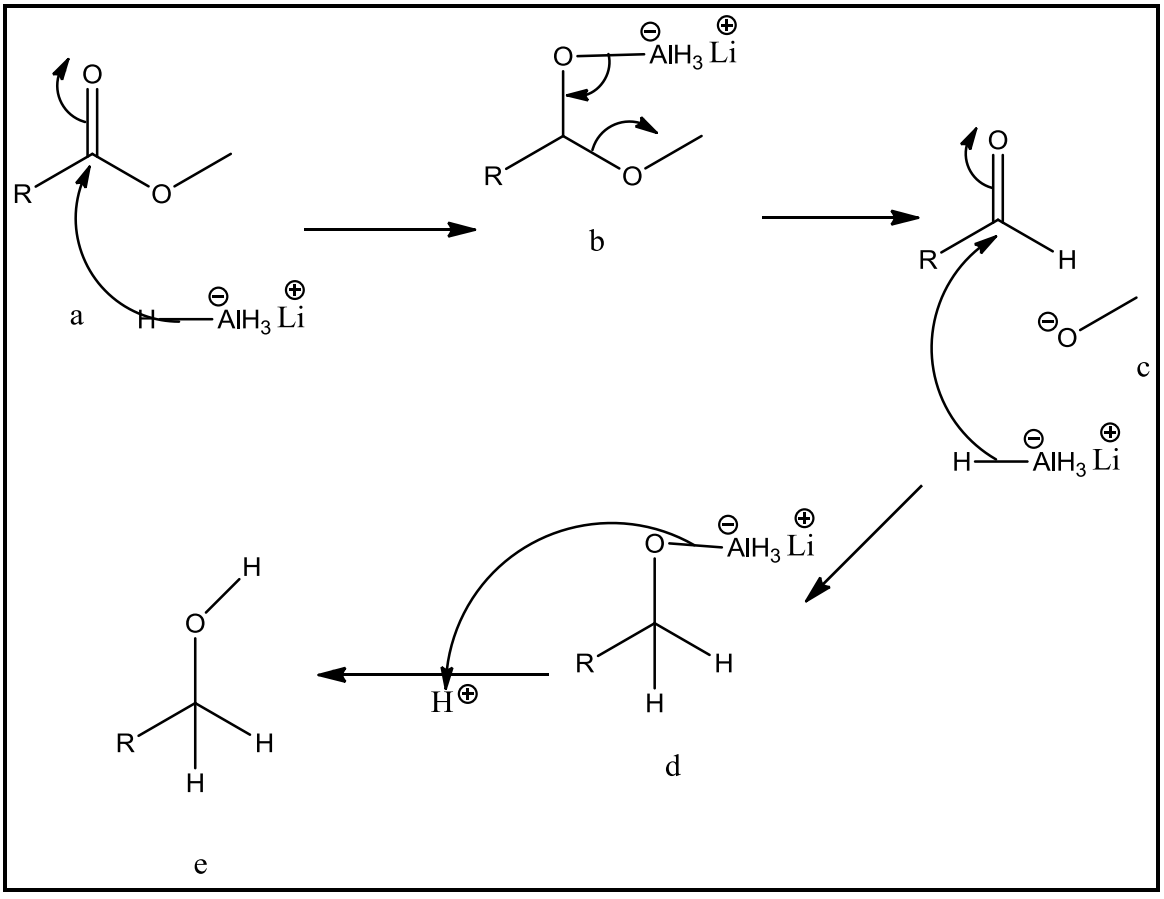

Scheme 2.7: Possible mechanism for the $LiAlH_4$ reduction of the ester

Due to the difficulty in obtaining pure 5,10,15,20-tetra-(4-hydroxymethylphenyl) porphyrin, the next step of the reaction, 5,10,15,20-tetra-(4-bromomethylphenyl) porphyrin [9] was aimed to be synthesised using a procedure found in the literature[210].

Briefly, 4-bromomethylbenzaldehyde and pyrrole were added to a solution of chloroform and after degassing the mixture for 30 minutes, boron trifluoride etherate ($BF_3.OEt_2$) was added and the reaction was allowed to stir at room temperature for an hour. After this period, triethylamine and tetrachlorobenzoquione were added, the temperature was raised and the reaction kept under reflux for 1 hour. The volume of the reaction was then reduced to approximately 250 mL and filtered through a short plug of silica gel. The product was obtained pure after precipitating with methanol over dichloromethane. The solvent was degassed under argon for 30 minutes. TLC (30:70 hexane:DCM). The product was confirmed by ^{1}HNMR, ^{13}CNMR and mass (MALDI) spectroscopy.

In parallel to this experiment, the following 5,10,15,20-tetrakis(2,3,5,6-tetrafluoro-4-{PEG(750)-sulfanyl}-phenyl)-porphyrin (PEG(750)Porphyrin) entrapped NPs was synthesised and observed leaching from the matrix. This observation ruled out taking forward the relatively less bulky 5, 10, 15, 20-tetra-(4-tributylaminomethylphenyl)porphyrin tetrabromide synthesis.

The attachment of a PEG chain with a high molecular weight to a porphyrin could enable to obtain a sterically bulky hydrophilic PS. Thus, the direct attachment of a PEG chain to the porphyrin molecule was explored (Scheme 2.8). A commercially available monomethoxy PEG (750) was first converted to its mono halide form. In the project,

methoxy PEG (average MW=750) chains with a primary bromide (Figure 2.26) was supplied by Dr Ryan E. Mewis, The University of Hull[211].

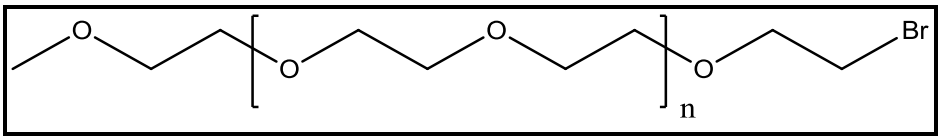

Figure 2.26: Structure of a methoxy PEG (average MW=750) chains with a primary bromide

To briefly outline the procedure: PBr_3 in DCM was added to a monomethoxy capped PEG with an average MW of 750 dissolved in DCM at 0°C over a 30 minutes period and left stirring for one hour. The reaction was quenched with brine, the organic layer separated, washed with brine repeatedly and concentrated *in vacuo* to give PEG(750)Br and was identified by ^{1}HNMR and ^{13}CNMR.

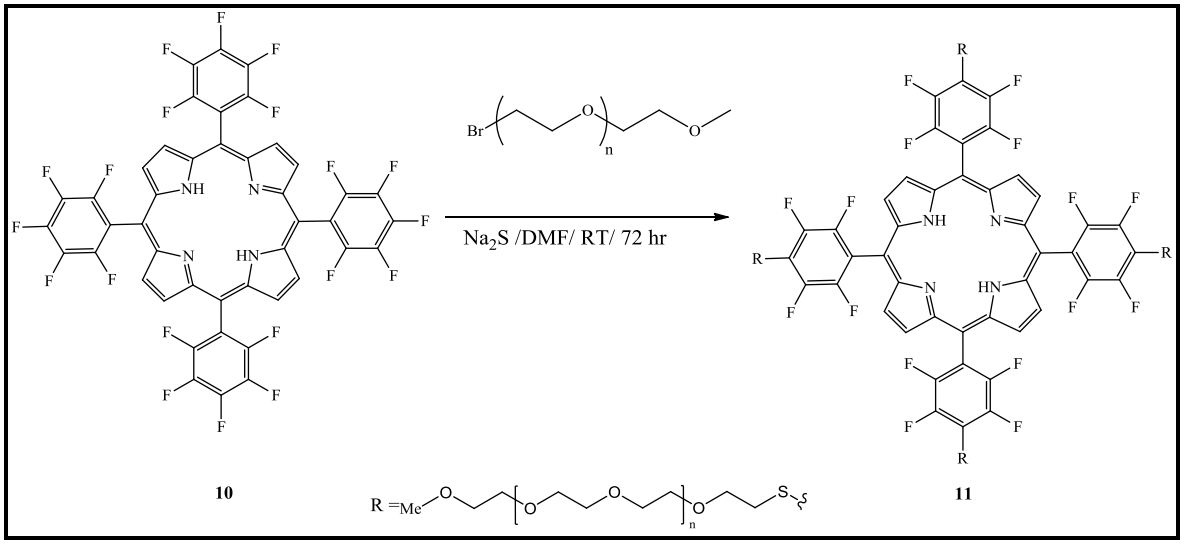

Scheme 2.8: 5,10,15,20-tetra(pentafluorophenyl)porphyrin and monomethoxy PEG (750) reaction

To synthesise 5,10,15,20-tetra(pentafluorophenyl)porphyrin [10] (5FPorphyrin), pyrrole was added drop wise to a refluxing mixture of acetic acid, nitrobenzene and pentafluorobenzaldehyde, refluxing was continued for 45 minutes. Once the mixture had cooled to room temperature, the solvents were removed *in vacuo*. The product was purified by flash chromatography (silica, eluent CH_2Cl_2:C_6H_6 3:7). The next step of the synthesis was to couple the synthesised porphyrin to the PEG(750)Br (Scheme 2.8). The mono-halogeno PEG was reacted with 5,10,15,20-tetra(pentafluorophenyl)porphyrin and sodium sulphide at room temperature until all the starting material was consumed (72 hours), followed by TLC. The reaction mixture was quenched with saturated sodium hydrogen carbonate. The precipitate was recovered by filtration. The filtrate was concentrated *in vacuo* and the resulting violet oil was washed thoroughly with ethanol to yield 5,10,15,20-tetrakis[2,3,5,6-tetrafluoro-4-{PEG(750)-sulfanyl}-phenyl]-porphyrin (PEG(750)Porphyrin) [11]. The porphyrin was characterised by several techniques. ^{1}H NMR confirmed the presence of the desired porphyrin and the PEG groups. Gel permeation chromatography confirmed that the PEG was attached to the porphyrin (eluent hexane). ^{19}F NMR spectra confirmed the substitution of the *para*-fluorine atom: the disappearance of the characteristic resonance of the *para*-fluorine atoms at -150 ppm, *meta*-fluorine atom shift from -160 ppm to -130 ppm and *ortho*-fluorine atoms resonances remaining near -140 ppm. The absorbance (Figure 2.27) and emission spectra (Figure 2.28) of the porphyrin before and after conjugation further confirmed the presence of the porphyrin in both instances.

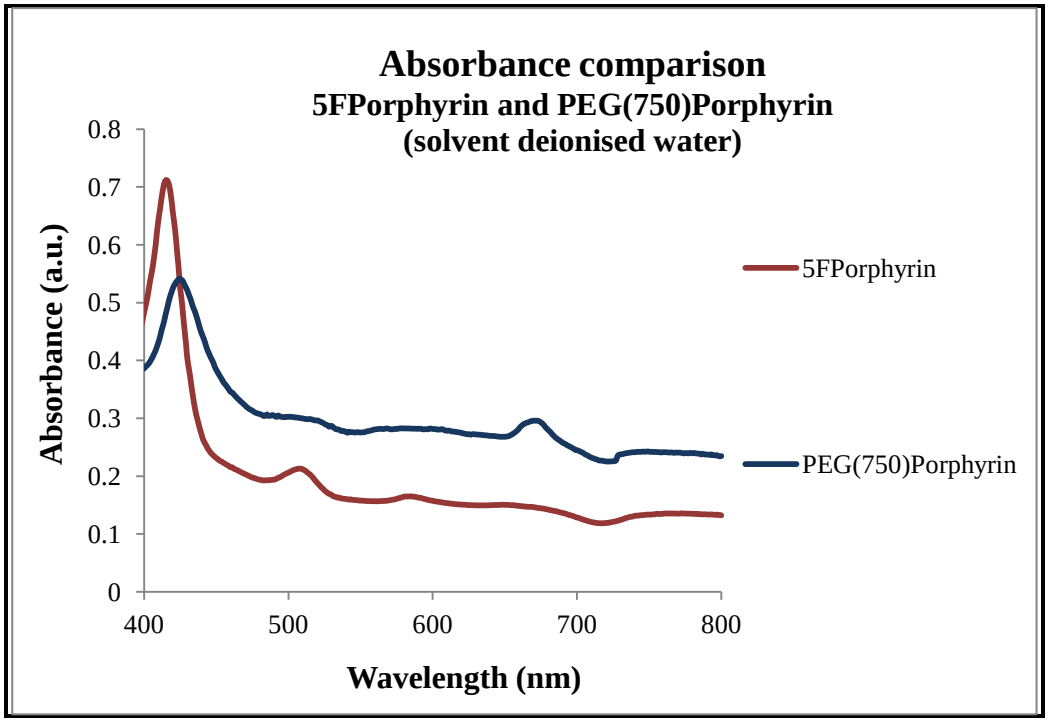

Figure 2.27: 5FPorphyrin and PEG(750)Porphyrin - absorbance spectra comparison

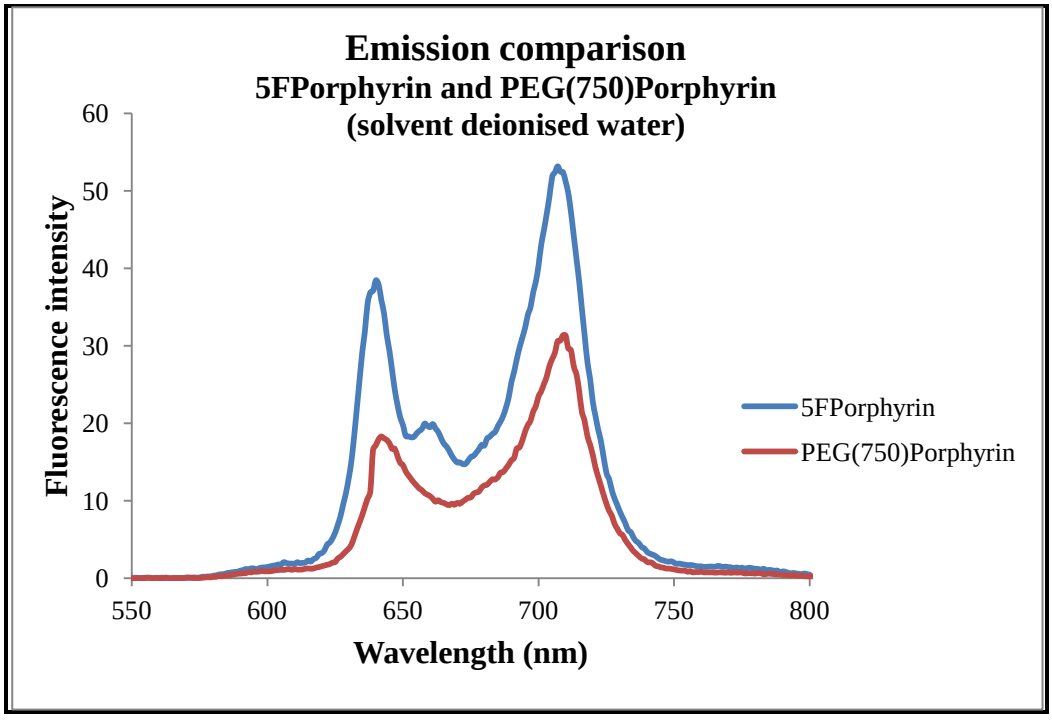

Figure 2.28: 5FPorphyrin and PEG(750)Porphyrin - emission spectra comparison

The successfully synthesised PEG(750)Porphyrin was then entrapped inside the polyacrylamide NPs [27]. In synthesising the NPs an aliquot (100 μL, 1.3 mmoldm^{-3}) of a solution of PEG(750)Porphyrin (5 mg, 1.3 μmol) in water (1 mL) was added along with the monomers to the NP reaction mixture (Scheme 2.2) to obtain polyacrylamide particles (Z_{ave}) 37 nm (Figure 2.29).

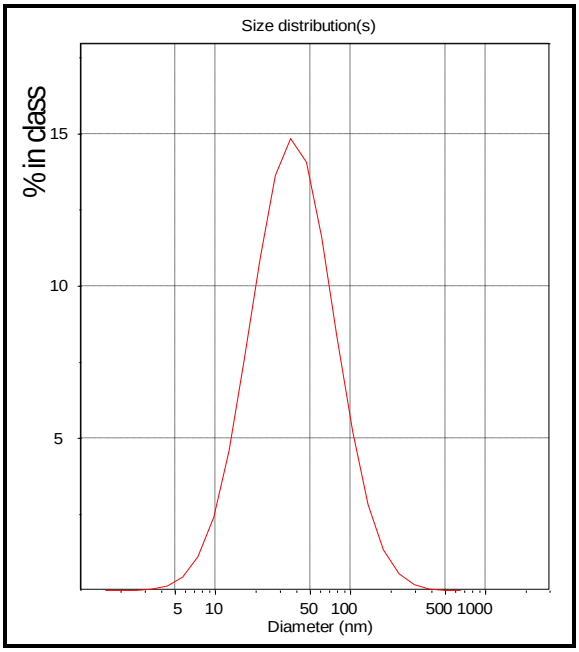

Figure 2.29: Size distribution of PEG(750)Porphyrin encapsulated NPs

The characteristic absorbance (Figure 2.30) and emission peaks (Figure 2.31) confirmed the presence of PEG(750)Porphyrin in the NPs.

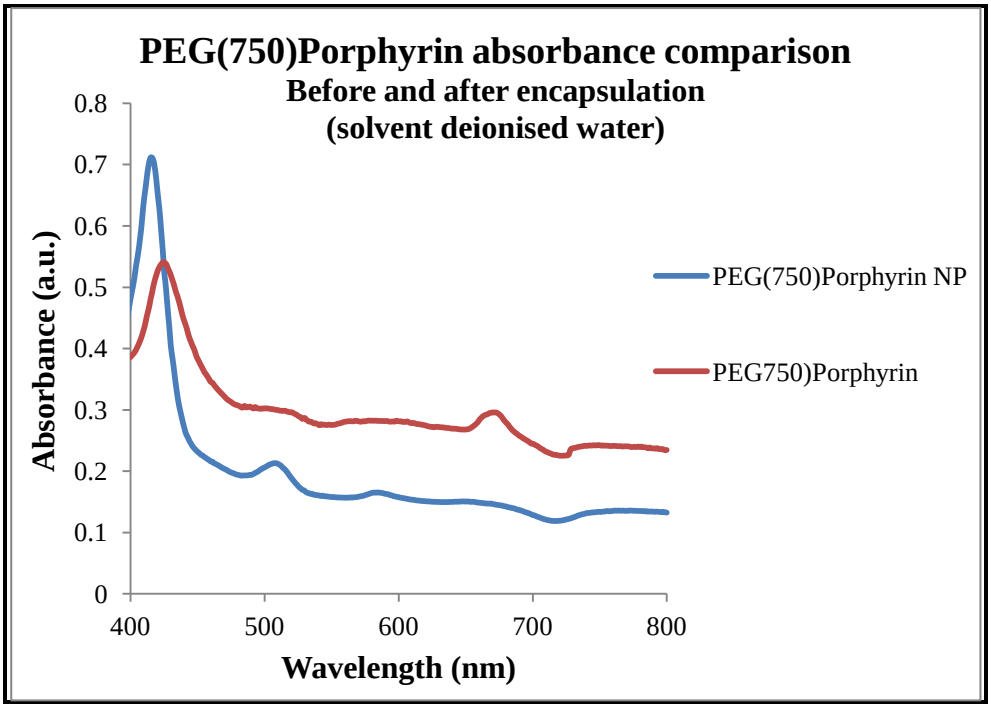

Figure 2.30: PEG(750)Porphyrin before and after encapsulation - absorbance spectra comparison

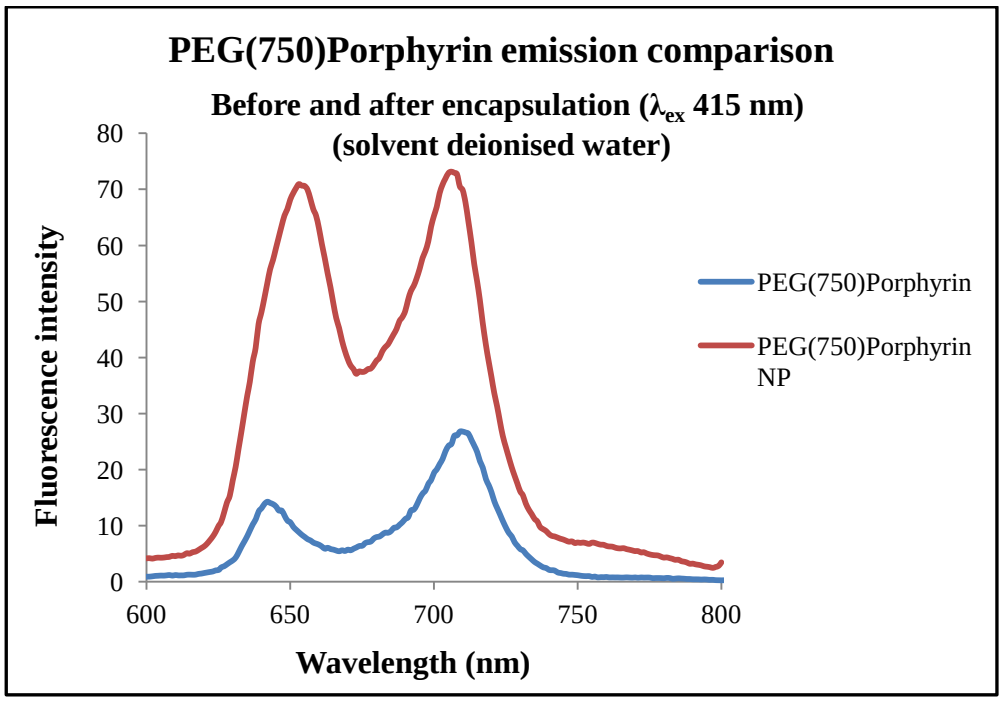

Figure 2.31: PEG(750)Porphyrin before and after encapsulation - emission spectra comparison

The calibration "straight" line for PEG(750)Porphyrin was plotted using the absorbance at 410 nm and known concentrations of the porphyrin (solvent deionised water) (Figure 2.32).

This calibration "straight" line was then used in quantifying the approximate concentrations of PEG(750)Porphyrin present in a pre-determined weight of NPs (*i.e.* 1 mg) in 1 mL of H_2O by measuring its absorbance. The concentration of PEG(750)Porphyrin per 1 mg of NPs in 1 mL of H_2O was 0.34 $\mu moldm^{-3}$.

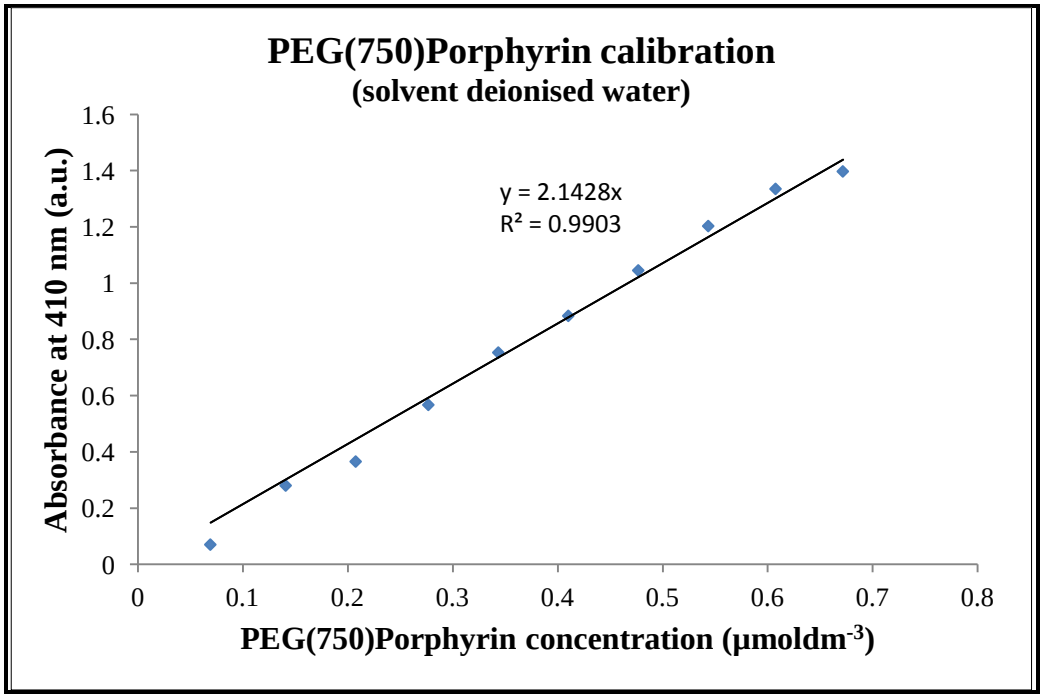

Figure 2.32: PEG(750)Porphyrin calibration "straight" line

Leaching of the synthesised porphyrin NP was studied using fluorescence spectroscopy. This technique was used due to its high sensitivity (approximately 1000 times more than absorption spectroscopy). In the experiment, hourly, three 2 mL aliquots were drawn from the suspension (200 mg of NPs in 80 mL MilliQ water), the NPs were microfiltered and

the supernatant was analysed by fluorescence microscopy over 24 hours. Maximum leaching of the porphyrin from the NPs peaked at 2 hours (Figure 2.33) and the level of fluorescence increased with the time. The relatively high increase within the first three hours may suggest that the majority of loosely trapped porphyrin molecules are 'removed' from the nanoparticle suspension within this time.

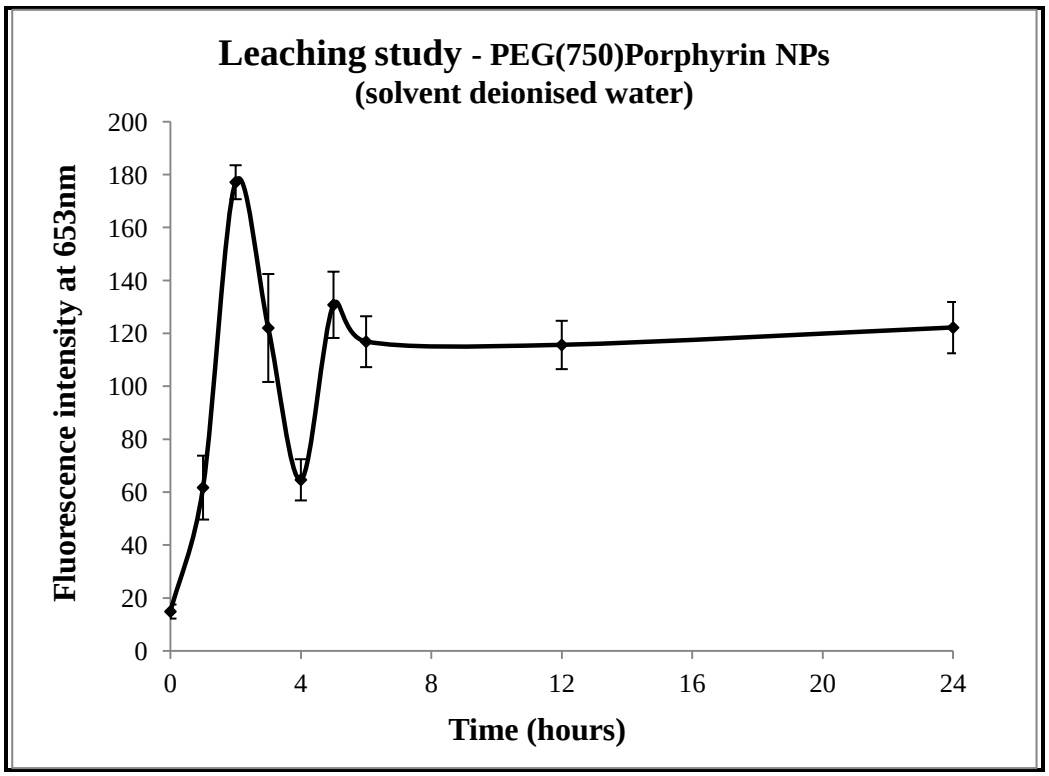

Figure 2.33: Leaching study of PEG(750)Porphyrin NPs

Since the PEG(750)Porphyrin (MW~3900) leached from the matrix, minimising leaching was addressed by an approach that relies on an increase in the overall (MW 10,000) size to retain the dye conjugates within the matrix: the incorporation of dextran conjugated dyes. This approach is limited by the number of commercially available dyes.

Following this initiative, as a useful bulky standard in the project, a NP system loaded with a commercial fluorescent probe, fluorescein conjugated to a dextran polymer (MW 10,000 Da) was designed. To synthesise the fluorescent NPs [29] the same synthetic method was followed as used in the production of acrylamide NPs, with the exception of the monomer phase. An aliquot (100 μL, 50 mmoldm^{-3}) of a solution of fluorescein conjugated to a dextran polymer (MW 10,000 Da) (5 mg, 50 μmol) in water (1 mL) was added to the hexane solution along with the monomers. Size (z_{ave}) 46 nm, emission 520 nm (λ_{ex} = 480 nm). The NPs containing the dextran-fluorescein conjugate were then used in initial investigations of leaching of bulky chromophores from NPs. The data from the leaching experiment can be seen in Figure 2.34. The sterically bulky dyes minimised leaching from the particles, however leaching was not completely suppressed. In the first 4 hours NPs clearly leach fluorescein. This could be due to the presence of surface bound fluorescein dextran which has leached from the complex polymeric matrix.

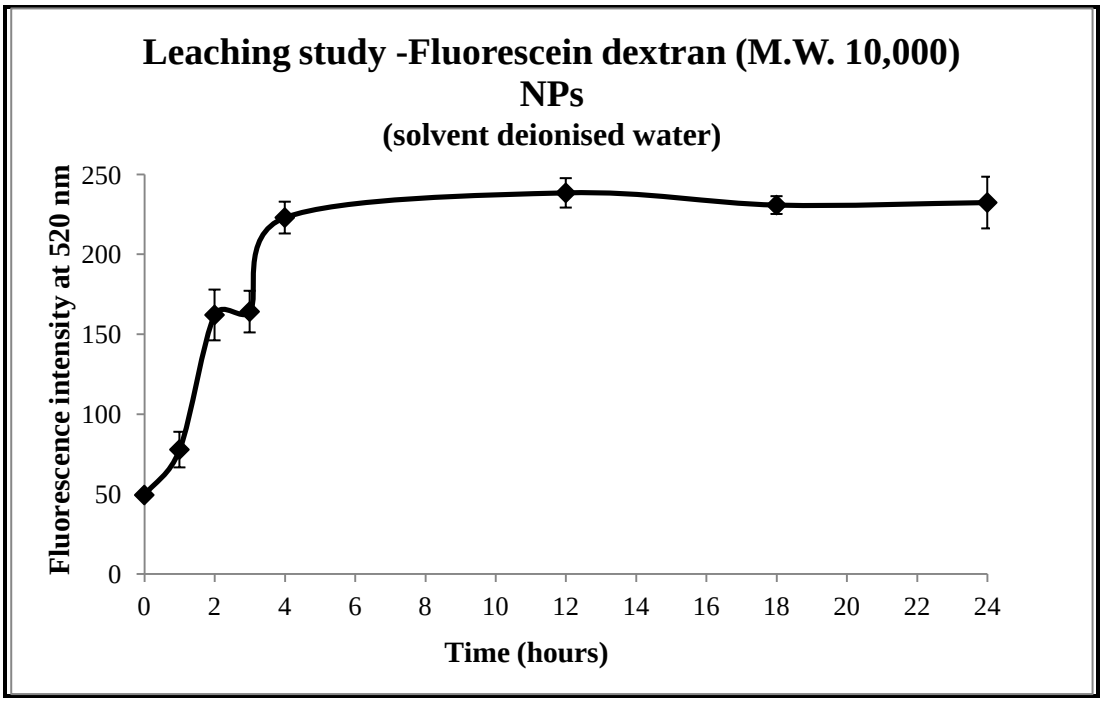

Figure 2.34: Leaching study of fluorescein dextran (M.W. 10,000) NPs

One of the main aims of the project was to study the activity of PS encapsulated NPs that have minimal or no PS leaching. Following from the dextran (MW 10,000 Da) fluorescein entrapped NPs it was decided to synthesise a variety of sterically bulky and linker anchored PSs suitable for incorporation into NPs. Initially, it was proposed to attach a PS (a phthalocyanine) to a soluble anchor, such that the size of the dye conjugate would be increased, preventing/minimising leaching from the NP structure.

Phthalocyanines can be excited *via* visible light with wavelengths higher than 630 nm and can effect a deeper penetration into the tissue and eradication of larger tumours[212]. However since the size of a phthalocyanine is approximately the same as porphyrin and since it is now established that porphyrins do leach (Figure 2.24 and Figure 2.33) from the polyacrylamide NPs it was decided to conjugate a phthalocyanine molecule to a high molecular weight polylysine.

The AlPC-tetrasulfonyl chloride reaction with 6-aminohexanoic acid published by Brasseur *et al.*[213] was adopted to synthesise the MW 15,000-30,000 polylysine conjugated aluminium phthalocyanine (POLPC) [12] (Scheme 2.9). In the reaction Al-phthalocyanine chloride, tetrasulfonic acid and chlorosulfonic acid was stirred at 100°C for 3 hours, followed by the addition of thionyl chloride. The reaction mixture was allowed to stir at 80°C for 2 hours. Once cooled to room temperature the solution was poured onto ice and the product was collected by centrifugation followed by filtration. The recovered product, Al phthalocyanine tetrasulfonyl chloride (PC), was concentrated *in vacuo* and added, in small portions, to a solution of MW 15,000-30,000 poly-D-lysine (4 equivalents) and

sodium carbonate in water. The solution was agitated (Vortex®) for 1 minute after each addition.

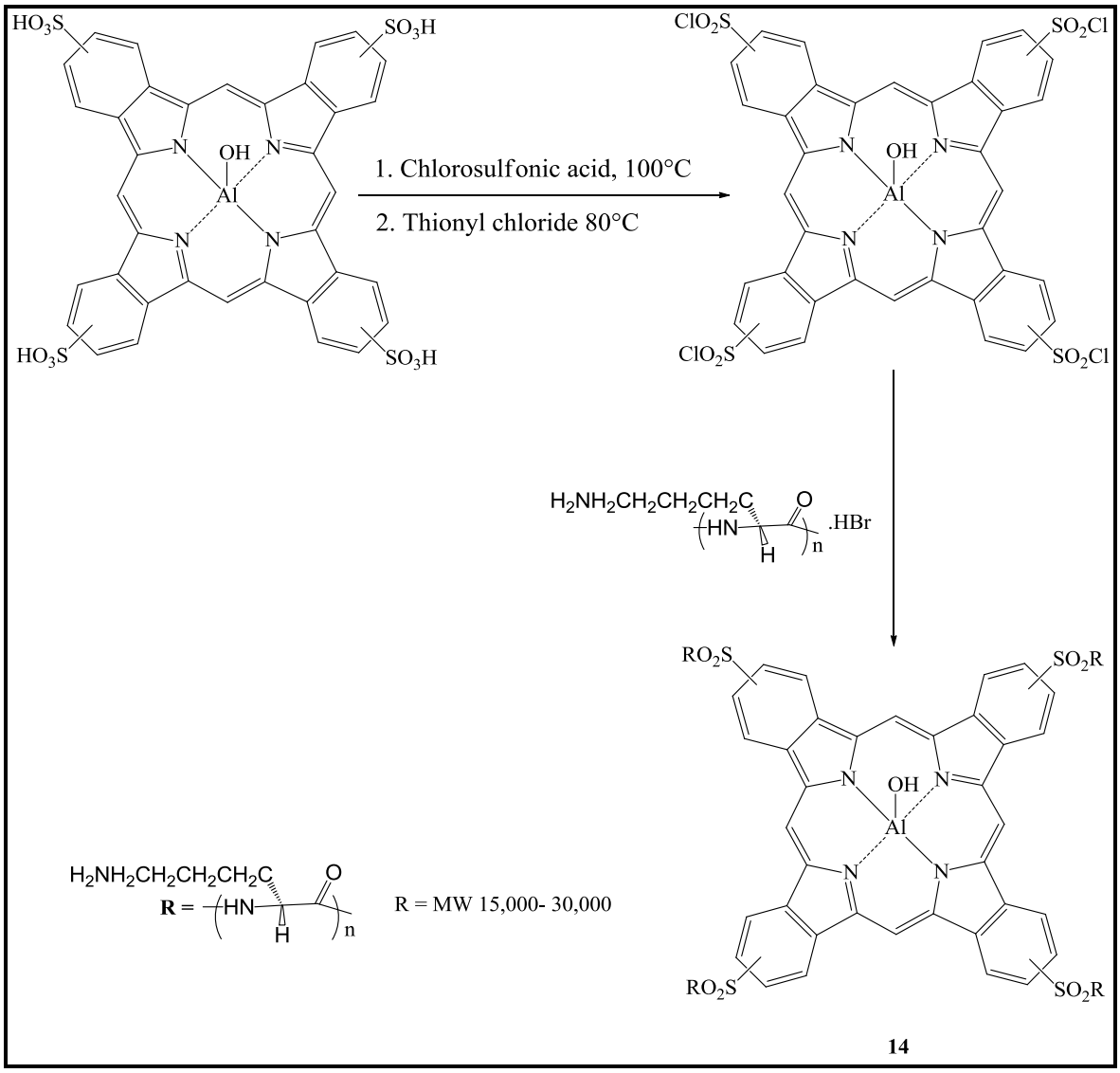

Scheme 2.9: Polylysine conjugated Al-phthalocyanine (POLPC) reaction

The dispersion was dialysed against PBS buffer using ultra membrane filters (MWCO 14,000) over 4 days to remove any unconjugated PC. The absorbance and emission spectra of the POLPC confirmed the presence of the phthalocyanine after conjugation (Figure 2.35).

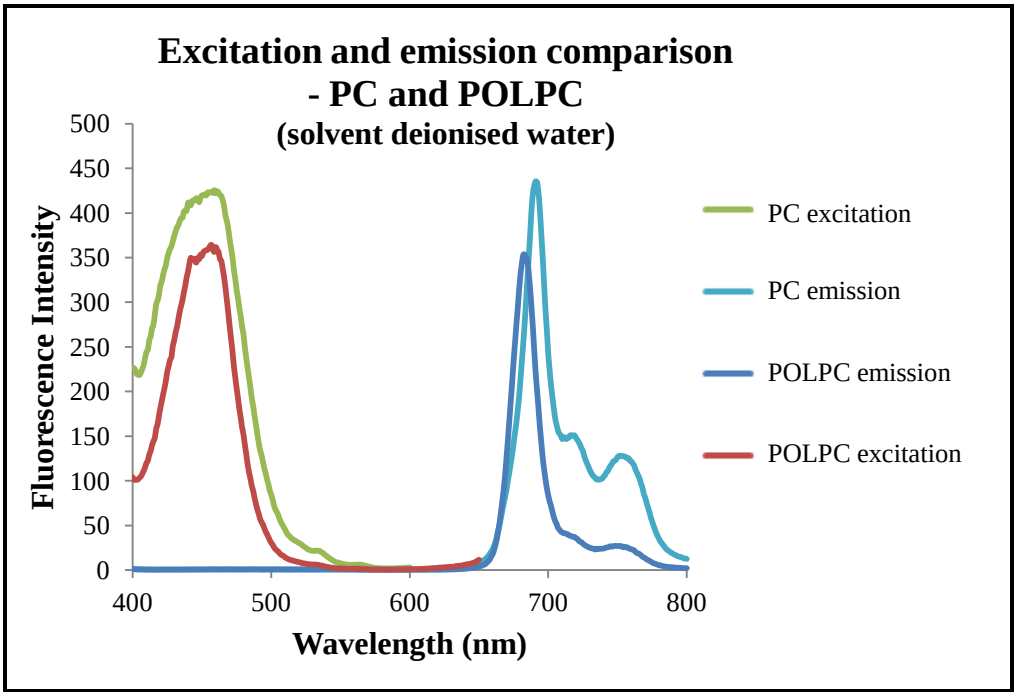

Figure 2.35: PC and POLPC excitation and emission spectra comparison

The synthesised POLPC were then entrapped in polyacrylamide NPs (PCNPs) [30] using the described method. The absorbance and emission spectra confirmed that the POLPC is entrapped intact within the nanoparticle matrix (Figure 2.36 and Figure 2.37). It should be noted that all the nanoparticle suspensions were prepared in deionised water and filtered through a Millex® GP, 0.22 µm filter unit prior to any preliminary characterisations or secondary experiments unless stated otherwise.

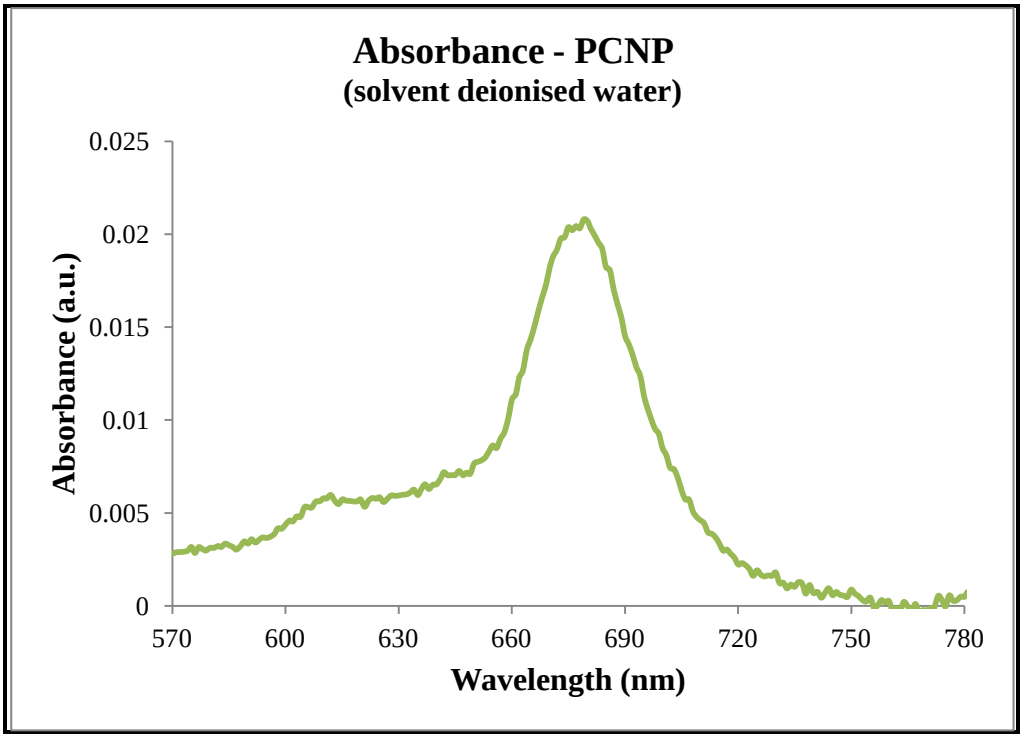

Figure 2.36: Absorbance spectrum of PCNP

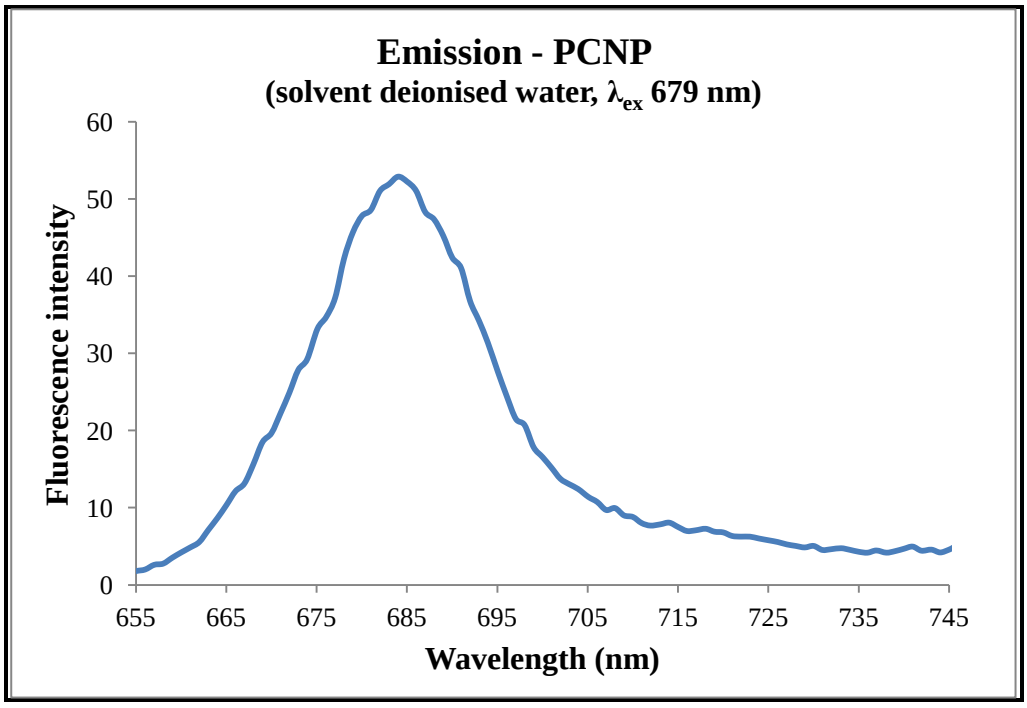

Figure 2.37: Emission spectrum of PCNP

The mean particle size, 45 (±10 nm) was determined by PCS and TEM images (Figure 2.38).

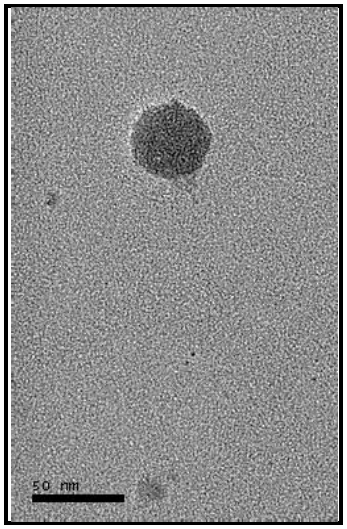

Figure 2.38: TEM image of a PCNP

Leaching of the PCNP was studied using fluorescence spectroscopy. In the experiment, three 2 mL aliquots (hourly) were drawn from the suspension (200 mg of NPs in 80 mL MilliQ water), the NPs were microfiltered and the supernatant was analysed by fluorescence microscopy. Maximum leaching of the POLPC (MW 15,000 – 30,000) from the NPs peaked at 3 hours (Figure 2.39) and the level of fluorescence remained the same. Interestingly, this is very similar to results obtained with the MW 10,000 dextran fluorescein conjugate encapsulated in the same NPs. This may suggest that the majority of loosely trapped POLPC molecules are 'removed' from the nanoparticle suspension within this time. The fluorescence intensity of the filtrate dropped slowly between 3-24 hours. Thus, it can be hypothesised that no further leaching occurred after the first three hours. The slight drop in the fluorescence level of the filtrate after three hours could be due to photobleaching due to the much smaller concentration of fluorescent material (POLPC) in the filtrate.

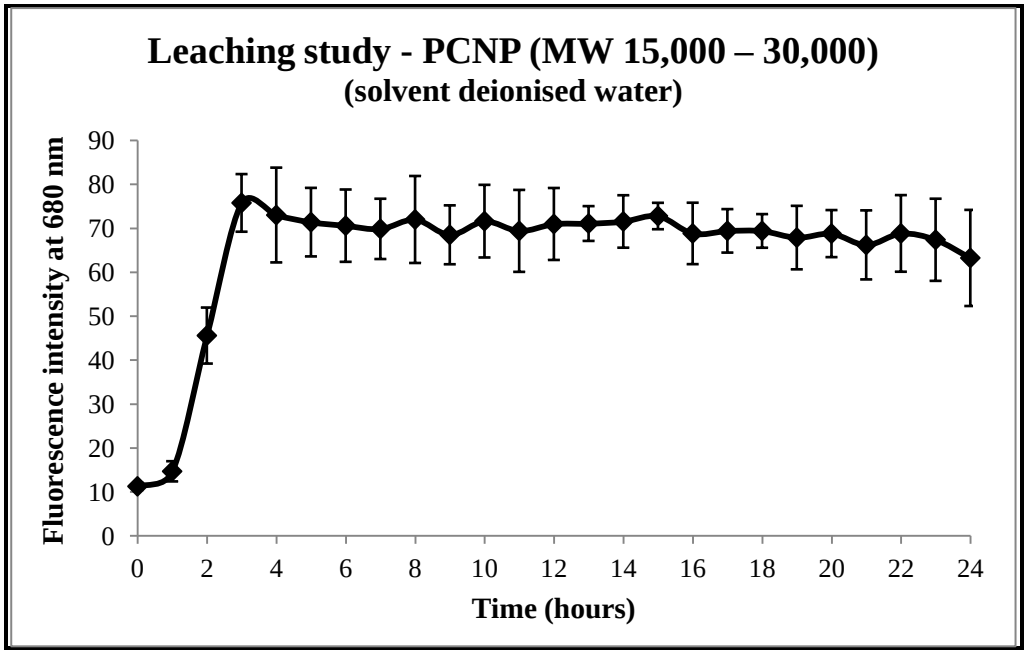

Figure 2.39: Leaching study of PCNPs (MW 15,000 – 30,000)

The concentration of the entrapped PC was quantified using the Beer-Lambert law and the reported molar extinction co-efficient (ε) 1.5 x 10^5 $M^{-1}cm^{-1}$ (for Al-Pc calculated from absorbance at 666 nm)[214] and was found to be 0.41 µmoldm^{-3} per 1 mg of PCNPs (MW 15,000 – 30,000) (ST DEV 3.5 x 10^{-8} moldm^{-3} (within 20%)). However, as the maximum absorbance of the PC used in the project was 680 nm, it was considered important to confirm the concentrations using a PC calibration "straight" line plotted against the absorbance at 680nm and known concentrations of the phthalocyanine (Figure 2.40). The approximate concentration of PC present per 1 mg of NPs in 1 mL obtained using the calibration "straight" line was 0.36 µmoldm^{-3}. This was within the standard deviation expected above.

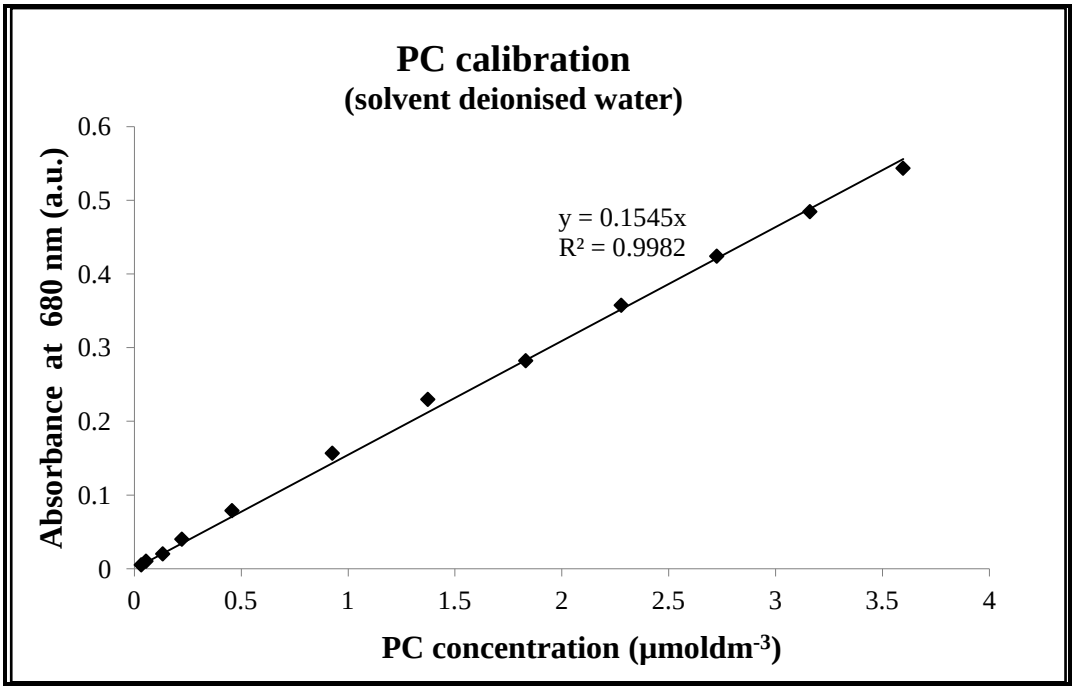

Figure 2.40: PC calibration "straight" line

2.5 Biofilms

Although the main focus of the project was to fully entrap dyes in NP matrix, slow release of PSs from NPs is known to be useful in many applications, mainly in PACT[215]. Thus having successfully entrapped the MB in NPs and quantifying the leachate, the project focused on *in-vitro* bacterial assay development, in order to study the possibility of using MB entrapped NPs in PACT.

There has been a variety of research carried out on the ability of NPs to circumvent antibacterial resistance over the years, primarily focusing on issues such as antibacterial drug uptake and altered drug targets[215, 216]. Unfortunately, to date these trials have not been successfully carried through to the clinic. This drew our attention to analysing the mode of action of nanoparticles in biofilms (models of bacterially infected wounds). Biofilm studies were undertaken in collaboration with Professor M. Wilson and his group at University College, London (UCL).

Biofilms are colonies of micro-organisms (single or multiple microbial species) growing in a polymeric matrix. The reason for bacterial resistance in biofilms is rather uncertain[217] however inefficient penetration and distribution of antibacterial agents is likely to be a significant factor. It was interesting to determine whether NP delivery could enhance the delivery of therapeutic agents into biofilms.

Fluorescein conjugated to a dextran polymer (M.W. 10,000 Da) entrapped within the NPs [29] were sent to Professor Wilson's research group to observe whether the NPs were able to penetrate through the biofilms. The observations were made using laser scanning confocal fluorescence microscopy (LSCM). Biofilms were grown in 6 microtitre plates.

Dextran fluorescein entrapped NPs were then incubated with the biofilm for one hour. Confocal images were taken from above and from the side of the film (side of the well) and *z*-series acquired from top to bottom of the film (Figure 2.41 and Figure 2.42). In the figures the fluorescence is produced by NPs in the biofilm.

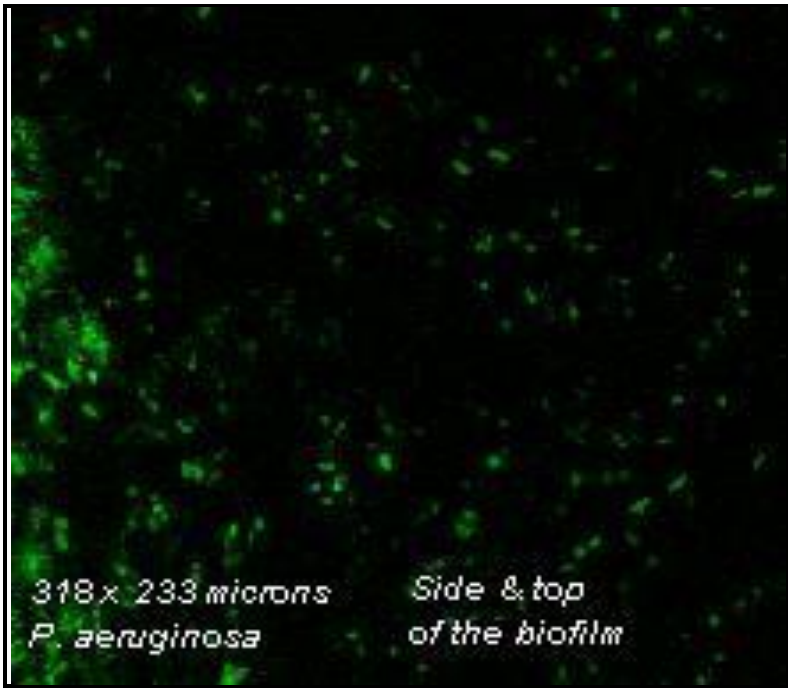

Figure 2.41: LSCM image of the biofilm from side and top

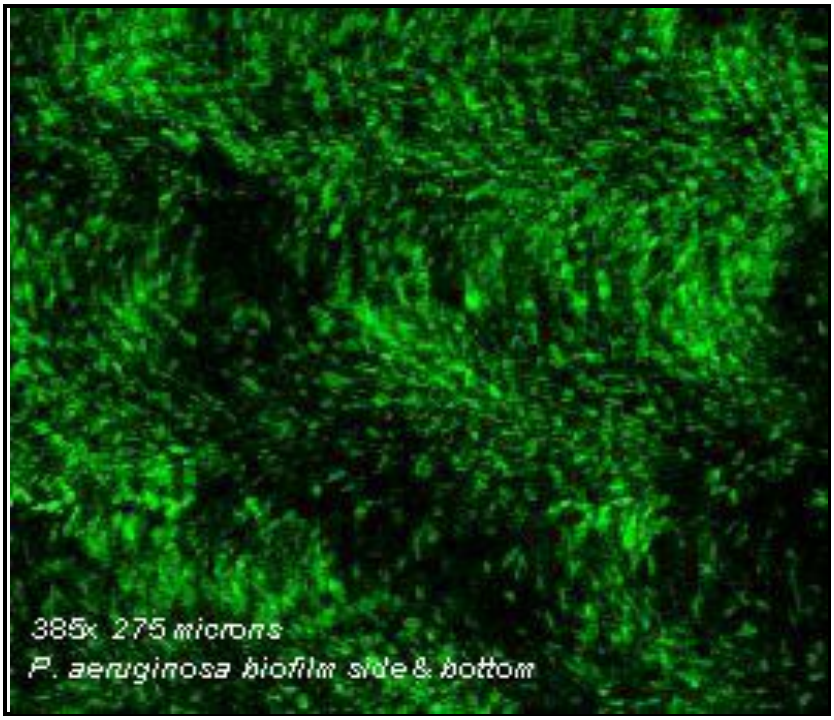

Figure 2.42: LSCM image of the biofilm from side and bottom

The images confirmed that the NPs do indeed penetrate through the biofilms to the bottom of the well. With this discovery the next step of the project was to use MB NPs in biofilms to use in PACT studies.

Prior to using MB NPs in PACT assays, a primary bacteria assay used a Gram negative and Gram positive bacteria with free MB. To this end, *Staphylococcus aureus* and *Staphylococcus epidermis* (Gram positive) and *Pseudomonas aeruginosa* and *Escherichia coli* (Gram negative) bacteria were chosen as the primary bacteria assay. Bacteria cultures were obtained from Dr. T.Paget's group at the Medway School of Pharmacy (Kent University).

2.6 Bacterial assays

The initial protocol consisted of two 96 well plates: dark control and light control. Two organisms were assayed on one plate and the detailed protocol can be found in 5.4.7 (Figure 2.43).

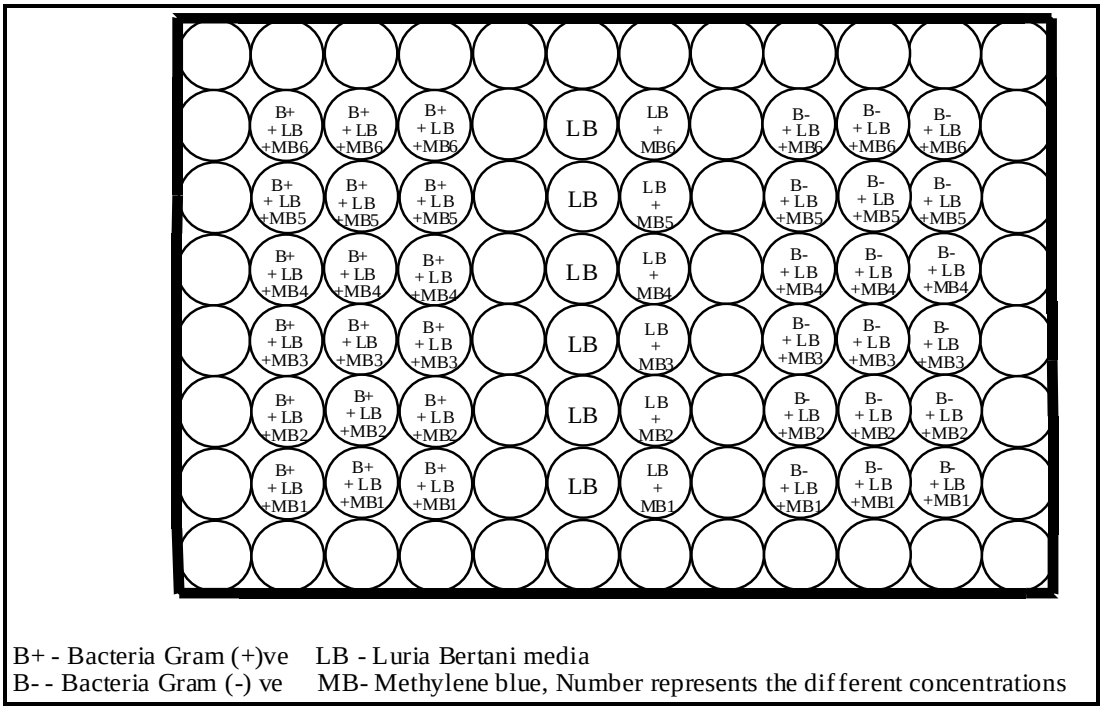

Figure 2.43: Schematic diagram of the 96 well plate in relation to general bacteria protocol

Briefly, overnight bacteria culture was added to each well of a 96 conical well plate followed by MB in distilled water and Luria-Bertani (LB) media. The cultures were incubated at 37°C, in an atmosphere of 5% CO_2 in a humidified shaker incubator. The plates were centrifuged, the supernatant was removed and fresh LB added. The pellets (cells) were thawed and transferred to a flat bottom 96 well plate. The light controlled assay was irradiated with red light (40 J/cm^2) and incubated for 30 minutes with shaking. The sample was irradiated (40 J/cm^2) again and incubated at 37°C, in an atmosphere of 5%

CO_2 in a humidified shaker incubator overnight. The dark controlled assay culture was transferred to a flat bottom well plate and was also incubated at 37°C in an atmosphere of 5% CO_2 in a humidified shaker incubator.

Following the overnight incubation period, the absorbance of each well was taken at 630 nm using a microtitre plate reader. 630 nm is considered one of the most appropriate wavelengths to measure the turbidity caused by bacteria to minimize absorbance by the medium because most bacterial growth media are brown or brownish-yellow. This was followed by a CellTiter 96® aqueous non-radioactive cell proliferation assay: 20 µL of MTS/PMS combined reagent was added to the wells, incubated for 1-4 hours and the absorbance of the samples read by a micropipette reader.

CellTiter 96® aqueous non-radioactive cell proliferation assay[218] is a colorimetric method that determines mammalian cell survival and proliferation. The reagents used in the assay are 3-(4,5-dimethyl thiazol-2-yl)-5-(3-carboxymethoxyphenyl)-2-(4-sulfophenyl)-2H-tetrazolium inner salt: MTS and an electronic coupling reagent (phenazine methosulfate, PMS).

The cells reduce MTS into formazan which is soluble in tissue culture medium (Scheme 2.10). Hence, this method can be used to measure the cytotoxicity, proliferation or activation of cells. The absorbance of formazan is measured at 490 nm and consequently can be read using a micropipette reader. The quantity of formazan produced is directly proportional to the number of living cells in culture.

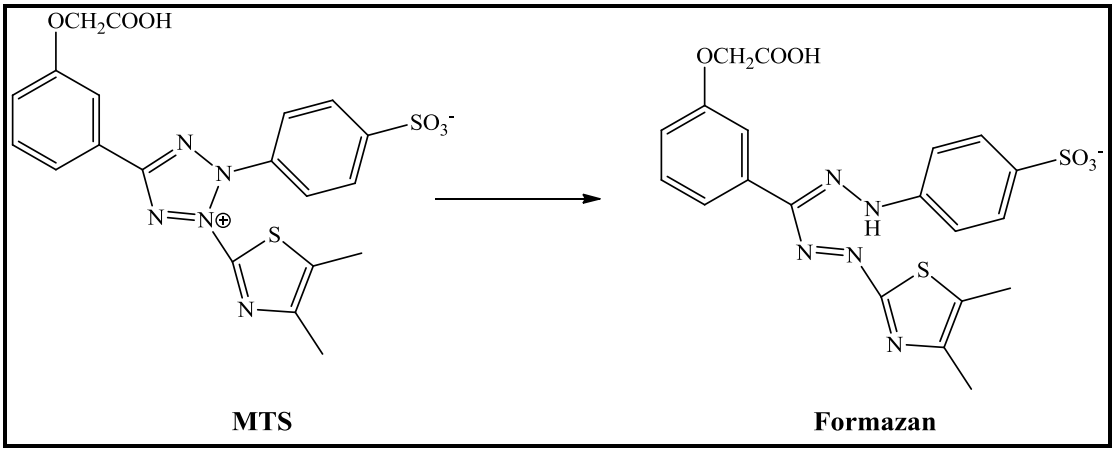

Scheme 2.10: MTS conversion to formazan in the MTS assay

The MTS assay is capable of providing quick[219] results and doesn't include any radio-isotopes that are typically used in killing assays or washing steps. The above protocol was repeated 3-5 times using the described conditions and parameters. The assays were prepared in triplicates. Unfortunately, no significant differences between the dark and light controls were observed with any of the organisms used. Hence, the protocol needed optimising.

Generally, in a bacteria assay post-PDT treatment, the bacteria culture needs incubating over night before the absorbance of the system is measured. Further, in measuring absorbance, to avoid any false readings, the turbidity of the culture should be at a low level, even at 100% growth (bacteria on its own in culture, without PS). Usacheva *et al.* have demonstrated due to scattering effects how the absorbance peak of MB (both at 631 and 665 nm) progressively decreased, reached a minimum and began to rise again when high concentrations of Gram-negative bacteria [more than 10^9 CFU/ml (colonies on the plate)] were added to the dye solutions[220]. Hence, before optimising the protocol it was

important to determine the bacteria concentration in the media that would be suitable for measuring absorbance.

The light doses used to irradiate the culture were varied according to the light source and PS concentration chosen. The light sources used were Omnilux® EL1000A with a wavelength of 633 ±3 nm and Oriel Model 66188 wavelength set from 550 to 2000 nm. In PDT treatments it is important to achieve a balance between the PS concentrations, light dosage and the light source. Further, the chosen PS, MB, can behave differently under certain circumstances, such as increasing dye concentration, presence of anionic polymers (chromotropes) or inorganic salts. In short, MB is a methacrymatic dye - appears different colours depending upon the wavelength of light under which they are viewed which results in different spectra. Generally, the accepted criteria for these changes (metachromasy effect) are a shift in the absorption maximum of the dye to a shorter wavelength (hypsochromic effect) and a decrease in its molar absorbance at the long wavelength absorption maximum (hypochromic effect)[220]. This is due to electrostatic and hydrophobic interactions between the dye molecules and the nearest partner and the interaction of the π-electrons between adjacent dye molecules. These interactions result in dye aggregation, which in some cases is restricted to dimerisation[221]: the process by which two molecules of the same chemical composition form a condensation product or polymer. Usacheva[220] *et al.* established that the spectral behaviour of increasing concentrations of MB was due to these metachromatic effects and was caused by the increase in dye concentration. The effect on MB in distilled water results in an enhancement of the dye dimerisation with increased concentrations[221]. Furthermore, it has suggested that low-level light irradiation may proliferate cell growth under certain conditions during a set of photochemical reactions, this is referred to as biostimulation[222]. However, phototoxic inhibitory reactions,

post-irradiation of natural or artificially inoculated cells, are possible with the appropriate dosage of light. Hence, it was vital to determine the appropriate light and dosage to stimulate a phototoxic effect using MB.

Further, the incubation time of a bacteria culture loaded with a PS is a significant factor. Additionally, the cell washing step is an important one in photodynamic experiments to remove any unbound PS from the bacteria wall in order to avoid any false positives. Bacterial organisms were tested to confirm their identity using several tests. Gram positive and Gram negative bacteria are differentiated according to a particular staining procedure. The technique was developed by Christian Gram, a Danish bacteriologist in the 1800's. The Gram stain protocol involves the application of a series of dyes. The detailed procedure is as described below. The dyes stain some bacteria purple (Gram-positive) and others pink (Gram-negative). In a Gram-staining test Gram-positive bacteria retain the blue-violet colour in the test (crystal violet dye) contrasting to Gram-negative bacteria, which does not retain the colour.

For the staining test (Table 2.2) a heat-fixed bacteria smear was prepared. A clean microscope slide was passed through a Bunsen flame twice to ensure that the slide was free of grease and contamination. A small sample of overnight bacteria was mixed with a drop of distilled water and placed in the middle of the slide. Once the sample was air dried (using a forceps to minimise contamination) the slide was passed rapidly through the hottest part of the flame and then cooled.

Procedure	Rationale
Flood the slide with crystal violet	Primary stain
After 1 minute rinse the slide with distilled water	To remove any excess stain
Flood the slide with iodine	Iodine is a mordant that binds with crystal violet, rendering it unable to exit the Gram-positive peptidoglycan cell wall
After 1 minute rinse the slide with water	To remove any excess stain
Flood the slide with acetone	Acetone is a decolouriser that removes the stain from the Gram-negative cells
After 2-3 seconds rinse the slide with water	Do not leave the decolouriser on too long or it may remove stain from the Gram-positive cells as well
Floodslide with safranin	The counter stain
After 1 minute rinse the slide with water	To remove any excess stain
Gently blot the slide dry	To view under oil immersion (x1000) with a bright-field compound microscope

Table 2.2: Procedure and the reason for the Gram staining test

After the staining procedure and having retained the primary stain, Gram-positive cells appeared purple, whereas Gram-negative cells appeared pink, retaining the counter stain after the primary stain is removed by the decolouriser. The test was carried out in order to identify all four organisms that were tested in the project: *Staphylococcus aureus* (Gram-

positive), *Staphylococcus epidermis* (Gram-negative), *Pseudomonas aeruginosa* (Gram-negative) and *Escherichia Coli* (Gram-negative).

Having confirmed the Gram charge of bacteria, they were further characterised. The API® 20 E system (Figure 2.44) following the procedure described in API® 20 E system 5.4.6.1 was used to identify and confirm the presence of *Escherichia coli*. This is a standardised system containing 20 microtubes of dehydrated substrates to identify *Enterobacteriaceae* and other non-fastidious Gram–rods which use 21 miniaturised biochemical tests and an international database.

Figure 2.44: API® 20E Strip

Every microtube on the API® 20E strip represents a test (Table 2.3).

Test sequence	Biochemical test	API abbreviation
1	o-Nitrophenyl-f8-D-galactosidase	ONPG
2	Arginine dihydrolase	ADH
3	Lysine decarboxylase	LDC
4	Ornithine decarboxylase	ODC
5	5 Citrate utilization	CIT
6	H_2S production	H_2S
7	Urease	URE
8	Tryptophan deaminase	TDA
9	Indole production	IND
10	Acetoin production	VP
11	Gelatinase GEL	GEL
12	Glucose fermentation	GLU
13	Mannitol fermentation	MAN
14	Inositol fermentation	INO
15	Sorbitol fermentation	SOR
16	Rhamnose fermentation	RHA
17	Sucrose fermentation	SAC
18	Melibiose fermentation	MEL
19	Amygdaline fermentation	AMY
20	Arabinose fermentation	ARA

Table 2.3: API® 20E biochemical tests

Staphylococci are perfectly spherical cells about 1 µm in diameter. *Staphylococcus aureus* form fairly large golden yellow colonies on agar whereas *S. epidermidis* forms a relatively small white colony. Further identification was possible using API STAPH strips. Roughly, the same procedure that was used for API® 20E was adopted in performing the API STAPH test. The strip was prepared in the same way as API® 20E, creating a humid atmosphere and the detailed of this test can be found in 5.4.6.2. Every micro tube on the API (Table 2.4) STAPH strip represents a test and the *Staphylococci* strains were identified.

Test sequence	Active ingredient	Test
1	No substrate	0
2	D-glucose	GLU
3	D-fructose	FRU
4	D-mannose	MNE
5	D-maltose	MAL
6	D-lactose (bovine origin)	LAC
7	D-trehalose	TRE
8	D-mannitol	MAN
9	xylitol	XLT
10	D-melibiose	MEL
11	Potassium nitrate	NIT
12	ß-naphthyl phosphate	PAL
13	Sodium pyruvate	VP
14	D-raffinose	RAF
15	D-xylose	XYL
16	D-saccharose (sucrose)	SAC
17	methyl-αd-glucopyranoside	MDG
18	N-acetyl-glucosamine	NAG
19	L-arginine	ADH
20	Urea	URE

Table 2.4: API STAPH biochemical tests

Pseudomonas aeruginosa was preliminarily identified by its rod shape and grape-like odour. This was further confirmed by its characteristic feature- the ability to grow at 42°C.

Once the bacteria had been tested, protocols with different concentrations of bacteria and MB were developed. However, a significant difference in the PDT effect (between the dark control and light control) could not be observed even with the optimised bacteria protocol. The final optimised protocol is detailed in 5.4.8. Throughout the experiment it was very important to protect both the dark and light control plates from any light (as practically as possible) in order to minimise any unwanted PDT effect on the cultures except from desired effect (the light irradiation on the light controlled plates). Due to the rapid growth of bacteria it was vital that pipetting was done with extra care to avoid any false absorbance readings.

The best results from Gram-positive bacteria - *Staphylococcus aureus* (Figure 2.45) and Gram-negative bacteria - *Pseudomonas aeruginosa* (Figure 2.46) are as below. According to the results, *Staphylococcus aureus* showed a significant difference between the dark and 25 µM will be considered as the optimum MB concentration for future experiments/assays. 12.5 µM concentration will be considered the optimum MB concentration for future *Pseudomonas aeruginosa* experiments/assays.

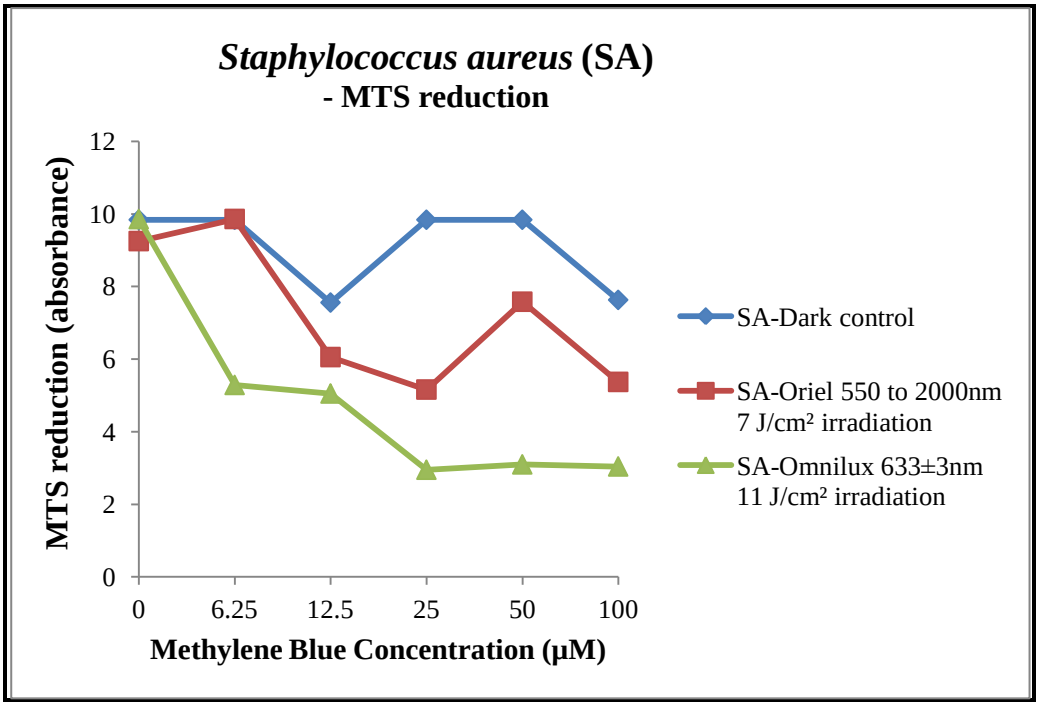

Figure 2.45: *Staphylococcus aureus* MTS reduction assay

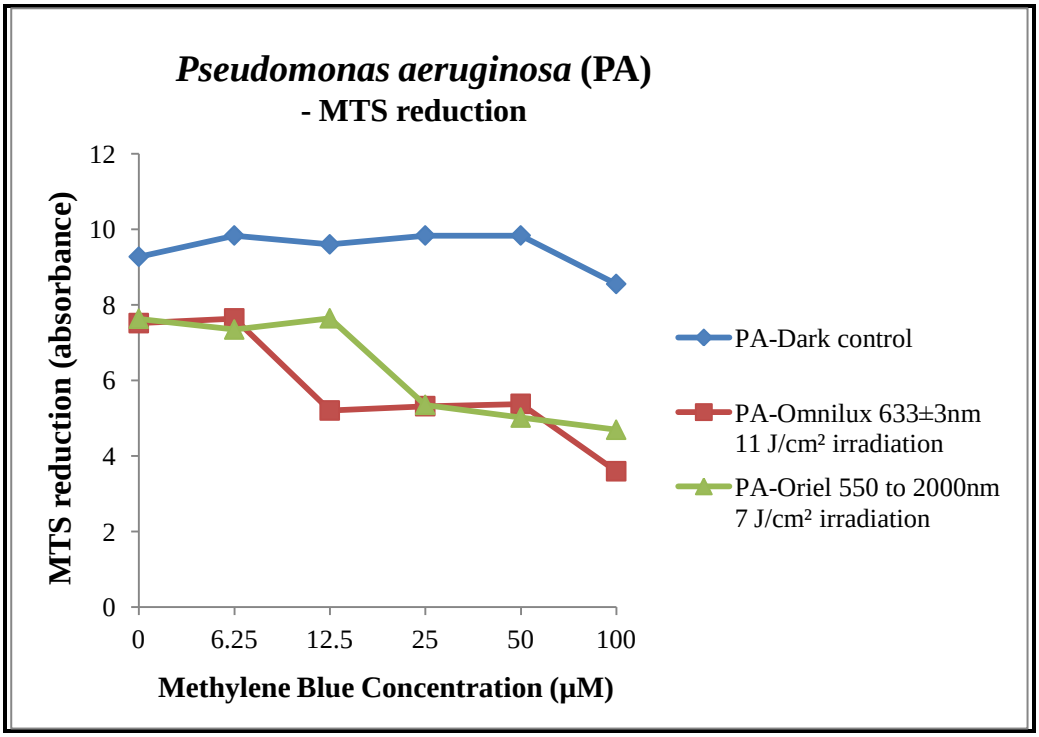

Figure 2.46: *Pseudomonas aeruginosa* MTS reduction assay

Even with the optimised protocol the bacteria kill was not satisfactory. However, a minor difference between the dark and light controls was observed. Due to the time restraints and with the intention of accomplishing the goal of the Project: to synthesise a multiple PS delivery system using polyacrylamide NPs and exploit its application in anticancer applications, the Project required more focus on investigating the biological effects of the PDT agents that were entrapped in NPs to establish an efficient and universal delivery system.

With this unsuccessful experiment series the project moved towards determining if PCNPs, the most successful entrapped PS in the project so far, could be internalised into cells *via* natural uptake.

As mentioned in Chapter 1 endocytosis is one of the major pathways of nanoparticle uptake by cells[91-93]. This process is both concentration and time dependent. Uptake of NPs *via* endocytosis can occur through phagocytosis, fluid phase pinocytosis or receptor mediated endocytosis. NPs less than 200 nm are known to be imported into cells by pinocytosis while larger particles (>500 nm) are internalised through phagocytosis[99]. Panyam and Labhasetwar reported no phagocytic activity with NPs approximately 100 nm in size[90].

2.7 Nanoparticle Cell Uptake – Quantification

It was found that polyacrylamide NPs do accumulate in cells provided they are incubated with cells for a sufficient time period. To this end, flow cytometry was used to develop a method for quantifying the NP uptake. Flow cytometry measures and analyses multiple physical and optical characteristics of individual cells/particles as they flow in a fluid stream through a beam of light.

Fluorescence-activated cell sorting (FACS) was used to sort the heterogeneous mixture of cells, with and without the NPs. FACS is based upon the fluorescent and light characteristics of the system and provides an objective and quantitative measure of fluorescent signals from individual cells as well physically separating the cells. The main parameters of FACS include: fluorescence intensity, particle size, granularity or internal complexity by the degree of forward scatter produced by the laser passing through the cell/particle.

To identify FACS as the method to quantify the internalisation it was important to identify that the blank NPs on their own do not appear as a population on their own and do not fluoresce. To this end, a NP suspension (made in water) was run through the flow cytometer and the resulting FSC, SSC and fluorescent plots were empty. Further more it was important to find out whether the media that the cells were to be grown (McCoy's media supplemented with 10% fetal calf serum (FCS) and 1% *L*-glutamine (all purchased from PAA)) fluoresced. Fluorescence – 1 detector (FL1, 515-545 nm) detected some fluorescence; however this was easily nullified by updating the settings of the FL1 detector. Further, by using a cell-only sample as a negative control at each time point any interference from the environment would be avoided.

2.7.1 Fluorescein dextran (MW 10,000 Da) entrapped NP uptake

Before studying the uptake of the synthesised PCNPs it was aimed to study NP uptake with a reference dye (fluorescein dextran (MW 10,000 Da) entrapped within the NPs. The human Caucasian colon adenocarcinoma cell line (HT29) was chosen for the cell uptake studies due to the large amount of data published on PDT effects of PSs using these cells[223].

The NPs were prepared using the method described in chapter 5.2.12. The average size of the synthesised NPs (Z_{ave}) was 45 nm. Fluorescein was chosen due to the close match of the excitation and emission properties of fluorescein with the argon ion laser and detectors found in commercial flow cytometers. NPs entrapped with fluorescein conjugated to dextran were used so that minimum fluorescein would leach into the aqueous media (due to the high molecular weight).

A time course experiment was carried out by setting up controls (cells only) and samples (cells and NPs). Cell-only controls contained 50,000 cells in 400 µL of McCoy's media (complete) and each sample contained 50,000 HT29 cells and 5 mg of filtered (through a 220 nm filter) dextran conjugated fluorescein encapsulated NPs in 400 µL media (*i.e.* 5 mg of NPs in 200 µL media were added to a sterile sample tube containing 50,000 cells in 200 µL media).

Both the control and NPs samples were incubated at 37°C in an atmosphere of 5% CO_2 within a humidified incubator. Every 15 minutes duplicate sample tubes and a control tube were taken out of the incubator, washed and resuspended in PBS/BSA/azide before preparation for flow cytometry.

Since both endocytosis and exocytosis are energy dependent functions[93] washing steps were considered to have a minimal[224] and/or constant effect on nanoparticle uptake study. Further, it should be noted that the HT29 cell line used in the experiment naturally divides with time effectively reducing the quantity of NPs in each cell by a factor of two with each division[189], which could potentially impact on the internalisation studies.

Following incubation, 4 mL of PBS/BSA/azide was added to all three tubes, the cells were pelleted by centrifugation at 404 x *g* for 5 minutes. The supernatant was removed and discarded and the cells were resuspended in 1 mL of PBS/BSA/azide and transferred to a clean tube. The cells were washed again by adding a further 3 mL of PBS/BSA/azide. The cells were pelleted by centrifugation at 404 x *g* for 5 minutes. The wash procedure was repeated twice more before the cells were resuspended in 200 µL of PBS/BSA/azide. Repeated washing steps washed away most of the fluorescein or NPs present in the surrounding media. Further, to quench any extracellular fluorescence, 10 µL of Trypan blue 4% was added to the washed cells to differentiate between membrane bound and internalised NPs.

After 5 minutes the cell suspension was loaded into a haemocytometer to count the cells. Trypan blue quenches extracellular fluorescence[225] therefore guaranteeing that any fluorescence seen was due to the internalised NPs and not due to those merely attached to the cell surface. Results were then acquired using a Becton Dickinson FACS Calibur™ flow cytometer with the following settings: forward scatter (FSC) E -1 752, side scatter (SSC) 369; fluorescence (FL1) log 415; fluorescence (FL2) log 550. A minimum of 10,000 cells was measured in each sample.

The fluorescein loaded NPs were detected in the fluorescence level (FL1) channel of the flow cytometer. Analysis was performed using CellQuest Pro V software (Becton Dickinson) and histograms plotted of FL1 fluorescence *vs* cell counts for each time point (Figure 2.47). The cell-only sample provided the negative control at each time point.

A gate was drawn on this control (M1) which contained less than 3% of the cell population (*i.e.* sample No.005 on Figure 2.47). The M1 gate was then copied and pasted onto the histogram plots generated from the cells plus NPs at each time point. Statistical analysis then determines the percentage of cells within the M1 gate, *i.e.* the percentage of cells containing fluorescent NPs. The M1 gate is always relative to the negative control at that particular time point. The experiment was continued for 4 hours.

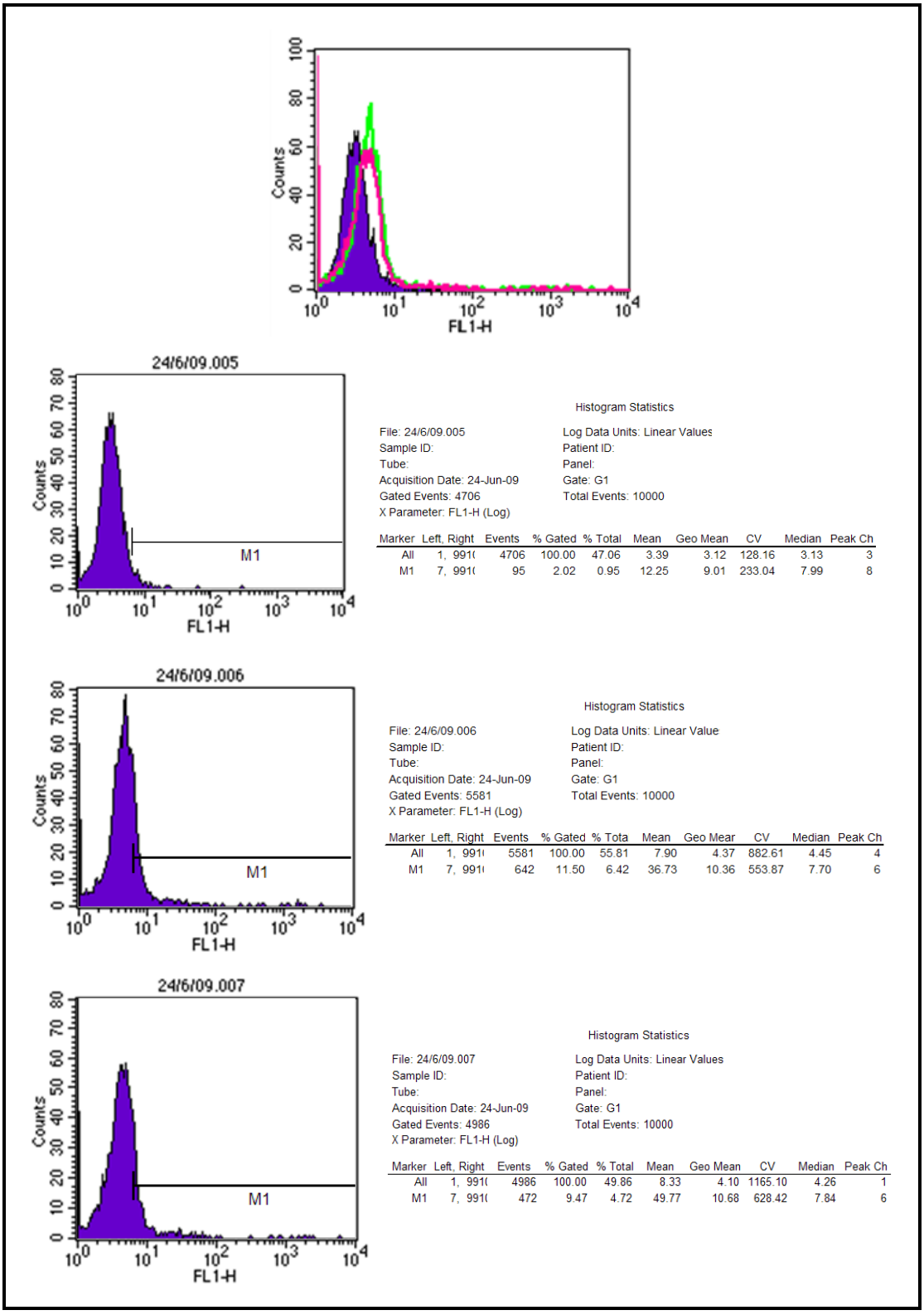

Figure 2.47: An example of a FACS reading *

*Key:

- Purple - negative control
- Pink and green - duplicate representation of cells incubated with fluorescein NPs
- Sample 5 - negative control (cells only)
- Sample 6 & 7 (cells and NPs)

Recorded uptake % at any given point is the difference between the sample and the negative control.

NP uptake was measured as a percentage of fluorescence detected (by FL1) in the cell population. Two different concentrations were studied to confirm whether 'uptake' was affected by the NP concentration (Figure 2.48).

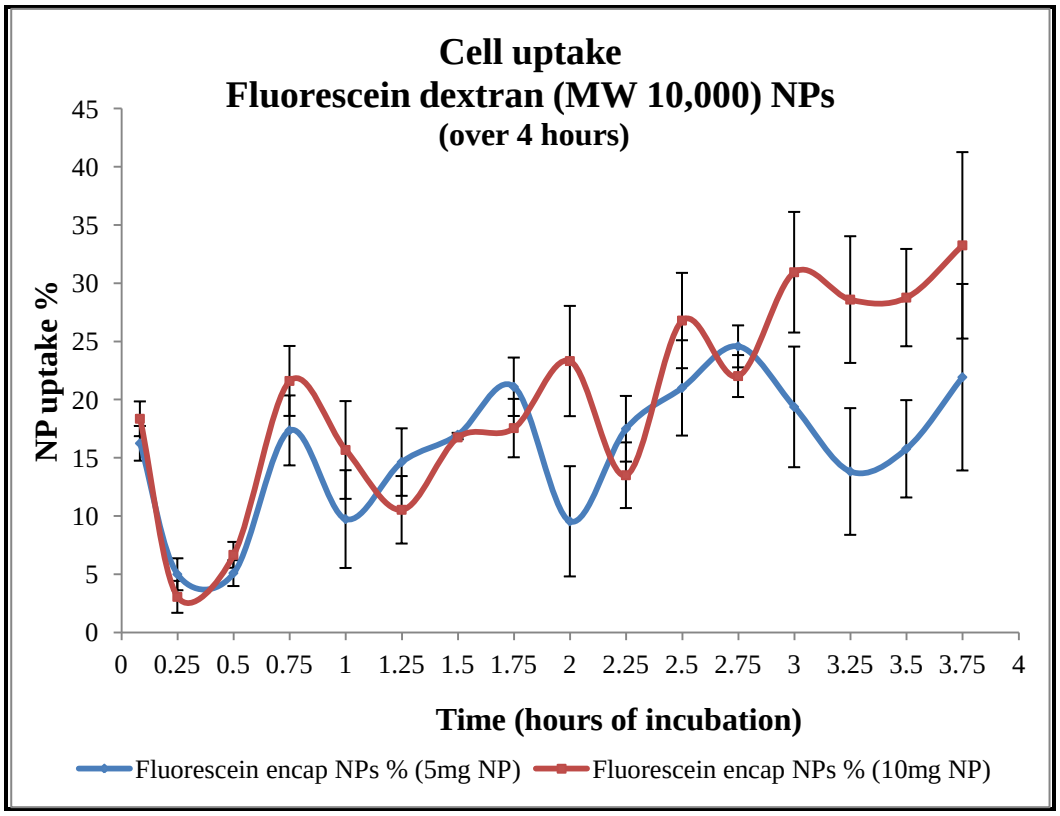

Figure 2.48: Cell uptake (Fluorescein dextran NPs) over 4 hours quantified using FACS

Now that the uptake of NPs had been established and an oscillation pattern observed within the first few hours, the uptake pattern at longer incubation times was determined. To enable this it was important to find out the time period over which the HT29 cells can be kept alive under the chosen conditions.

Propidium iodide (PI) is a DNA intercalator used to label the dead cells *via* the FL3 channel of the flow cytometer, which measures PI signals at 617 nm. PI is membrane impermeant and generally excluded from viable cells. However, it has the potential to bind to dead cell DNA as well as to RNA. Although its molar absorptivity (extinction coefficient) is relatively low once the dye is bound to nucleic acids its fluorescence is enhanced 20 to 30 fold. Further, the fluorescence excitation maximum shifts approximately 30–40 nm towards the red end of the spectrum and the fluorescence emission maximum approximately 15 nm towards the blue part of the spectrum, exhibiting an adequately large Stokes shift to allow simultaneous detection of nuclear DNA and fluorescein entrapped NPs. Thus, PI was chosen for use in the flow cytometry experiments in order to determine cell death over a given period of time in the presence of NPs.

Cell viability by flow cytometry was studied over 48 hours using fluorescein dextran NPs with HT29 cells incubated at 37°C in a humidified environment of 5% CO_2. Every 3 hours, for the duration of the experiment, duplicate sample tubes and a control tube were taken out of the incubator, cells washed and resuspended cells in 30 µL PI/Triton X-100 staining solution before preparation for flow cytometry.

Results were then acquired using a Becton Dickinson FACS Calibur^{TM} flow cytometer with the following settings: forward scatter (FSC) E -1 752, side scatter (SSC) 369;

fluorescence (FL1) log 412; fluorescence (FL2) log 474, fluorescence (FL3) log 427. A minimum of 10,000 events (counts) was measured in each sample.

No peaks were observed in the FL3 and FL4 detectors. Only a FL1 peak was observed, the fluorescence peak of fluorescein. Although it could have been possible to continue the experiment and observe how much longer these cells can be kept alive under the present conditions, as 48 hours is generally much more time than required for assay experiments, the study was discontinued at 48 hours and it was confirmed that the HT29 cells can be used in NP assays up to 48 hours.

This method could have been developed to quantify the cytotoxicity of PSs in PDT by using PI provided the PSs encapsulated in the NPs absorb at lower wavelengths. However, since the main PS that would be used in the project was a PC which absorbs at approximately 670 nm, the cell cytotoxicity would not be measured with PI, but with MTT assays.

2.7.2 PCNP uptake

Next, the fluctuation of the NP net uptake by flow cytometry was studied over 28 hours using PCNP with HT29 cells incubated at 37°C in a humidified environment of 5% CO_2 (Figure 2.49). At every hour for the duration of the experiment, duplicate sample tubes and a control tube were taken out of the incubator, the cells washed and resuspended in PBS/BSA/azide solution before their preparation for flow cytometry.

Two concentrations (3 mg/mL and 5 mg/mL) of NPs were studied and the percentage uptake values confirmed that NP uptake by HT29 was concentration dependent (Figure 2.49).

According to the quantified NP uptake profile, NP uptake reaches its maximum within 18 hours and then remains constant but with regular fluctuations. Alberola and Rädler showed a similar oscillation pattern in uptake of NPs by epithelial cells using fluorescence microscopy[226].

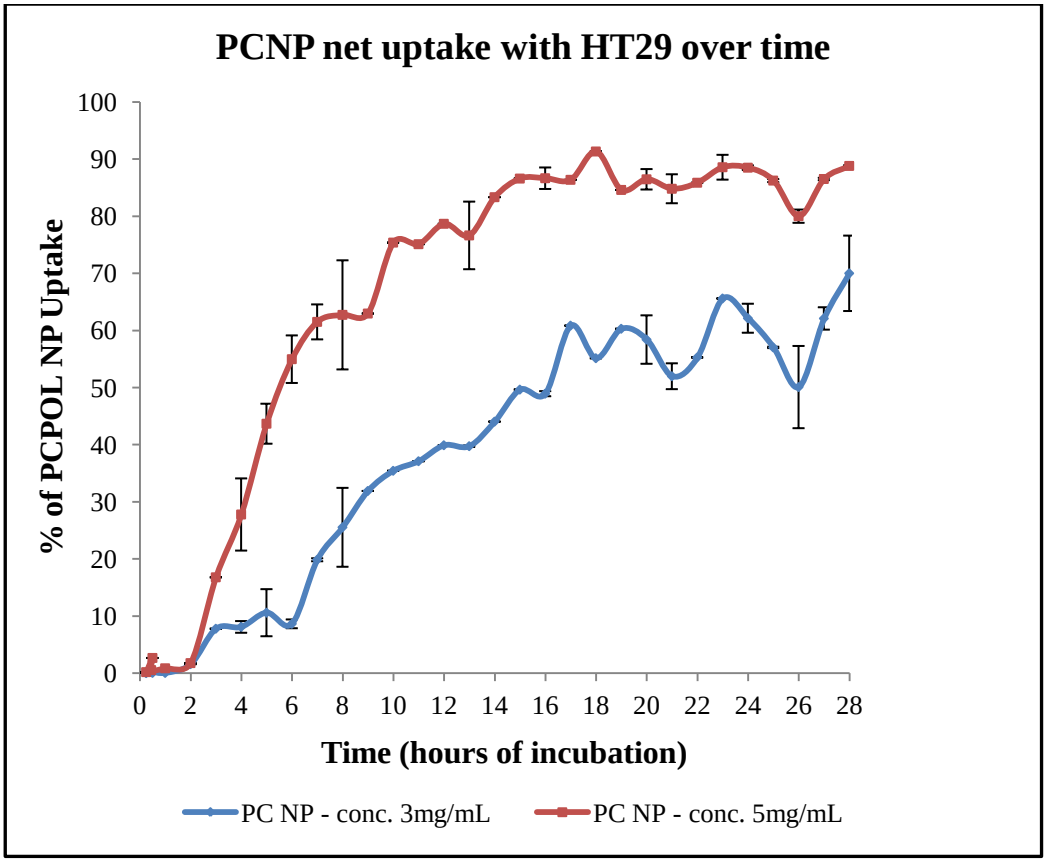

Figure 2.49: PCNP net uptake with HT29 over time quantified using FACS

The PCNP uptake study was carried out to develop a protocol for PDT *in vitro* studies. In PDT a PS does not need to be internalised but mere attachment to the cells surface can be suffice to cause cell kill. Thus, external fluorescence does not need to be quenched.

2.8 Intracellular distribution of NPs

According to the cell uptake studies the maximum uptake of NPs should have been reached within 18 hours. The confocal microscopy images below display the localisation of the PCNP which have been incubated with HT29 cells for 20 hours and washed three times with media prior to imaging. The confocal images were captured by exciting at 633 nm (Figure 2.50) by Leica Microsystems CMS GmbH (LAS AF version: 2.2.1 build 4842).

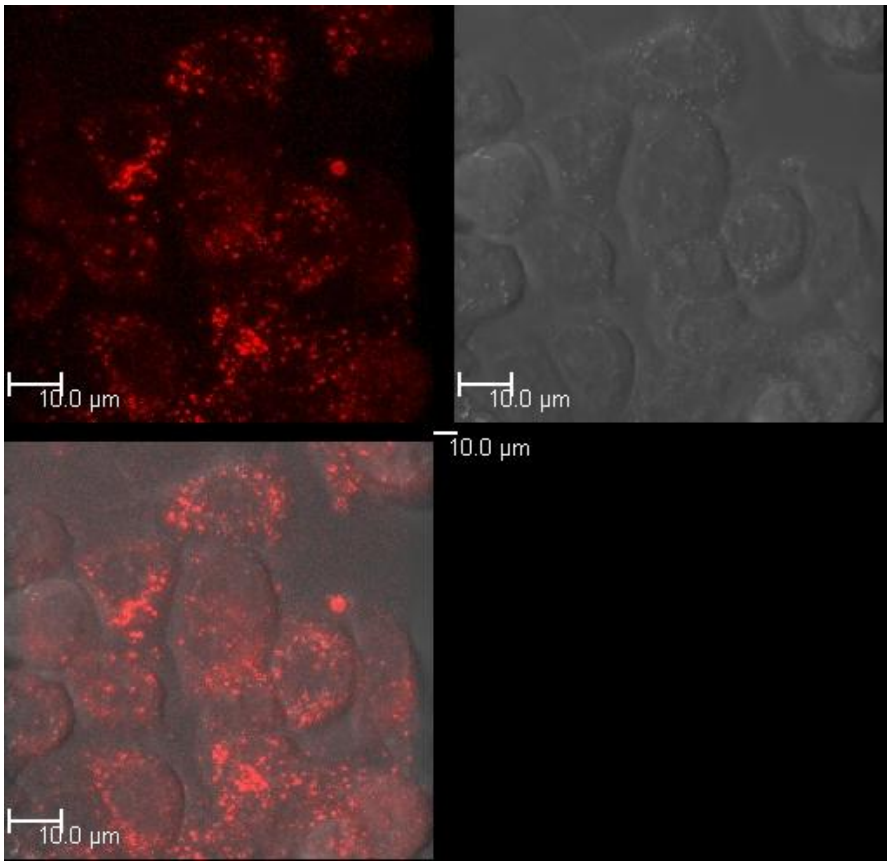

Figure 2.50: Confocal images of PCNP internalised in HT29 cells*

*After incubating for 20 hours; A - HT29 cells only, B - PC emission, C - merged image

Further, if a PS is to be used in PDT the polyacrylamide matrix (*i.e.* the NP) should facilitate the production and diffusion of singlet oxygen by the PS and be compatible with the biological environment to be able to be useful in PDT.

2.9 Determination of singlet oxygen production

Singlet oxygen is known to reactive with cholesterol *via* an oxidation pathway to give a dihydroxy sterol product which can be visualised by TLC and quantified by HPLC.

DCM and cholesterol 10 mM (1:9 DCM:MeOH) were added to a PCNP (MW 15,000–30,000 Da., 5 mg/mL MeOH) suspension. Oxygen was bubbled through the resulting suspension mixture which was then irradiated with white light (400 – 700 nm) for one hour. The mixture volume was reduced to dryness by flowing argon into the suspension. 1 mL of MeOH was added and the suspension was filtered through a 15 nm filter (Whatman Nuclepore-Track Etch membrane; 25 mm, 0.015 µm). 200 µL of this solution was transferred to an Eppendorf® tube and 200 µL of methanol was added. 1-2 crystals of $NaBH_4$ were added to the solution which was left for 1 minute until complete reduction had taken place. The volume of the solvent was reduced to approximately 100–150 µL by flowing argon over the solution.

TLC plate development was carried out using the method described by van Lier (1991)[227]. Briefly, a TLC plate was placed in a tank containing a 1:1 hexane: ethyl acetate mixture. The solvent was allowed to migrate 2/3 of the way up the plate; the plate was then removed from the TLC chamber and allowed to air dry. Once dried, the plate was returned to the tank and the solvent was allowed to migrate to the top of the plate and was left dry again. To visualise the sterols on the TLC plate, a 5% H_2SO_4 in ethanol mist was sprayed onto the TLC plate and the plate placed on a 100-120°C hot plate to allow development of the blue coloured spot at TLC retention factor (R_f = 0.38) indicating the presence of the dihydroxy product than the purple spot indicating the cholesterol starting material at R_f = 1.0.

The HPLC method for quantifying and analysing the singlet oxygen production was adopted from Osada *et al.*[228]. Cholesterol and its oxidised derivatives were separated on a Phenomenex Luna 5 µm C18 column (250 x 4.60 mm) using a mixture of methanol:acetonitrile (60:40 vol/vol) mobile phase. The flow rate was maintained at 1.0mL/ min. for 20 minutes prior to analysis. UV detection was performed at 205 nm. 10 µL of the sample was injected manually into the HPLC analysis system and the separation was detected using the Azur software version 5.0.

The HPLC chromatogram showed a mixture of 7α-, 7β-, 25-, 26- hydroxycholesterols, 7-ketocholesterols. The oxidised derivatives were quantified as a percentage of the intensity of cholesterol (0.59%). The aim of this excercise was to quantify the singlet oxygen production of PS entrapped NPs and to compare it to other NPs that will be synthesised in the project. Thus, this value cannot be directly compared to the PC only. However, the above value will be used for comparison purposes (with other NPs) in the project.

Since the singlet oxygen production and leaching was established and quantified, the next step of the project was to study the PCNP PDT cytotoxicity upon maximum internalisation.

2.10 PDT – *In vitro* studies (Maximum uptake)

Prior to using the NPs in the cytotoxicity assays it was important to sterilise them to avoid any bacterial growth in the culture. Thus 10 mg of 15,000-30,000 M.W. PC entrapped NPs were added to ethanol, decanted and dried in the class II biological hood. Then, 1 mL McCoy's media was added, vortexed (60 seconds), sonicated (60 seconds) and was added to a volume of cells (2.5×10^5 cells/1 mL) in a Falcon polystyrene (12 x 75 mm) tube. As concluded from the uptake studies the maximum amount of NPs were internalised within 24 hours and thereafter remained fluctuating around the maximum region. Thus, in the Project, the cell populations were incubated with NPs for 25 hours before preparing the samples for PDT cytotoxicity analysis. The volume of the media was adjusted to 4 mL and the supernatant discarded to eliminate any interference from NP conjugates that had not been internalised or attached to the HT29 cells. The volume of media was adjusted to the initial volume (1 mL). HT29 cells were plated with 100 µL per well in two 96 well plates. One row of 96 well plates with cells was used as control without the addition of NPs.

One plate was irradiated with 25 J/cm^2 [~23 min] of light from the Patterson system with a filter chosen to match the PC absorbance 630 nm centred. The second plate was kept in the dark outside the incubator while the previous plate was being irradiated. The plates were left to incubate overnight for 18-24 hours in the dark. To determine cell viability, the colorimetric MTT (3-[4, 5-dimethylthiazol-2-yl]-2, 5 diphenyltetrazolium bromide; purchased from Sigma) metabolic activity assay developed by Mossman[219] and subsequently modified by Prasad and co-workers (to incorporate a cell irradiation protocol[149]) was used. The cell viability was determined using a Biotek ELX80 universal microplate reader.

However, even after repeated experiments, no noticeable cell viability difference was observed in both the irradiated and the dark control. NPs gave 31.9% and 32.8% cell survival rate for the irradiated (light control) and non-irradiated (dark control) respectively. It is reported that ethanol has the potential to disrupt the cell membranes even when present in small quantities[229]. Thus, it is possible that the unpredicted cell toxicity was observed when incubating for longer periods due to minute amounts of ethanol present from the NP sterilisation step. This hypothesis was further confirmed by the cytoxicity results of NPs alone without the sterilisation step that showed no effect on the viability of the cells. The NPs 'sterilised' in ethanol indicated that the effect was none or minimal if the cells were not in contact with them for too long (<1 hour). Long contact however halved the viability.

Thus, the experiment was repeated without washing NPs in ethanol. Without any sterilisation method in place the cells were contaminated with bacteria in the 25 hour incubation (prior addition of MTT).

Following from these unfortunate results a new sterilisation approach was considered. It was decided to filter the NPs through a 220 nm filter syringe. The experimental set up was followed as described earlier with the exception of the sterilising step. After 25 hours of incubation cells were not contaminated with bacteria and no unexpected cell death was observed. However with the irradiated experiment no significant PDT toxicity was observed (Figure 2.51).

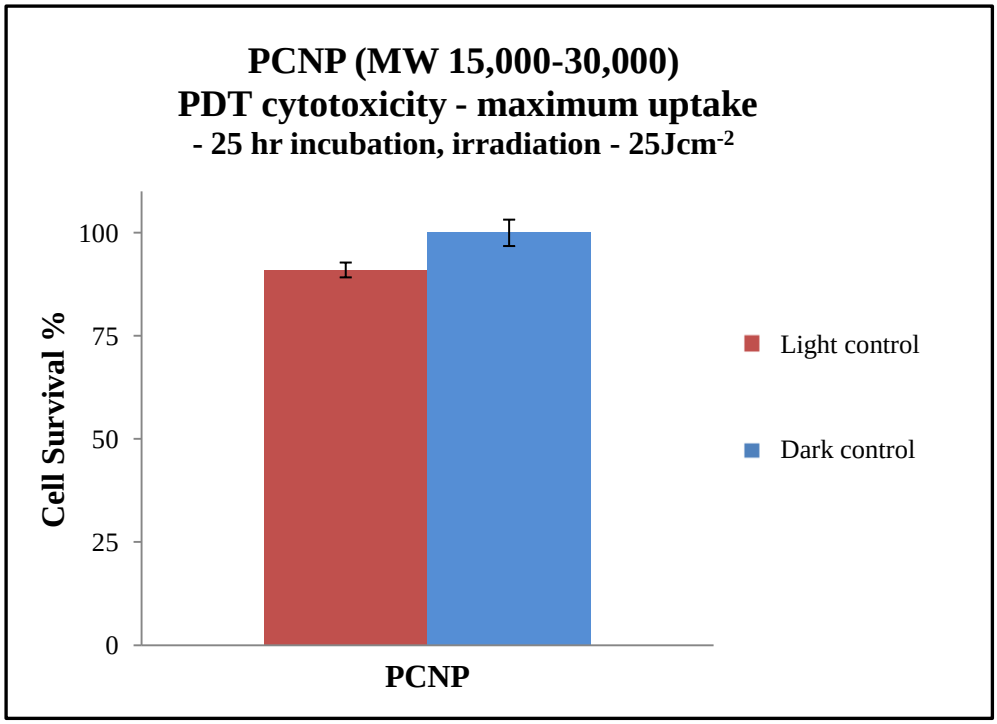

Figure 2.51: PDT cytotoxicity of PCNP (MW 15,000-30,000)

at its maximum uptake 25 hr incubation period

This insignificant difference could be a result of the low concentration of the PC present in the NPs. The concentration of PC in the NPs can be increased by either increasing the amount of NPs used in the assays or by synthesising NPs with more PC entrapped. Although, increasing the amount of NPs used in the assays seems to be the easier option, it was found to be problematic to make a homogeneous suspension with more NPs. Thus, NPs with a higher concentration of entrapped PC were synthesised.

To this end, first it was attempted to synthesis three batches of PCNPs with (PC attached to polylysine with MW 15,000-30,000 Da) using the procedure described in 5.2.13 with more POLPC concentrations. However, after the washing steps the similar concentrations of PC were present in the NPs.

Thus as another approach, a relatively higher molecular weight polylysine *i.e.* 30,000 – 70,000 to the PC was conjugated. In synthesising NPs with the MW 30,000 -70,000 POLPC, three batches with different concentrations of POLPC were synthesised using the same NP synthesis procedure (Chapter 5.2.15)

The mean particle size 45 (±10 nm) was determined by PCS and TEM. After a series of experiments with different PC concentrations it was found that the highest concentration of PC that can be entrapped in NPs was with the initial concentration 1.34 moldm^{-3} (30 mg/mL) (Figure 2.52).

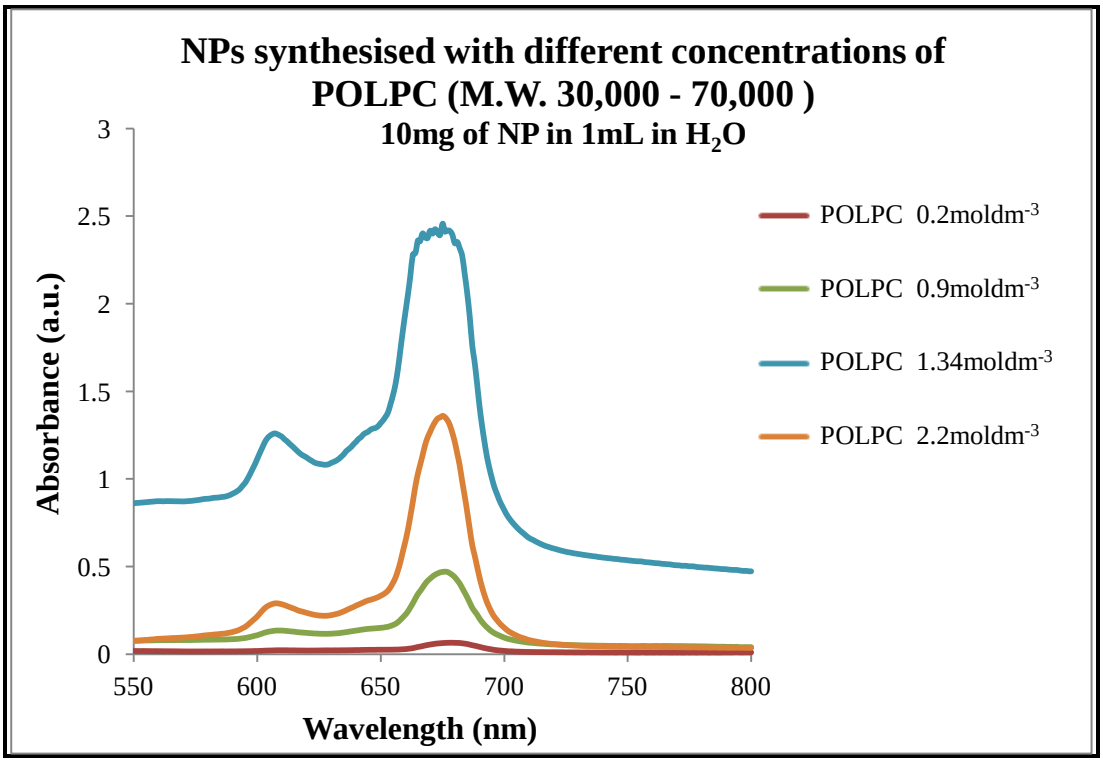

Figure 2.52: NPs synthesised with different concentrations of POLPC (M.W. 30,000 - 70,000)

The concentration of PC entrapped has a direct correlation to the amount of singlet oxygen produced (for procedure details see Chapter 5.3.5). MW 30,000 – 70,000 Da PCNP produced 360% more singlet oxygen compared to the MW 15,000 – 30,000 Da PCNP.

The concentration of the entrapped PC was quantified using the calibration "straight" line (Figure 2.40): 1.9 x 10^{-4} M per 1 mg of nanoparticles (ST DEV 5.09 x 10^{-8} (within 30%) in 1 mL of H_2O. Leaching experiments using these NPs showed the similar pattern to POLPC (MW15,000 – 30,000) study (Figure 2.39).

The PDT experiments (procedure details Chapter 5.4.3) carried out also showed a relatively high cell toxicity (Figure 2.53). Thus, optimising the PC concentration entrapped in NPs was an important step in the project.

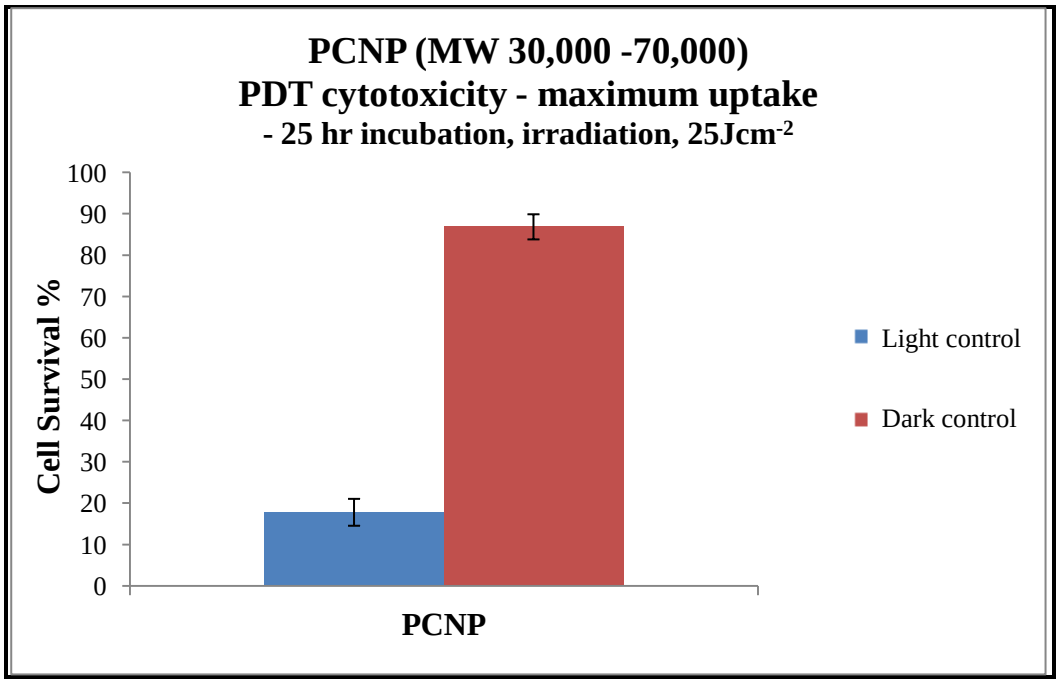

Figure 2.53: PDT cytotoxicity (maximum uptake) of PCNP (MW 30,000 -70,000)

2.11 PDT – *In vitro* studies (Minimum uptake)

NPs are reported to accumulate in tumour neovasculature due to selective retention[134]. Exploiting this notion *in vitro* HT29 cells surrounded with NPs in the extracellular media and at the minimum uptake time (<5 minutes) were irradiated under identical conditions to those used for the 25 hour uptake time. MTT assays were then performed as before and cell viabilities determined (Figure 2.54).

The cell viability of PCNP was 33%. However, no noticeable dark toxicity was observed with PCNP. This result could be due to, in this instance, the NPs being mixed with cells only for the duration of the irradiation (approximately 90 minutes).

These results are potentially very interesting from a clinical perspective as it is likely that a significant proportion of NPs would accumulate in the stroma of the tumour *i.e.* in the extracellular space. It is demonstrated here that if this localised NP concentration is high enough cancer cells can be effectively killed without the requirement that the NPs be internalised.

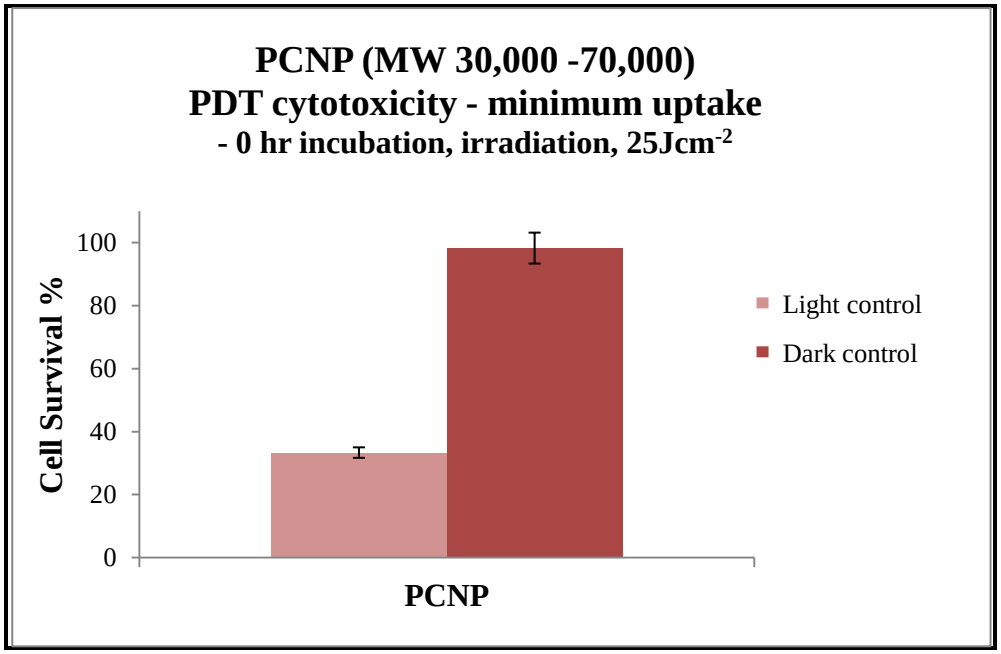

Figure 2.54: PCNP - PDT cytotoxicity (minimum uptake)

2.12 Summary

The primary intent of the Project was to synthesise PSs/probes suitable for entrapping within NPs and to study their behaviour in cellular uptake, PDT and PACT. To this end, a number of PSs/dyes have been entrapped within a range of polyacrylamide NPs: MB, DSRuCl, PyPorphyrin. However, as leaching from the matrix was identified as a challenge to overcome, sterically bulky groups were attached to the PSs/probes entrapped within the NPs and characterised. To this end, dextran (MW 10,000) conjugated fluorescein (reference dye), PEG(750)Porphyrin and PCNP (MW 15,000- 30,000 and 30,000-70,000) were successfully entrapped in the polyacrylamide matrix. Once the PSs/probes were entrapped, the NPs were characterised for their size, presence of PSs/probes within the NPs by spectroscopic investigation (absorbance and/or fluorescence) and the concentration of entrapped PSs/probes (using absorbance spectroscopy).

5-(4-Phenylpropenoate)-10,15,20-triphenylporphyrinatozinc was successfully synthesised to be copolymerised using GTP. However, the porphyrin molecule (monomer) did not copolymerise in the reaction and thus, with the limited time frame of the Project this concept has not been pursued further.

Another interesting result that was not pursued further was the NP penetration into biofilms. This would be an interesting area for future research.

Uptake of the NPs by HT29 cells was quantified using the encapsulated fluorescein reference dye (fluorescein dextran 10,000MW) and PCNP. Intracellular distribution of NPs was determined by confocal microscopy and maximum uptake was observed after 18 hours of incubation. Production of the main PDT agent, singlet oxygen, was quantified and

the PDT cytotoxicity assays were carried out using the maximum and minimum uptake times with the chosen NP-PCNP.

Chapter 3: Investigations and synthesis of photosensitiser entrapped and conjugated nanoparticle systems

In addition to the synthesis of PS entrapped NPs another objective of the project was to selectively add features to the PS entrapped NPs. This was attempted *via* altering the net charge and lipophilic character of the NPs. This chapter describes the attempts taken to optimise the functionality of the most successful PS (entrapped within the nanoparticle) discussed in the previous chapter; PCNP (MW 30,000 – 70,000Da). Once the alterations have been established the effect on NP penetration and distribution in cells will be investigated.

3.1 Surface functionalisation of photoactive NPs

The size, composition, network porosity and surface chemistry of NPs dictate the selectivity and the functionality of the NPs in cellular environments. In the synthesis of polyacrylamide NPs in the Project, these parameters were selectively controlled by varying the ratio of the synthetic reagents and the microemulsion environment. The ability to control surface chemistry is useful in increasing the retention/circulation time of the NPs in the body.

In targeting NPs to tumour tissue, provided the NPs can avoid sequestration by the reticuloendothelial system (RES), accumulation can occur in the stroma as a result of the enhanced permeability and retention effect[48]. Particles synthesised to avoid the RES can

lead to longer circulation times[230], resulting in a greater potential to reach the site of interest[35]. These NPs are approximately 100 nm in size with a hydrophilic surface (to avoid clearance by fixed macrophages). This can be achieved by coating the NPs with hydrophilic polymers (*i.e.* PEGylation) that create a cloud of chains on the particle surface repelling plasma proteins[48]. To this end, there are few functional groups that can be incorporated into the surface of the NPs *i.e.* hydroxyl (OH), sulphonate (SO_3^-), carboxylic acid (COOH) and amino (NH_2) groups or bio-reactive groups such as folate and antibodies. The addition of secondary functional groups can be incorporated into the NP surface either during particle synthesis or post-synthesis, *i.e.* functionalised monomers can be incorporated into the microemulsion reaction mixture or can be grafted directly onto the NP surface.

3.1.1 Amino functionalisation

Josefsen[28] previously synthesised amino functionalised NPs (see Chapter 5.2.2 for procedure). In this way net charge and lipophilic character can be altered to investigate the effect on penetration and distribution in cells and bacteria. The procedure differed only from the above described polyacrylamide NP synthesis by the addition of N-(3-aminopropyl)methacrylamide hydrochloride (1% equivalent to acrylamide) to obtain amino functionalisation. A similar procedure was followed in the project to synthesis NPs in the range Z_{ave} 42 nm. The presence and reactivity of the primary amino groups was confirmed using a non-fluorescent reagent, fluorescamine (Figure 3.1).

Fluorescamine reacts with primary amines to form a fluorescent product which can be identified through optical spectroscopy and is commonly used in the assay of primary

amines. The reaction is almost instant in aqueous media at room temperature and forms highly fluorescent products ($\lambda_{ex.}$ ~365 nm and $\lambda_{em.}$ ~ 465-485 nm).

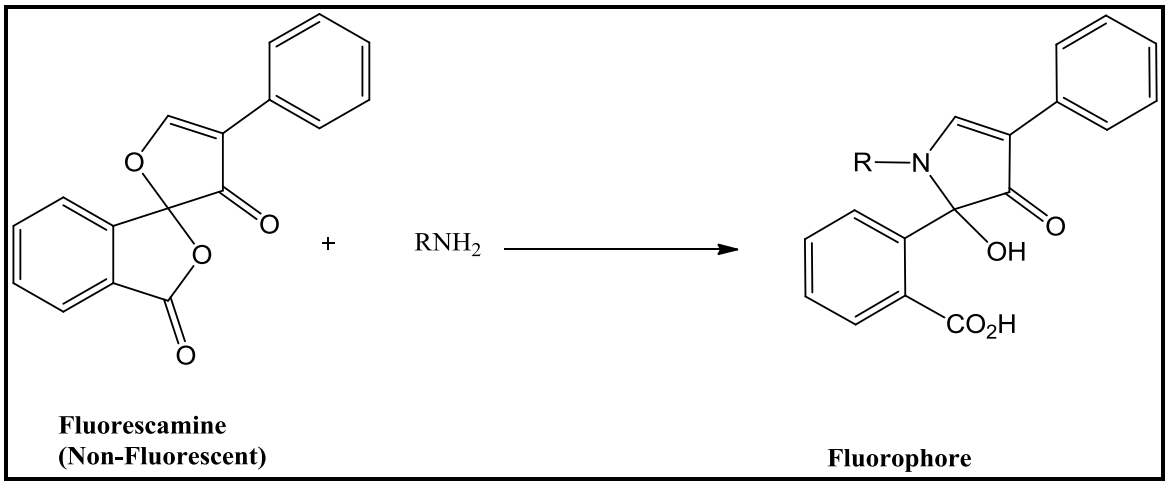

Figure 3.1: Reaction of Fluorescamine and Primary Amines

The fluorescence of a solution containing primary amines plus fluorescamine is proportional to the quantity of free amine groups present.

3.1.2 Amine quaternisation

As the study of charge effects on NP uptake and biological activity was of interest, amino functionalised NPs were quaternised using methyl iodide (Figure 3.2).

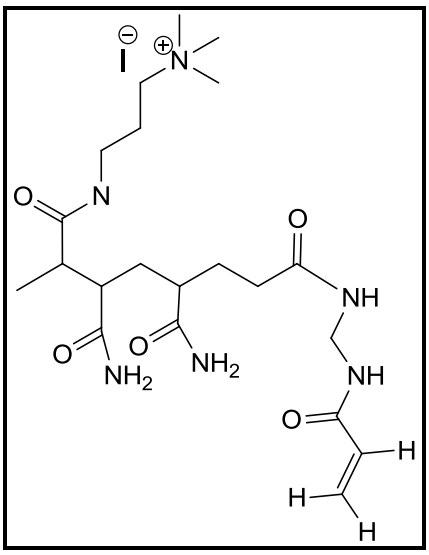

Figure 3.2: Structure of a quaternised amino group

Blank amino NPs (no surface functionalisation/no PS entrapped) and methyl iodide were added to a dry DMF solution at 40°C under an argon atmosphere. After one hour, the argon supply was removed and the solution was kept stirring for 72 hours at 40°C. Aqueous triethylamine was added and the solution was microfiltered (Whatman® Anodisc 25, 0.02 µm, 25 mm filter). The particles were then repeatedly washed with ethanol (4-5 times). The product was filtered and vacuum dried (5 hours) to obtain dry cationic polyacrylamide NPs.

These NPs were characterised using solid-phase ^{1}H NMR and ^{13}C NMR. The spectra were obtained using a 4 mm double resonance magic angle spinning probe on a Bruker Avance II. 500MHz NMR instrument and the samples were spun at 8 kHz. The chemical shifts were referenced externally to TMS at 0 ppm.

^{1}H NMR suggested the presence of methyl groups (CH_3) attached to nitrogen atoms, indicated by a characteristic peak around 3.3-3.4 ppm (Figure 3.3). In spite of the expected singlet, a multiplet is observed. The resolution of a MAS NMR spectrum (Magic-Angle Spinning Nuclear Magnetic Resonance) is generally too poor to resolve J-coupling splitting. However, this resonance can be attributed to the 2 CH_3 groups in differing environments. The ^{13}C NMR spectrum shows a peak around 55-60 ppm, where a CH_3 group attached to a nitrogen atom would be expected (Figure 3.4).

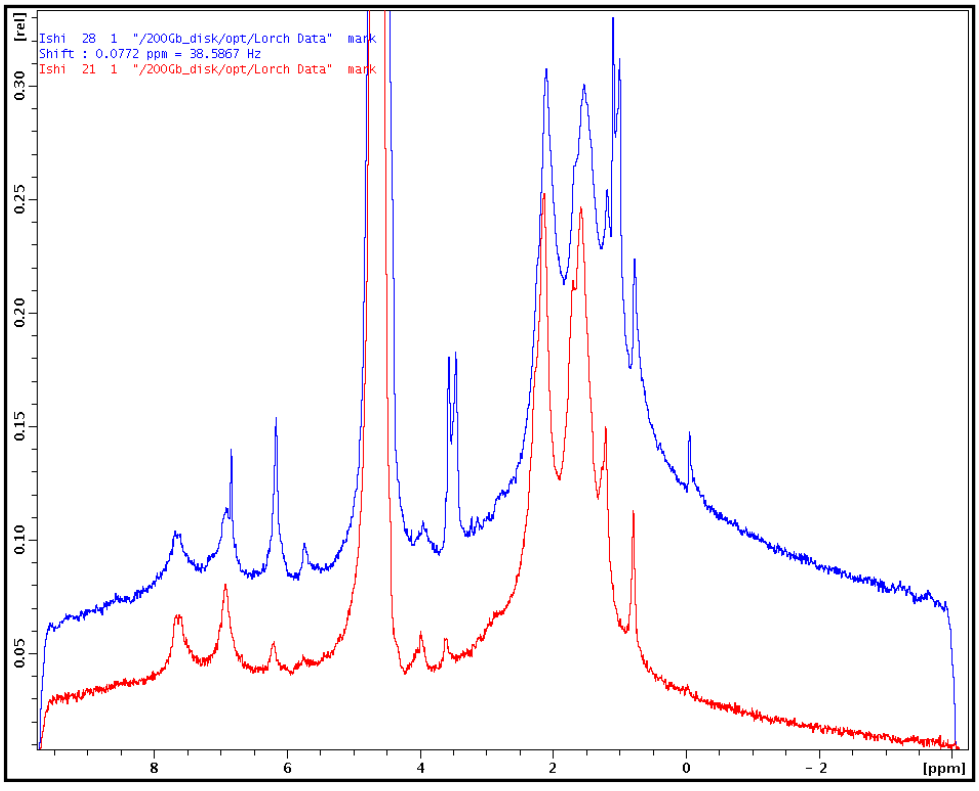

Figure 3.3: Solid phase ^{1}H NMR spectra: red - blank NPs, blue - cationic NPs

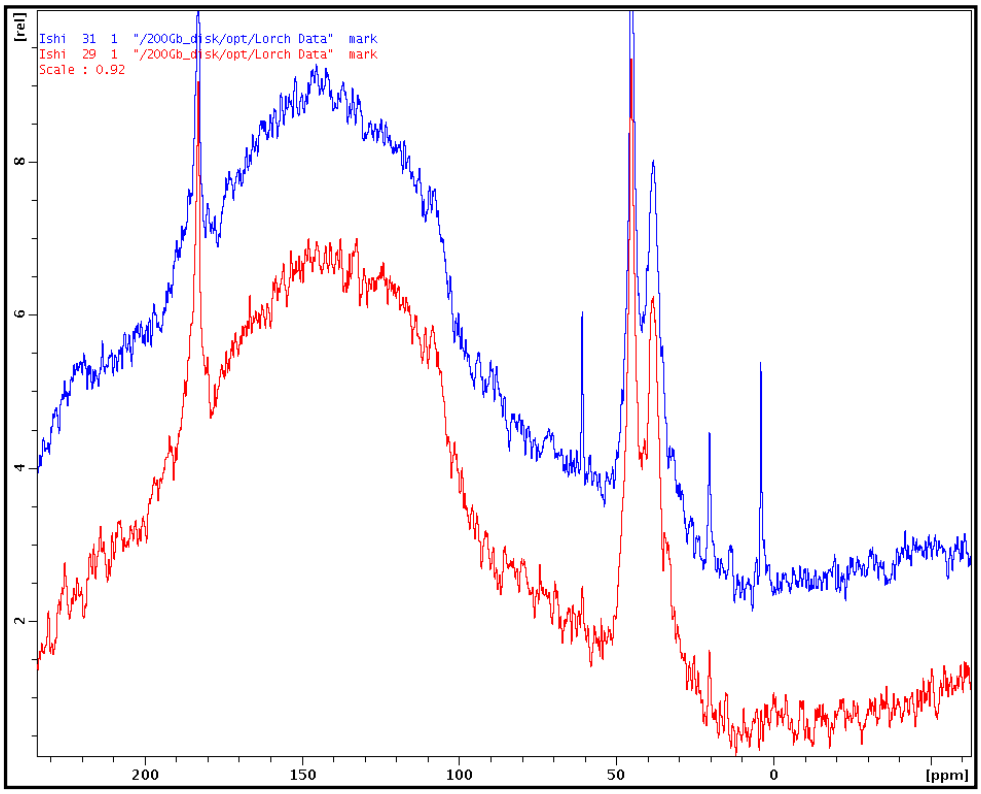

Figure 3.4: Solid phase ^{13}C NMR spectra: red - blank NPs, blue - cationic NPs

3.1.3 Attaching a second PS

Amino functionalised NPs can be used to conjugate a further photosensitising moiety to the NP. While synthesising a multi PS conjugated NP system, this would also enable a hydrophilic polymer cloud around the NP to be created. As discussed previously in this Chapter, if such a NP was introduced to human cells, this would minimise NP clearance by the RES pathway. In order to assemble a conjugated system of this nature, the NPs and the PS molecules must possess reactive functional groups capable of promoting the binding reaction. It was anticipated that this coupling criteria could be easily met, provided the functional group that would enable the desired coupling of the two components be accomplished and a desired hydrophilic PS is identified.

Since the entrapped PS in the chosen NP is a phthalocyanine it was decided to attach a PS which absorbs around 400-500 nm enabling the use of a wider window in the visible spectrum. To this end, a porphyrin was chosen to attach to the surface of the PCNP. The ability to deliver more than one class of PS could be advantageous clinically as the larger spectral region covered could lead to more efficient absorption of light.

3.1.3.1 *N*-hydroxysuccinimide functionalised porphyrins (NHS Porphyrin)

Porphyrins can be functionalised while protecting the hydrophilicity of the molecule to enable the creation of a bifunctional system for applications such as directed delivery in PDT and cellular imaging tools. Following the procedure of Boyle *et al.*[231] 5-[4-(succinimide-N-oxycarbonyl)phenyl]-10,15,20-tris-(4-*N*-methylpyridimiumyl)porphyrin trichloride [17] was synthesised. Briefly, the Rothemund reaction[232] was followed to

synthesis 5-(4-carboxyphenyl)-10,15,20-tri-(4-pyridyl)porphyrin [14] from 4-formylbenzoic acid, 4-pyridinecarboxaldehyde and pyrrole. At the next step, although activation with NHS decreases water solubility of the modified carboxylate molecule, the reactive arm, *N*-hydroxysuccinimide, was introduced to the reaction, followed by addition of methyl iodide to increase the hydrophilicity of the other three pyridyl groups. Increased water-solubility of the charged porphyrin was consequently achieved *via* an anion exchange reaction utilising the Dowex 1x8 20-400 Cl, whereby the counter iodide ions of porphyrin [17] were replaced by the chloride ions from the resin (Scheme 3.1).

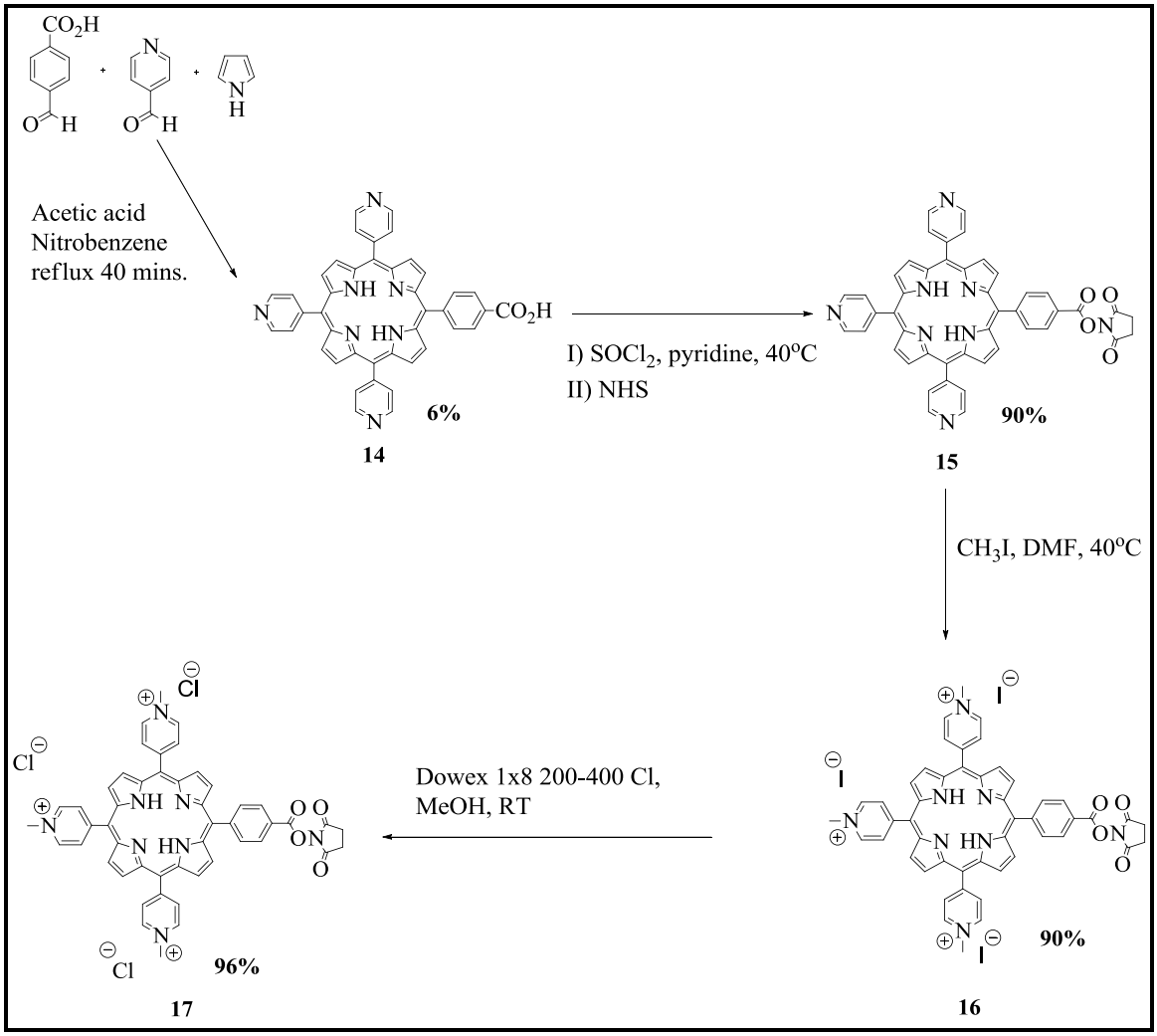

Scheme 3.1: *N*-hydroxysuccinimide functionalised porphyrin (NHS Porphyrin) synthesis

3.1.3.2 NHS Amino coupling reaction

In order to maintain the primary amino groups of the NPs in a non-protonated (reactive form), it was necessary to carry out the coupling reaction in a slightly basic medium, that itself is free from any primary amines. A sodium bicarbonate buffer, pH 9, was first considered for the conjugation. The reaction was carried out ranging from a 5 minute to 2 hours period in the basic suspension and filtered through the microfiltration kit. There were some practical problems faced during this step.

Polyacrylamide NPs formed a creamy suspension in water which appeared to block the microfiltration kit (Millipore filter unit (fritted glass) with 0.02 mm, 25 mm, Whatman® Anodisc 25 filters). It was found that the creamy suspension could only be precipitated using very high rpm centrifuge (*i.e.* 60,000) for 1 hour. The product required washing at least 3 times to remove any sodium bicarbonate residue. These NPs were dried under vacuum at 37°C. However, after drying, the NPs seemed to have lost their characteristic suspension properties, *i.e.* forming a clear suspension in water, thought to be due to huge variations in the nanoparticle size. Freeze drying was chosen as an option to dry the NPs, however the NPs no longer showed suspension properties once again.

Generally polyacrylamide NPs were washed with ethanol in the project. NPs, precipitate in ethanol without any difficulty. However, since the above experiment requires a basic medium, ethanol could not be used. Thus, triethyl amine was identified as a basic solution that would remain as a liquid in both water and ethanolic media while being compatible with the polyacrylamide matrix and the synthesised porphyrin.

3.1.3.3 Conjugation of porphyrin to NPs

To synthesise the PCNP-P (Figure 3.5) briefly, polymer bound amino functionalised tetrasulfonato-aluminium phthalocyanine entrapped nanoparticles (PCNP-A) (in suspension) was mixed with the porphyrin engineered to bear a single amine-reactive succinimide–N-oxycarbonyl-phenyl group in water. An aliquot of 5-[4-(succinimide-N-oxycarbonyl)phenyl]-10,15,20-tris-(4-*N*-methylpyridimiumyl)porphyrin trichloride (500 µL, 2.2 mmoldm^{-3}) was added to a dispersion (10 mL) of filtered (Millex® GP, 0.22 µm Filter unit) amino functionalised PC-polylysine entrapped NPs (50 mg) and triethylamine (250 µL). The mixture was spun in Falcon polystyrene tubes (12x75 mm) for 2 hours on a spinning rotator at room temperature, protected from light. The resulting suspension was washed with ethanol, centrifuged (7x50 mL, 10 minutes, 5500 rpm), microfiltered (Whatman® Anodisc 25, 0.02 µm, 25 mm filters) and dried for 8 hours at 40°C to yield the desired porphyrin conjugated PC entrapped NPs as a green solid. Yield 78% (39 mg). The NPs were then precipitated and washed (5 times, 50 mL) with ethanol.

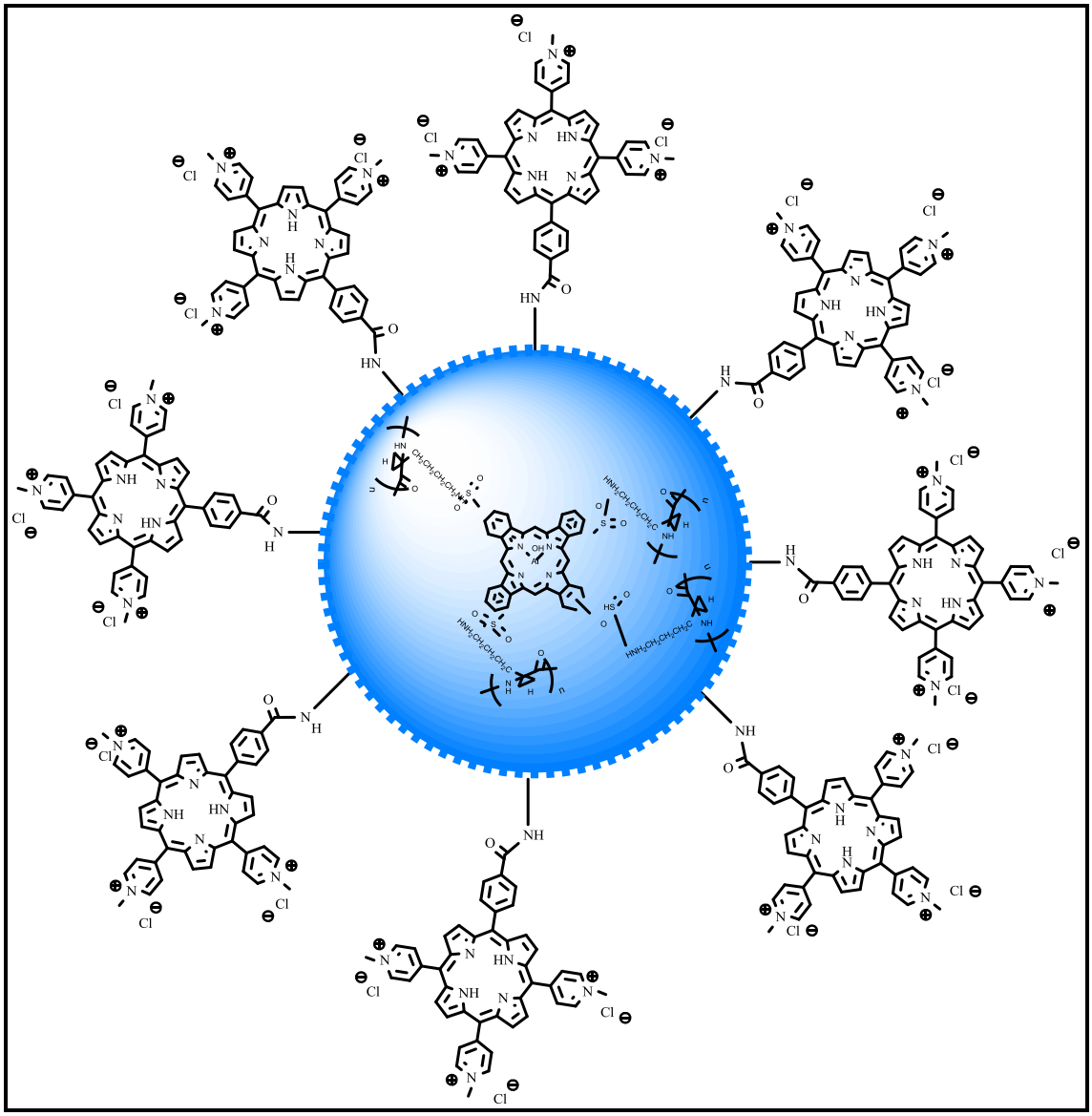

Figure 3.5: PCNP –P

The successful conjugation of the NHS Porphyrin to PCNP-A was confirmed by clear absorbance peaks at 424 nm (porphyrin Soret band) and 680 nm (PC Q band) respectively (Figure 3.6). When excited at 424 nm, the PCNP-P emission spectra showed two clear fluorescence peaks (656 nm and 708 nm) corresponding to the porphyrin and a minor peak relative to PC at 685 nm (Figure 3.7). However, when excited at 650 nm (close to the PC λ_{max} of 680 nm), a clear emission peak relating to the PC at 685 nm was observed (Figure 3.8).

.

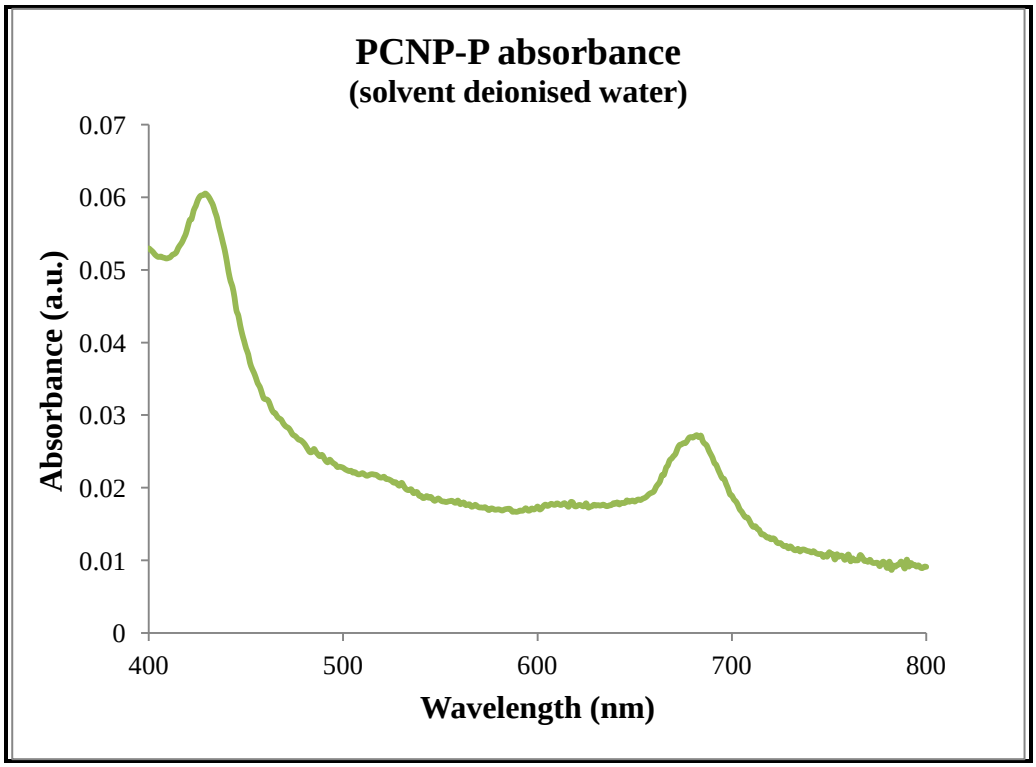

Figure 3.6: Absorbance spectrum of PCNP-P

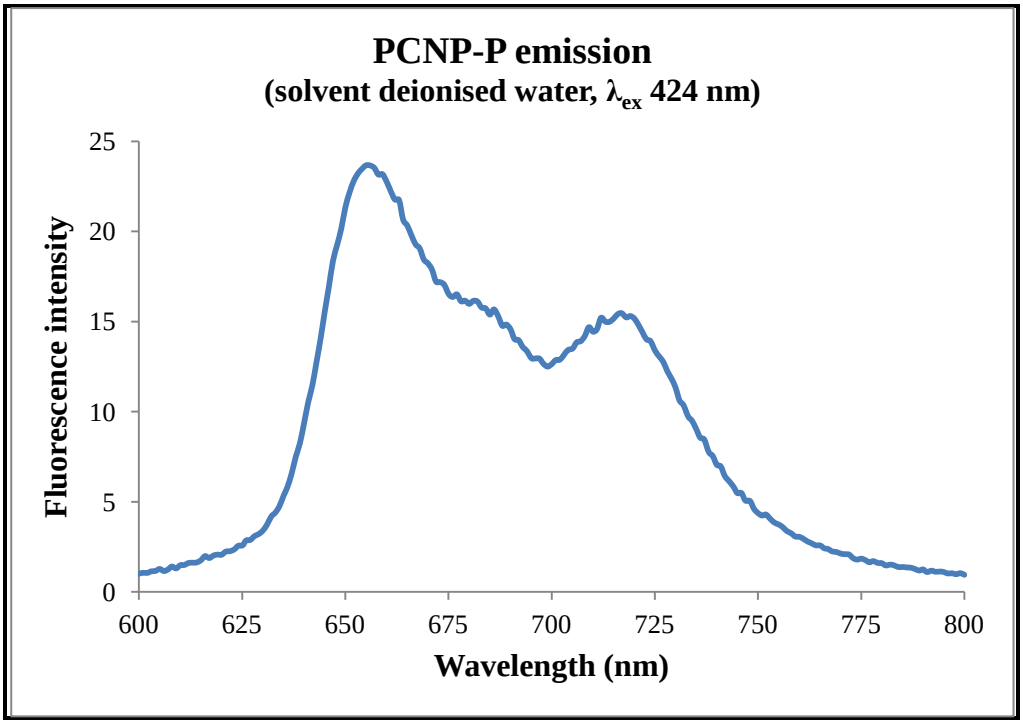

Figure 3.7: Emission spectrum of PCNP-P (λ_{ex} 424 nm)

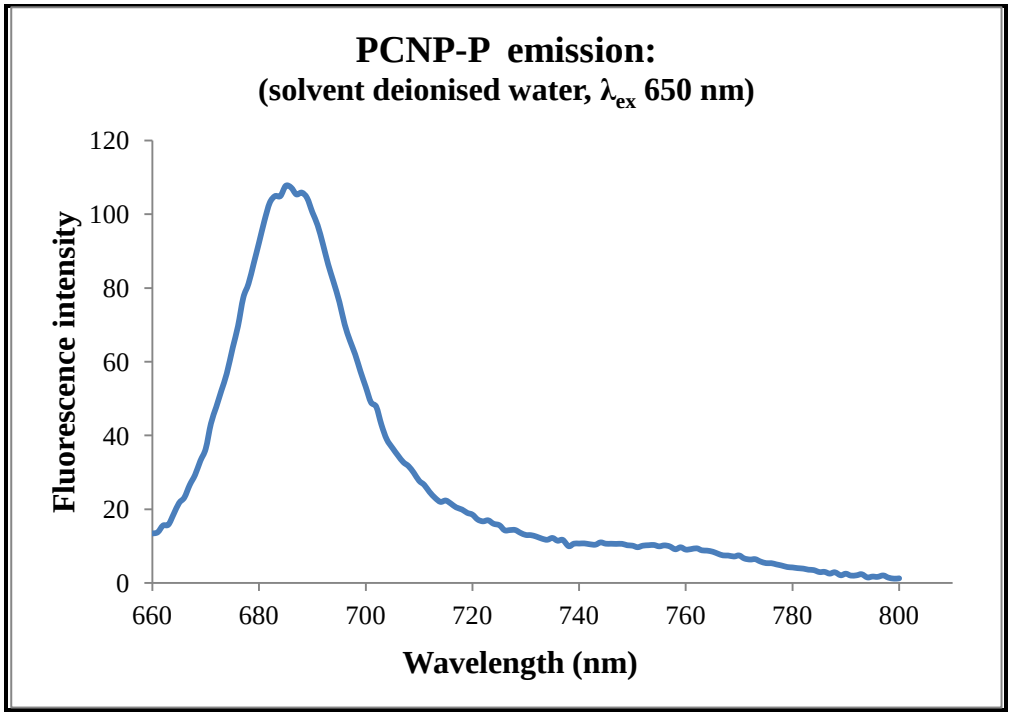

Figure 3.8: Emission spectrum of PCNP-P (λ_{ex} 650 nm)

As confirmed by PCS and TEM images the mean size of the PCNP-P was 95±10 nm (Figure 3.9). The size of a porphyrin molecule is 18 Å and thus the maximum size increase that was expected was ~36 Å. Experiments were carried out to study the reasons for this unexpected increase in size of PCNP-A after conjugation to the porphyrin molecule.

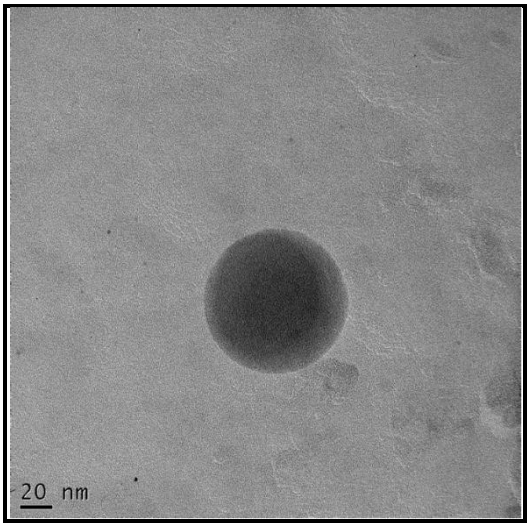

Figure 3.9: TEM - PCNP-P

One hypothesis was that the increase in the mean particle size upon porphyrin conjugation to PCNPs could be a result of aggregation caused by porphyrin interactions on adjacent particles. This type of π-π interaction could be detected in the fluorescence spectra of the NHS porphyrin used for conjugation and is similar to the split fluorescence peaks reported for the interactions with the related 5,10,15,20-tetrakis(4-N-methylpyridyl)porphyrin[233] (Figure 3.10).

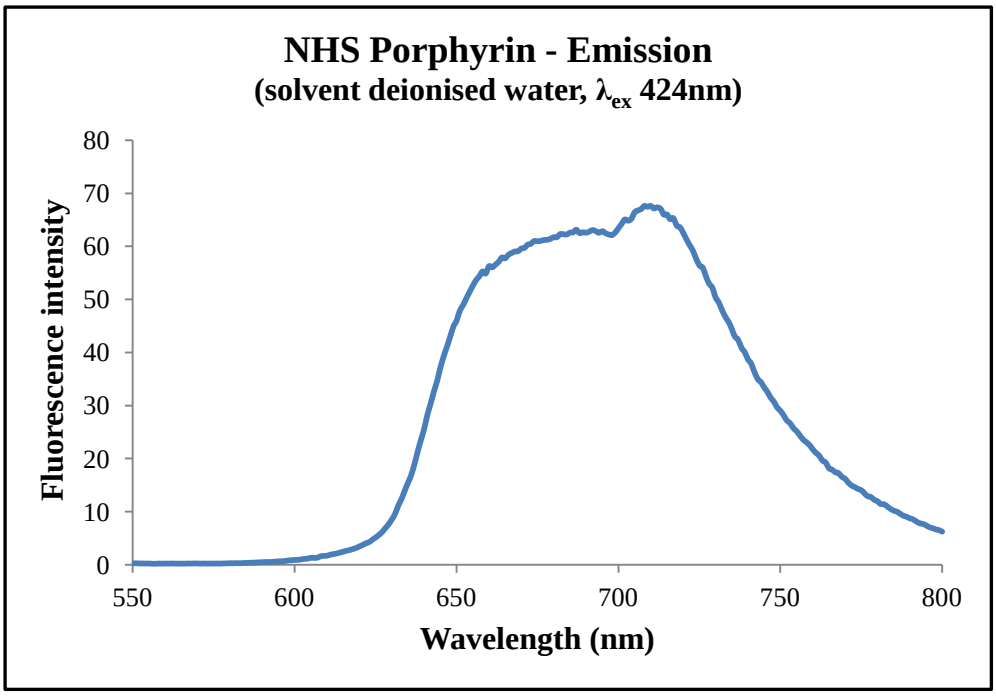

Figure 3.10: Fluorescence spectra - 5,10,15,20-tetrakis(4-N-methylpyridyl)porphyrin

Polyacrylamide hydrogels/nanogels are known to swell in aqueous environments[234]. Thus, an alternative hypothesis was that this effect was due to polyacrylamide swelling. In water the swelling is controlled by several factors: the cross linker concentration, pH and ionic strength[234, 235]. However, experiments were carried out to study whether the diameter increase was a result of this swelling behaviour; the studies indicated that these parameters were not involved.

Leaching studies carried out with the PCNP-P showed no filtrate fluorescence: two PSs (PC and porphyrin) were successfully conjugated to a polyacrylamide nanoparticle system (without leaching).

1 mg of each PCNP-P and PCNP-A were prepared in water. The absorbance spectra were compared to observe any differences in the PC concentration. The Q band of PCNP-P showed a slight decrease (15-20%) in intensity than PCNP-A (Figure 3.11).This could be either any loosely entrapped PC being washed away during the conjugation procedure and/or the mass added by the conjugated porphyrin in the total weighed sample. The porphyrin–nanoparticle conjugation procedure generally takes approximately 3 hours and the PC leached only in the first 3 hours. During the conjugation procedure it is possible that any loosely entrapped PC was washed away leaving only the tightly entrapped PC in the nanoparticle.

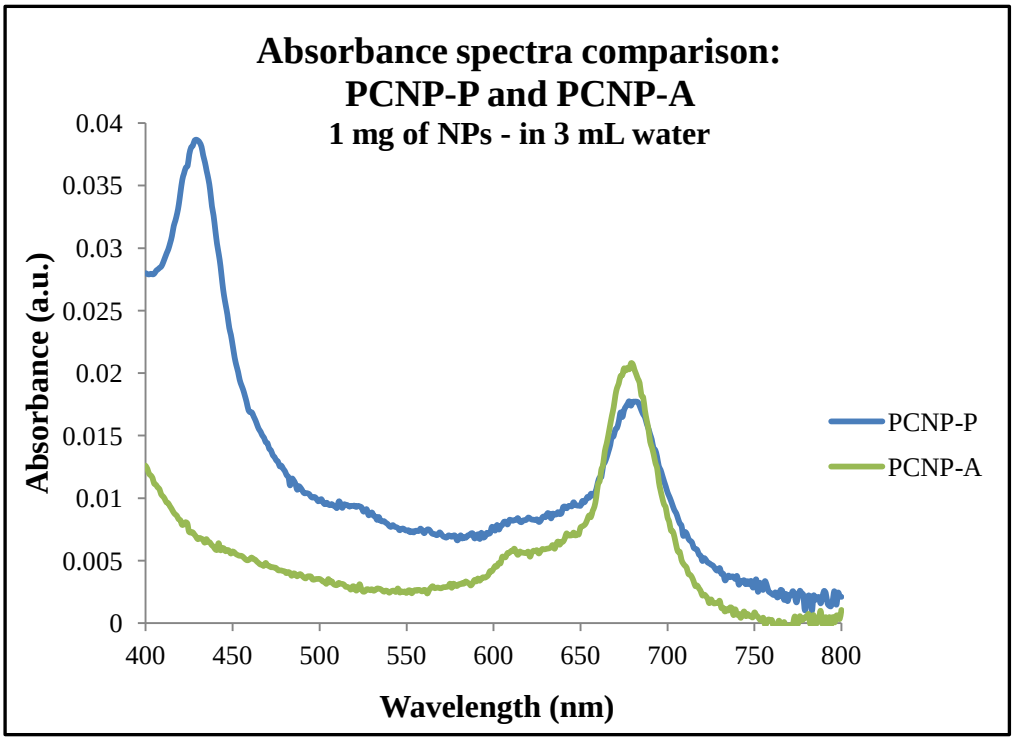

Figure 3.11: PCNP-A and PCNP-P absorbance spectra comparison

The concentration of the entrapped PC and porphyrin were quantified using the Beer-Lambert law and the plotted calibration "straight" lines (Figure 2.40 and Figure 3.12): 1.6

x 10^{-4} moldm^{-3} of PC and 1.8 x 10^{-4} moldm^{-3} porphyrin respectively for PCNP-P (ST DEV 5.09 x 10^{-8} moldm^{-3}; within 30%).

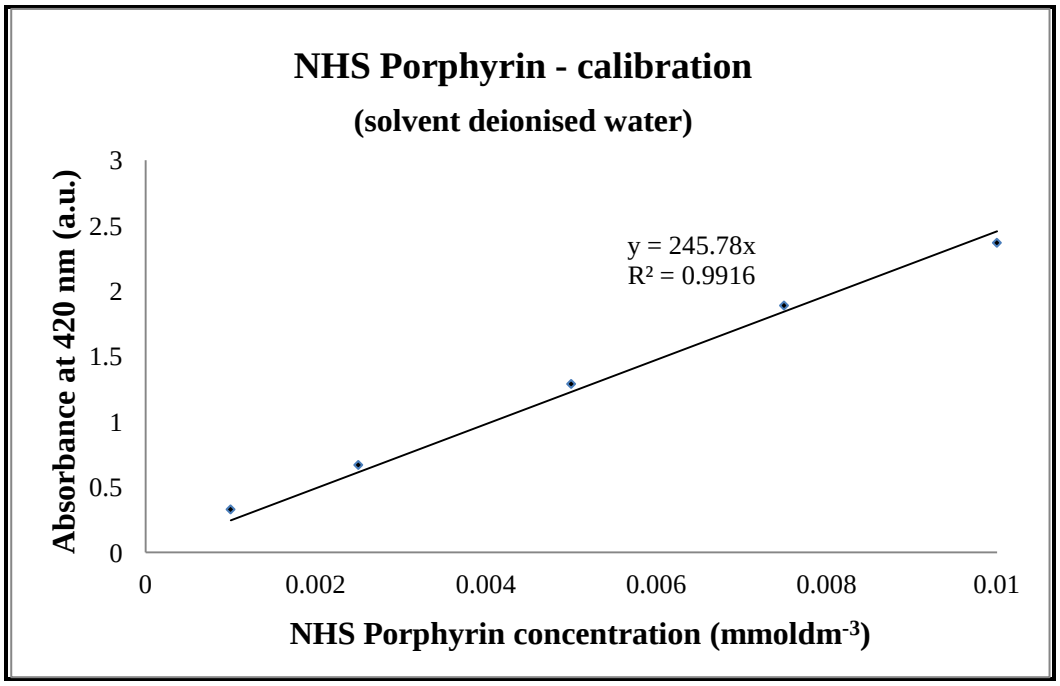

Figure 3.12: NHS Porphyrin calibration "straight" line

3.2 Singlet oxygen production quantification

Following the procedure described in chapter 2.9, the production of singlet oxygen by PCNP-P was qualitatively (by TLC) and quantitatively (by HPLC) measured. The HPLC chromatogram showed a mixture of 7α-, 7β-, 25-, 26-hydroxychoelsterols, 7ketocholesterols. The oxidised derivatives were quantified as a percentage of the cholesterol. This was a 20% increase in singlet oxygen production in comparison to PCNP (MW 30,000 -70,000).

Theoretically, the singlet oxygen ($^1O_2$) produced *via* the Type II process act near to their site of origin, within a radius of action of approximately 20 nm. Size of PCNP-P was 95±10 nm and PCNP was 45 (±10 nm). As the radius of the NPs is above 20 nm, any singlet oxygen produced at the centre of the NP might have not reached the cholesterol in the suspension. PC closer to the NP surface and the surface bound porphyrin should be the key singlet oxygen originators contributed to the oxidised derivatives produced by the PCNP-P system.

Ideally, NPs synthesised to avoid the RES should be ~100 nm in size, with a hydrophilic surface (to avoid clearance by fixed macrophages)[36, 47, 48]. Thus, one of the aims of the project was to synthesise a NP system that would produce sufficient amount of singlet oxygen while maintaining the NP size ~100 nm and PCNP-P nano system fulfilled these criteria.

3.3 Nanoparticle uptake dynamics

The percentage of nanoparticle uptake was quantified using the procedure described in Chapter 2.7.2. Identical concentration (5 mg/1 mL) of PCNP-A and PCNP-P were used in the experiment and both demonstrated a similar but more intense fluctuation pattern as for PCNP (Figure 3.13).

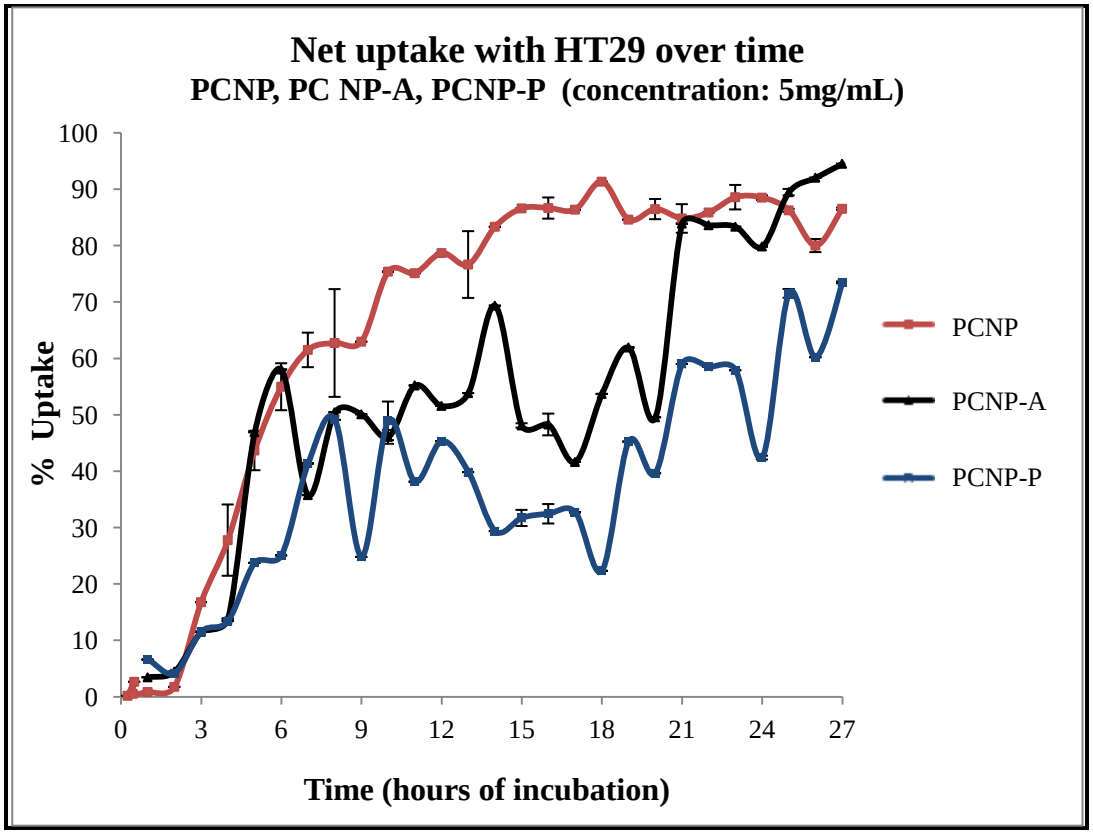

Figure 3.13: Net uptake with HT29 over time - PCNP, PC NP-A, PCNP-P

All three nanoparticle types showed a relatively high uptake at 25 hours. Thus, in the PDT cytotoxicity assays cells were incubated with NPs for 25 hours before irradiation.

3.4 PDT – *In vitro* studies (Maximum uptake)

Since PCNP-P contained both porphyrin and phthalocyanine the Patterson light system with one filter was not appropriate for irradiation. To this end, the Oriel light system (> 580 nm, with a red Schott glass filter, 51310/59510) was chosen to irradiate both PSs. However, to provide the same amount of energy with the Oriel system, it was necessary to irradiate the NP system for approximately 82 minutes. Due to the stress this longer duration could cause, it was important to find an amount of energy that was sufficient to observe a PDT effect with minimum damage caused to the cells due to temperature strains.

In vivo PDT one parameter that limits direct tumour cell destruction is the availability of oxygen within the tissue that is targeted. Oxygen shortage can arise as a result of photochemical consumption of oxygen during the photodynamic process. Two ways to reduce oxygen consumption rates are (i) fractionate the PDT light dose to re-oxygenate the tissue and (ii) to lower the light fluence rate[136]. Fractionated drug dose have been found to be the most effective way to target tumour cells. Compared to the single dose regimens this type of PDT is able to induce long term tumour growth control[236].

Thus, multiple fractionated radiation could benefit from a higher volume of oxygen to a single extensive photoirradiation process. This model is employed in several occasions in the literature[135].

After trial experiments to find the optimum amount of energy using the fractionated modaility, the Oriel light system was used to compare the PDT activity of PCNP and PCNP using the following measures. As per Chapter 2.10, NPs were filtered through a 200 nm filter to ‘sterilise’ the particles. The plated NPs were incubated for 25 hours with HT29

and the cells were irradiated with a dose of energy (7 J/cm^2,~23 min) followed by 40 minute recovery period in the incubator and a further dose of 7 J/cm^2. The light dose (14 J/cm^2) was fractionated with a 40 minute recovery period to allow re-oxygenation of the media. The plates were left in the incubator overnight (18-24 hours) in the dark. MTT activity assays were then used to determine the cell viability.

PCNP-P showed improved cell viability post PDT treatment. After irradiation the viability of cells loaded with PCNP-P was 20% while the non-irradiated dark control was 91%. To elaborate the results, if the NPs were 100% efficient, irradiated cell viability is expected to be 0% and non-irradiated 100%. Using the same conditions as for PCNP-P, cell viability of the PCNP loaded cells post irradiation was 30% and the dark control was 70% (Figure 3.14). The dark toxicity of the PCNP could have been due to the leached phthalocyanine from the NPs during the incubation period. This hypothesis further confirmed that PCNP-P, which does not leach from the NPs, showed almost no dark toxicity.

Russell *et al*.[156] reported cell viability (after irradiation) of 43% and 77% for an analogous experiment without irradiation with gold NPs coated on the surface with phthalocyanines (diameter 2-4 nm). In this case, HeLa cells were incubated with the NPs for 4 hours and irradiated with light at 690 nm (1.84 mWcm^{-2}) for 20 minutes.

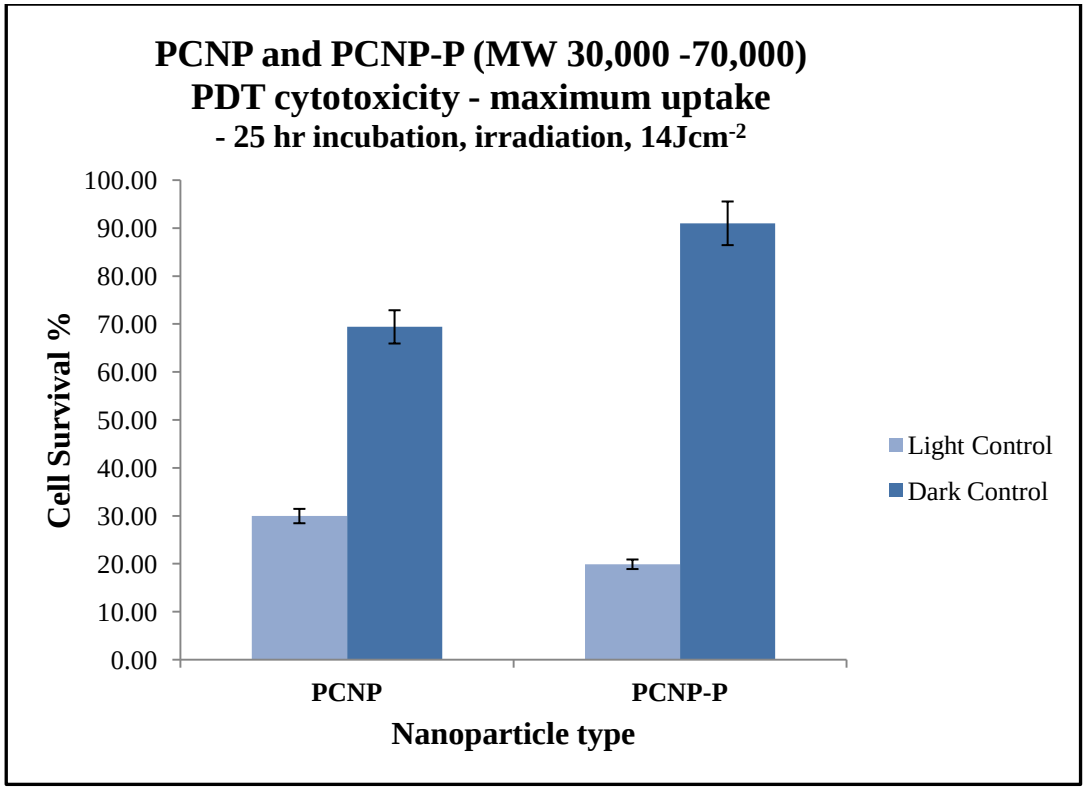

Figure 3.14: PDT cytotoxicity (maximum uptake) - PCNP and PCNP-P (MW 30,000 -70,000)

3.5 PDT - *In vitro* studies (Minimum uptake)

As discussed in Chapter 2, NPs accumulate in tumour neovasculature due to selective retention[134]. It is interesting to try and determine whether there is also an impact by having a component attached to the surface of a particle. Exploiting this notion *in vitro*, HT29 cells surrounded with PCNP-P in the extracellular media and at the minimum uptake time (<5 minutes) were irradiated under identical conditions to those used for the 25 hour uptake time. MTT assays were then performed as before and cell viabilities determined (Figure 3.15).

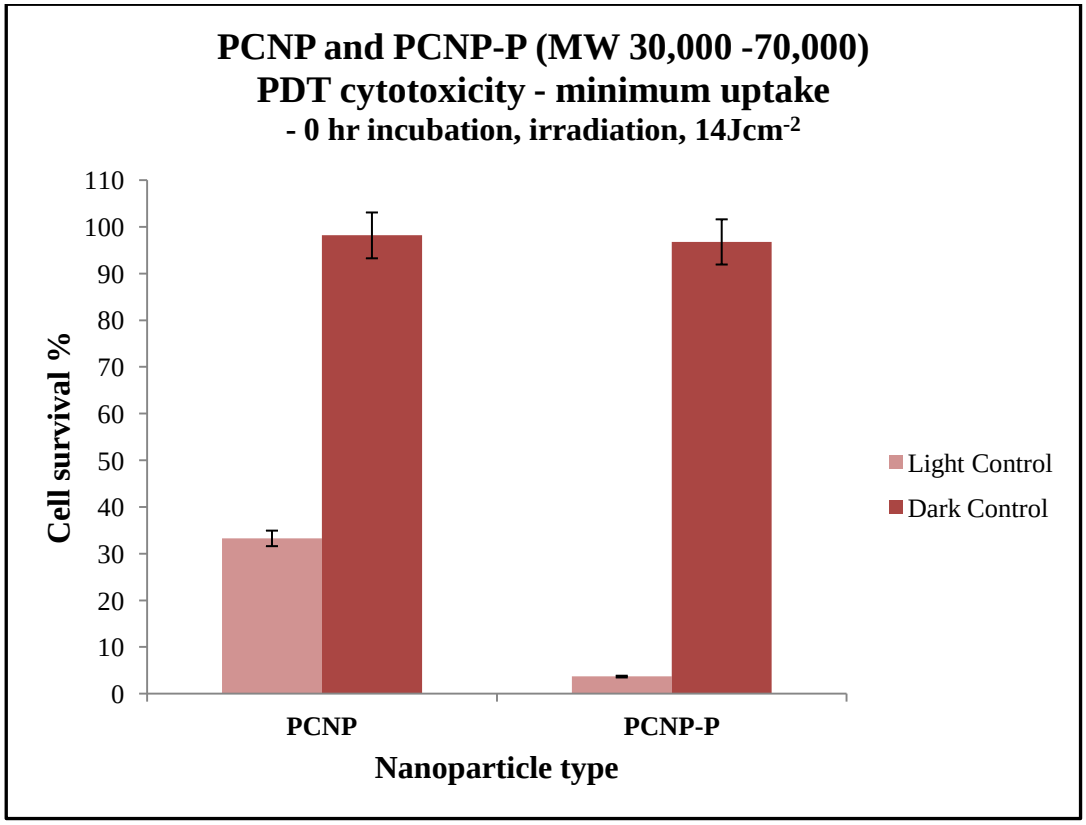

Figure 3.15: PDT cytotoxicity (minimum uptake) - PCNP and PCNP-P (MW 30,000 -70,000)

PCNP-P showed the lowest cell viability post irradiation with only 3.7% of cells surviving whereas the cell viability of PCNP was 33%. However, the cell survival with both non-irradiated PCNP and PCNP-P was 100%. This result could be due to, in this instance, the NPs being mixed with cells only for the duration of the irradiation (approximately 90 minutes). These results are potentially very interesting from a clinical perspective, as it is likely that a significant proportion of NPs would accumulate in the stroma of the tumour *i.e.* in the extracellular space. It is demonstrated here that if this localised concentration is high enough cancer cells can be effectively killed without the requirement that the NPs be internalised.

The reason for the high PDT activity of the minimum nanoparticle uptake study could be due to the presence of NPs in the surrounding area during irradiation. A higher concentration of NPs carries more PSs enabling greater singlet oxygen production. From the nanoparticle uptake studies it was established that only 60 - 90% of the NPs were internalised at the maximum uptake time. However, in the minimum uptake studies, irradiation was performed while 100% of the NPs were present in the cell environment.

3.6 Intracellular distribution of NPs

According to the cell uptake studies, the maximum uptake of NPs should have been reached in 18 hours. The confocal microscopy images below display the localisation of the PCNP-P which have been incubated with HT29 cells for 20 hours and washed three times with media prior to imaging. The confocal images were captured at 633 and 405 nm (Figure 3.16) using Leica Microsystems CMS GmbH (LAS AF version: 2.2.1 build 4842). Although, the PC absorbs significantly at approximately 400 nm, excitation at 405 nm gave no fluorescence from the PCNP. Thus, the fluorescence observed with PCNP-P (excited at 405 nm) was considered to be only that emitted by the porphyrin. PC emission was captured by NP excitation at 633 nm.

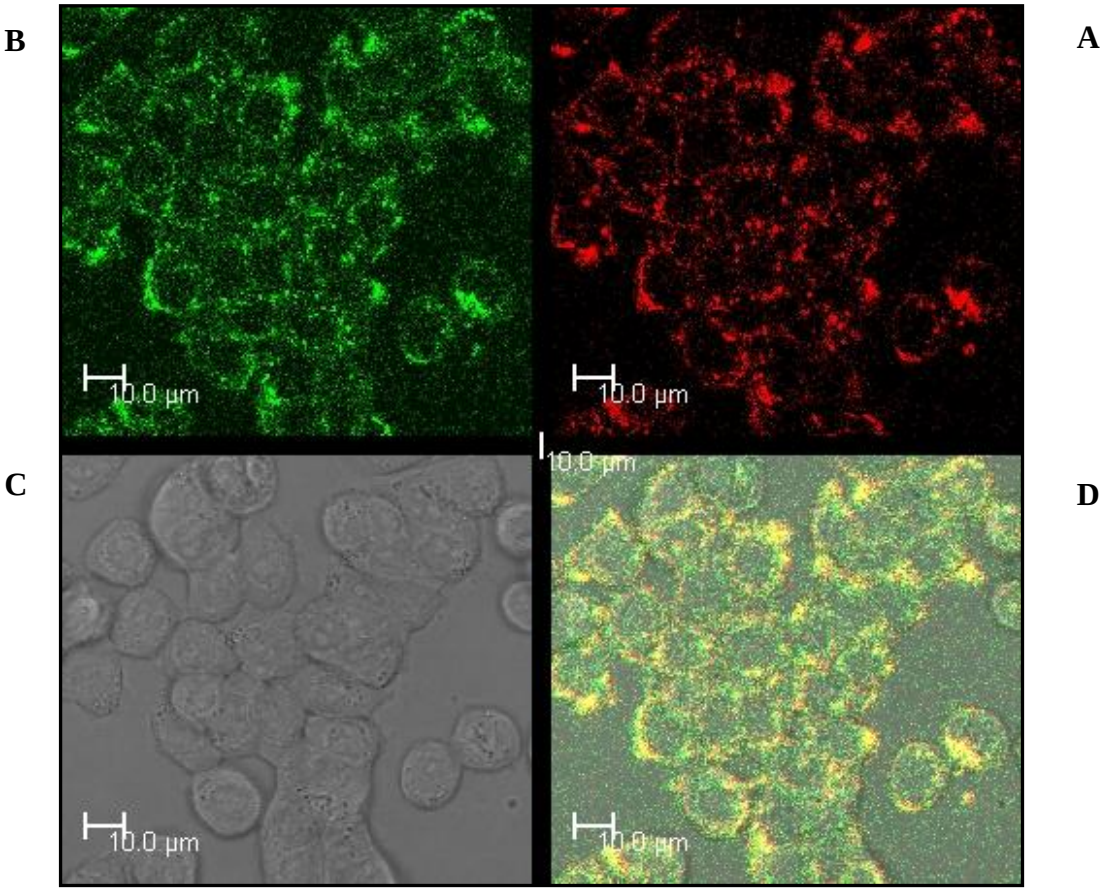

Figure 3.16: Confocal images (Leica) of PCNP-P internalised in HT29 cells*

*After incubating for 20 hours - (Red – excited at 633 nm; green – excited at 405 nm); A - PC emission, B - porphyrin emission, C - HT29 cells only, D - merged image

As can be seen from Figure 3.16, cells show granular fluorescence (PC and porphyrin) suggesting localisation of the NPs in endocytic vessels [58].

3.7 Summary

Successfully entrapped photosensitiser NP systems described in Chapter 2 were functionalised and a chosen PCNP was further developed to conjugate another photosensitiser (porphyrin) onto the matrix. This enhanced system was studied for *in vitro* uptake and intracellular distribution in HT29 cells. Production of singlet oxygen was quantified and the PDT cytotoxicity assays were carried out using the maximum and minimum uptake times with the chosen NP–PCNP-P system and showed some excellent results. After irradiation (maximum uptake) the viability of cells loaded with PCNP-P was 20% while the non-irradiated dark control was 91%. In the minimum uptake study, PCNP-P showed the lowest cell viability post-irradiation with only 3.7% of cells surviving and the cell survival for non-irradiated cells was 100%. In the project, PCNP-P is established as a potential delivery system to use *in vivo* (Table 3.1).

Positive characteristic of the PCNP-P	**The advantage for efficient delivery**
These NPs are 95±10 nm in size	NPs less than 100 nm are able to avoid the RES[36, 237]
The ability to deliver more than one class of PS	Larger spectral region covered could lead to more efficient absorption of light
Cationic nature of PCNP-P	Could potentially be attractive for PACT
No leaching from the NPs	Assured maximum passive targeting
Almost no dark toxicity	Selective targeting – efficient PDT treatment

Table 3.1: PCNP-P Summary

Chapter 4: Concluding remarks

The aim of the project was to synthesise PSs/dyes suitable for encapsulation within NPs, both functionalised and non-functionalised, and to study their behaviour in cell uptake, PDT and PACT.

To this end, a number of PSs/dyes have been entrapped within a range of polyacrylamide NPs and amino functionalised: MB, DSRuCl, PyPorphyrin. However, leaching from the matrix was identified as a challenge to overcome. To this end, sterically bulky groups, PEG(750)Porphyrin and PCNP (MW 15,000- 30,000 and 30,000-70,000) were synthesised whilst dextran (MW 10,000) conjugated fluorescein (reference dye) and MB dyes were purchased to entrap in the polyacrylamide matrix. The mean NP size, 45 (±10 nm) was determined by PCS and TEM images. Further they were characterised for the presence of PSs within the NPs by spectroscopic investigation (absorbance and/or fluorescence) and the concentration of entrapped PSs/probes (using absorbance spectroscopy).

Production of the main PDT agent, singlet oxygen, was quantified to observe the relationship between the singlet oxygen production and cell cytoxicity assays. Singlet oxygen production of PCNP (30,000 – 70,000 Da) was 360% more than the singlet oxygen production of PCNP (15,000 - 30,000 Da). The singlet oxygen production of PCNP-P (30,000 – 70,000 Da) was 20% more than PCNP (30,000 – 70,000 Da).

Uptake of the NPs by HT29 cells was investigated using flow cytometry. First, fluorescein reference dye (fluorescein dextran 10,000MW) entrapped NPs were used to conduct the time course experiment that established an oscillation pattern with the NP uptake. PI was

used to confirm how long HT29 cells can be kept alive under the experimental conditions. No peaks were observed in the FL3 and FL4 detectors in the experiment. Only the fluorescence peak from fluorescein (FL1 peak) was observed. Although it could have been possible to continue the experiment and observe how much longer these cells can be kept alive under the present conditions, as 48 hours is generally much more time than required for assay experiments, the study was discontinued at 48 hours and it was confirmed that the HT29 cells can be used in NP assays up to 48 hours.

Subsequently, the fluctuation of the NP net uptake by flow cytometry was studied over 28 hours using PCNP with HT29 cells incubated at 37°C in a humidified environment of 5% CO_2. Two concentrations (3 mg/mL and 5mg/mL) of NPs were studied and the percentage uptake values confirmed that NP uptake by HT29 was concentration dependent. According to the quantified NP uptake profile, NP uptake reaches its maximum within 18 hours and then remains constant but with regular fluctuations.

Intracellular distribution of NPs was determined by confocal microscopy and maximum uptake was observed after 18 hours of incubation. Cells showed granular fluorescence from the PSs suggesting localisation of the NPs in endocytic vessels.

PDT cytotoxicity assays were carried out using the maximum and minimum uptake times with the chosen NP-PCNP and PCNP-P.

When irradiated at the maximum uptake time (25 hour), the cell viability of the light controlled PCNP experiment was 18% and the cell viability of the dark controlled

experiment was 87%. After irradiation (maximum uptake) the viability of cells loaded with PCNP-P was 20% while the non-irradiated dark control was 91%.

The cell viability of HT29 cells surrounded with PCNP in the extracellular media at the minimum uptake time (<5 minutes) was 33%. However, no noticeable dark toxicity was observed with PCNP. This result could be due to, in this instance, the NPs being mixed with cells only for the duration of the irradiation (approximately 90 minutes). In the minimum uptake study, PCNP-P showed the lowest cell viability post-irradiation with only 3.7% of cells surviving and the cell survival for non-irradiated cells was 100%. In the project, PCNP-P is established as a potential delivery system to use *in vivo.*

The results presented here indicate that polyacrylamide NPs have potential as delivery vehicles for photodynamic agents in PDT for cancer. Both internally trapped PSs and analogues with a second PS conjugated to the particles after formation were active against HT-29 cells, but the latter was the more powerful PDT agent when the particles were internalised. The ability to deliver more than one class of PS could be advantageous clinically as the larger spectral region covered could lead to more efficient absorption of light. The cationic nature of PCNP-P also makes it potentially attractive for Photodynamic Antimicrobial Chemotherapy (PACT).

Results also show that cellular internalisation is not necessary to photodynamically kill cancer cells, although internalised particles are also active, this could be important *in vivo* as significant amounts of nanoparticle would be expected to accumulate in the extracellular space in tumours due to the enhance permeability and retention effect.

4.1 Future work

The project compares the PDT cytotoxicity of PCNP with PCNP-P. Another interesting step could be to synthesise a nanoparticle system with only the 5-[4-(Succinimide-N-oxycarbonyl)phenyl]-10,15,20-tris-(4-*N*-methylpyridimiumyl)porphyrin trichloride attached external to the nanoparticle and compare the PDT assay results with PCNP and PCNP-P.

In the project, 5-(4-phenylpropenoate)-10,15,20-triphenylporphyrinatozinc was successfully synthesised to use in GTP. However, the porphyrin molecule (monomer) did not copolymerise in the reaction and thus, with the limited time frame of the Project, this concept has not been pursued further.

Steps to consider, facilitating the reaction:

- Increase the length of the link between the functional handle of the porphyrin to enable spacing the steric bulk of the porphyrin further from the polymerisation centre.

- Perform the reaction over a longer period.

In the study with biofilms, it was shown that NPs have the potential to penetrate efficiently into a biofilm. This would be an interesting area to investigate with a photosensitiser NP delivery system.

In the Project the system relies on passive targeting due to the attractive physical properties of the NPs. To enhance the current system, targeting agents can be attached to NPs to increase localised tumour concentrations[146, 157, 169].

Chapter 5: Experimental

5.1 Organic synthesis

General

- Starting materials were purchased from Fluka, Lancaster or Sigma Aldrich and used without further purification unless otherwise stated.

- Solvents were of general purpose or HPLC grade and were purchased from Fischer Scientific.

- All NMR spectra were acquired in the solvent indicated with chemical shifts (δ) quoted as parts per million values (ppm) and coupling constants (J) quoted in Hertz (Hz). NMR spectra were obtained from either a JEOL JNM-ECP 400 MHZ FT-NMR spectrometer or JEOL JNM-LA400 FT NMR spectrometer, at a frequency of 400MHz for ^{1}H, 100 MHz for ^{13}C and 376 Hz for ^{19}F spectra. Chemical shifts are quoted in ppm relative to $SiMe_4$, which was used as an internal standard, unless the solvent used was DMSO, in which case ppm values are relative to the DMSO singlet at 2.62.

- Ultra violet/visible absorption spectra were recorded on a Varian Cary 50Bio UV- Vis spectrometer. Cuvettes used were Starna opti glass 2 type 23 (optical glass, 10 mm) and a VWR International, uv-vis. Optical glass, 10 mm, from Starna (Hainault) and VWR International Limited (Leicestershire) respectively.

- Fluorescence spectra were recorded on a Cary Eclipse Fluorescence spectrometer.

- Analytical TLC was carried out using aluminium backed silica gel 60 F254 (Merck plates) and visualised using UV light (254/365 nm).

- Column chromatography was performed using ICN silica 32-63, 60Å.

- All water used was deionised, ELGASTAT Prima Reverse Osmosis unless otherwise stated.

- Mass spectrometry results, where the most abundant peak of the M+ is quoted, were obtained *via* services provided by:
  - EPSRC National Mass Spectrometry Service Centre, Chemistry Department University of Wales Swansea. Analyses were made using the following instrumentation: MALDI Applied Biosystems
  - Mass spectra were recorded on a Bruker Reflex IV matrix assisted laser desorption ionisation-time of flight (MALDI-TOF) mass spectrometer.

- Gel Permeation Chromatography (GPC) was performed using Viscotek 270 Dual detector

- Elemental analyses were obtained on a Fisons EA1108 CHN

- THF was dried over sodium under a nitrogen atmosphere with benzophenone as the indicator.

Synthesis

5.1.1 Disulphonated 4,7-diphenyl-1,10-phenanthroline ruthenium (II) chloride (DSRuCl) synthesis (1)

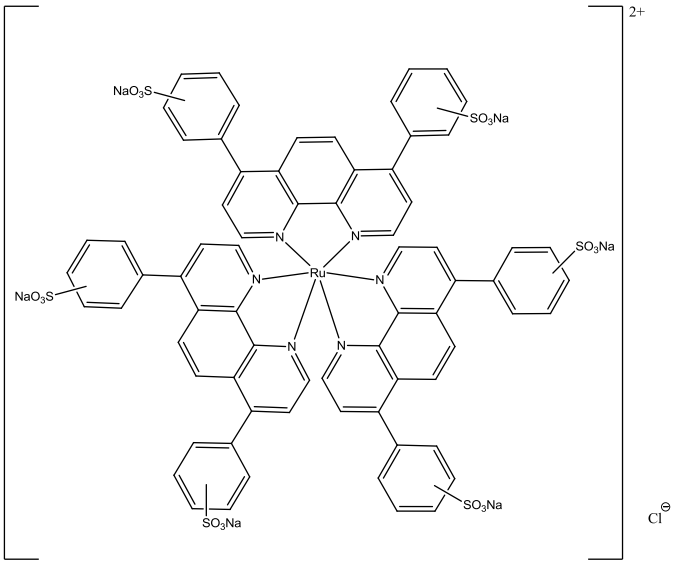

The compound was synthesised according to literature procedures[198, 199]. $RuCl_3$ (57 mg, 0.0276 mmol) was refluxed while stirring in 4,7-diphenyl-1,10-phenanthrolinedisulfonic acid disodium salt (518 mg, 0.0965 mmol, 3.5 equiv.) in 20 mL of deionised water for 48 hours. The colour of the reaction mixture changed from dark green to red over the period. The solution was cooled to room temperature, filtered and excess solvent removed *in vacuo*.

The resultant red-brown solid was purified by size exclusion chromatography with a Sephadex-medium (solvent distilled water). The bright red fraction was collected and concentrated *in vacuo* to obtain the product, DSRuCl (yield 44.8 mg, 90%).

λ_{ex} (DI water)/nm 461 (λ_{em} 612 nm)

Elemental analysis:

Element	**Expected results %**	**Actual results %**
Carbon	47.18	42.61
Hydrogen	3.96	2.81
Nitrogen	4.23	4.08
Sulphur	9.69	7.88

The discrepancy between the calculated and results obtained is discussed in Chapter 2.2 (page 76).

5.1.2 5,10,15,20-Tetrakis (4-N-methylpyridiniumyl)porphyrin tetraiodide synthesis (2)

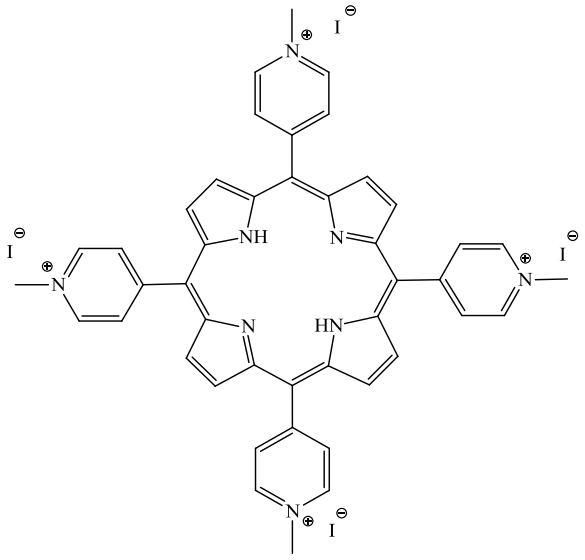

The compound was synthesised according to literature procedure[231]. Iodomethane (2 mL, 32.326 mmol, 200 equiv.) was added to a stirred solution of 5,10,15,20-tetra 4-pyridyl porphyrin (100 mg, 0.161 mmol) in dry DMF (20 mL). The reaction was stirred at 40°C for 17 hours. The crude product was precipitated with ice cold diethyl ether after cooling the solution to room temperature. The precipitate was washed several times with diethyl ether to remove any trace of iodomethane. The precipitate was dissolved in water:acetone (1:1). The solvents were removed under reduced pressure. The porphyrin was precipitated from acetone (190 mg, 99.44%) as a purple solid.

^{1}H NMR [400MHz, $(CD_3)_2SO$], δ: -3.12 (2H, br s, NH), 4.71 (12H, s, CH_3), 8.99 (8H, d, *J* = 6.2Hz Ar-3, 5-H), 9.20 (8H, s, β-H), 9.48 (8H, d, *J*= 6.2Hz Ar- 2, 6-H); **^{13}C NMR [100MHz, $(CD_3)_2SO$], δ:** 47.9, 120.5, 127.7, 133.9, 134.6, 135.8, 142.3, 156.2; **UV-Vis (H_2O) λ_{max}** 423, 512, 519 nm; **Mass (MALDI) *m/z*** 677[M+3e].

5.1.3 5-(4-Hydroxyphenyl)-10,15,20-triphenylporphyrin synthesis (3)

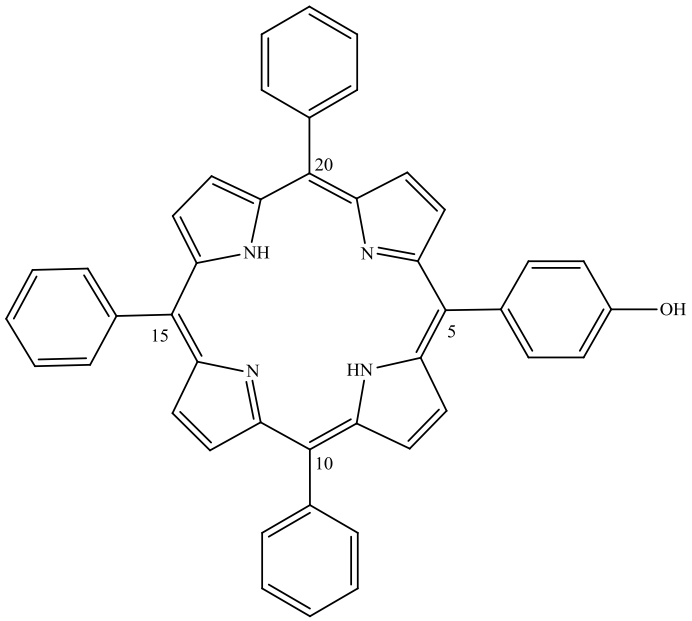

The compound was synthesised adopting the Adler method[201]. 4-Hydroxybenzaldehyde (1.808 g, 14.81 mmol) and benzaldehyde (4.5 mL, 44.43 mmol) were added to the refluxing propionic acid (222.5 mL). Once the aldehydes were dissolved, pyrrole (4 mL, 59.25 mmol) was added cautiously. The reaction mixture was reacted at reflux for one hour and then the solvent was removed *in vacuo*. The resulting solid was separated by flash chromatography (silica, eluent dichloromethane), to obtain 5-(4-hydroxyphenyl)-10,15,20-triphenylporphyrin (0.54 g, 5.8%).

^{1}H NMR [400MHz, $CDCl_3$] δ: -2.79 (2H, br s, CH_2), 5.35 (1H, br s, OH), 7.22 (2H, m, 5-Ar-*o*-H), 7.70-7.82 (9H, m, 10,15,20-Ar-*m,p*-H), 8.08 (2H, m, 5-Ar-*o*-H), 8.22 (6H, m, 10,15,20-Ar-*o*-H), 8.09-8.85 (6H, m, β-H), 8.88 (2H, m, β-H); **^{13}C NMR [100MHz, $CDCl_3$],δ:** 113.7, 120.1, 120.5, 126.7, 127.3, 127.7, 133.7, 133.9, 134.6, 135.8, 142.3, 156.7; **UV-Vis ($CDCl_3$) λ_{max}** 416, 417,419, 420,516,552,593,647 nm; **Mass (MALDI) *m/z*** 630 (M+).

5.1.4 5-(4-Hydroxyphenyl)-10,15,20-triphenylporphyrinatozinc synthesis (4)

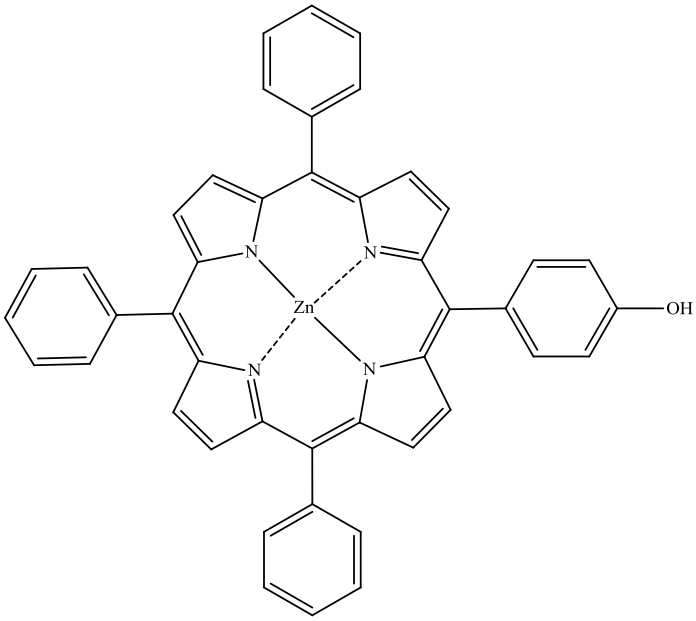

The compound was synthesised according to the literature procedure[238]. A solution of zinc acetate (1.87 g, 8.56 mol) dissolved in methanol (40 mL) was added to a solution of 5-(4-hydroxyphenyl)-10,15,20-triphenylporphyrin (0.54 g, 0.856 mmol) dissolved in DCM (100 mL). The mixture was stirred at 40°C for 2 hours protected from light. The residue was washed with water (2 x 100 mL) and brine (100 mL) followed by an extraction with DCM (200 mL). A fine purple residue was obtained after removal of the solvent under reduced pressure (0.549 g, 92.4%).

^{1}H NMR [400MHz, $CDCl_3$] δ 5.35 (1H, br s, OH), 7.14 (2H, d, *J*= 8.0Hz, 5-Ar-*o*-H), 7.71-7.75 (9H, m, 10,15,20-Ar-*m,p*-H), 8.04 (2H, d, *J*= 8.0Hz, 5-Ar-*o*-H), 8.21 (6H, m, 10,15,20-Ar-*o*-H), 8.89 (6H, d, *J* = 4.5Hz, β-H), 8.95 (2H, d, *J* = 4.5Hz, β-H); **^{13}C NMR**

[100MHz, $CDCl_3$],δ: 113.4, 126.4, 127.3, 131.7, 131.9, 134.5, 135,6, 143.2, 150.1; **UV-Vis ($CDCl_3$) λ_{max}** 417, 419, 421, 548, 588 nm; **Mass (MALDI) *m/z*** 692 (M+).

5.1.5 5-(4-Phenylpropenoate)-10,15,20-triphenylporphyrinatozinc synthesis (5)

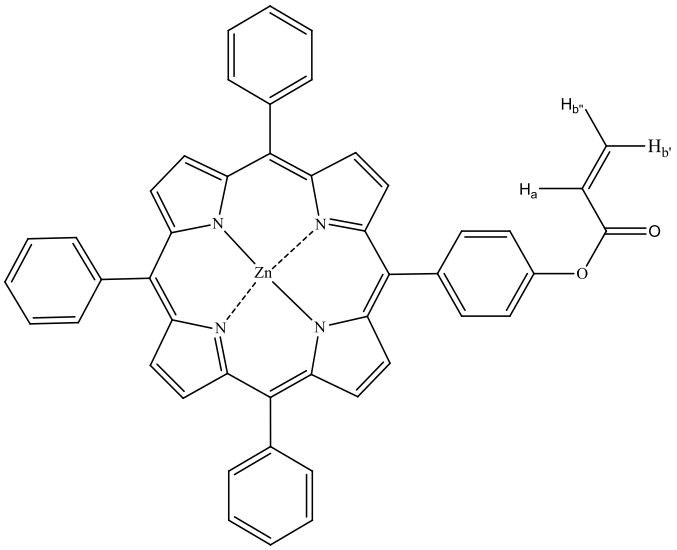

The compound was synthesised adopting the literature procedure[204]. Triethylamine (1.32 mL, 7.9 mmol) was added to the solution of 5-(4-hydroxyphenyl)-10,15,20-triphenylporphyrinatozinc (0.549 g, 0.79 mmol) in dry DCM under nitrogen. Acryloyl chloride (0.64 mL, 7.9 mmol) was added dropwise, by syringe, to the solution at 5°C and the solution was left stirring for 25 minutes. Saturated sodium hydrogen carbonate (30 mL) solution was added to quench the reaction and the organic phase was washed with water (3 x 100 mL). The solvent was removed *in vacuo* and the crude purple solid was purified by flash chromatography (silica, eluent hexane:DCM (90:10)). Purified yield: 0.33 g, (55.8%).

^{1}H NMR [400MHz, $CDCl_3$] – δ: 6.06 (1H, d, *J*=10.4Hz, $H_{b'}$), 6.41 (1H, dd, *J*=10.4Hz and 17.5Hz, H_a), 6.69 (1H, d, *J*=17.5Hz, $H_{b''}$), 7.37-7.54 (2H, m, 5-Ar-*o*-H), 7.57 -7.82 (9H, m, 10,15,20-Ar-*m*,*p*-H), 8.05-8.30 (8H, m, 10,15,20-Ar-*o*-H),8.82-9.05 (2H, m, β-H);

^{13}C NMR [100MHz, $CDCl_3$], δ: 119.4, 126.4, 127.3, 128.0, 131.6, 131.8, 132.9, 150.1; **UV-Vis ($CDCl_3$) $\lambda_{max/nm}$** 419, 548, 581 nm; **Mass (MALDI) *m/z*** 746 $[M]^+$

5.1.6 4-Toluenesulfonic acid-1-(2-(2-(2-methoxy)ethoxy)ethoxy)ethyl ester (TEGTs) synthesis (6)

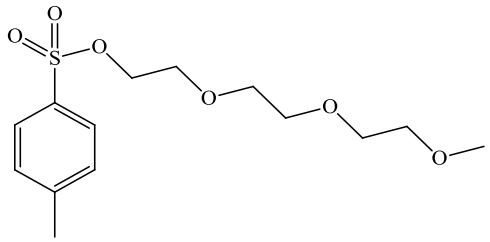

The compound was synthesised according to the literature procedure[206]. Monomethoxy tri(ethyleneglycol) (9.9 g, 60.51 mmol) was added to a solution of triethyl amine (9.10 g, 12.7 mL, 90.8 mmol) in dry, alcohol-free chloroform (200 mL) under nitrogen. After cooling the mixture to 0°C in an ice/salt bath, 4-toluenesulfonyl chloride (15.0 g, 78.7 mmol) was added and the reaction was stirred for 20 minutes. Ice/salt bath was removed and the reaction was stirred at room temperature for 17 hours under nitrogen. Toluene (100 mL) was added to the reaction mixture and the solvent was removed *in vacuo*. The residue was dissolved in ethyl acetate (300 mL) and the triethylammonium chloride was removed by vacuum filtration. The residue was further washed with ethyl acetate (2 x 50 mL). The organic filtrates were combined and the ethyl acetate solution was washed once with potassium hydrogen sulphate 1M solution (100 mL) followed by saturated sodium hydrogen carbonate solution (100 mL) and twice with water (100 mL). The organic phase was dried over anhydrous magnesium sulphate, filtered and the solvent removed from the filtrate *in vacuo*. The crude product was purified by flash chromatography (silica, eluent: ethyl acetate: hexane (60:40)), Yield 3.89 g, 20.2%.

^{1}H NMR [400 MHz, $CDCl_3$],δ: 2.45 (3H, s, CH_3), 3.37 (3H, s, OCH_3), 3.52- 3.54 (2H, t, *J*= 4.7Hz CH_2), 3.59 – 3.62 (6H, s, CH_2), 3.67-3.70(2H, t, *J*= 4.7Hz CH_2), 4.15- 4.17 (2H,

t, *J*= 4.7Hz CH_2), 7.35 (2H, d, J=8.0Hz, Ar-3, 5-H), 7.80 (2H, d, *J*= 8.0Hz, Ar- 2, 6-H); **^{13}C NMR [100 MHz, $CDCl_3$],δ:** 21.5, 58.7, 68.3, 70.2, 71.6, 127.7, 129.6, 130.0, 132.7, 144.6; **Mass (Nanospray Ionisation)** ***m/z*** 318 (M+).

5.1.7 5,10,15,20-Tetra-(4-carbomethoxyphenyl)porphyrin synthesis (7)

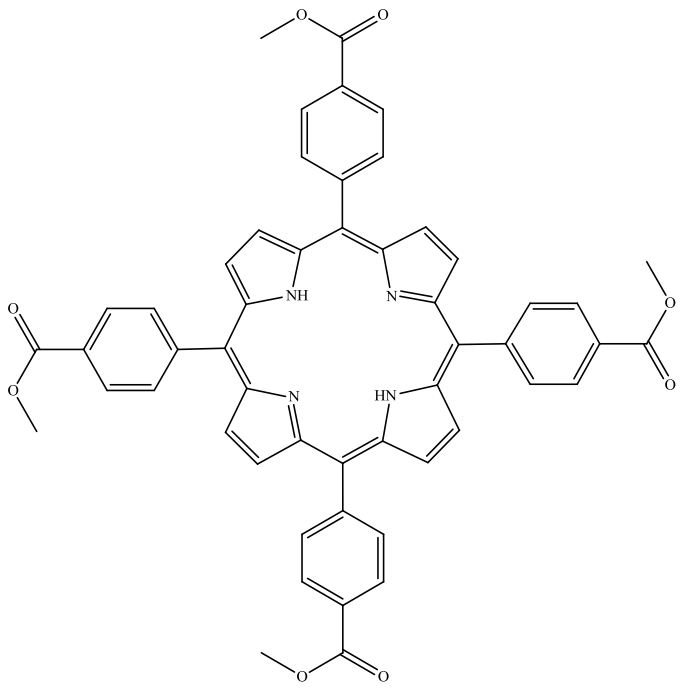

The compound was synthesised adopting the Adler method[201] according to the method described in the literature[207]. Methyl 4-formylbenzoate (19.45 g, 0.1185 mol) was added to refluxing propionic acid (445 mL). Pyrrole (8 mL, 0.1185 mol) was added cautiously to the solution. The mixture was refluxed for 30 minutes and left at room temperature for 16 hours, then filtered to yield a purple solid. Using a mixture of dichloromethane/methanol (98:2) as an eluent and precipitation with methanol over dichloromethane the pure product was obtained as a purple solid in 22.20% yield (5.57 g).

R*f* = 0.25 (silica, 0.05% MeOH: CH_2Cl_2); **^{1}H NMR [400MHz, $CDCl_3$], δ:** -2.79 (2H, br s, NH), 4.09 (12H, s, OCH_3), 8.30 (8H, d, *J* = 8.0Hz, Ar-3,5-H), 8.46 (8H, d, *J*= 8.0Hz, Ar-2, 6-H), 8.83 (8H, s, β-H); **^{13}C NMR [100MHz, $CDCl_3$], δ**: 52.5 ($O\underline{C}H_3$), 119.4, 128.0, 130.0, 134.5, 146.6, 167.2 ($\underline{C}O_2CH_3$); **UV-Vis ($CHCl_3$) λ_{max}** 421, 516, 551, 591, 625, 646 nm ; **Mass (MALDI) *m/z*** 847 $[M+H]^+$

5.1.8 5,10,15,20-Tetra-(4-hydroxymethylphenyl)porphyrin synthesis (8)

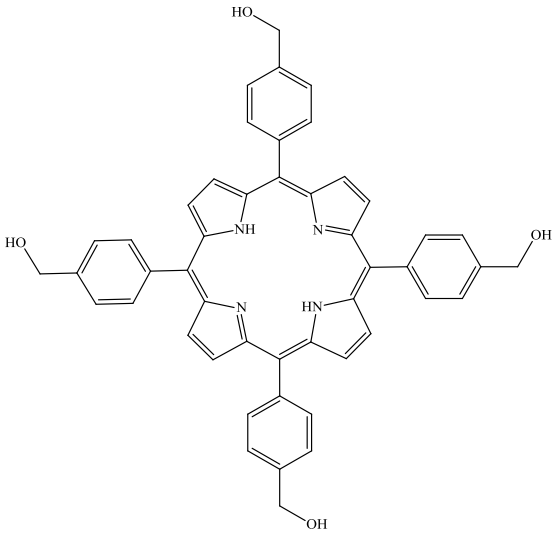

The compound was synthesised adopting the Adler method[201] according to the method described in the literature[207]. 5,10,15,20-Tetra(4-carbomethoxyphenyl) porphyrin (100 mg, 0.118 mmol) was added to freshly distilled (dried and degassed) tetrahydrofuran (75 mL), stirred under nitrogen and cooled to 0°C. Once the porphyrin was fully dissolved, lithium aluminium hydride (516 mg, 13.6 mmol, 115 equiv.) was added to the reaction mixture and left stirring in the dark at room temperature for 48 hours. The unreacted $LiAlH_4$ was decomposed with moist ether at 0°C and the solution was filtered through a celite bed. The colourless filtrate was extracted with dichloromethane:methanol (70:30). The combined extracts were distilled *in vacuo*. The solid was washed with DCM followed by MeOH and this was recrystallised from hexane - DCM. The residual lithium aluminium hydroxide was washed with water (2 x 200 mL) followed by MeOH (2 x 200 mL). A fine purple solid was obtained after filtration (1.2 mg, 1.38%).

^{1}H NMR [400MHz, $(CD_3)_2SO$], δ: -2.93 (2H, br s, NH), 4.86 (8H, s, CH_2) 5.51(4H, br s, OH), 7.75 (8H, d, *J* = 7.8Hz Ar-3, 5-H), 8.15 (8H, d, *J*= 7.8Hz, Ar- 2, 6-H), 8.82(8H, s, β-

H); **^{13}C NMR [100MHz, $CDCl_3$], δ**: 62.9, 120.0, 125.0, 134.0, 139.3, 142.3; **UV-Vis $(CD_3)_2SO$) λ_{max}** 417, 419, 515, 550,590,648 nm ; **Mass (MALDI) *m/z*** 734 (M+).

5.1.9 5,10,15,20-Tetra-[4-(bromomethyl)phenyl]porphyrin synthesis (9)

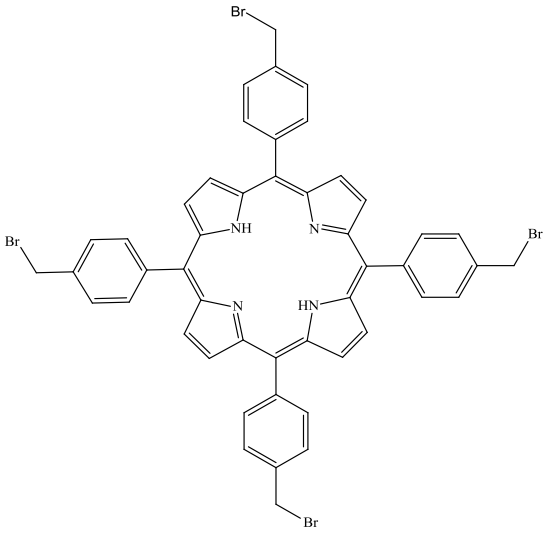

The compound was synthesised adopting the Lyndsey method[239]. To 1.5 L of chloroform were added 4-bromomethylbenzaaldehyde (2.99 g, 0.015 mol) and pyrrole (1.05 mL, 0.015 mol). After degassing the mixture (under nitrogen for 30 minutes), $BF_3.OEt_2$ (0.6 mL, 5 mmol) was added and the reaction was allowed to stir at room temperature, protected from the light and under a nitrogen atmosphere for one hour. After this period, triethylamine (0.84 mL, 16 mmol) and tetrachlorobenzoquinone (2.78 g, 11.3 mmol) were added, the temperature was raised and the reaction kept under reflux for one hour. The volume of the reaction was then reduced to c.a.250 mL and filtered through a short plug of silica gel (eluent CH_2Cl_2/MeOH initially 99:1 rising to 9:1). The product was obtained pure after precipitation with methanol over dichloromethane (1.29 g, 32.44%).

^{1}H NMR [400MHz, $CDCl_3$], δ: -2.81 (2H, br s, NH), 4.86 (8H, s, CH_2), 7.80 (8H, d, *J*=8.1Hz, 5,10,15,20-Ar-*m*-H), 8.19 (8H, d, *J*=8.1Hz, 5,10,15,20-Ar-*o*-H), 8.85 (8H, br s, H-β); **^{13}C NMR [100MHz, $CDCl_3$], δ**:33.5 ($\underline{\mathbf{C}}H_2$), 119.5 (*meso*-C), 127.5 (5,10,15,20-Ar-*m*-C), 130.0 (5,10,15,20-Ar-*o*-C), 134.9, 137.4, 142.2; **UV-Vis ($CHCl_3$) λ_{max}** 419, 421, 423, 425, 516, 552, 591, 646 nm ; **Mass (MALDI) *m/z*** 987 $[M+H]^+$.

5.1.10 5,10,15,20-Tetra(pentafluorophenyl) porphyrin synthesis (10)

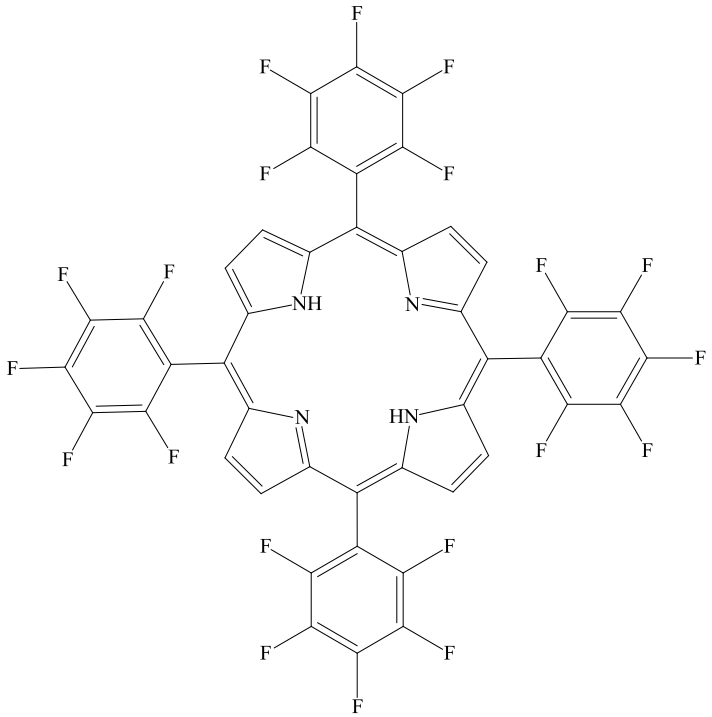

The compound was synthesised according to literature procedure[211]. Pyrrole (6 mL, 0.0865 mol) was added drop wise to a refluxing mixture of acetic acid (300 mL), nitrobenzene (150 mL) and pentafluorobenzaldehyde (10.68 mL, 0.0865 mol) and the mixture was refluxed for a further 45 minutes. Once the mixture had cooled to room temperature, methanol (100 mL) was added to induce crystallisation and the solvents were removed *in vacuo.* The product was purified by flash chromatography (silica, eluent CH_2Cl_2:C_6H_6 3:7) and was concentrated *in vacuo* to give 5,10,15,20-tetra(pentafluorophenyl) porphyrin as a purple solid (1.26 g, 5.98%). Note: hexane was used to remove the last traces of nitrobenzene. The spectral data for the compound was consistent with the data reported in the literature and the assignments of the signals were carried out accordingly[240].

^{1}H NMR [400MHz, $CDCl_3$], δ: -2.9 (2H, s, NH), 8.92 (8H, s, β-H); **^{19}F NMR [376MHz, $CDCl_3$], δ:** -160.9 (m, 2F, *m*-F), -151.1 (t, 1F, *J*=18.4Hz, *p*-F), -136.35 (m, 2F, 51.4Hz, *o*-F); **UV-Vis ($CHCl_3$) λ_{max}** 410, 516, 552, 591, 636 nm ; **MS (MALDI): *m/z*** 975 (M+).

5.1.11 5,10,15,20-Tetrakis[2,3,5,6-tetrafluoro-4-{PEG(750)-sulfanyl}-phenyl]-porphyrin synthesis (11)

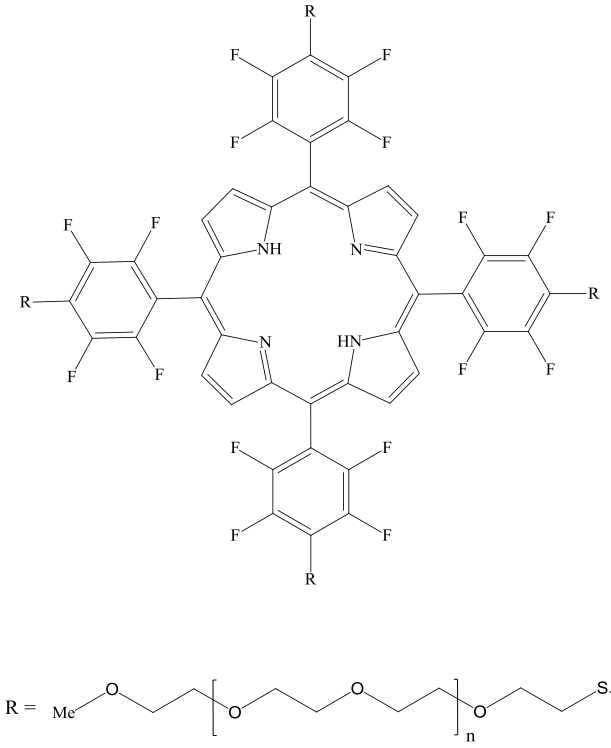

The compound was synthesised according to literature procedure procedures[211].5,10,15,20-Tetra(pentafluorophenyl) porphyrin (20 mg, 0.021 mmol) and polyethylene glycol(750)Br (130 mg, 0.21 mmol) were dissolved in DMF (5 mL). Na_2S (18 mg, 0.21 mmol) was then added and solution stirred at RT for 72 hours. Saturated $NaHCO_{3(aq)}$ (10 mL) was then added and the precipitate that formed was removed by filtration. The filtrate was concentrated under reduced pressure and the isolated violet oil was then washed repeatedly with hexane until the washings were clear to give a purple oil (70 mg, 85%).

The spectral data for the compound was consistent with the data reported in the literature and the assignments of the signals were carried out accordingly[240].

^{1}H NMR [400MHz, $CDCl_3$], δ: -2.9 (2H, br s, NH), 2.9 (xH, t, *J*=6.15 Hz, PEG), 3.54-3.7 (xH, m, PEG), 3.9 (xH, t, *J*=6.01Hz, PEG), 8.8-9.1 (8H, m, H-β); **^{19}F NMR [376MHz, $CDCl_3$], δ:** -137.1 (m, 2F, *p*-F), -133.7 (m, 2F, *m*-F); **UV-Vis ($CHCl_3$) λ_{max}** 415, 518, 548, 591, 645 nm.

5.1.12 MW 15,000-30,000 Poly-D-lysine conjugated phthalocyanine synthesis (12)

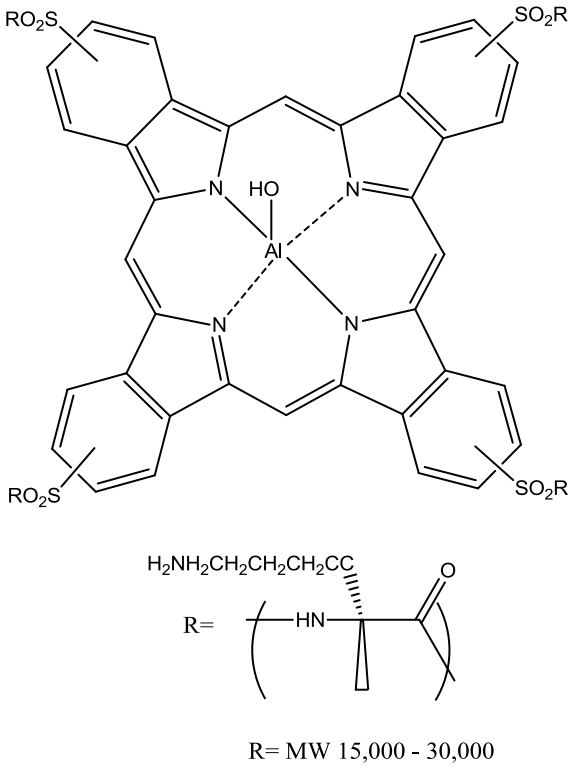

R= MW 15,000 - 30,000

Aluminium phthalocyanine(AlPc) tetrasulfonyl chloride 0.22 g (95%) was synthesised adopting the procedure described in Brasseur *et al.*,[213]. Briefly, AlPc-tetrasulfonic acid (200 mg, 0.23 mmol) and chlorosulfonic acid (0.8 mL) were stirred for 3 hours at 100°C. Thionyl chloride (1.2 mL) was added followed by stirring for 2 hours at 80°C. Once cooled to room temperature, the solution was poured onto ice and the AlPc-tetrasulfonyl chloride collected by centrifugation, filtration and was dried *in vacuo* to receive Aluminium phthalocyanine(AlPc) tetrasulfonyl chloride in 95% yield (0.22 g).

AlPc-tetrasulfonyl chloride (100 mg, 0.1 mmol) was added, in small portions, to a solution of poly-D-lysine hydrobromide (MW 15,000-30,000) (50 mg, 0.4 mmol, 4 equiv., with

respect to lysine groups) and sodium carbonate (85 mg, 0.8 mmol, 8 equiv.) in water (4 mL), while mixing (vortex) for 1 minute between each addition. 10 mL of the dispersion was dialysed against PBS buffer using ultra membrane filters (MWCO 14,000) over 4 days to remove any unconjugated PC. MW 15,000-30,000 POLPC was collected and dried *in vacuo* to yield 110 mg.

λ_{ex} (DI water)/nm 681 (λ_{em} 686 nm).

5.1.13 MW 30,000-70,000 Poly-D-lysine conjugated phthalocyanine synthesis (13)

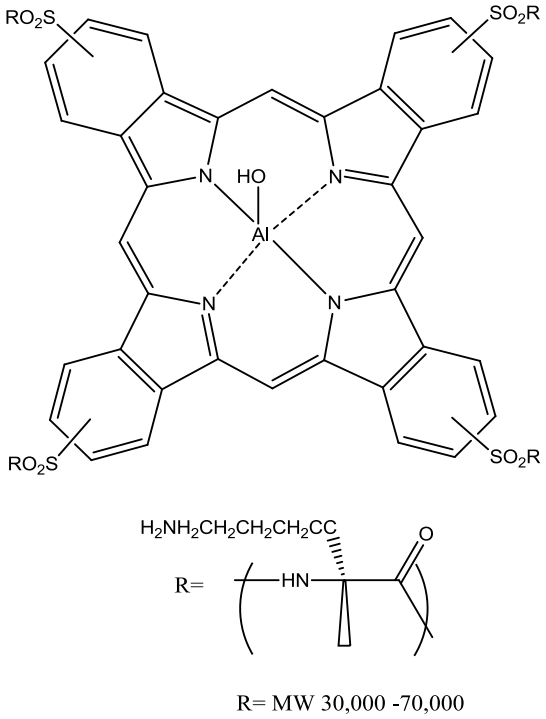

R= MW 30,000 -70,000

Aluminium phthalocyanine(AlPc) tetrasulfonyl chloride 0.22 g (95%) was synthesised adopting the procedure described in Brasseur *et al.*,[213]. Briefly, AlPc-tetrasulfonic acid (200 mg, 0.23 mmol) and chlorosulfonic acid (0.8 mL) were stirred for 3 hours at 100°C. Thionyl chloride (1.2 mL) was added followed by stirring for 2 hours at 80°C. Once cooled to room temperature, the solution was poured onto ice and the AlPc-tetrasulfonyl chloride collected by centrifugation, filtration and was dried *in vacuo* to receive Aluminium phthalocyanine(AlPc) tetrasulfonyl chloride in 95% yield (0.22 g).

AlPc-tetrasulfonyl chloride (100 mg, 0.1 mmol) was added, in small portions, to a solution of poly-D-lysine hydrobromide (MW 30,000-70,000) (50 mg, 0.4 mmol, 4 equiv., with

respect to lysine groups) and sodium carbonate (85 mg, 0.8 mmol, 8 equiv.) in water (4 mL), while mixing (vortex) for 1 minute between each addition. 10 mL of the dispersion was dialysed against PBS buffer using ultra membrane filters (MWCO 14,000) over 4 days to remove any unconjugated PC. MW 30,000-70,000 polylysine conjugated PC was collected and dried *in vacuo* to yield 104 mg.

λ_{ex} (DI water)/nm 681 (λ_{em} 686 nm).

5.1.14 5-(4-Carboxyphenyl)-10,15,20-tri-(4-pyridyl)porphyrin synthesis (14)

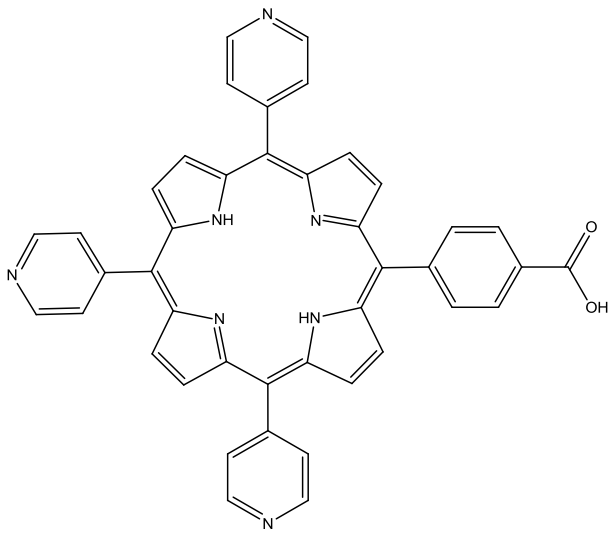

The compound was synthesised according to literature procedure[231]. Dropwise, pyrrole (4 mL, 57.8 mmol) was added to a refluxing mixture of 4-formylbenzoic acid (2.54 g, 17 mmol) and 4-pyridinecarboxaldehyde (9.78 mL, 104 mmol) in acetic acid (200 mL) and nitrobenzene (150 mL). The reaction mixture was kept under reflux and intense stirring for 1 hour. The solvents were removed under reduced pressure and the residue was purified by column chromatography using a mixture of 15% dichloromethane/methanol as an eluent system. Pure 5-(4-carboxyphenyl)-10,15,20-tri-(4-pyridyl)porphyrin was obtained after precipitation from methanol over chloroform in 5.3% yield (510 mg).

^{1}H NMR ($CDCl_3$, 400MHz) δ: -2.79 (2H, br s, CH_2), 8.2 (9H, m, 10,15,20-Ar-*m*,*p*-H), 8.2 (2H, d, *J*= 7.8Hz, 5-Ar-*o*-H), 8.4 (2H, d, *J*=7.8Hz, 5-Ar-*o*-H), 8.8 (6H, s, 5-Ar-*o*-H), 8.97 (8H, m, β-H); **^{13}C NMR ($CDCl_3$, 100MHz)** δ: 117.1, 120.6, 128.3, 129.5, 129.6, 134.4, 145.8, 147.3, 150.9, 168.8; **UV Vis** 420, 519, 555, 580, 636 nm; **Mass (MALDI) *m/z***: 662 [M^++H].

5.1.15 5-[4-(Succinimide-N-oxycarbonyl)phenyl]-10,15,20-tri-(4-pyridyl)porphyrin synthesis (15)

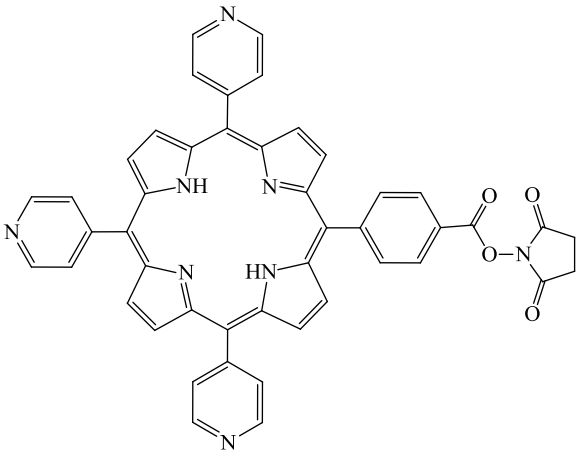

The compound was synthesised according to literature procedure[231]. To a stirred solution of 5-(4-carboxyphenyl)-10,15,20-tri-(4-pyridyl)porphyrin (51.1 mg, 0.077 mmol) in dry pyridine (5 mL) was slowly added thionyl chloride (0.1 mL, 1.37 mmol, 18 equiv.). The reaction was stirred at 50^{o}C, protected from light and atmospheric moisture, for 30 minutes. *N*-Hydroxysuccinimide (200 mg, 1.74 mmol, 22.6 equiv.) was then added and the mixture was kept stirring under the previous conditions for further 3 hours. Pyridine was removed under vacuum, the residue taken up in dichloromethane and washed with an aqueous saturated solution of sodium carbonate. The organic layer was dried over sodium sulphate and evaporated to dryness under reduced pressure. Crystallisation of the residue in light petroleum over chloroform afforded pure 5-[4-(succinimide-N-oxycarbonyl)phenyl]-10,15,20-tri-(4-pyridyl)porphyrin in 89.5% yield (52.3 mg).

^{1}H NMR ($CDCl_3$, 400MHz), δ: -2.90 (2H, br s, NH), 3.10 (4H, br s, CH_2), 8.24 (6H, dd, *J*=1.4, 1.4Hz, 10,15,20-H-Ar-o), 8.44 (2H, dd, *J*=1.4, 1.4 Hz, 5-H-Ar-m), 8.64 (2H, dd, *J*=1.4, 1.6Hz, 5-H-Ar-o), 8.87-8.978 (8H, m, H-β), 9.13 (6H, dd, *J*=1.4, 1.6Hz, 10,15,20-

H-Ar-*m*). **^{13}C NMR ($CDCl_3$, 100MHz)** δ: 25.8, 26.0 (**C**H_2), 117.7, 129.1, 129.3 (10,15,20-Ar-o-**C**), 134.8, 148.4 (10,15,20-Ar-*m*-**C**),149.8, 150.0, 161.7 (**C**O_2N), 169.3 (**C**ON); **UV Vis** 420, 519, 555, 580, 636 nm; **Mass (MALDI) *m/z*** 759$[M+H]^+$.

5.1.16 5-[4-(Succinimide-N-oxycarbonyl)phenyl]-10,15,20-tris-(4-*N*-methylpyridimiumyl)porphyrin triiodide synthesis (16)

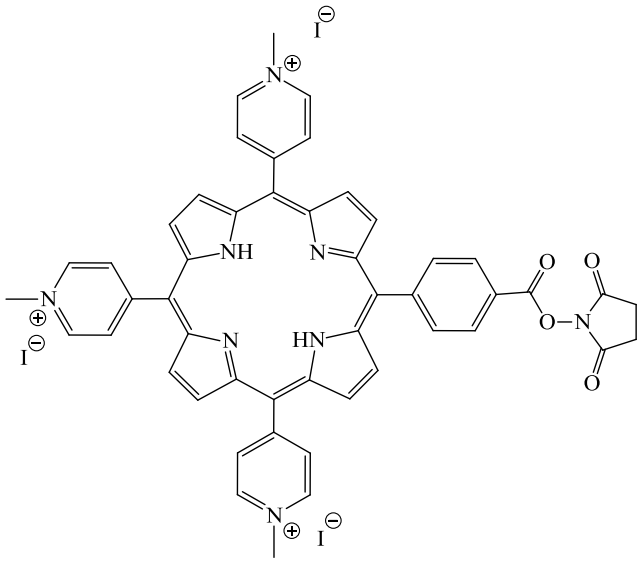

The compound was synthesised according to literature procedure[231]. To a stirred solution of 5-[4-(succinimide-*N*-oxycarbonyl)phenyl]-10,15,20-tri-(4-pyridyl)porphyrin (26 mg, 0.0343 mmol) in dry DMF (5 mL) a large excess of methyl iodide (0.5 mL, 8.03 mmol) was added *via* syringe. The reaction mixture was kept stirring at 40^{o}C, under a nitrogen atmosphere and protected from light overnight. The product was then precipitated with diethyl ether to remove any trace of methyl iodide and DMF. The resulting solid was filtered, dissolved in acetone/water (50:50) and the solvents removed under reduced pressure. Pure 5-[4-(succinimide-*N*-oxycarbonyl)phenyl]-10,15,20-tris-(4-*N*-methylpyridimiumyl)porphyrin triiodide was obtained after precipitation in acetone over water in 77.8% yield (31.6 mg).

^{1}H NMR ($CDCl_3$, 400MHz), δ: -3.05 (2H, br s, NH), 3.01 (4H, br s, CH_2), 4.71 and 4.72 (6+3H, 2s, CH_3), 8.50 (2H, d, *J*=8.2 Hz, 5-H-Ar-m), 8.60 (2H, d, *J*=8.2 Hz, 5-H-Ar-o),

9.00 (6H, d, *J*=6.6Hz, 10,15,20-H-Ar-o), 9.06-9.15 and 9.15-9.26 (8H, 2m, H-β), 9.48 (6H, d, *J*=6.6Hz, 10,15,20-H-Ar-m); **^{13}C NMR ($CDCl_3$, 100MHz)** δ: 25.8, 29.7 (**C**H_2), 117.8, 129.1, 129.3 (10,15,20-Ar-o-**C**), 134.8, 148.4 (10,15,20-Ar-*m*-**C**),149.8, 150.3, 162.0 (**C**O_2N), 169.3 (**C**ON); **UV Vis** 420, 520, 554, 582, 635 nm; **Mass (MALDI) *m/z*** 804 $[M+H]^+$.

5.1.17 5-[4-(Succinimide-N-oxycarbonyl)phenyl]-10,15,20-tris-(4-*N*-methylpyridimiumyl)porphyrin trichloride synthesis (17)

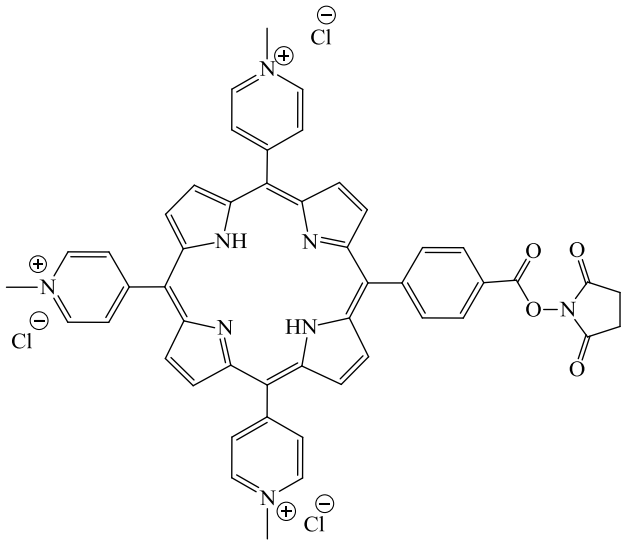

The compound was synthesised according to literature procedure[231]. To a solution of 5-[4-(succinimide-*N*-oxycarbonyl)phenyl]-10,15,20-tris-(4-*N*-methylpyridimiumyl)porphyrin triiodide (56.9 mg, 0.0481 mmol) in anhydrous methanol (57 mL) Dowex 1x8 200-400 Cl (1.81 g) was added and the reaction mixture was allowed to stir at room temperature for 1 hour, protected from moisture and light. The resin was separated by filtration and the reaction mixture concentrated under reduced pressure. After precipitation with acetone, pure 5-[4-(succinimide-*N*-oxycarbonyl)phenyl]-10,15,20-tris-(4-*N*-methylpyridimiumyl)porphyrin trichloride was obtained as a brown solid in 95.5% yield (41.8 mg).

^{1}H NMR (DMSO-d6, 400MHz), δ: -3.05 (2H, br s, NH), 3.01 (4H, br s, CH_2), 4.72 and 4.73 (6+3H, 2s, CH_3), 8.51 (2H, d, *J*=7.8Hz, 5-H-Ar-m), 8.61 (2H, d, *J*=7.8Hz, 5-H-Ar-o), 9.00 (6H, d, *J*=5.6 Hz, 10,15,20-H-Ar-o), 9.04-9.13 and 9.13-9.23 (8H, 2m, H-β), 9.52

(6H, d, *J*=5.6 Hz, 10,15,20-H-Ar-m); **^{13}C NMR (DMSO-d6, 100MHz):** δ: 25.8 (**C**H_2), 47.9 (**C**H_3), 117.8, 119.1, 120.1, 124.9, 129.3, 134.8 (10,15,20-Ar-o-**C**), 135.1, 144.2 (10,15,20-Ar-m-**C**), 148.4, 149.8, 150.4 (**C**O_2N), 169.3 (**C**ON); **UV Vis** 421, 519, 554, 584, 637 nm; **Mass (MALDI) *m/z*** 804$[M+H]^+$.

5.2 Nanoparticle synthesis

General

- All starting materials were purchased from Fluka, Lancaster or Sigma Aldrich and used without further purification unless otherwise stated.
- Photocorrelation spectra were recorded on a Malvern Zetasizer 1000/2000/3000.
- Centrifugation was carried out Denley BS400.
- A Millipore filter unit (fritted glass) with 0.02 mm, 25 mm, Whatman® Anodisc 25 filters and 0.22 µm in-line Millex GP filters (Millipore) were used to recover the nanoparticles or sterilise them before biological experiments.
- Cuvettes used were Starna opti glass 2 type 23 (optical glass, 10 mm) and a VWR International, uv-vis. Optical glass, 10 mm, from Starna (Hainault) and VWR International Limited (Leicestershire) respectively.
- Jeol 2010 transmission electron microscope (Jeol (UK) Ltd. Welwyn Garden City), and UltraScan 4000 digital camera (Gatan UK, Abingdon) were used for NP TEM imaging.
- Hydrophilic carbon coated copper grid used in TEM imaging were from Agar Scientific Ltd, Stansted, Essex, UK.
- High performance liquid chromatography (HPLC) was performed on a HPLC system with a UV detector, Phenomenex Luna 5 µm C18 column (250 x 4.60 mm) and analysed using Azur software version 5.0
- The solid NMR on the nanoparticles was performed on a Bruker Avance II. 500 MHz. Measurements were conducted with a 4 mm double resonance Magic angle spinning probe. Samples were spun at 8 Khz. The chemical shifts were referenced externally to TMS at 0 ppm.

Synthesis

5.2.1 Polyacrylamide nanoparticles synthesis (18)

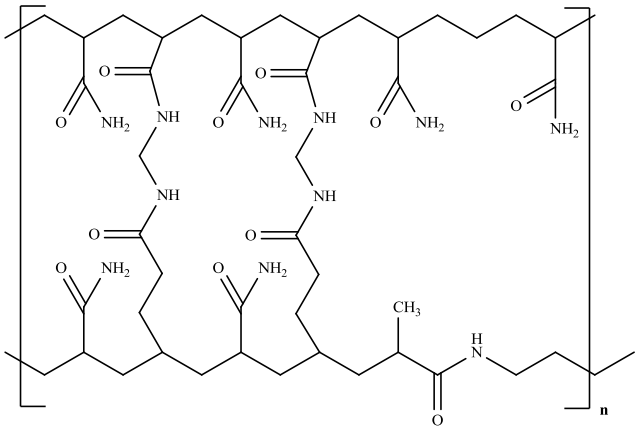

The compound was synthesised according to literature procedure[28]. A final volume (2.00 mL) of solution containing acrylamide (540 mg, 7.60 mmol) and N,N'-methylenebisacrylamide (160 mg, 1.04 mmol) in water (1.8 mL) were added to a deoxygenated hexane (42 mL) solution containing Brij® 30 (3.08 g, 8.49 mmol) and completely dissolved dioctyl sulfosuccinate sodium salt (1.59 g, 3.58 mmol). A solution (30 µL, 0.4382 moldm^{-3}) of ammonium persulphate (100 mg, 0.4382 mmol) in water (1 mL) followed by TEMED (15 µL, 0.1 µmol) were added and the reaction was stirred for 2 hours under a positive argon pressure at room temperature. Excess hexane was removed *in vacuo*. The resulting viscous solid was washed with ethanol, centrifuged (8 x 50 mL, 10 minutes, 4500 rpm) and was recovered by microfiltration (Whatman® Anodisc 25, 0.02 µm, 25 mm filters) to yield the desired polyacrylamide nanoparticles (610 mg, 87%). An optically clear dispersion was obtained from the nanoparticles upon addition to aqueous media (water or $NaHCO_{3\,(aq)}$).

PCS *mean* (z_{ave}, DI water)/nm 38; *fluorescamine test* (λ_{ex}/nm 365) negative.

5.2.2 Amino functionalised nanoparticles synthesis (19)

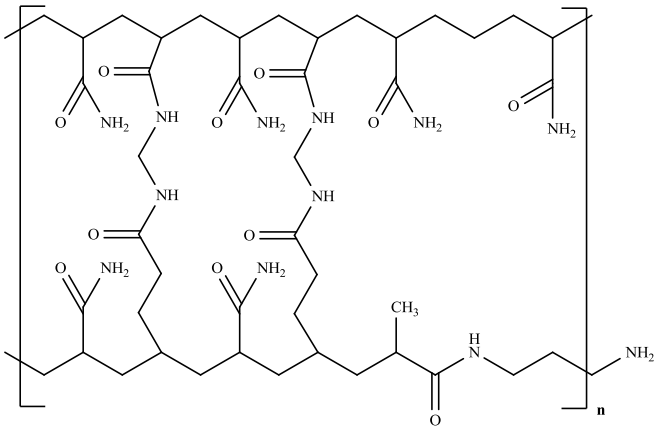

The compound was synthesised according to literature procedure[28]. A final volume of (2.00 mL) containing acrylamide (527 mg, 7.41 mmol), N,N'-methylenebisacrylamide (160 mg, 1.04 mmol) and N-(3-aminopropyl)methacrylamide hydrochloride (13 mg, 0.073 mmol) in water (1.8 mL) were added to a deoxygenated hexane (42 mL) solution containing Brij® 30 (3.08 g, 8.49 mmol) and completely dissolved dioctyl sulfosuccinate sodium salt (1.59 g, 3.58 mmol). A solution (30 µL, 0.4382 $moldm^{-3}$) of ammonium persulphate (100 mg, 0.4382 mmol) in water (1 mL) followed by TEMED (15 µL, 0.1 µmol) was added and the reaction was stirred for 2 hours under a positive argon pressure at room temperature.

Excess hexane was removed *in vacuo*. The resulting viscous solid was washed with ethanol, centrifuged (8 x 50 mL, 10 minutes, 4500 rpm) and was recovered by microfiltration (Whatman® Anodisc 25, 0.02 µm, 25 mm filters) to yield the amino functionalised nanoparticles (630 mg, 90.0%). An optically clear dispersion was obtained from the nanoparticles upon addition to aqueous media (water or $NaHCO_{3\,(aq)}$).

PCS *mean* (z_{ave}, DI water)/nm 37; *fluorescamine test* (λ_{ex}/nm 365) positive.

5.2.3 Cationic nanoparticles synthesis (20)

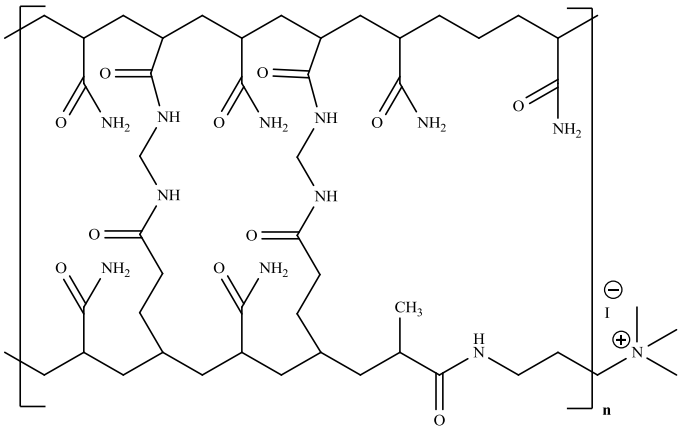

Blank amino nanoparticles (90 mg) and methyl iodide (2.0 mL) were added to a dry DMF (5 mL) solution at 40°C under an argon atmosphere. After one hour the argon supply was removed and the solution was kept stirring for 72 hours at 40°C. Aqueous triethylamine (10 mL) was added and the solution was microfiltered (Whatman® Anodisc 25, 0.02 µm, 25 mm filter). The particles were then repeatedly washed with ethanol (4-5 times). The product was filtered and vacuum dried (5 hours) to obtain dry cationic polyacrylamide nanoparticles (80 mg, 89%).

^{1}H NMR [500MHz], δ: 3.35 (3H, d, C**H$_3$**-N); **^{13}C NMR [500MHz], δ**: 57.5 (**C**H$_3$-N); PCS *mean* (z_{ave}, DI water)/nm 38; *fluorescamine test* (λ_{ex}/nm 365) negative.

5.2.4 Methylene blue entrapped nanoparticles synthesis (21)

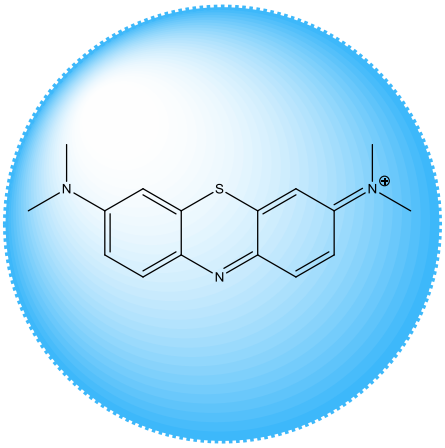

The compound was synthesised adopting literature procedure[28]. A final volume of (1.90 mL) containing acrylamide (540 mg, 7.60 mmol) and N,N'-methylenebisacrylamide (160 mg, 1.04 mmol) in water (1.8 mL) followed by an aliquot (100 µL, 15.6 mmoldm^{-3}) of a solution of MB (5 mg, 15.6 µmol) in water (1 mL) were added to a deoxygenated hexane (42 mL) solution consisting of Brij® 30 (3.08 g, 8.49 mmol) and completely dissolved dioctyl sulfosuccinate sodium salt (1.59 g, 3.58 mmol). A solution (30 µL, 0.4382 moldm^{-3}) of ammonium persulphate (100 mg, 0.4382 mmol) in water (1 mL) followed by TEMED (15 µL, 0.1 µmol) was added and the reaction was stirred for 2 hours under a positive argon pressure at room temperature. Excess hexane was removed *in vacuo*. The resulting viscous yellow solid was washed with ethanol, centrifuged (8 x 50 mL, 10 minutes, 4500 rpm) and recovered by microfiltration (Whatman® Anodisc 25, 0.02 µm, 25 mm filters) to yield the desired MB entrapped nanoparticles (451 mg, 64%). An optically clear blue dispersion was obtained from the nanoparticles upon addition to aqueous media (water or $NaHCO_{3\ (aq)}$).

PCS *mean* (z_{ave}, DI water)/nm 36; *fluorescamine test* (λ_{ex}/nm 365) negative; λ_{ex} (DI water)/nm 658(λ_{em} 674 nm); concentration of MB present in 1 mg of nanoparticles ~ 5.6

$\mu moldm^{-3}$, $R^2 = 0.9998$, $y = 30.243x$ (5.6 $\mu moldm^{-3}$ of MB per 1 mg of MB entrapped NPs in 1 mL of H_2O).

5.2.5 Methylene blue entrapped amino functionalised nanoparticles synthesis (22)

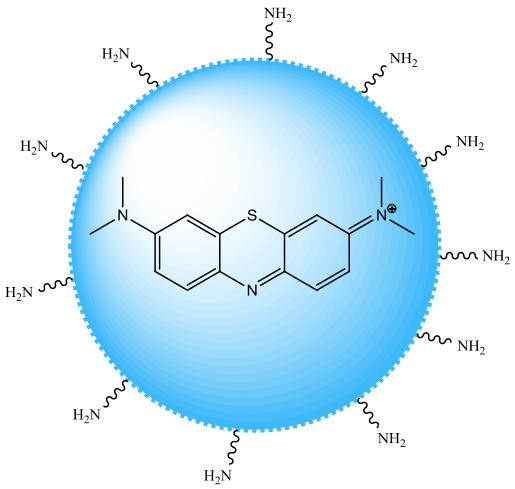

The compound was synthesised adopting literature procedure[28]. A final volume of (1.90 mL) containing acrylamide (527 mg, 7.41 mmol), N,N'-methylenebisacrylamide (160 mg, 1.04 mmol) and N-(3-aminopropyl)methacrylamide hydrochloride (13 mg, 0.073 mmol) in water (1.8 mL) followed by an aliquot (100 µL, 15.6 mmoldm^{-3}) of a solution of MB (5 mg, 15.6 µmol) in water (1 mL) were added to a deoxygenated hexane (42 mL) solution consisting of Brij® 30 (3.08 g, 8.49 mmol) and completely dissolved dioctyl sulfosuccinate sodium salt (1.59 g, 3.58 mmol). A solution (30 µL, 0.4382 moldm^{-3}) of ammonium persulphate (100 mg, 0.4382 mmol) in water (1 mL) followed by TEMED (15 µL, 0.1 µmol) was added and the reaction was stirred for 2 hours under a positive argon pressure at room temperature. Excess hexane was removed *in vacuo*. The resulting viscous yellow solid was washed with ethanol, centrifuged (8 x 50 mL, 10 minutes, 4500 rpm) and recovered by microfiltration (Whatman® Anodisc 25, 0.02 µm, 25 mm filters) to yield the desired MB entrapped nanoparticles (681 mg, 97%). An optically clear blue dispersion

was obtained from the nanoparticles upon addition to aqueous media (water or $NaHCO_{3\,(aq)}$).

PCS *mean* (z_{ave}, DI water)/nm 42; *fluorescamine test* (λ_{ex}/nm 365) positive; λ_{ex} (DI water)/nm 658(λ_{em} 674 nm); concentration of MB present in 1 mg of nanoparticles ~ 4.9 $\mu moldm^{-3}$, $R^2 = 0.9998$, $y = 30.243x$ (4.9 $\mu moldm^{-3}$ of MB per 1 mg of MB entrapped NPs in 1 mL of H_2O).

5.2.6 Uranyl acetate entrapped polyacrylamide nanoparticles synthesis (23)

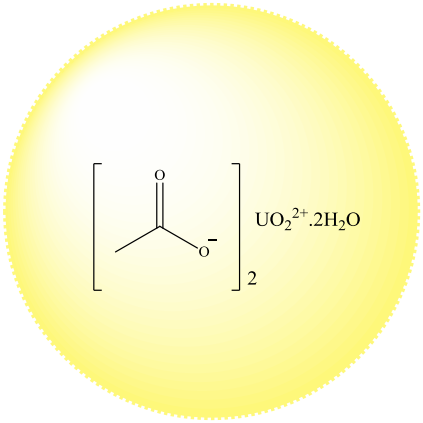

The compound was synthesised adopting literature procedure[28]. A final volume of (1.95 mL) containing acrylamide (540 mg, 7.60 mmol) and N,N'-methylenebisacrylamide (160 mg, 1.04 mmol) in water (1.8 mL) followed by a solution of uranyl acetate (1 mg, 2.4 µmol) in water (50 µL) were added to a deoxygenated hexane (42 mL) solution consisting of Brij® 30 (3.08 g, 8.49 mmol) and completely dissolved dioctyl sulfosuccinate sodium salt (1.59 g, 3.58 mmol). A solution (30 µL, 0.4382 mol dm^{-3}) of ammonium persulphate (100 mg, 0.4382 mmol) in water (1 mL) followed by TEMED (15 µL, 0.1 µmol) was added and the reaction was stirred for 2 hours under a positive argon pressure at room temperature. Excess hexane was removed *in vacuo*. The resulting viscous yellow solid was washed with ethanol, centrifuged (8 x 50 mL, 10 minutes, 4500 rpm) and recovered by microfiltration (Whatman® Anodisc 25, 0.02 µm, 25 mm filters) to yield the desired uranyl acetate entrapped nanoparticles (580 mg, 83%). An optically clear yellow dispersion was obtained from the nanoparticles upon addition to aqueous media (water or $NaHCO_{3\,(aq)}$).

PCS *mean* (z_{ave}, DI water)/nm 51.5; *fluorescamine test* (λ_{ex}/nm 365) negative; *TEM imaging* stain positive.

5.2.7 Disulphonated 4,7-diphenyl-1,10-phenanthroline ruthenium (II) chloride (DSRuCl) entrapped NPs synthesis (24)

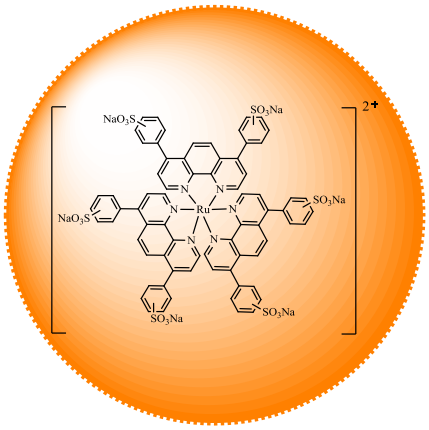

The compound was synthesised adopting literature procedure[28]. A final volume of (1.90 mL) containing acrylamide (540 mg, 7.60 mmol) and N,N'-methylenebisacrylamide (160 mg, 1.04 mmol) in water (1.8 mL) followed by an aliquot (100 µL, 2.8 mmoldm^{-3}) of a solution of DSRuCl (5 mg, 2.8 µmol) in water (1 mL) were added to a deoxygenated hexane (42 mL) solution containing Brij® 30 (3.08 g, 8.49 mmol) and completely dissolved dioctyl sulfosuccinate sodium salt (1.59 g, 3.58 mmol). A solution (30 µL, 0.4382 moldm^{-3}) of ammonium persulphate (100 mg, 0.4382 mmol) in water (1 mL) followed by TEMED (15 µL, 0.1 µmol) was added and the reaction was stirred for 2 hours under a positive argon pressure at room temperature. Excess hexane was removed *in vacuo*. The resulting viscous orange solid was washed with ethanol, centrifuged (8 x 50 mL, 10 minutes, 4500 rpm) and was recovered by microfiltration (Whatman® Anodisc 25, 0.02 µm, 25 mm filters) to yield the desired DSRuCl entrapped nanoparticles (570 mg, 81%). An optically clear dispersion was obtained from the nanoparticles upon addition to aqueous media (water or $NaHCO_{3\,(aq)}$).

PCS *mean* (z_{ave}, DI water)/nm 58; *fluorescamine test* (λ_{ex}/nm 365) negative; λ_{ex} (DI water)/nm 461(λ_{em} 610 nm); concentration of DSRuCl present in 1 mg of nanoparticles ~4.0 μmoldm^{-3}, R^2 = 0.9968, y = 11.973x (4.0 μmoldm^{-3} of DSRuCl per 1 mg of DSRuCl entrapped NPs in 1 mL of H_2O).

5.2.8 Disulphonated 4,7-diphenyl-1,10-phenanthroline ruthenium (II) chloride (DSRuCl) entrapped amino functionalised nanoparticles synthesis (25)

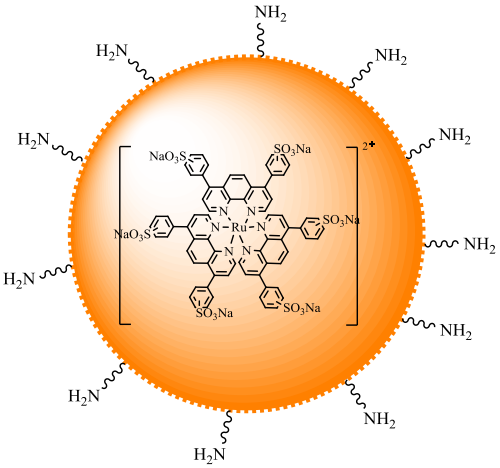

The compound was synthesised adopting literature procedure[28]. A final volume of (1.90 mL) containing acrylamide (527 mg, 7.41 mmol), N,N'-methylenebisacrylamide (160 mg, 1.04 mmol) and N-(3-aminopropyl)methacrylamide hydrochloride (13 mg, 0.073 mmol) in water (1.8 mL) followed by an aliquot (100 µL, 2.8 mmoldm^{-3}) of a solution of DSRuCl (5 mg, 2.8 µmol) in water (1 mL) were added to a deoxygenated hexane (42 mL) solution containing Brij® 30 (3.08 g, 8.49 mmol) and completely dissolved dioctyl sulfosuccinate sodium salt (1.59 g, 3.58 mmol). A solution (30 µL, 0.4382 moldm^{-3}) of ammonium persulphate (100 mg, 0.4382 mmol) in water (1 mL) followed by TEMED (15 µL, 0.1 µmol) was added and the reaction was stirred for 2 hours under a positive argon pressure at room temperature. Excess hexane was removed *in vacuo*. The resulting viscous orange solid was washed with ethanol, centrifuged (8 x 50 mL, 10 minutes, 4500 rpm) and was recovered by microfiltration (Whatman® Anodisc 25, 0.02 µm, 25 mm filters) to yield the

desired DSRuCl entrapped nanoparticles (580 mg, 83%). An optically clear dispersion was obtained from the nanoparticles upon addition to aqueous media (water or $NaHCO_{3\,(aq)}$).

PCS *mean* (z_{ave}, DI water)/nm 58; *fluorescamine test* (λ_{ex}/nm 365) positive; λ_{ex} (DI water)/nm 461(λ_{em} 610 nm); concentration of DSRuCl present in 1 mg of nanoparticles ~4.9 μmoldm^{-3}, R^2 = 0.9968, y = 11.973x (4.9 μmoldm^{-3} of DSRuCl per 1 mg of DSRuCl entrapped NPs in 1 mL of H_2O).

5.2.9 5,10,15,20-Tetrakis(4-N-methylpyridiniumyl)porphyrin tetraiodide entrapped polyacrylamide nanoparticles synthesis (26)

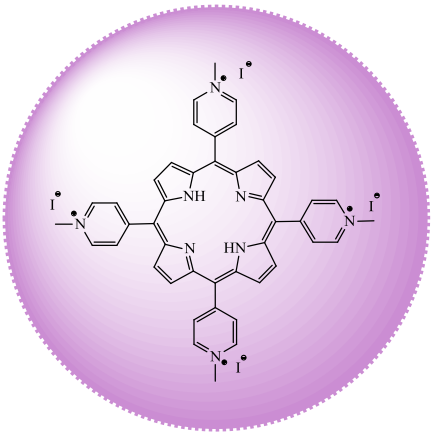

The compound was synthesised adopting literature procedure[28]. A final volume of (1.90 mL) containing acrylamide (540 mg, 7.60 mmol) and N,N'-methylenebisacrylamide (160 mg, 1.04 mmol) in water (1.8 mL) followed by an aliquot (100 µL, 4.2 $mmoldm^{-3}$) of a solution of PyPorphyrin (5 mg, 4.2 µmol) in water (1 mL) were added to a deoxygenated hexane (42 mL) solution consisting of Brij® 30 (3.08 g, 8.49 mmol) and completely dissolved dioctyl sulfosuccinate sodium salt (1.59 g, 3.58 mmol). A solution (30 µL, 0.4382 $moldm^{-3}$) of ammonium persulphate (100 mg, 0.4382 mmol) in water (1 mL) followed by TEMED (15 µL, 0.1 µmol) was added and the reaction was stirred for 2 hours under a positive argon pressure at room temperature. Excess hexane was removed *in vacuo*. The resulting viscous yellow solid was washed with ethanol, centrifuged (8 x 50 mL, 10 minutes, 4500 rpm) and recovered by microfiltration (Whatman® Anodisc 25, 0.02 µm, 25 mm filters) to yield the desired porphyrin entrapped nanoparticles (640 mg, 91.4%). An optically clear yellow dispersion was obtained from the nanoparticles upon addition to aqueous media (water or $NaHCO_{3\,(aq)}$).

PCS *mean* (z_{ave}, DI water)/nm 51.5; *fluorescamine test* (λ_{ex}/nm 365) negative; λ_{ex} (DI water)/nm 429(λ_{em} 665 nm); concentration of PyPorphyrin present in 1 mg of nanoparticles ~ 0.34 μmoldm^{-3}, R^2 = 0.996, y = 1.7894x (0.34 μmoldm^{-3} of PyPorphyrin per 1 mg of PyPorphyrin entrapped NPs in 1 mL of H_2O).

5.2.10 5,10,15,20-Tetrakis(2,3,5,6-tetrafluoro-4-{PEG(750)-sufanyl}-phenyl)-porphyrin entrapped polyacrylamide nanoparticles synthesis (27)

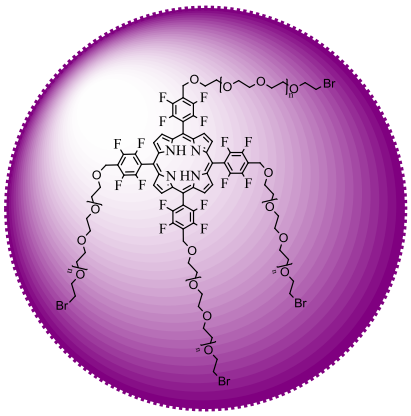

The compound was synthesised adopting literature procedure[28]. A final volume of (1.90 mL) containing acrylamide (540 mg, 7.60 mmol) and N,N'-methylenebisacrylamide (160 mg, 1.04 mmol) in water (1.8 mL) followed by an aliquot (100 µL, 1.3 mmoldm^{-3}) of a solution of PEG(750)Porphyrin (5 mg, 1.3 µmol) in water (1 mL) was added to a deoxygenated hexane (42 mL) solution containing Brij® 30 (3.08 g, 8.49 mmol) and completely dissolved dioctyl sulfosuccinate sodium salt (1.59 g, 3.58 mmol). A solution (30 µL, 0.4382 moldm^{-3}) of ammonium persulphate (100 mg, 0.4382 mmol) in water (1 mL) followed by TEMED (15 µL, 0.1 µmol) was added and the reaction was stirred for 2 hours under a positive argon pressure at room temperature. Excess hexane was removed *in vacuo*. The resulting viscous yellow solid was washed with ethanol, centrifuged (8 x 50 mL, 10 minutes, 4500 rpm) and was recovered by microfiltration (Whatman® Anodisc 25, 0.02 µm, 25 mm filters) to yield the desired 5,10,15,20-tetrakis(2,3,5,6-tetrafluoro-4-{PEG(750)-sufanyl}-phenyl)-porphyrin entrapped nanoparticles (552 mg, 79%). An optically clear dispersion was obtained from the nanoparticles upon addition to aqueous media (water or $NaHCO_{3\,(aq)}$).

PCS *mean* (z_{ave}, DI water)/nm 37; *fluorescamine test* (λ_{ex}/nm 365) negative; λ_{ex} (DI water)/nm 410 (λ_{em} 653 nm); concentration of PEG(750)Porphyrin present in 1 mg of nanoparticles 0.34 $\mu moldm^{-3}$, R^2 = 0.9944, y = 2.1428x (0.34 $\mu moldm^{-3}$ of PEG(750)Porphyrin per 1 mg of PEG(750)Porphyrin entrapped NPs in 1 mL of H_2O).

5.2.11 5,10,15,20-Tetrakis(2,3,5,6-tetrafluoro-4-{PEG(750)-sufanyl}-phenyl)-porphyrin entrapped amino functionalised polyacrylamide nanoparticles synthesis (28)

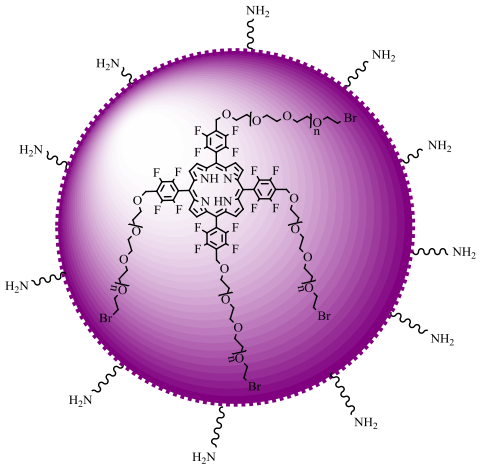

The compound was synthesised adopting literature procedure[28]. A final volume of (1.90 mL) containing acrylamide (527 mg, 7.41 mmol), N,N'-methylenebisacrylamide (160 mg, 1.04 mmol) and N-(3-aminopropyl)methacrylamide hydrochloride (13 mg, 0.073 mmol) in water (1.8 mL) followed by an aliquot (100 µL, 1.3 mmoldm^{-3}) of a solution of PEG(750)Porphyrin (5 mg, 1.3 µmol) in water (1 mL) was added to a deoxygenated hexane (42 mL) solution containing Brij® 30 (3.08 g, 8.49 mmol) and completely dissolved dioctyl sulfosuccinate sodium salt (1.59 g, 3.58 mmol). A solution (30 µL, 0.4382 moldm^{-3}) of ammonium persulphate (100 mg, 0.4382 mmol) in water (1 mL) followed by TEMED (15 µL, 0.1 µmol) was added and the reaction was stirred for 2 hours under a positive argon pressure at room temperature. Excess hexane was removed *in vacuo*. The resulting viscous yellow solid was washed with ethanol, centrifuged (8 x 50 mL, 10 minutes, 4500 rpm) and was recovered by microfiltration (Whatman® Anodisc 25, 0.02 µm, 25 mm filters) to yield the desired 5,10,15,20-tetrakis(2,3,5,6-tetrafluoro-4-{PEG(750)-sufanyl}-phenyl)-porphyrin entrapped nanoparticles (601 mg, 86%). An

optically clear dispersion was obtained from the nanoparticles upon addition to aqueous media (water or $NaHCO_{3\,(aq)}$).

PCS *mean* (z_{ave}, DI water)/nm 40; *fluorescamine test* (λ_{ex}/nm 365) positive; λ_{ex} (DI water)/nm 410 (λ_{em} 653 nm); concentration of PEG(750)Porphyrin present in 1 mg of nanoparticles 0.42 μmoldm^{-3}, R^2 = 0.9944, y = 2.1428x (0.42 μmoldm^{-3} of PEG(750)Porphyrin per 1 mg of PEG(750)Porphyrin entrapped NPs in 1 mL of H_2O).

5.2.12 MW 10,000 dextran fluorescein entrapped polyacrylamide nanoparticles synthesis (29)

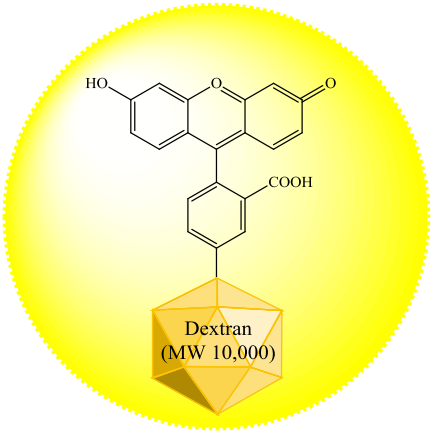

The compound was synthesised adopting literature procedure[28]. A final volume of (1.90 mL) containing acrylamide (540 mg, 7.60 mmol) and N,N'-methylenebisacrylamide (160 mg, 1.04 mmol) in water (1.8 mL) followed by an aliquot (100 µL, 50 mmoldm^{-3}) of a solution of fluorescein conjugated to a dextran polymer (MW 10,000 Da) (5 mg, 50 µmol) in water (1 mL) was added to a deoxygenated hexane (42 mL) solution consisting of Brij® 30 (3.08 g, 8.49 mmol) and completely dissolved dioctyl sulfosuccinate sodium salt (1.59 g, 3.58 mmol). A solution (30 µL, 0.4382 moldm^{-3}) of ammonium persulphate (100 mg, 0.4382 mmol) in water (1 mL) followed by TEMED (15 µL, 0.1 µmol) was added and the reaction was stirred for 2 hours under a positive argon pressure at room temperature. Excess hexane was removed *in vacuo*. The resulting viscous light orange solid was washed with ethanol, centrifuged (8 x 50 mL, 10 minutes, 4500 rpm) and recovered by microfiltration (Whatman® Anodisc 25, 0.02 µm, 25 mm filters) to yield the desired fluorescein entrapped nanoparticles (660 mg, 94%). An optically clear dispersion was obtained from the nanoparticles upon addition to aqueous media (water or $NaHCO_{3\,(aq)}$).

PCS *mean* (z_{ave}, DI water)/nm 46; *fluorescamine test* (λ_{ex}/nm 365) negative; λ_{ex} (DI water)/nm 480(λ_{em} 520 nm).

5.2.13 MW 15,000-30,000 Poly-D-lysine conjugated phthalocyanine entrapped polyacrylamide nanoparticles synthesis (30)

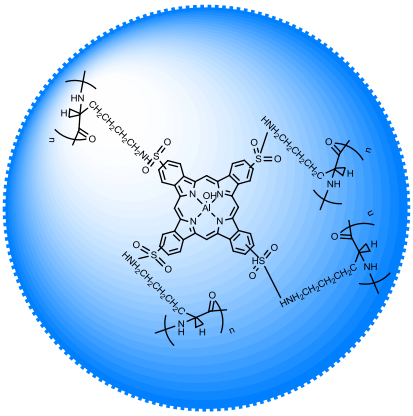

The compound was synthesised adopting literature procedure[28]. A final volume of (1.90 mL) containing acrylamide (540 mg, 7.60 mmol) and N,N'-methylenebisacrylamide (160 mg, 1.04 mmol) in water (1.8 mL) followed by a solution (100 µL) of PCPOL (1.34 moldm^{-3}) were added to a deoxygenated hexane (42 mL) solution containing Brij® 30 (3.08 g, 8.49 mmol) and completely dissolved dioctyl sulfosuccinate sodium salt (1.59 g, 3.58 mmol). A solution (30 µL, 0.4382 moldm^{-3}) of ammonium persulphate (100 mg, 0.4382 mmol) in water (1 mL) followed by TEMED (15 µL, 0.1 µmol) was added and the reaction was stirred for 2 hours under a positive argon pressure at room temperature. Excess hexane was removed *in vacuo*. The resulting viscous yellow solid was washed with ethanol, centrifuged (8 x 50 mL, 10 minutes, 4500 rpm) and was recovered by microfiltration (Whatman® Anodisc 25, 0.02 µm, 25 mm filters) to yield the desired PCPOL entrapped nanoparticles (590 mg, 84%). An optically clear dispersion was obtained from the nanoparticles upon addition to aqueous media (water or $NaHCO_{3\,(aq)}$).

PCS *mean* (z_{ave}, DI water)/nm 40; *fluorescamine test* (λ_{ex}/nm 365) negative; λ_{ex} (DI water)/nm 681 (λ_{em} 686 nm); concentration of phthalocyanine loaded to 1 mg of

nanoparticles ~0.36 μmoldm^{-3}, ε Al-Pc 1.5 x 10^5 M^{-1}cm^{-1} (λ_{ex} (DI water)/666 nm), R^2 = 0.9987, y = 0.1545x (0.36 μmoldm^{-3} of phthalocyanine per 1 mg of NPs in 1 mL of H_2O).

5.2.14 MW 15,000-30,000 Poly-D-lysine conjugated phthalocyanine entrapped amino functionalised polyacrylamide nanoparticles synthesis (31)

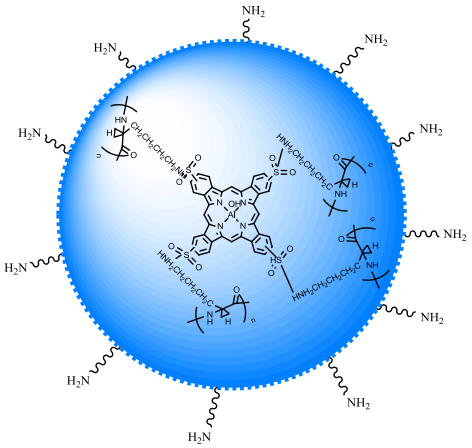

The compound was synthesised adopting literature procedure[28]. A final volume of (1.90 mL) containing acrylamide (527 mg, 7.41 mmol), N,N'-methylenebisacrylamide (160 mg, 1.04 mmol) and N-(3-aminopropyl)methacrylamide hydrochloride (13 mg, 0.073 mmol) in water (1.7 mL) followed by a solution (100 µL) of PCPOL (1.34 moldm^{-3}) were added to a deoxygenated hexane (42 mL) solution containing Brij® 30 (3.08 g, 8.49 mmol) and completely dissolved dioctyl sulfosuccinate sodium salt (1.59 g, 3.58 mmol). A solution (30 µL, 0.4382 moldm^{-3}) of ammonium persulphate (100 mg, 0.4382 mmol) in water (1 mL) followed by TEMED (15 µL, 0.1 µmol) was added and the reaction was stirred for 2 hours under a positive argon pressure at room temperature. Excess hexane was removed *in vacuo*. The resulting viscous yellow solid was washed with ethanol, centrifuged (8 x 50 mL, 10 minutes, 4500 rpm) and was recovered by microfiltration (Whatman® Anodisc 25, 0.02 µm, 25 mm filters) to yield the desired Pc polylysine entrapped nanoparticles (625 mg, 89%). An optically clear dispersion was obtained from the nanoparticles upon addition to aqueous media (water or $NaHCO_{3\,(aq)}$).

PCS *mean* (z_{ave}, DI water)/nm 40 (±10 nm); *fluorescamine test* (λ_{ex}/nm 365) positive; λ_{ex} (DI water)/nm 681 (λ_{em} 686 nm); concentration of phthalocyanine loaded to 1 mg of nanoparticles ~0.36 μmoldm^{-3}, ε Al-Pc 1.5 x 10^5 $M^{-1}cm^{-1}$ (λ_{ex} (DI water)/666 nm), R^2 = 0.9987, y = 0.1545x (0.36 μmoldm^{-3} of phthalocyanine per 1 mg of NPs in 1 mL of H_2O).

5.2.15 MW 30,000-70,000 Poly-D-lysine conjugated PC entrapped polyacrylamide nanoparticles synthesis (32)

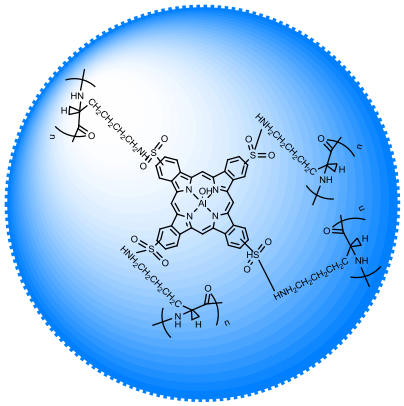

The compound was synthesised adopting literature procedure[28]. A final volume of (1.90 mL) containing acrylamide (540 mg, 7.60 mmol) and *N,N'*-methylenebisacrylamide (160 mg, 1.04 mmol) in water (1.7 mL) followed by a solution (100 µL) of PCPOL (1.34 moldm^{-3}) were added to a deoxygenated hexane (42 mL) solution containing Brij® 30 (3.08 g, 8.49 mmol) and completely dissolved dioctyl sulfosuccinate sodium salt (1.59 g, 3.58 mmol). A solution (30 µL, 0.4382 moldm^{-3}) of ammonium persulphate (100 mg, 0.4382 mmol) in water (1 mL) followed by TEMED (15 µL, 0.1 µmol) was added and the reaction was stirred for 2 hours under a positive argon pressure at room temperature. Excess hexane was removed *in vacuo*. The resulting viscous yellow solid was washed with ethanol, centrifuged (8 x 50 mL, 10 minutes, 4500 rpm) and was recovered by microfiltration (Whatman® Anodisc 25, 0.02 µm, 25 mm filters) to yield the desired Pc polylysine entrapped nanoparticles (602 mg, 86%).

PCS *mean* (z_{ave}, DI water)/nm 45 (±10 nm); *fluorescamine test* (λ_{ex}/nm 365) negative; λ_{ex} (DI water)/nm 681 (λ_{em} 686 nm); concentration of phthalocyanine loaded to 1 mg of nanoparticles ~1.9 x 10^{-4} moldm^{-3} (ST DEV 5.09 x 10^{-8} moldm^{-3}), ε AlPc 1.5 x 10^{5} $M^{-1}cm^{-1}$

(λ_{ex} (DI water)/666 nm), $R^2 = 0.9987$, $y = 0.1545x$ (1.9×10^{-4} $moldm^{-3}$ of phthalocyanine per 1 mg of NPs in 1 mL of H_2O).

5.2.16 MW 30,000-70,000 Poly-D-lysine conjugated PC entrapped amino functionalised polyacrylamide nanoparticles synthesis (33)

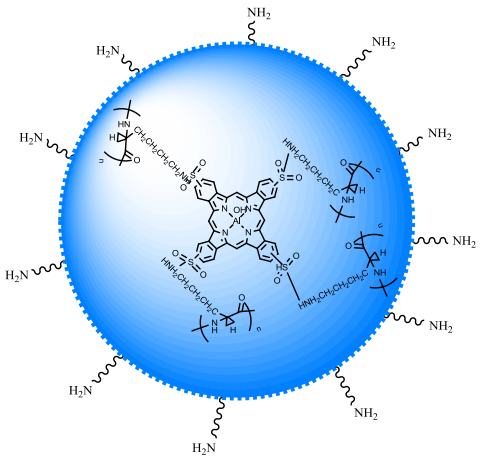

The compound was synthesised adopting literature procedure[28]. A final volume of (1.90 mL) containing acrylamide (527 mg, 7.41 mmol), N,N'-methylenebisacrylamide (160 mg, 1.04 mmol) and N-(3-aminopropyl)methacrylamide hydrochloride (13 mg, 0.073 mmol) in water (1.7 mL) followed by a solution (100 µL) of PCPOL (1.34 moldm^{-3}) were added to a deoxygenated hexane (42 mL) solution containing Brij® 30 (3.08 g, 8.49 mmol) and completely dissolved dioctyl sulfosuccinate sodium salt (1.59 g, 3.58 mmol). A solution (30 µL, 0.4382 moldm^{-3}) of ammonium persulphate (100 mg, 0.4382 mmol) in water (1 mL) followed by TEMED (15 µL, 0.1 µmol) was added and the reaction was stirred for 2 hours under a positive argon pressure at room temperature. Excess hexane was removed *in vacuo*. The resulting viscous yellow solid was washed with ethanol, centrifuged (8 x 50 mL, 10 minutes, 4500 rpm) and was recovered by microfiltration (Whatman® Anodisc 25, 0.02 µm, 25 mm filters) to yield the desired Pc polylysine entrapped nanoparticles (616 mg, 88%).

PCS *mean* (z_{ave}, DI water)/nm 45 (±10 nm); *fluorescamine test* (λ_{ex}/nm 365) positive; λ_{ex} (DI water)/nm 681 (λ_{em} 686 nm); concentration of phthalocyanine loaded to 1 mg of nanoparticles ~1.9×10^{-4} moldm^{-3} (ST DEV 5.09×10^{-8} moldm^{-3}), ε AlPc 1.5×10^{5} M^{-1}cm^{-1} (λ_{ex} (DI water)/666 nm), $R^2 = 0.9987$, $y = 0.1545x$ (1.9×10^{-4} moldm^{-3} of phthalocyanine per 1 mg of NPs in 1 mL of H_2O).

5.2.17 MW 30,000-70,000 Poly-D-lysine conjugated phthalocyanine entrapped methylated NHS ester conjugated nanoparticles synthesis (34)

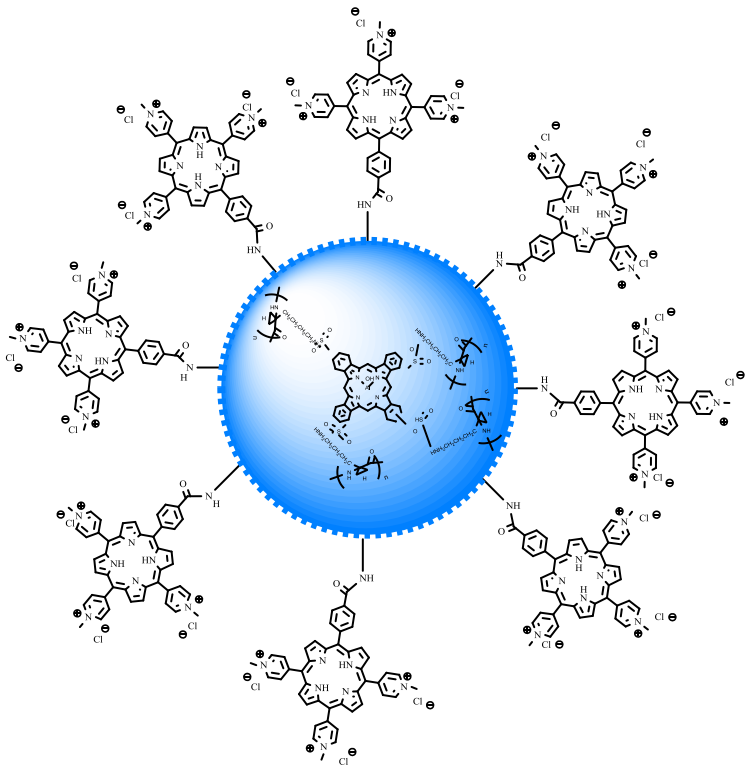

The compound was synthesised adopting literature procedure[28]. An aliquot of (500 µL, 2.2 mmoldm^{-3}) of 5-[4-(succinimide–N-oxycarbonyl)phenyl]-10,15,20-tri(4-N-methylpyridiniumyl)porphyrin trichloride [17] was added to a dispersion (10 mL) of filtered (Millex® GP, 0.22 µm filter unit) amino functionalised PC-polylysine entrapped nanoparticles (50 mg) and triethylamine (250 µL). The mixture was spun in Falcon polystyrene (12x75 mm) tubes for 2 hours on a spinning rotator at room temperature, protected from light. The resulting suspension was washed with ethanol, centrifuged (7x50 mL, 10 minutes, 5500 rpm), microfiltered (Whatman® Anodisc 25, 0.02 µm, 25 mm

filters) and dried for 8 hours at 40°C to yield the desired porphyrin conjugated PC entrapped nanoparticles as a green solid (39 mg, 78%).

PCS *mean* (z_{ave}, DI water)/nm 95 ± 10 nm; *fluorescamine test* (λ_{ex}/nm 365) negative; λ_{ex} (DI water)/nm 424 (λ_{em} 656 nm and 708 nm); λ_{ex} (DI water)/nm 680 (λ_{em} 685 nm); concentration of phthalocyanine loaded to 1 mg of nanoparticles ~1.6 x 10^{-4} moldm^{-3} (ST DEV 5.09 x 10^{-8} moldm^{-3}), ε AlPc 1.5 x 10^{5} M^{-1}cm^{-1} (λ_{ex} (DI water)/666 nm), R^2 = 0.9987, y = 0.1545x, (1.6 x 10^{-4} moldm^{-3} of phthalocyanine per 1 mg of NPs in 1 mL of H_2O); concentration of porphyrin loaded to 1 mg of nanoparticles ~1.8 x 10^{-4} moldm^{-3} (ST DEV 5.09 x 10^{-8} moldm^{-3}), ε NHS Porphyrin 2.3 x 10^{5} M^{-1}cm^{-1} (λ_{ex} (DI water)/520 nm) (1.8 x 10^{-4} moldm^{-3} of porphyrin per 1 mg of NPs in 1 mL of H_2O).

5.3 Nanoparticle characterisation Methods

5.3.1 Particle Size

The particle size and size distribution properties of the nanoparticles were measured by PCS, Zetaplus™ particle size analyzer (Malvern 3000) at 25°C and at a scattering angle of 90°. A dilute sample of nanoparticles (1 mg/mL) was prepared in MilliQ water, sonicated for 30s and filtered (Millex® GP, 0.22 µm filter unit) before analysis. The value was recorded as the average of 30 data measurements.

5.3.2 TEM Imaging

The nanoparticles were suspended in deionised water and placed in an ultrasonic bath for 3 minutes. The suspension was then passed through a Millex® GP, 0.22 µm filter unit and the resulting suspension returned to the ultrasonic bath for a further 2 minutes to disperse any aggregates. 5 µL of the suspension was immediately put onto a hydrophilic carbon coated copper grid (Agar Scientific Ltd, Stansted, Essex, UK) and allowed to air dry. Dry ethanol (5 µL) was then added to the grid and left to air dry. TEM images were obtained using an UltraScan 4000 digital camera (Gatan UK, Abingdon) attached to a Jeol 2010 transmission electron microscope (Jeol (UK) Ltd., Welwyn Garden City) running at 120 kV.

5.3.3 Entrapped/conjugated PS/probe concentration quantification

1 mg of filtered (Millex® GP, 0.22 µm filter unit) nanoparticles were dispersed in 1 ml of deionised water and the absorbance of the particles measured by UV spectrophotometry (Varian Cary50 Bio, Cary WinUV) between the wavelengths 400-800 nm.

5.3.3.1 DSRuCl NP

The calibration "straight" line for DSRuCl was plotted against the absorbance of the DSRuCl at 461 nm for a known concentration range of the (DSRuCl) (solvent deionised water). The calibration "straight" line was then used in measuring the approximate concentrations of DSRuCl present in a pre-determined weight of NPs by measuring its absorbance.

5.3.3.2 MB NP

The calibration "straight" line was plotted using the MB absorbance at 665 nm against known concentrations of MB. This calibration "straight" line was used in quantifying the approximate concentrations of MB present in a given weight of NPs by measuring its absorbance.

5.3.3.3 PyPorphyrin NP

A calibration "straight" line was used to measure the approximate concentrations of PyPorphyrin present per set weight of NPs by measuring its absorbance (solvent deionised water) at 421 nm.

5.3.3.4 PEG(750)Porphyrin NP

The calibration "straight" line for 5,10,15,20-tetrakis(2,3,5,6-tetrafluoro-4-{PEG(750)-sulfanyl}-phenyl)-porphyrin was plotted using the porphyrin absorbance at 410 nm and known concentrations of the porphyrin (solvent deionised water). This calibration "straight" line was then used to measure the approximate concentrations of porphyrin present per specified weight of NPs.

5.3.3.5 PCNP

The concentrations of the entrapped PC was quantified using the Beer-Lambert Law ($A=\varepsilon cl$; A- Absorbance, ε- extinction coefficient of the compound, c- concentration, l- path length). The reported extinction coefficient for AlPc was 1.5 x 10^5 $M^{-1}cm^{-1}$ (λ_{ex} (DI water)/666 nm)[214]. A calibration "straight" line for PC was also plotted using the published PC absorbance maxima at 680 nm and known concentrations of the PC (solvent deionised water). This calibration "straight" line was then used to measure the approximate concentrations of PC present per specified weight of NPs. The results obtained using both reported extinction coefficient and the plotted curve were within the standard deviation.

5.3.3.6 PCNP-P

Above detailed PC calibration "straight" line (5.3.3.5) and the measured extinction coefficient for NHS porphyrin, 2.3 x 10^5 $M^{-1}cm^{-1}$(λ_{ex} (DI water)/520 nm) was used to estimate the concentration of the photosensitisers present in the PCNP-P.

5.3.4 Leaching studies

The absorbance reading of the leachates with the MB NP was significant. Thus, it was possible to calculate the percentage of MB leached from the MB NPs. For all the other NPs synthesised in the Project, fluorescence intensity was measured in the leaching experiment.

5.3.4.1 MB NP

200 mg of NPs were dispersed in 80 mL of MilliQ water and the dispersion was kept stirring at room temperature. At given time intervals (hourly), three 2 mL samples were drawn from the suspension and the absorbances were measured using UV-vis. NP suspensions were microfiltered (Whatman® Anodisc 25, 0.02 µm, 25 mm filter) and the absorbance readings of the leachates were analysed. Average readings at each time point before and after filtration were taken for 24 hours. Percentage of leached dye was calculated using the formulae below.

$$\% \text{ Leached} = (\text{Filtrate absorbance}/\text{NP suspension aliquot absorbance}) * 100$$

5.3.4.2 All the other NPs produced

Leaching of the POLPC from the nanoparticles was studied to assess the porosity of the nanoparticles. Nanoparticles (200 mg) were dispersed in 80 mL of MilliQ water. The dispersion was kept stirring at room temperature. At given time intervals (hourly), three 2 mL samples were drawn from the suspension and the nanoparticles were microfiltered (Whatman® Anodisc 25, 0.02 µm, 25 mm filter). The filtrate was analysed by fluorescence spectroscopy.

5.3.5 Determination of singlet oxygen production

2 mL of DCM followed by 3 mL of cholesterol 10 mM (1:9 DCM:MeOH) were added to a nanoparticle (5 mg/1 mL MeOH) suspension. Oxygen was bubbled through the resulting suspension mixture, which was then irradiated with white light (400–700 nm) for one hour. The volume was reduced to dryness by flowing argon into (over) the suspension. 1 mL of MeOH was added and the suspension was filtered through a 15 nm filter (Whatman® Nuclepore Track Etch membrane; 25 mm, 0.015 µm). 200 µL of this solution was transferred to an Epindorf® tube and 200 µL of methanol was added. 1-2 crystals of $NaBH_4$ were added to the solution, which was left for 1 minute until complete reduction had taken place. The volume of the solvent was reduced to approximately 100–150 µL by flowing argon over the solution.

A TLC plate was placed in a tank containing a 1:1 hexane:ethyl acetate mixture. The solvent was allowed to migrate 2/3 of the way up the plate; the plate was then removed from the TLC chamber and allowed to air dry. Once dried, the plate was returned to the tank and the solvent was allowed to migrate to the top of the plate and was left to dry again. To visualise the sterols on the TLC plate, a 5% H_2SO_4 in ethanol mist was sprayed onto the TLC plate and the plate placed on a 100-120°C hot plate to allow development of the coloured spots.

Cholesterol and its oxidation products were separated on a Phenomenex Luna 5 µm C18 column (250 x 4.60 mm) using a mixture of methanol:acetonitrile (60:40 vol/vol) mobile phase. The flow rate was maintained at 1.0 mL/min. for 20 minutes prior to analysis. UV detection was performed at 205 nm. 10 µL of the sample was injected manually into the HPLC analysis system and the separation was detected using the Azur software version 5.

5.4 Biological methods

General

- All starting materials were purchased from Sigma Aldrich.
- FACS – Becton Dickinson FACS calibur BD Biosciences software.
- Autoclavable Nichiryo Nichipet Ex Plus micropipettes (Japan) were used for measuring/pipetting small volumes.
- The white light source was a 3M Overhead Projector, 1700 A4, Visual Systems Division, Austin, Texas, U.S.A.
- Paterson PDT light system BL1000A equipped with red Glens 100 367 0134 filter (670WB, 630 110).
- Omnilux EL1000A LED light system (Phototherapeutics Limited) with a wavelength of 633±3 nm.
- Oriel light system (1000W quartz tungsten halogen lamp model 66188, Newport power supply Model 69935) equipped with a red Schott glass filter (wavelength 560 to 1940 nm).
- Biotek ELX80 Universal Microplate Reader was used to determine the cell viability after MTT assay.
- Centrifuge: Heraeus Biofuge Primo was used to pellet cells during washing steps.
- Heraeus Hera Cell incubator was used to incubate the biological assay.
- UltraScan 4000 digital camera (Gatan UK, Abingdon) attached to a Jeol 2010 transmission electron microscope (Jeol (UK) Ltd. Welwyn Garden City).
- Hydrophilic carbon coated copper grid for TEM imaging was obtained from Agar Scientific Ltd, Stansted, Essex, UK.
- Leica Microsystems CMS GmbH (LAS AF version: 2.2.1 build 4842).

5.4.1 Cell culture

Human Caucasian colon adenocarcinoma cells (HT29) cells were routinely cultured in 75cm^3 tissue culture flasks in McCoy's media supplemented with 10% fetal calf serum (FCS), 1% *L*-glutamine (all purchased from PAA) at 37°C in a humidified environment of 5% CO_2. The medium was replenished daily and the cells were sub-cultured after reaching confluence. PBS, BSA and sodium azide were purchased from Sigma Aldrich,UK.

5.4.2 Cellular uptake

5.4.2.1 Fluorescein entrapped NP uptake

A time course experiment was carried out by setting up controls (cells only) and samples (cells and NPs). Cell-only controls contained 50,000 cells in 400 µL of McCoy's media (complete) and each sample contained 50,000 HT29 cells and 5 mg of filtered (through a 220 nm filter) dextran conjugated fluorescein encapsulated NPs in 400 µL media (*i.e.* 5 mg of NPs in 200 µL media were added to a sterile sample tube containing 50,000 cells in 200 µL media).

Both the control and NPs samples were incubated at 37°C, in an atmosphere of 5% CO_2 within a humidified incubator. Every 15 minutes, duplicate sample tubes and a control tube were taken out of the incubator, washed and resuspended in PBS/BSA/azide before preparation for flow cytometry. Following incubation, 4 mL of PBS/BSA/azide was added to all three tubes, the cells were pelleted by centrifugation at 404 x *g* for 5 minutes. The supernatant was removed and discarded, and the cells were resuspended in 1 mL of PBS/BSA/azide and transferred to a clean tube. The cells were washed again by adding a

further 3 mL of PBS/BSA/azide. The cells were pelleted by centrifugation at 404 x *g* for 5 minutes. The wash procedure was repeated twice more before the cells were resuspended in 200 µL of PBS/BSA/azide. Repeated washing steps washed away most of the fluorescein or NPs present in the surrounding media. Further, to quench any extracellular fluorescence, 10 µL of Trypan blue 4% was added to the washed cells. After 5 minutes the cell suspension was loaded into a haemocytometer to count the cells.

Results were then acquired using a Becton Dickinson FACS Calibur^{TM} flow cytometer with the following settings: forward scatter (FSC) E -1 752, side scatter (SSC) 369; fluorescence (FL1) log 415; fluorescence (FL2) log 550. A minimum of 10,000 cells were measured in each sample. The fluorescein loaded NPs were detected in the fluorescence level (FL1) channel of the flow cytometer. Analysis was performed using CellQuest Pro V software (Becton Dickinson) and histograms plotted of FL1 fluorescence *vs* cell counts for each time point. The cell-only sample provided the negative control at each time point.

5.4.2.2 Cell viability over longer periods (~48 hours)

A time course experiment was carried out by setting up controls (cells only) and samples (cells and NPs). Cell-only controls contained 50,000 cells in 400 µL of McCoy's media (complete) and each sample contained 50,000 HT29 cells and 5 mg of filtered (through a 220 nm filter) dextran conjugated fluorescein encapsulated NPs in 400 µL media (*i.e.* 5 mg of NPs in 200 µL media were added to a sterile sample tube containing 50,000 cells in 200 µL media).

Both the control and NP samples were incubated at 37°C, in an atmosphere of 5% CO_2 within a humidified incubator. Every 3 hours, for the duration of the experiment, duplicate sample tubes and a control tube were taken out of the incubator, cells were washed and resuspended in 30 µL PI/Triton X-100 staining solution before preparation for flow cytometry.

Following incubation, 4 mL of PBS/BSA/azide was added to all three tubes and the cells were pelleted by centrifugation at 404 x *g* for 5 minutes. The supernatant was removed and discarded, and the cells were resuspended in 1 mL of PBS/BSA/azide and transferred to a clean tube. The cells were washed again by adding a further 3 mL of PBS/BSA/azide. The cells were pelleted by centrifugation at 404 x *g* for 5 minutes. The wash procedure was repeated twice more before the cells were resuspended in 200 µL of PBS/BSA/azide. 30 µL of PI/Triton X-100 staining solution was added to the washed cells and after 5 minutes the cell suspension was loaded into a haemocytometer to count the cells.

Results were then acquired using a Becton Dickinson FACS Calibur™ flow cytometer with the following settings: forward scatter (FSC) E -1 752, side scatter (SSC) 369;

fluorescence (FL1) log 412; fluorescence (FL2) log 474, fluorescence (FL3) log 427. A minimum of 10,000 cells were measured in each sample.

During the entire experiment no peaks were observed in the FL3 and FL4 detectors. Only a FL1 peak was observed - the fluorescence peak of fluorescein.

5.4.2.3 Nanoparticle uptake (PCNP, PCNP-A and PCNP-P)

A time course experiment using HT29 was set up with a control (cells only) and 2 samples (cells and nanoparticles) at each given time point. Cell-only controls contained 50,000 cells in 400 µL of McCoy's high glucose media and each sample contained 50,000 HT29 cells and 10 mg of the nanoparticles in 400 µL media (10 mg nanoparticles suspension of 200 µL media were added to a sterile Falcon polystyrene (12x75 mm) tube containing 50,000 cells in 200 µL media).

Both the control and sample systems were incubated at 37°C, in an atmosphere of 5% CO_2 within a humidified incubator. At given time points, duplicate sample tubes and a control tube were taken out of the incubator, cells washed and resuspended in PBS/BSA/azide solution before preparation of the material for flow cytometry.

Following incubation, 4 mL of the PBS/BSA/azide solution was added to all three tubes, the cells were pelleted by centrifugation at 404 x *g* for 5 minutes. The supernatant was removed and discarded and the cells were resuspended in 1 mL of PBS/BSA/azide solution and transferred to a clean tube. The cells were washed again by adding a further 3 mL of PBS/BSA/azide. The cells were pelleted once again by centrifugation at 404 x *g* for 5 minutes. The washing procedure was repeated twice before the cells were resuspended in 200 µL of PBS/BSA/azide solution.

The cell suspension was loaded into a haemocytometer after 5 minutes to count the cells. Results were then acquired using a Becton Dickinson FACS Calibur™ flow cytometer with the following settings: forward scatter (FSC) E -1 752, side scatter (SSC) 369;

fluorescence (FL1) log 412; fluorescence (FL2) log 474, fluorescence (FL3) log 427, fluorescence (FL4) log 377 . A minimum of 10,000 cells were measured in each sample.

PC entrapped in the NPs was detected in the fluorescence level (FL4) channel of the flow cytometer. Analysis was performed using CellQuest Pro V software (Becton Dickinson) and histograms were plotted of FL4 fluorescence *versus* cell counts for each time point. The cell-only sample provided the negative control at each time point.

5.4.3 Phototoxicity - *In vitro* (Maximum uptake)

10 mg of nanoparticles were added to 1 mL McCoy's media, agitated (Vortex™) (60 seconds), sonicated (60 seconds) and filtered (Millex® GP, 0.22 µm filter unit). The obtained volume (approximately 800 µL) was added to the same volume of cells (2.5×10^5cells/mL) in a Falcon polystyrene (12x75 mm) tube. The tube was incubated for 25 hours at 37°C in a humidified environment of 5% CO_2. The volume of the media was increased to 4 mL and the supernatant discarded to eliminate any interference from nanoparticle conjugates that had not been internalised or attached to the HT29 cells. The volume of media was increased to the initial volume (approximately 800 µL). HT29 cells were plated with 100 µL of cell suspension per well in two 96 well plates. The two controls, cells only (100% cell survival) and media only (background control) were plated onto each plate.

One plate was irradiated with 7J/cm^2 [~23 minutes] of cooled red light followed by a 40 minute recovery period in the incubator (at 37°C in a humidified environment of 5% CO_2) and another 7J/cm^2 using an Oriel light system (>580 nm red Schott glass filter, 51310/59510). The second plate was kept in the dark outside the incubator while the other plate was being irradiated. The plates were left to incubate overnight for 18-24 hours in the dark. The cell viability was determined using the MTT colorimetric assay. Briefly, 10 µL of 12 mM MTT solution was added to each well and incubated between 1 and 4 hours at 37°C to allow MTT metabolisation. The crystals formed were dissolved by adding 150 µL of acid-alcohol mixture (0.04 M HCl in absolute 2-propanol). The absorbance at 570 nm was measured on a Biotek ELX80 Universal Microplate Reader. The results were expressed with respect to control values (cells without NPs).

5.4.4 Phototoxicity - *In vitro* (Minimum uptake)

10 mg of nanoparticles were added to 1 mL McCoy's media, agitated (Vortex™) (60 seconds), sonicated (60 seconds) and filtered (Millex® GP, 0.22 µm filter unit). The obtained volume (approximately 800 µL) was added to the same volume of cells (2.5×10^5cells/mL) in a Falcon polystyrene (12x75 mm) tube. The cells were plated with 100 µL cell suspension per well in two 96 well plates. The two controls, cells only (100% cell survival) and media only (background control) were transferred onto each plate.

The light control plate was irradiated with the same system described above soon after plating (<5 minutes) 7J/cm^2 [~23 minutes] of cooled red light followed by a 40 minute recovery period in the incubator (at 37°C in a humidified environment of 5% CO_2) and another 7J/cm^2. Meanwhile the dark control plate was kept outside the incubator in the dark.

The wells were washed with 3x100 µL of media. 100 µL of media was added to the wells and the plates were left to incubate overnight for 18-24 hours in the dark. The cell viability was using MTT colorimetric assay. Briefly, 50 µL of 0.5% MTT solution was added to each well and incubated for 4 hours at 37°C to allow MTT metabolisation. The crystals formed were dissolved adding 100 µL of HCl. The absorbance at 570 nm was measured on a Microtiter® Plate reader. The results were expressed with respect to control values (cells without NPs).

5.4.5 Fluorescence confocal microscopy

5.4.5.1 PCNP

1 mL of the PCNP (10 mg/mL) were added to separate Falcon polystyrene (12x75 mm) tubes containing 1 mL ($2.5x10^5$/mL) of HT29. These were incubated for 20 hours at 37°C in a humidified environment of 5% CO_2 and washed three times with McCoy's media.

The intracellular localisation of the nanoparticles was observed with a Leica Microsystems CMS GmbH (LAS AF version: 2.2.1 build 4842). To observe the PCNP the incubated cells with PCNP were excited at 633 nm and the emission was collected between 648-790 nm.

5.4.5.2 PCNP-P

1 mL of the PCNP-P (10 mg/mL) were added to separate Falcon polystyrene (12x75 mm) tubes containing 1 mL ($2.5x10^5$/mL) of HT29. These were incubated for 20 hours at 37°C in a humidified environment of 5% CO_2 and washed three times with McCoy's media.

The intracellular localisation of the nanoparticles was observed with a Leica Microsystems CMS GmbH (LAS AF version: 2.2.1 build 4842). PCNP-P localisation was observed by exciting the incubated cells with PCNP-P at 405 nm and 633 nm and emission collected between 420-790 nm and 648-794 nm respectively.

5.4.6 Bacteria identification experiments

5.4.6.1 API® 20 E system

This system was used to identify *Escherichia coli*. This is a standardised system containing 20 microtubes of dehydrated substrates to identify *Enterobacteriaceae* and other non-fastidious Gram–rods which use 21 miniaturised biochemical tests and an international database.

The first step in the test is to prepare the incubation box with the tray and lid provided in the API® 20 E kit. To create a humid atmosphere in the incubation box approximately 5 mL of distilled water was distributed into the honeycombed wells of the tray. The API® 20E strip was then placed into the box. Every microtube on the API® 20E strip represents a test (Table 2.3). These tubes were inoculated with a bacterial suspension (a colony from an overnight cultured E.*coli* plate emulsified in 5 mL saline). The microtubes where then filled up, avoiding the formation of any bubbles, with the bacterial suspension following the procedure below. Both the tube and the capsule were filled in CIT, VP and GEL tests. ADH, LDC, ODC, H_2S, URE tubes were filled with the bacterial suspension and anaerobiosis was created by covering the suspension with a drop of mineral oil. For the remaining tests only the tubes were filled with bacterial suspension. The strip was incubated at 37°C, in an atmosphere of 5% CO_2 in a humidified incubator for 24 hours. During incubation, metabolism resulted in colour changes that were either spontaneous or revealed by addition of reagents after the incubation period. The reactions were read referencing the Reading Table from API® 20E Analytical Profile Index or/and using the identification software. *Escherichia Coli* identification was confirmed.

5.4.6.2 API STAPH test

Staphylococci are perfectly spherical cells about 1µm in diameter. *Staphylococcus aureus* form fairly large golden yellow colonies on agar whereas *S. epidermidis* forms a relatively small white colony.

Further identification was possible using API STAPH strips. The first step in the test is to prepare the incubation box with the tray and lid provided in the API STAPH kit. To create a humid atmosphere in the incubation box approximately 5 mL of distilled water was distributed into the honeycombed wells of the tray. The API STAPH strip was then placed into the box. Every microtube on the API STAPH strip represents a test (Table 2.4). The *Staphylococcus* strains (sub-cultured on agar and incubated at 37°C, in an atmosphere of 5% CO_2 within a humidified incubator for 24 hours) were emulsified on an API STAPH medium. In inoculating the strip the bacterial suspension was added to all the microtubes to fill only the tube. Anaerobiosis was created only on ADH and URE tests by filling the capsules with mineral oil.

The strip was incubated at 37°C, in an atmosphere of 5% CO_2 in a humidified incubator for 24 hours. The identification was facilitated by the use of the API STAPH Analytical Profile Index or/and the identification software. Both the *Staphylococci* strains were identified.

5.4.7 Primary bacteria assay

The initial protocol consisted of two 96 well plates: dark control and light control. Two organisms were assayed on one plate (Figure 2.43). 10 µL of overnight bacteria culture was added to each well of a 96 conical well plate, fllowed by 10 µL of MB in distilled water (final drug concentration 0–50 µM) and 180 µL Luria-Bertani (LB) media. The cultures were incubated at 37°C, in an atmosphere of 5% CO_2 in a humidified shaker incubator for 5 minutes. The plates were centrifuged for 10 minutes (404 *g*), the supernatant was removed and fresh LB added. The pellets (cells) were thawed and transferred to a flat bottom 96 well plate. The light controlled assay was irradiated with red light (40 J/cm^2) and incubated for 30 minutes with shaking. The sample was irradiated (40 J/cm^2) again and incubated at 37°C, in an atmosphere of 5% CO_2 in a humidified shaker incubator over night. The dark controlled assay culture was transferred to a flat bottom well plate and was also incubated at 37°C in an atmosphere of 5% CO_2 in a humidified shaker incubator.

Following the overnight incubation period the absorbance of each well was taken at 630 nm using a microtitre plate reader. This was followed by the CellTiter 96® aqueous non-radioactive cell proliferation assay: 20 µL of MTS/PMS combined reagent was added to the wells, incubated for 1-4 hours and the absorbance of the samples read by a micropipette reader.

5.4.8 Optimised bacteria assay

The protocol consisted of two plates: 1. dark control and 2. light control. Two organisms were assayed on one plate (Figure 2.43).

10 µL of $32x10^5$ dilution of overnight bacteria culture, 10 µL of photosensitiser (*i.e.* MB) in distilled water (final drug concentration in the well 0-100 µM) and 160 µL of LB were placed in three 96 conical well plates. The amount of LB added to the wells was reduced to avoid any spillage while centrifuging the plates. The cultures were incubated at 37°C, in an atmosphere of 5% CO_2 within a humidified shaker incubator for 15 minutes (15 minutes was found to be the best MB uptake time). The bacteria cultures were washed three times whilst changing plates at each washing (plates were centrifuged for 10 minutes, (404 *g*) of supernatant removed, fresh LB added and the cell pellets were thawed and then transferred to new plates). During the washings cultures were transferred to conical well plates with the exception of the last washing where the cultures were transferred to flat-bottom well plates.

One light controlled plate was irradiated with Omnilux® EL1000A with a wavelength of 633±3 nm providing a dose of $11J/cm^2$ (~23 minutes) and the other light controlled plate was irradiated with Oriel Model 66188 wavelength set from 550 to 2000 nm providing a dose of $7J/cm^2$ (~23 minutes). The plates were incubated at 37°C, in an atmosphere of 5% CO_2 within a humidified shaker incubator for 30 minutes (as above), and the irradiation step was repeated. The dark control assay was incubated at 37°C, in an atmosphere of 5% CO_2 (as above conditions) in a humidified shaker incubator and the culture was transferred to flat-bottom well plates.

After the PDT treatment, the plates were incubated overnight (approximately 14 hours) at 37°C, in an atmosphere of 5% CO_2 within a humidified shaker incubator. The next day, 20 µL of MTS reagent was added to the bacteria cultures to determine the bacteria viability. The cultures were incubated at 37°C, in an atmosphere of 5% CO_2 within a humidified shaker incubator for 1 hour (this was found to be the optimum duration for MTS assays), protected from light. Absorbance of each well was taken at 490 nm using a microtitre plate reader.

References

1. Campbell, I. M., *Introduction to Synthetic Polymers*. ed.; Wiltshire: Oxford University Press. Oxford.: **1994**, Chapter 1.
2. O'Shaughnessy, B.; Vavylonis, D. Dynamics of Living Polymers. *Eur. Phys. J. E* **2003,** *12*, (3), 481-496.
3. Patten, T. E.; Matyjaszewski, K. Atom Transfer Radical Polymerization and The Synthesis of Polymeric Materials. *Adv. Mater.* **1998,** *10*, (12), 901-+.
4. Owens III, D. E.; Peppas, N. A. Opsonization, Biodistribution, and Pharmacokinetics of Polymeric Nanoparticles. *Int. J. Pharm.* **2006,** *307*, (1), 93-102.
5. Vijayaraghavan, R.; MacFarlane, D. R. Group Transfer Polymerisation in Hydrophobic Ionic Liquids. *Chem. Commun.* **2005**, (9), 1149-1151.
6. Feynman, R. P., There's Plenty of Room at the Bottom. In *Annual meeting of the American Physical Society at the California Institute of Technology (Caltech)*, **1959**.
7. Schmid, G., *Nanoparticles From Theory to Application*, John Wiley & Sons, **2004**; Vol. 1st Edition, Chapter 1.
8. Narducci, D. An Introduction to Nanotechnologies: What's in it for us? *Vet. Res. Commun.* **2007,** *31*, 131-137.
9. Ferrari, M. Cancer Nanotechnology: Opportunities and Challenges. *Nat. Rev. Cancer* **2005,** *5*, (3), 161-171.

10. Gu, F. X.; Karnik, R.; Wang, A. Z.; Alexis, F.; Levy-Nissenbaum, E.; Hong, S.; Langer, R. S.; Farokhzad, O. C. Targeted Nanoparticles for Cancer Therapy. *Nano Today* **2007,** *2*, (3), 14-21.

11. Moghimi, S. M.; Hunter, A. C.; Murray, J. C. Nanomedicine: Current Status and Future Prospects. *Faseb J.* **2005,** *19*, (3), 311-330.

12. Jiang, G.; Park, K.; Kim, J.; Kim, K. S.; Oh, E. J.; Kang, H. G.; Han, S. E.; Oh, Y. K.; Park, T. G.; Hahn, S. K. Hyaluronic Acid-Polyethyleneimine Conjugate for Target Specific Intracellular Delivery of siRNA. *Biopolymers* **2008,** *89*, (7), 635-642.

13. Sunderland, C. J.; Steiert, M.; Talmadge, J. E.; Derfus, A. M.; Barry, S. E. Targeted Nanoparticles for Detecting and Treating Cancer. *Drug Dev. Res.* **2006,** *67*, (1), 70-93.

14. Hone, D. C.; Haines, A. H.; Russell, D. A. Rapid, Quantitative Colorimetric Detection of a Lectin Using Mannose-Stabilized Gold Nanoparticles. *Langmuir* **2003,** *19*, (17), 7141-7144.

15. Park, J. H.; Lee, S.; Kim, J. H.; Park, K.; Kim, K.; Kwon, I. C. Polymeric Nanomedicine for Cancer Therapy. *Prog. Polym. Sci.* **2008,** *33*, (1), 113-137.

16. Xu, H.; Aylott, J. W.; Kopelman, R. Fluorescent Nano-PEBBLE Sensors Designed for Intracellular Glucose Imaging. *Analyst* **2002,** *127*, (11), 1471-1477.

17. Sumner, J. P.; Aylott, J. W.; Monson, E.; Kopelman, R. A Fluorescent PEBBLE Nanosensor for Intracellular Free Zinc. *Analyst* **2002,** *127*, (1), 11-16.

18. Hild, W. A.; Breunig, M.; Goepferich, A. Quantum Dots - Nano-Sized Probes for the Exploration Of Cellular And Intracellular Targeting. *Eur. J. Pharm. Biopharm.* **2008,** *68*, (2), 153-168.

19. Orringer, D. A.; Koo, Y. E.; Chen, T.; Kopelman, R.; Sagher, O.; Philbert, M. A. Small Solutions for Big Problems: The Application of Nanoparticles to Brain Tumor Diagnosis and Therapy. *Clin. Pharmcol. Ther.* **2009,** *85*, (5), 531-534.

20. Leggett, R.; Lee-Smith, E. E.; Jickells, S. M.; Russell, D. A. "Intelligent" Fingerprinting: Simultaneous Identification of Drug Metabolites and Individuals by using Antibody-Functionalized Nanoparticles. *Angew. Chem. Int. Edit.* **2007,** *46*, (22), 4100-4103.

21. Sun, H.; Scharff-Poulsen, A. M.; Gu, H.; Jakobsen, I.; Kossmann, J. M.; Frommer, W. B.; Almdal, K. Phosphate Sensing by Fluorescent Reporter Proteins Embedded in Polyacrylamide Nanoparticles. *Acs. Nano.* **2008,** *2*, (1), 19-24.

22. Almdal, K.; Sun, H. H.; Poulsen, A. K.; Arleth, L.; Jakobsen, I.; Gu, H.; Scharff-Poulsen, A. M. Fluorescent Gel Particles in the Nanometer Range for Detection of Metabolites in Living Cells. *Polym. Adv. Technol.* **2006,** *17*, (9-10), 790-793.

23. Sun, H.; Scharff-Poulsen, A. M.; Gu, H.; Almdal, K. Synthesis and Characterization of Ratiometric, pH Sensing Nanoparticles with Covalently Attached Fluorescent Dyes. *Chem. Mater.* **2006,** *18*, (15), 3381-3384.

24. Poulsen, A. K.; Scharff-Poulsen, A. M.; Olsen, L. F. Horseradish Peroxidase Embedded In Polyacrylamide Nanoparticles Enables Optical Detection of Reactive Oxygen Species. *Anal. Biochem.* **2007,** *366*, (1), 29-36.

25. Koo, Y. E. L.; Cao, Y. F.; Kopelman, R.; Koo, S. M.; Brasuel, M.; Philbert, M. A. Real-time Measurements of Dissolved Oxygen Inside Live Cells by Organically Modified Silicate Fluorescent Nanosensors. *Anal. Chem.* **2004,** *76*, (9), 2498-2505.

26. Cao, Y. F.; Koo, Y. E. L.; Koo, S. M.; Kopelman, R. Ratiometric Singlet Oxygen Nano-Optodes and Their use for Monitoring Photodynamic Therapy Nanoplatforms. *Photochem. Photobiol.* **2005,** *81*, (6), 1489-1498.

27. Josefsen, L. B.; Aylott, J. W.; Beeby, A.; Warburton, P.; Boyle, J. P.; Peers, C.; Boyle, R. W. Porphyrin-Nanosensor Conjugates. New Tools for the Measurement of Intracellular Response to Reactive Oxygen Species. *Photochem. Photobiol. Sci.* **2010,** *9*, (6), 801-811.

28. Josefsen, L. B. Porphyrin-Nanosensor Conjugates: Novel Tools for the Study of Cellular Response to Oxidative Stress. PhD Thesis, University of Hull, **2007**.

29. Quarta, A.; Di Corato, R.; Manna, L.; Ragusa, A.; Pellegrino, T. Fluorescent-Magnetic Hybrid Nanostructures: Preparation, Properties, and Applications in Biology. *Ieee T. Nanobiosci.* **2007,** *6*, (4), 298-308.

30. Venugopal, J.; Prabhakaran, M. P.; Low, S.; Choon, A. T.; Zhang, Y. Z.; Deepika, G.; Ramakrishna, S. Nanotechnology for Nanomedicine and Delivery of Drugs. *Curr. Pharm. Design.* **2008,** *14*, (22), 2184-2200.

31. Rawat, M.; Singh, D.; Saraf, S.; Saraf, S. Nanocarriers: Promising Vehicle for Bioactive Drugs. *Biol. Pharm. Bull.* **2006,** *29*, (9), 1790-1798.

32. Rosi, N. L.; Giljohann, D. A.; Thaxton, C. S.; Lytton-Jean, A. K. R.; Han, M. S.; Mirkin, C. A. Oligonucleotide-Modified Gold Nanoparticles for Intracellular Gene Regulation. *Science.* **2006,** *312*, 1027-1030.

33. Mirkin, C. A.; Letsinger, R. L.; Mucic, R. C.; Storhoff, J. J. A DNA-Based Method for Rationally Assembling Nanoparticles into Macroscopic Materials. *Nature.* **1996,** *382*, (6592), 607-609.

34. Panyam, J.; Labhasetwar, V. Biodegradable Nanoparticles for Drug and Gene Delivery to Cells and Tissue. *Adv. Drug Deliv. Rev.* **2003,** *55*, (3), 329-347.

35. Faraji, A. H.; Wipf, P. Nanoparticles in Cellular Drug Delivery. *Bioorgan. Med. Chem.* **2009,** *17*, (8), 2950-2962.

36. Cho, K. J.; Wang, X.; Nie, S. M.; Chen, Z.; Shin, D. M. Therapeutic nanoparticles For Drug Delivery In Cancer. *Clin. Cancer Res.* **2008,** *14*, (5), 1310-1316.

37. Subramani, K.; Hosseinkhani, H.; Khraisat, A.; Hosseinkhani, M.; Pathak, Y. Targeting Nanoparticles as Drug Delivery Systems for Cancer Treatment. *Curr. Nanosci.* **2009,** *5*, (2), 135-140.

38. Rancan, F.; Papakostas, D.; Hadam, S.; Hackbarth, S.; Delair, T.; Primard, C.; Verrier, B.; Sterry, W.; Blume-Peytavi, U.; Vogt, A. Investigation of Polylactic Acid (PLA) Nanoparticles as Drug Delivery Systems for Local Dermatotherapy. *Pharm. Res.* **2009,** *26*, (8), 2027-2036.

39. Neuberger, T.; Schopf, B.; Hofmann, H.; Hofmann, M.; von Rechenberg, B. Superparamagnetic Nanoparticles for Biomedical Applications: Possibilities and Limitations of a New Drug Delivery System. *J. Magn. Magn. Mater.* **2005,** *293*, (1), 483-496.

40. Agnihotri, S. A.; Mallikarjuna, N. N.; Aminabhavi, T. M. Recent Advances on Chitosan-Based Micro- and Nanoparticles in Drug Delivery. *J. Controlled Release* **2004,** *100*, (1), 5-28.

41. Hans, M. L.; Lowman, A. M. Biodegradable Nanoparticles for Drug Delivery and Targeting. *Curr. Opin. Solid St. M.* **2002,** *6*, (4), 319-327.

42. Soppimath, K. S.; Aminabhavi, T. M.; Kulkarni, A. R.; Rudzinski, W. E. Biodegradable Polymeric Nanoparticles as Drug Delivery Devices. *J. Controlled Release* **2001,** *70*, (1-2), 1-20.

43. Müller, R. H.; Mader, K.; Gohla, S. Solid Lipid Nanoparticles (SLN) for Controlled Drug Delivery - A Review of The State of The Art. *Eur. J. Pharm. Biopharm.* **2000,** *50*, (1), 161-177.

44. Xu, Z. P.; Zeng, Q. H.; Lu, G. Q.; Yu, A. B. Inorganic Nanoparticles as Carriers for Efficient Cellular Delivery. *Chem. Eng. Sci.* **2006,** *61*, (3), 1027-1040.

45. Breunig, M.; Bauer, S.; Goefferich, A. Polymers and Nanoparticles: Intelligent Tools for Intracellular Targeting. *Eur. J. Pharm. Biopharm.* **2008,** *68*, (1), 112-128.

46. Tang, W.; Xu, H.; Park, E. J.; Philbert, M. A.; Kopelman, R. Encapsulation of Methylene Blue in Polyacrylamide Nanoparticle Platforms Protects its Photodynamic Effectiveness. *Biochem. Biophys. Res. Commun.* **2008,** *369*, (2), 579-583.

47. Ehrenberg, M. S.; Friedman, A. E.; Finkelstein, J. N.; Oberdörster, G.; McGrath, J. L. The Influence of Protein Adsorption on Nanoparticle Association with Cultured Endothelial Cells. *Biomaterials* **2009,** *30*, (4), 603-610.

48. Brannon-Peppas, L.; Blanchette, J. O. Nanoparticle and Targeted Systems for Cancer Therapy. *Adv. Drug Deliver. Rev.* **2004,** *56*, (11), 1649-1659.

49. Sahoo, S. K.; Labhasetwar, V. Nanotech Approaches to Delivery and Imaging Drug. *Drug Discov. Today* **2003,** *8*, (24), 1112-1120.

50. Pinto Reis, C.; Neufeld, R. J.; Ribeiro, A. J.; Veiga, F. Nanoencapsulation I. Methods for Preparation of Drug-Loaded Polymeric Nanoparticles. *Nanomedicine-UK* **2006,** *2*, (1), 8-21.

51. Sahoo, S. K.; Parveen, S.; Panda, J. J. The Present and Future of Nanotechnology in Human Health Care. *Nanomed.-Nanotechnol.* **2007,** *3*, (1), 20-31.

52. Maeda, H. The Enhanced Permeability and Retention (EPR) Effect in Tumor Vasculature: The Key Role of Tumor-Selective Macromolecular Drug Targeting. *Adv. Enzyme Regul.*, **2001,** *41*, 189-207.

53. Allen, T. M. Ligand-Targeted Therapeutics in Anticancer Therapy. *Nat. Rev. Cancer* **2002,** *2*, (10), 750-763.

54. Emerich, D. F.; Thanos, C. G. The Pinpoint Promise of Nanoparticle-Based Drug Delivery and Molecular Diagnosis. *Biomol. Eng.* **2006,** *23*, (4), 171-184.

55. Katz, E.; Willner, I. Integrated nanoparticle-Biomolecule Hybrid Systems: Synthesis, Properties, and Applications. *Angew. Chem. Int. Edit.* **2004,** *43*, (45), 6042-6108.

56. Mucic, R. C.; Storhoff, J. J.; Mirkin, C. A.; Letsinger, R. L. DNA-Directed Synthesis of Binary Nanoparticle Network Materials. *J. Amer. Chem. Soc.* **1998,** *120*, (48), 12674-12675.

57. Chen, S. H.; Kimura, K. Synthesis and Characterization of Carboxylate-Modified Gold Nanoparticle Powders Dispersible in Water. *Langmuir* **1999,** *15*, (4), 1075-1082.

58. Panyam, J.; Zhou, W. Z.; Prabha, S.; Sahoo, S. K.; Labhasetwar, V. Rapid Endo-Lysosomal Escape of Poly(DL-lactide-co-glycolide) Nanoparticles: Implications for Drug and Gene Delivery. *Faseb J.* **2002,** *16*, (10).

59. Kaul, G.; Amiji, M. Long-Circulating Poly(ethylene glycol)-Modified Gelatin Nanoparticles for Intracellular Delivery. *Pharm. Res.* **2002,** *19*, (7), 1061-1067.

60. Mecerreyes, D.; Lee, V.; Hawker, C. J.; Hedrick, J. L.; Wursch, A.; Volksen, W.; Magbitang, T.; Huang, E.; Miller, R. D. A Novel Approach to Functionalized Nanoparticles: Self-Crosslinking of Macromolecules in Ultradilute Solution. *Adv. Mater.* **2001,** *13*, (3), 204-208.

61. Vihola, H.; Laukkanen, A.; Hirvonen, J.; Tenhu, H. Binding and Release of Drugs Into and From Thermosensitive Poly(N-vinyl caprolactam) Nanoparticles. *Eur. J. Pharm. Sci.* **2002,** *16*, (1-2), 69-74.

62. Sablong, R.; Schlotterbeck, U.; Vogt, D.; Mecking, S. Catalysis with Soluble Hybrids of Highly Branched Macromolecules with Palladium Nanoparticles in a

Continuously Operated Membrane Reactor. *Adv. Synth. Catal.* **2003,** *345*, (3), 333-336.

63. Zhang, M. F.; Drechsler, M.; Muller, A. H. E. Template-controlled Synthesis of Wire-Like Cadmium Sulfide Nanoparticle Assemblies Within Core-Shell Cylindrical Polymer Brushes. *Chem. Mater.* **2004,** *16*, (3), 537-543.

64. Pavel, F. M.; Mackay, R. A. Reverse Micellar Synthesis of a Nanoparticle/Polymer Composite. *Langmuir* **2000,** *16*, (23), 8568-8574.

65. Ugelstad, J.; Elaasser, M. S.; Vanderho. J. W. Emulsion Polymerization - Initiation of Polymerization in Monomer Droplets. *J. Pol. Sci. Pol. Lett.* **1973,** *11*, (8), 503-513.

66. Maxwell, I. A.; Morrison, B. R.; Napper, D. H.; Gilbert, R. G. Entry of Free-Radicals into Latex-Particles in Emulsion Polymerization. *Macromolecules* **1991,** *24*, (7), 1629-1640.

67. Hansen, F. K.; Ugelstad, J. Particle Nucleation in Emulsion Polymerization .1. Theory for Homogeneous Nucleation. *J. Polm.Sci.Part a* **1978,** *16*, (8), 1953-1979.

68. Goodall, A. R.; Wilkinson, M. C.; Hearn, J. Mechanism of Emulsion Polymerization of Styrene in Soap-Free Systems. *J. Polym. Sci. Part a* **1977,** *15*, (9), 2193-2218.

69. Feeney, P. J.; Napper, D. H.; Gilbert, R. G. Coagulative Nucleation and Particle-Size Distributions in Emulsion Polymerization. *Macromolecules* **1984,** *17*, (12), 2520-2529.

70. Barton, J., Capek, I., *Radical Polymerization in Disperse Systems*. 1 ed.; Ellis Horwood series in Polymer Chemistry: Slovakia, **1994**.

71. Gao, H. X.; Jiang, T.; Han, B. X.; Wang, Y.; Du, J. M.; Liu, Z. M.; Zhang, J. L. Aqueous/Ionic Liquid Interfacial Polymerization for Preparing Polyaniline Nanoparticles. *Polymer* **2004,** *45*, (9), 3017-3019.

72. Sun, Q. H.; Deng, Y. L. *In Situ* Synthesis of Temperature-Sensitive Hollow Microspheres *via* Interfacial Polymerization. *J. Amer. Chem. Soc.***2005,** *127*, (23), 8274-8275.

73. Yang, S.; Liu, H. R. A Novel Approach to Hollow Superparamagnetic Magnetite/Polystyrene Nanocomposite Microspheres *via* Interfacial Polymerization. *J. Mater. Chem.* **2006,** *16*, (46), 4480-4487.

74. Krauel, K.; Davies, N. M.; Hook, S.; Rades, T. Using Different Structure Types of Microemulsions for the Preparation of Poly(alkylcyanoacrylate) Nanoparticles by Interfacial Polymerization. *J. Control Release* **2005,** *106*, (1-2), 76-87.

75. Xie, X. L.; Tang, C. Y.; Zhou, X. P.; Li, R. K. Y.; Yu, Z. Z.; Zhang, Q. X.; Mai, Y. W. Enhanced Interfacial Adhesion Between PPO and Glass Beads in Composites by Surface Modification of Glass Beads *via In Situ* Polymerization and Copolymerization. *Chem. Mater.* **2004,** *16*, (1), 133-138.

76. Poulsen, A. K.; Arleth, L.; Almdal, K.; Scharff-Poulsen, A. M. Unusually Large Acrylamide Induced Effect on the Droplet Size in AOT/Brij30 Water-In-Oil Microemulsions. *J. Colloid. Interf. Sci.* **2007,** *306*, (1), 143-153.

77. Tantillo, C.; Ding, J. P.; Jacobomolina, A.; Nanni, R. G.; Boyer, P. L.; Hughes, S. H.; Pauwels, R.; Andries, K.; Janssen, P. A. J.; Arnold, E. Locations of Anti-Aids Drug-Binding Sites and Resistance Mutations in the 3-Dimensional Structure of HIV-1 Reverse-Transcriptase - Implications for Mechanisms of Drug-Inhibition and Resistance. *Journal of Mol. Biol.* **1994,** *243*, (3), 369-387.

78. Walsh, C. Molecular Mechanisms That Confer Antibacterial Drug Resistance. *Nature* **2000,** *406*, (6797), 775-781.

79. Gottesman, M. M. Mechanisms of Cancer Drug Resistance. *Annu. Rev. Med.* **2002,** *53*, 615-627.

80. Borst, P.; Ouellette, M. New Mechanisms of Drug-Resistance in Parasitic Protozoa. *Annu.l Rev. Microbiol.***1995,** *49*, 427-460.

81. Longley, D. B.; Johnston, P. G. Molecular Mechanisms of Drug Resistance. *J. Pathol.* **2005,** *205*, (2), 275-292.

82. Gottesman, M. M.; Fojo, T.; Bates, S. E. Multidrug Resistance in Cancer: Role of ATP-Dependent Transporters. *Nat. Rev. Cancer* **2002,** *2*, (1), 48-58.

83. Huang, I. P.; Sun, S. P.; Cheng, S. H.; Lee, C. H.; Wu, C. Y.; Yang, C. S.; Lo, L. W.; Lai, Y. K. Enhanced Chemotherapy of Cancer Using pH-Sensitive Mesoporous Silica Nanoparticles to Antagonize P-Glycoprotein-Mediated Drug Resistance. *Mol. Cancer Ther.* **2011,** *10*, (5), 761-769.

84. Wong, H. L.; Bendayan, R.; Rauth, A. M.; Xue, H. Y.; Babakhanian, K.; Wu, X. Y. A Mechanistic Study of Enhanced Doxorubicin Uptake and Retention in Multidrug Resistant Breast Cancer Cells Using a Polymer-Lipid Hybrid Nanoparticle System. *J. Pharmacol. Exp. Ther.* **2006,** *317*, (3), 1372-1381.

85. Sahoo, S. K.; Labhasetwar, V. Enhanced Anti-Proliferative Activity of Transferrin-Conjugated Paclitaxel-Loaded Nanoparticles is Mediated *via* Sustained Intracellular Drug Retention. *Mol. Pharm.* **2005,** *2*, (5), 373-383.

86. Lee, E. S.; Na, K.; Bae, Y. H. Doxorubicin loaded pH-Sensitive Polymeric Micelles for Reversal of Resistant MCF-7 Tumor. *J. Control. Release* **2005,** *103*, (2), 405-418.

87. Conner, S. D.; Schmid, S. L. Regulated Portals of Entry into the Cell. *Nature* **2003,** *422*, (6927), 37-44.

88. Rogers, W. J.; Basu, P. Factors Regulating Macrophage Endocytosis of Nanoparticles: Implications for Targeted Magnetic Resonance Plaque Imaging. *Atherosclerosis* **2005,** *178*, (1), 67-73.

89. Raynal, I.; Prigent, P.; Peyramaure, S.; Najid, A.; Rebuzzi, C.; Corot, C. Macrophage Endocytosis of Superparamagnetic Iron Oxide Nanoparticles - Mechanisms and Comparison of Ferumoxides and Ferumoxtran-10. *Invest. Radiol.* **2004,** *39*, (1), 56-63.

90. Panyam, J.; Labhasetwar, V. Dynamics of endocytosis and Exocytosis of Poly(D,L-lactide-co-glycolide) Nanoparticles in Vascular Smooth Muscle Cells. *Pharm. Res.* **2003,** *20*, (2), 212-220.

91. Gratton, S. E. A.; Ropp, P. A.; Pohlhaus, P. D.; Luft, J. C.; Madden, V. J.; Napier, M. E.; DeSimone, J. M. The Effect of Particle Design on Cellular Internalization Pathways. *P. Natl. Acad. Sci. USA* **2008,** *105*, (33), 11613-11618.

92. Zhang, L. W.; Monteiro-Riviere, N. A. Mechanisms of Quantum Dot Nanoparticle Cellular Uptake. *Toxicol. Sci.* **2009,** *110*, (1), 138-155.

93. Wartlick, H.; Spankuch-Schmitt, B.; Strebhardt, K.; Kreuter, J.; Langer, K. Tumour Cell Delivery of Antisense Oligonucleotides by Human Serum Albumin Nanoparticles. *J. Control. Release* **2004,** *96*, (3), 483-495.

94. Aderem, A.; Underhill, D. M. Mechanisms of Phagocytosis in Macrophages. *Annu. Rev. Immun.* **1999,** *17*, 593-623.

95. Berlin, R. D.; Oliver, J. M.; Walter, R. J. Surface Functions During Mitosis .1. Phagocytosis, Pinocytosis and Mobility of Surface-Bound Cona. *Cell* **1978,** *15*, (2), 327-341.

96. Brandt, P. W. A Study of the Mechanism of Pinocytosis. *Exp. Cell Res.* **1958,** *15*, (2), 300-313.

97. Goldstein, J. L.; Anderson, R. G. W.; Brown, M. S. Coated Pits, Coated Vesicles, and Receptor-Mediated Endocytosis. *Nature* **1979,** *279*, (5715), 679-685.

98. Goldstein, J. L.; Brown, M. S.; Anderson, R. G. W.; Russell, D. W.; Schneider, W. J. Receptor-Mediated Endocytosis - Concepts Emerging from the Ldl Receptor System. *Annu. Revi. Cell Biol.* **1985,** *1*, 1-39.

99. Hu, L.; Mao, Z. W.; Gao, C. Y. Colloidal Particles for Cellular Uptake and Delivery. *J. Mater. Chem.* **2009,** *19*, (20), 3108-3115.

100. Hed, J.; Stendahl, O. Differences in the Ingestion Mechanisms of Igg and C3b Particles in Phagocytosis by Neutrophils. *Immunology.* **1982,** *45*, (4), 727-736.

101. Pommier, C. G.; Inada, S.; Fries, L. F.; Takahashi, T.; Frank, M. M.; Brown, E. J. Plasma Fibronectin Enhances Phagocytosis of Opsonized Particles by Human Peripheral-Blood Monocytes. *J. Exp. Med.* **1983,** *157*, (6), 1844-1854.

102. Innes, N. P. T.; Ogden, G. R. A Technique for the Study of Endocytosis in Human Oral Epithelial Cells. *Arch. Oral Biol.* **1999,** *44*, (6), 519-523.

103. Swanson, J. A.; Watts, C. Macropinocytosis. *Trends. Cell Biol.* **1995,** *5*, (11), 424-428.

104. Marsh, M.; McMahon, H. T. Cell biology - The Structural Era of Endocytosis. *Science.* **1999,** *285*, (5425), 215-220.

105. Pelkmans, L.; Helenius, A. Endocytosis *via* Caveolae. *Traffic.* **2002,** *3*, (5), 311-320.

106. Larsen, A. K.; Escargueil, A. E.; Skladanowski, A. Resistance Mechanisms Associated with Altered Intracellular Distribution of Anticancer Agents. *Pharmacol. Therapeut.* **2000,** *85*, (3), 217-229.

107. Hillaireau, H.; Couvreur, P. Nanocarriers' Entry into the Cell: Relevance to Drug Delivery. *Cell. Mol. Life Sci.* **2009,** *66*, (17), 2873-2896.

108. Besterman, J. M.; Low, R. B. Endocytosis - A Review of Mechanisms and Plasma-Membrane Dynamics. *Biochem. J.* **1983,** *210*, (1), 1-13.

109. Jin, H.; Heller, D. A.; Strano, M. S. Single-Particle Tracking of Endocytosis and Exocytosis of Single-Walled Carbon Nanotubes in NIH-3T3 Cells. *Nano Lett.* **2008,** *8*, (6), 1577-1585.

110. Raab, O. Uber die Wirkung Fluoreszierender Stoffen auf Infusoria. *Z. Biol*, **1900,** *39*, 524.

111. McCaughan, J. S. Photodynamic Therapy - A Review. *Drugs & Aging* **1999,** *15*, (1), 49-68.

112. MacDonald, I. J.; Dougherty, T. J. Basic Principles of Photodynamic Therapy. *J. Porphyr.Phthalocya.* **2001,** *5*, (2), 105-129.

113. Josefsen, L. B.; Boyle, R. W. Photodynamic Therapy: Novel Third-Generation Photosensitizers One Step Closer? *Br. J. Pharmacol.* **2008,** *154*, (1), 1-3.

114. Sharman, W. M.; Allen, C. M.; van Lier, J. E. Photodynamic Therapeutics: Basic Principles and Clinical Applications. *Drug Discov. Today* **1999,** *4*, (11), 507-517.

115. Hopper, C. Photodynamic Therapy: A Clinical Reality in the Treatment of Cancer. *Lancet Oncol.* **2000,** *1*, 212-219.

116. Girotti, A. W. Photosensitized Oxidation of Membrane Lipids: Reaction Pathways, Cytotoxic Effects, and Cytoprotective Mechanisms. *J. Photochem. Photobiol. B-Biol.* **2001,** *63*, (1-3), 103-113.

117. Christie, R. M., *Colour Chemistry*. ed.; RSC: Royal society of Chemistry: **2001**.

118. Nassau, K., The physics and Chemistry of Color: The Fifteen Causes of Color. In ed.; A Wiley-Interscience Publication: John Wiley & Sons: **1983**.

119. Zhang, P.; Steelant, W.; Kumar, M.; Scholfield, M. Versatile Photosensitizers for Photodynamic Therapy at Infrared Excitation. *J. Am. Chem. Soc.* **2007,** *129*, (15), 4526-+.

120. Kübler, A. C. Photodynamic Therapy. *Medical Laser Application* **2005,** *20*, (1), 37-45.

121. Anstey, A. Photodynamic Therapy. *Medicine* **2004,** *32*, (12), 24-25.

122. Fuchs, J.; Thiele, J. The Role of Oxygen in Cutaneous Photodynamic Therapy. *Free Radical Bio. Med.* **1998,** *24*, (5), 835-847.

123. Schmidt-Erfurth, U.; Hasan, T. Mechanisms of Action of Photodynamic Therapy with Verteporfin® for the Treatment of Age-Related Macular Degeneration. *Surv. Ophthalmol.* **2000,** *45*, (3), 195-214.

124. Valenzeno, D. P. Photomodification of Biological Membranes with Emphasis on Singlet Oxygen Mechanisms. *Photochem. Photobiol.* **1987,** *46*, (1), 147-160.

125. Schweitzer, C.; Mehrdad, Z.; Noll, A.; Grabner, E. W.; Schmidt, R. Mechanism of Photosensitized Generation of Singlet Oxygen During Oxygen Quenching of Triplet States and the General Dependence of the Rate Constants and Efficiencies of $O_2(^1\Sigma_g^+)$, $O_2(^1\Delta_g)$, and $O_2(^3\Sigma_g^-)$ Formation on Sensitizer Triplet State Energy and Oxidation Potential. *J. Phys. Chem. A.* **2003,** *107*, (13), 2192-2198.

126. Schweitzer, C.; Schmidt, R. Physical Mechanisms of Generation and Deactivation of Singlet Oxygen. *Chem. Rev.* **2003,** *103*, (5), 1685-1757.

127. Plaetzer, K.; Krammer, B.; Berlanda, J.; Berr, F.; Kiesslich, T. Photophysics and Photochemistry of Photodynamic Therapy: Fundamental Aspects. *Laser. Med. Sci.* **2009,** *24*, (2), 259-268.

128. Ochsner, M. Photophysical and Photobiological Processes in the Photodynamic Therapy of Tumours. *J. Photochem. Photobiol. B-Biol.* **1997,** *39*, (1), 1-18.

129. Schmidt, R.; Bodesheim, M. Radiationless Deactivation of the Second Excited Singlet State $^1\Sigma_g^+$ *of* O_2 in Solution. *J. Phys. Chem. A* **1998,** *102*, (25), 4769-4774.

130. Moreno, M. J.; Monson, E.; Reddy, R. G.; Rehemtulla, A.; Ross, B. D.; Philbert, M.; Schneider, R. J.; Kopelman, R. Production of Singlet Oxygen by Ru(Dpp(SO_3)($_2$))($_3$) Incorporated in Polyacrylamide PEBBLES. *Sensor. Actuat. B-Chem.* **2003,** *90*, (1-3), 82-89.

131. Harada, Y.; Suzuki, K.; Hashimoto, M.; Tsukagoshi, K.; Kimoto, H. Chemiluminescence from Singlet Oxygen that was Detected at Two Wavelengths and Effects of Biomolecules On It. *Talanta* **2009,** *77*, (3), 1223-1227.

132. Wainwright, M. Photodynamic Antimicrobial Chemotherapy (PACT). *J. Antimicrob. Chemoth.* **1998,** *42*, (1), 13-28.

133. Konan, Y. N.; Gurny, R.; Allémann, E. State of the Art in the Delivery of Photosensitizers for Photodynamic Therapy. *J. Photochem. Photobiol. B: Biol.* **2002,** *66*, (2), 89-106.

134. Greish, K. Enhanced Permeability and Retention of Macromolecular Drugs in Solid Tumors: A Royal Gate for Targeted Anticancer Nanomedicines. *J. Drug Target.* **2007,** *15*, (7-8), 457-464.

135. Nishiyama, N.; Okazaki, S.; Cabral, H.; Miyamoto, M.; Kato, Y.; Sugiyama, Y.; Nishio, K.; Matsumura, Y.; Kataoka, K. Novel Cisplatin-Incorporated Polymeric Micelles Can Eradicate Solid Tumors in Mice. *Cancer Res.* **2003,** *63*, (24), 8977-8983.

136. Dolmans, D.; Fukumura, D.; Jain, R. K. Photodynamic Therapy for Cancer. *Nature Rev. Cancer* **2003,** *3*, (5), 380-387.

137. Henderson, B. W.; Waldow, S. M.; Mang, T. S.; Potter, W. R.; Malone, P. B.; Dougherty, T. J. Tumor Destruction and Kinetics of Tumor-Cell Death in 2

Experimental Mouse-Tumors Following Photodynamic Therapy. *Cancer Res.* **1985,** *45*, (2), 572-576.

138. Chen, W.; Zhang, J. Using Nanoparticles to Enable Simultaneous Radiation and Photodynamic Therapies for Cancer Treatment. *J. Nanosci. Nanotechnol.* **2006,** *6*, (4), 1159-1166.

139. Nann, T. Nanoparticles in Photodynamic Therapy. *Nano Biomed. Eng.* **2011,** *3*, (2), 137-143.

140. Bechet, D.; Couleaud, P.; Frochot, C.; Viriot, M.-L.; Guillemin, F.; Barberi-Heyob, M. Nanoparticles as Vehicles for Delivery of Photodynamic Therapy Agents. *Trends in Biotechnol.* **2008,** *26*, (11), 612-621.

141. Couleaud, P.; Morosini, V.; Frochot, C.; Richeter, S.; Raehm, L.; Durand, J.-O. Silica-Based Nanoparticles for Photodynamic Therapy Applications. *Nanoscale* **2010,** *2*, (7), 1083-1095.

142. Juzenas, P.; Chen, W.; Sun, Y.-P.; Neto Coelho, M. A.; Generalov, R.; Generalova, N.; Christensen, I. L. Quantum Dots and Nanoparticles for Photodynamic and Radiation Therapies of Cancer. *Adv. Drug Deliv. Rev.* **2008,** *60*, (15), 1600-1614.

143. Chatterjee, D. K.; Fong, L. S.; Zhang, Y. Nanoparticles in Photodynamic Therapy: An Emerging Paradigm. *Adv. Drug Deliv. Rev.* **2008,** *60*, (15), 1627-1637.

144. Lee, Y.-E. K.; Kopelman, R. Polymeric Nanoparticles For Photodynamic Therapy. *Method. mol. biol.* **2011,** *726*, 151-178.

145. Allison, R. R.; Mota, H. C.; Bagnato, V. S.; Sibata, C. H. Bio-Nanotechnology and Photodynamic Therapy - State of The Art Review. *Photodiagn. Photodyn.* **2008,** *5*, (1), 19-28.

146. Brevet, D.; Gary-Bobo, M.; Raehm, L.; Richeter, S.; Hocine, O.; Amro, K.; Loock, B.; Couleaud, P.; Frochot, C.; Morere, A.; Maillard, P.; Garcia, M.; Durand, J.-O.

Mannose-Targeted Mesoporous Silica Nanoparticles for Photodynamic Therapy. *Chem. Commun.* **2009**, (12), 1475-1477.

147. Rosenholm, J. M.; Sahlgren, C.; Linden, M. Multifunctional Mesoporous Silica Nanoparticles for Combined Therapeutic, Diagnostic and Targeted Action in Cancer Treatment. *Curr. Drug Targets* **2011,** *12*, (8), 1166-1186.

148. Gupta, A.; Goswami, L. N.; Ethirajan, M.; Missert, J.; Rao, K. V. R.; Ohulchanskyy, T.; Roy, I.; Morgan, J.; Prasad, P. N.; Pandey, R. K. Organically Modified Silica Nanoparticles as Drug Delivery Vehicles in Photodynamic Therapy. *J. Porphyr. Phthalocya.* **2011,** *15*, (5-6), 401-411.

149. Roy, I.; Ohulchanskyy, T. Y.; Pudavar, H. E.; Bergey, E. J.; Oseroff, A. R.; Morgan, J.; Dougherty, T. J.; Prasad, P. N. Ceramic-Based Nanoparticles Entrapping Water-Insoluble Photosensitizing Anticancer Drugs: A Novel Drug-Carrier System for Photodynamic Therapy. *J. Am. Chem. Soc.* **2003,** *125*, (26), 7860-7865.

150. Liu, Y.; Lou, C.; Yang, H.; Shi, M.; Miyoshi, H. Silica Nanoparticles as Promising Drug/Gene Delivery Carriers and Fluorescent Nano-Probes: Recent Advances. *Curr. Cancer Drug Tar.* **2011,** *11*, (2), 156-163.

151. Huang, P.; Li, Z.; Lin, J.; Yang, D.; Gao, G.; Xu, C.; Bao, L.; Zhang, C.; Wang, K.; Song, H.; Hu, H.; Cui, D. Photosensitizer-Conjugated Magnetic Nanoparticles for *in vivo* Simultaneous Magnetofluorescent Imaging and Targeting Therapy. *Biomaterials* **2011,** *32*, (13), 3447-3458.

152. Wang, F.; Chen, X. L.; Zhao, Z. X.; Tang, S. H.; Huang, X. Q.; Lin, C. H.; Cai, C. B.; Zheng, N. F. Synthesis of Magnetic, Fluorescent and Mesoporous Core-Shell-Structured Nanoparticles for Imaging, Targeting and Photodynamic Therapy. *J. Mater. Chem.* **2011,** *21*, (30), 11244-11252.

153. Chen, Z.-L.; Sun, Y.; Huang, P.; Yang, X.-X.; Zhou, X.-P. Studies on Preparation of Photosensitizer Loaded Magnetic Silica Nanoparticles and Their Anti-Tumor Effects for Targeting Photodynamic Therapy. *Nanoscale Res. Lett.* **2009,** *4*, (5), 400-408.

154. Sun, Y.; Chen, Z.-l.; Yang, X.-x.; Huang, P.; Zhou, X.-p.; Du, X.-x. Magnetic Chitosan Nanoparticles as a Drug Delivery System for Targeting Photodynamic Therapy. *Nanotechnology* **2009,** *20*, (13), 135102

155. Arvizo, R.; Bhattacharya, R.; Mukherjee, P. Gold Nanoparticles: Opportunities and Challenges in Nanomedicine. *Exp. Opin. Drug Del.* **2010,** *7*, (6), 753-763.

156. Wieder, M. E.; Hone, D. C.; Cook, M. J.; Handsley, M. M.; Gavrilovic, J.; Russell, D. A. Intracellular Photodynamic Therapy with Photosensitizer-Nanoparticle Conjugates: Cancer Therapy using a 'Trojan Horse'. *Photochem. Photobiol. Sci.* **2006,** *5*, (8), 727-734.

157. Stuchinskaya, T.; Moreno, M.; Cook, M. J.; Edwards, D. R.; Russell, D. A. Targeted Photodynamic Therapy of Breast Cancer Cells using Antibody-Phthalocyanine-Gold Nanoparticle Conjugates. *Photochem. Photobiol. Sci.* **2011,** *10*, (5), 822-831.

158. Oo, M. K. K.; Yang, X.; Du, H.; Wang, H. 5-aminolevulinic Acid-Conjugated Gold Nanoparticles for Photodynamic Therapy of Cancer. *Nanomedicine* **2008,** *3*, (6), 777-786.

159. Cheng, Y.; Meyers, J. D.; Broome, A.-M.; Kenney, M. E.; Basilion, J. P.; Burda, C. Deep Penetration of a PDT Drug into Tumors by Noncovalent Drug-Gold Nanoparticle Conjugates. *J. Am. Chem. Soc.* **2011,** *133*, (8), 2583-2591.

160. Zaruba, K.; Kralova, J.; Rezanka, P.; Pouckova, P.; Veverkova, L.; Kral, V. Modified Porphyrin-Brucine Conjugated to Gold Nanoparticles and their

Application in Photodynamic Therapy. *Org. Biomol. Chem.* **2010,** *8*, (14), 3202-3206.

161. Xu, H.; Aylott, J. W.; Kopelman, R.; Miller, T. J.; Philbert, M. A. A Real-Time Ratiometric Method for the Determination of Molecular Oxygen Inside Living Cells using Sol-Gel-Based Spherical Optical Nanosensors with Applications to Rat C6 Glioma. *Anal. Chem.* **2001,** *73*, (17), 4124-4133.

162. Orringer, D. A.; Koo, Y.-E. L.; Chen, T.; Kim, G.; Hah, H. J.; Xu, H.; Wang, S.; Keep, R.; Philbert, M. A.; Kopelman, R.; Sagher, O. *In Vitro* Characterization of a Targeted, Dye-Loaded Nanodevice for Intraoperative Tumor Delineation. *Neurosurgery* **2009,** *64*, (5), 965-971.

163. Kuruppuarachchi, M.; Savoie, H.; Lowry, A.; Alonso, C.; Boyle, R. W. Polyacrylamide Nanoparticles as a Delivery System in Photodynamic Therapy. *Mol. Pharmaceutics.* **2011**, 8, (3), 920 -931.

164. Wenger, Y.; Schneider, R. J., II; Reddy, G. R.; Kopelman, R.; Jolliet, O.; Philbert, M. A. Tissue Distribution and Pharmacokinetics of Stable Polyacrylamide Nanoparticles Following Intravenous Injection in the Rat. *Toxicol. Appl. Pharm.* **2011,** *251*, (3), 181-190.

165. Hah, H. J.; Kim, G.; Lee, Y.-E. K.; Orringer, D. A.; Sagher, O.; Philbert, M. A.; Kopelman, R. Methylene Blue-Conjugated Hydrogel Nanoparticles and Tumor-Cell Targeted Photodynamic Therapy. *Macromol. Biosci.* **2011,** *11*, (1), 90-99.

166. Qin, M.; Hah, H. J.; Kim, G.; Nie, G.; Lee, Y.-E. K.; Kopelman, R. Methylene Blue Covalently Loaded Polyacrylamide Nanoparticles for Enhanced Tumor-Targeted Photodynamic Therapy. *Photochem. Photobiol. Sci.* **2011,** *10*, (5), 832-841.

167. Reddy, G. R.; Bhojani, M. S.; McConville, P.; Moody, J.; Moffat, B. A.; Hall, D. E.; Kim, G.; Koo, Y.-E. L.; Woolliscroft, M. J.; Sugai, J. V.; Johnson, T. D.; Philbert, M. A.; Kopelman, R.; Rehemtulla, A.; Ross, B. D. Vascular Targeted Nanoparticles for Imaging and Treatment of Brain Tumors. *Clin. Cancer Res.* **2006,** *12*, (22), 6677-6686.

168. Gao, X. H.; Cui, Y. Y.; Levenson, R. M.; Chung, L. W. K.; Nie, S. M. *In Vivo* Cancer Targeting and Imaging with Semiconductor Quantum Dots. *Nature Biotech.* **2004,** *22*, (8), 969-976.

169. Morosini, V.; Bastogne, T.; Frochot, C.; Schneider, R.; Francois, A.; Guillemin, F.; Barberi-Heyo, M. Quantum Dot-Folic Acid Conjugates as Potential Photosensitizers in Photodynamic Therapy of Cancer. *Photochem. Photobiol. Sci.* **2011,** *10*, (5), 842-851.

170. Bakalova, R.; Ohba, H.; Zhelev, Z.; Nagase, T.; Jose, R.; Ishikawa, M.; Baba, Y. Quantum Dot Anti-CD Conjugates: Are They Potential Photosensitizers or Potentiators of Classical Photosensitizing Agents in Photodynamic Therapy Of Cancer? *Nano Letters* **2004,** *4*, (9), 1567-1573.

171. Samia, A. C. S.; Dayal, S.; Burda, C. Quantum Dot-Based Energy Transfer: Perspectives and Potential for Applications in Photodynamic Therapy. *Photochem. Photobiol.* **2006,** *82*, (3), 617-625.

172. Yaghini, E.; Seifalian, A. M.; MacRobert, A. J. Quantum Dots and Their Potential Biomedical Applications in Photosensitization for Photodynamic Therapy. *Nanomedicine* **2009,** *4*, (3), 353-363.

173. Nikaido, H. Molecular Basis of Bacterial Outer Membrane Permeability Revisited. *Microbiol. Mol. Biol. R.* **2003,** *67*, (4), 593-+.

174. Orenstein, A., Klein D., Kopolovic J., Winkler E., Malik, Z, Keller, N., Nitzan, Y. The Use of Porphyrins for Eradication of *Staphylococcus Aureus* in Burn Wound Infections. *FEMS Immunol. Med. Mic.* **1998,** *19*, (4), 307-314.

175. Soukos, N. S., Ximenez-Fyvie, L. A.; Hamblin, M. R.; Socransky, S. S.; Hasan, T. Targeted Antimicrobial Photochemotherapy. *Antimicrob. Agents Ch.* **1998,** *42*, (10), 2595-2601.

176. Woodburn, K. W.; Fan, Q.; Kessel, D.; Luo, Y.; Young, S. W. Photodynamic Therapy of B16F10 Murine Melanoma with Lutetium Texaphyrin. *J. Invest. Dermatol.* **1998,** *110*, (5), 746-751.

177. Malik, Z.; Ladan, H.; Nitzan, Y. Photodynamic Inactivation of Gram-Negative Bacteria - Problems and Possible Solutions. *J. Photochem. Photobiol. B. Biol.* **1992,** *14*, (3), 262-266.

178. Banfi, S.; Caruso, E.; Buccafurni, L.; Battini, V.; Zazzaron, S.; Barbieri, P.; Orlandi, V. Antibacterial Activity Of Tetraaryl-porphyrin Photosensitizers: An *In Vitro* Study on Gram Negative and Gram Positive Bacteria. *J. Photochem. Photobiol. B. Biol.* **2006,** *85*, (1), 28-38.

179. Hamblin, M. R.; Hasan, T. Photodynamic Therapy: A New Antimicrobial Approach to Infectious Disease. *Photochem. Photobiol. Sci.* **2004,** *3*, (5), 436-450.

180. Bertoloni, G.; Lauro, F. M.; Cortella, G.; Merchat, M. Photosensitizing Activity of Hematoporphyrin on S*taphylococcus Aureus* Cells. *BBA. Gen. Subjects* **2000,** *1475*, (2), 169-174.

181. Perni, S.; Prokopovich, P.; Pratten, J.; Parkin, I. P.; Wilson, M. Nanoparticles: Their Potential Use in Antibacterial Photodynamic Therapy. *Photochem. Photobiol. Sci.* **2011,** *10*, (5), 712-720.

182. Salmon-Divon, M.; Nitzan, Y.; Malik, Z. Mechanistic Aspects of *Escherichia Coli* Photodynamic Inactivation by Cationic Tetra-meso(n-methylpyridyl)porphine. *Photochem. Photobiol. Sci.* **2004,** *3*, (5), 423-429.

183. Polo, L.; Segalla, A.; Bertoloni, G.; Jori, G.; Schaffner, K.; Reddi, E. Polylysine-Porphycene Conjugates as Efficient Photosensitizers for the Inactivation of Microbial Pathogens. *J. Photochem. Photobiol. B. Biol.* **2000,** *59*, (1-3), 152-158.

184. Konan, Y. N.; Gurny, R.; Allemann, E. State of the Art in the Delivery of Photosensitizers for Photodynamic Therapy. *J. Photochem. Photobiol. B. Biol.* **2002,** *66*, (2), 89-106.

185. Clark, H. A.; Barker, S. L. R.; Brasuel, M.; Miller, M. T.; Monson, E.; Parus, S.; Shi, Z. Y.; Song, A.; Thorsrud, B.; Kopelman, R.; Ade, A.; Meixner, W.; Athey, B.; Hoyer, M.; Hill, D.; Lightle, R.; Philbert, M. A. Subcellular Optochemical Nanobiosensors: Probes Encapsulated By Biologically Localised Embedding (PEBBLEs). *Sensor. Actuat. B-Chem.* **1998,** *51*, (1-3), 12-16.

186. Buck, S. M.; Xu, H.; Brasuel, M.; Philbert, M. A.; Kopelman, R. Nanoscale Probes Encapsulated By Biologically Localized Embedding (PEBBLEs) for Ion Sensing and Imaging in Live Cells. *Talanta.* **2004,** *63*, (1), 41-59.

187. Cao, Y. F.; Koo, Y. E. L.; Kopelman, R. Poly(decyl methacrylate)-Based Fluorescent PEBBLE Swarm Nanosensors for Measuring Dissolved Oxygen in Biosamples. *Analyst* **2004,** *129*, (8), 745-750.

188. Clark, H. A.; Hoyer, M.; Parus, S.; Philbert, M. A.; Kopelman, R. Optochemical Nanosensors and Subcellular Applications in Living Cells. *Microchim. Acta.* **1999,** *131*, (1), 121-128.

189. Clark, H. A.; Hoyer, M.; Philbert, M. A.; Kopelman, R. Optical Nanosensors for Chemical Analysis Inside Single Living Cells. 1. Fabrication, Characterization, and

Methods for Intracellular Delivery of PEBBLE Sensors. *Anal. Chem.* **1999,** *71*, (21), 4831-4836.

190. Clark, H. A.; Kopelman, R.; Tjalkens, R.; Philbert, M. A. Optical Nanosensors for Chemical Analysis inside Single Living Cells. 2. Sensors for pH and Calcium and the Intracellular Application of PEBBLE Sensors. *Anal. Chem.* **1999,** *71*, (21), 4837-4843.

191. Moreno, M. J.; Monson, E.; Reddy, R. G.; Rehemtulla, A.; Ross, B. D.; Philbert, M.; Schneider, R. J.; Kopelman, R. Production of Singlet Oxygen by $Ru(dpp(SO_3)_2)_3$ Incorporated in Polyacrylamide PEBBLES. *Sensor. Actuat. B-Chem.* **2003,** *90*, (1-3), 82-89.

192. Hansen, J. N.; Pheiffer, B. H.; Boehnert, J. A. Chemical and Electrophoretic Properties of Solubilizable Disulfide Gels. *Anal. Biochem.* **1980,** *105*, (1), 192-201.

193. Shi Q., J. G., *One-Dimensional Polyacrylamide Gel Electrophoresis* 3rd ed.; Oxford University Press: Oxford, 1998.

194. Habaue, S.; Okamoto, Y. Stereocontrol in Radical Polymerization. *Chem. Rec.* **2001,** *1*, (1), 46-52.

195. Gomes, A. J.; Lunardi, L. O.; Marchetti, J. M.; Lunardi, C. N.; Tedesco, A. C. Indocyanine Green Nanoparticles useful for Photomedicine. *Photomed. Laser Surg.* **2006,** *24*, (4), 514-521.

196. Giroldo, L.; Felipe, M.; de Oliveira, M.; Munin, E.; Alves, L.; Costa, M. Photodynamic Antimicrobial Chemotherapy (PACT) with Methylene Blue Increases Membrane Permeability in *Candida Albicans*. *Laser. Med. Sci.* **2009,** *24*, (1), 109-112.

197. Orth, K.; Beck, G.; Genze, F.; Ruck, A. Methylene Blue Mediated Photodynamic Therapy in Experimental Colorectal Tumors in Mice. *J. Photochem. Photobiol. B. Biol.* **2000,** *57*, (2-3), 186-192.

198. Castellano, F. N.; Lakowicz, J. R. A Water-Soluble Luminescence Oxygen Sensor. *Photochem. Photobiol.* **1998,** *67*, (2), 179-183.

199. Webster, A. Development and Application of Nanosensors for Intracellular Chemical Analysis. PhD Thesis, Hull University, Hull, **2005**.

200. Carvalho, C. M. B.; Gomes, A. T. P. C.; Fernandes, S. C. D.; Prata, A. C. B.; Almeida, M. A.; Cunha, M. A.; Tomé, J. P. C.; Faustino, M. A. F.; Neves, M. G. P. M. S.; Tomé, A. C.; Cavaleiro, J. A. S.; Lin, Z.; Rainho, J. P.; Rocha, J. Photoinactivation of Bacteria in Wastewater by Porphyrins: Bacterial [beta]-galactosidase Activity and Leucine-Uptake as Methods to Monitor The Process. *J. Photochem. Photobiol. B. Biol.* **2007,** *88*, (2-3), 112-118.

201. Adler, A. D.; Longo, F. R.; Finarelli, J. D.; Goldmacher, J.; Assour, J.; Korsakoff, L. A Simplified Synthesis for Meso-Tetraphenylporphine. *J. Org. Chem.* **1967,** *32*, (2), 476-476.

202. Park, E. J.; Brasuel, M.; Behrend, C.; Philbert, M. A.; Kopelman, R. Ratiometric Optical PEBBLE Nanosensors for Real-Time Magnesium Ion Concentrations Inside Viable Cells. *Anal. Chem.* **2003,** *75*, (15), 3784-3791.

203. Stanca, S. E.; Nietzsche, S.; Fritzsche, W.; Cranfield, C. G.; Biskup, C. Intracellular Ion Monitoring Using a Gold-Core Polymer-Shell Nanosensor Architecture. *Nanotechnology* **2010,** *21*, (5), 055501.

204. Qin, Y.; Bakker, E. Elimination of Dimer Formation in In(III)Porphyrin-Based Anion-Selective Membranes by Covalent Attachment of the Ionophore. *Anal. Chem.* **2004,** *76*, (15), 4379-4386.

205. Roberts, M. J.; Bentley, M. D.; Harris, J. M. Chemistry for Peptide and Protein PEGylation. *Adv. Drug Deliv. Rev.* **2002,** *54*, (4), 459-476.

206. Batinic-Haberle, I.; Spasojevic, I.; Stevens, R. D.; Bondurant, B.; Okado-Matsumoto, A.; Fridovich, I.; Vujaskovic, Z.; Dewhirst, M. W. New PEG-ylated Mn(III) Porphyrins Approaching Catalytic Activity of SOD Enzyme. *Dalton T.* **2006**, (4), 617-624.

207. Hall, C. E. The Synthesis Of Cationic Porphyrins for use in Photodynamic Antimicrobial Chemotherapy (PACT), PhD Thesis, Hull university, **2008**.

208. N. Datta-Gupta a, T. J. B. Synthetic Porphyrins. I. Synthesis and Spectra of Some Para-Substituted Meso - Tetraphenylporphines. *J. Heterocyclic Chem.* **1966,** *3*, (4), 495 - 502.

209. Robic, N.; Biedcharreton, C.; Perrefauvet, M.; Vercherebeaur, C.; Salmon, L.; Gaudemer, A. Synthesis and Preliminary DNA-Interaction Studies of a New Cationic Porphyrin. *Tetrahedron Lett.* **1990,** *31*, (33), 4739-4742.

210. Wen, L. Q.; Li, M.; Schlenoff, J. B. Polyporphyrin Thin Films from the Interfacial Polymerization of Mercaptoporphyrins. *J. Am. Chem. Soc.* **1997,** *119*, (33), 7726-7733.

211. Mewis, R. E. Synthesis of Tetraazamacrocyclic Complexes: Biomedical Applications , PhD Thesis, Hull University, **2009**.

212. Krammer, B. Vascular Effects Of Photodynamic Therapy. *Anticancer Res.* **2001,** *21*, (6B), 4271-4277.

213. Brasseur, N.; Langlois, R.; La Madeleine, C.; Ouellet, R.; van Lier, J. E. Receptor-Mediated Targeting of Phthalocyanines to Macrophages *via* Covalent Coupling to Native or Maleylated Bovine Serum Albumin. *Photochem. Photobiol.* **1999,** *69*, (3), 345-352.

214. Chan, W. S.; Marshall, J. F.; Svensen, R.; Bedwell, J.; Hart, I. R. Effect of Sulfonation on the Cell and Tissue Distribution of the Photosensitizer Aluminium Phthalocyanine. *Cancer Res.* **1990,** *50*, (15), 4533-4538.

215. Anthony W, S. Biofilms and Antibiotic Therapy: Is There a Role for Combating Bacterial Resistance by the use of Novel Drug Delivery Systems? *Adv. Drug Deliv. Rev.* **2005,** *57*, (10), 1539-1550.

216. Taylor, P. W.; Stapleton, P. D.; Paul Luzio, J. New Ways to Treat Bacterial Infections. *Drug Discov. Today* **2002,** *7*, (21), 1086-1091.

217. Saginur, R.; Denis, M. S.; Ferris, W.; Aaron, S. D.; Chan, F.; Lee, C.; Ramotar, K. Multiple Combination Bactericidal Testing of Staphylococcal Biofilms from Implant-associated Infections. *Antimicrob. Agents Chemother.* **2006,** *50*, (1), 55-61.

218. Volety, A. K.; Oliver, L. M.; Genthner, F. J.; Fisher, W. S. A Rapid Tetrazolium Dye Reduction Assay to Assess the Bactericidal Activity of Oyster (Crassostrea Virginica) Hemocytes Against Vibrio Parahaemolyticus. *Aquaculture.* **1999,** *172*, (1-2), 205-222.

219. Mosmann, T. Rapid Colorimetric Assay for Cellular Growth and Survival: Application to Proliferation and Cytotoxicity Assays. *J. Immunol. Methods.* **1983,** *65*, (1-2), 55-63.

220. Usacheva, M. N.; Teichert, M. C.; Biel, M. A. The Role of the Methylene Blue and Toluidine Blue Monomers And Dimers in the Photoinactivation of Bacteria. *J. Photochem. Photobiol. B.Biol.* **2003,** *71*, (1-3), 87-98.

221. Michaelis, L.; Granick, S. Metachromasy of Basic Dyestuffs. *J. Am. Chem. Soc.* **2002,** *67*, (7), 1212-1219.

222. Dadras, S.; Mohajerani, E.; Eftekhar, F.; Hosseini, M. Different Photoresponses of Staphylococcus Aureus and Pseudomonas Aeruginosa to 514, 532, and 633nm Low Level Lasers *In Vitro*. *Curr. Microbiol.* **2006,** *53*, (4), 282-286.

223. Hudson, R.; Savoie, H.; Boyle, R. W. Lipophilic Cationic Porphyrins as Photodynamic Sensitisers—Synthesis and Structure–Activity Relationships. *Photodiagn. Photodyn.* **2005,** *2*, (3), 193-196.

224. Kim, J. S.; Yoon, T. J.; Yu, K. N.; Noh, M. S.; Woo, M.; Kim, B. G.; Lee, K. H.; Sohn, B. H.; Park, S. B.; Lee, J. K.; Cho, M. H. Cellular Uptake of Magnetic Nanoparticle is Mediated Through Energy-Dependent Endocytosis in A549 Cells. *J. Vet. Sci.* **2006,** *7*, (4), 321-326.

225. Vanamersfoort, E. S.; Vanstrijp, J. A. G. Evaluation of a Flow Cytometric Fluorescence Quenching Assay of Phagocytosis of Sensitized Sheep Erythrocytes by Polymorphonuclear Leukocytes. *Cytometry* **1994,** *17*, (4), 294-301.

226. Alberola, A. P.; Rädler, J. O. The Defined Presentation of Nanoparticles to Cells and their Surface Controlled Uptake. *Biomaterials*. **2009,** *30*, (22), 3766-3770.

227. van Lier, J. E., Photosensitization: reaction pathways, in Valenzeno, D. P., Pottier, R.H., Mathis, P., Douglas, R. H. (eds.), Advanced Study Institute on Photobiological, T. In *Photobiological techniques: [Proceedings of a NATO Advanced Study Institute on Photobiological Techniques, held July 1 - 4, 1990, in Kingston, Ontario, Canada]*, New York u.a, **1991**, Plenum Press: New York.

228. Osada, K.; Ravandi, A.; Kuksis, A. Rapid Analysis of Oxidized Cholesterol Derivatives by High-Performance Liquid Chromatography Combined with Diode-Array Ultraviolet and Evaporative Laser Light-Scattering Detection. *J. Am. Oil. Chem. Soc*. **1999,** *76*, (7), 863-871.

229. Castilla, R.; Gonzalez, R.; Fouad, D.; Fraga, E.; Muntane, J. Dual Effect of Ethanol on Cell Death in Primary Culture of Human and Rat Hepatocytes. *Alcohol. Alcoholism.* **2004,** *39*, (4), 290-296.

230. Oh, J. K.; Drumright, R.; Siegwart, D. J.; Matyjaszewski, K. The Development of Microgels/Nanogels for Drug Delivery Applications. *Prog. Polym. Sci.* **2008,** *33*, (4), 448-477.

231. Alonso, C. M. A.; Palumbo, A.; Bullous, A. J.; Pretto, F.; Neri, D.; Boyle, R. W. Site-Specific and Stoichiometric Conjugation of Cationic Porphyrins to Antiangiogenic Monoclonal Antibodies. *Bioconjugate. Chem.* **2010,** *21*, (2), 302-313.

232. Rothemund, P. Formation of Porphyrins from Pyrrole and Aldehydes. *J. Am. Chem. Soc.* **1935,** *57*, (10), 2010-2011.

233. Kano, K.; Miyake, T.; Uomoto, K.; Sato, T.; Ogawa, T.; Hashimoto, S. Evidence for Stacking of Cationic Porphyrin in Aqueous-Solution. *Chemist. Lett.* **1983**, (12), 1867-1870.

234. McAllister, K.; Sazani, P.; Adam, M.; Cho, M. J.; Rubinstein, M.; Samulski, R. J.; DeSimone, J. M. Polymeric Nanogels Produced *via* Inverse Microemulsion Polymerization as Potential Gene and Antisense Delivery Agents. *J. Am. Chem. Soc.* **2002,** *124*, (51), 15198-15207.

235. Bajpai, A. K.; Giri, A. Water Sorption Behaviour of Highly Swelling (Carboxy Methylcellulose-G-Polyacrylamide) Hydrogels and Release of Potassium Nitrate as Agrochemical. *Carbohyd. Polym.* **2003,** *53*, (3), 271-279.

236. Peng, Q.; Moan, J.; Nesland, J. M. Correlation of Subcellular and Intratumoral Photosensitizer Localization with Ultrastructural Features After Photodynamic Therapy. *Ultrastruct. Pathol.* **1996,** *20*, (2), 109-129.

237. Storm, G.; Belliot, S. O.; Daemen, T.; Lasic, D. D. Surface Modification of Nanoparticles to Oppose Uptake by the Mononuclear Phagocyte System. *Adv. Drug. Deliver. Rev.* **1995,** *17*, (1), 31-48.

238. Yu L.H.; Muthukumaran K.; Sazanovich I.V.; Kirmaier C.; Hindin E.; Diers, J.R.; Boyle, P.D.; Bocian DF, Holten, D.; Lindsey, J. S., Inorg. Chem. **2003; 42**: 6629-6647.

239. Kadish, K. M.; Smith, K.M.; Guilard, R., The Porphyrin Handbook: Synthesis and organic chemistry Volume 1, **1990**, Page 60.

240. Birnbaum, E.R.; Hodge, J.A.; Grinstaff, M.W.; Schaefer, W.P.; Henling, L.; Labinger, J.A.; Bercaw, J.E.; Gra, H.B. 19F NMR Spectra and Structures of Halogenated Porphyrins. *Inorg. Chem.* **1995, 34,** 3625-3632.